ISSI Scientific Report SR-004

Heat and Gas Diffusion in Comet Nuclei

W.F. Huebner, J. Benkhoff, M-T. Capria,
A. Coradini, C. De Sanctis, R. Orosei & D. Prialnik

INTERNATIONAL SPACE SCIENCE INSTITUTE

HEAT AND GAS DIFFUSION IN COMET NUCLEI

Walter F. Huebner
Southwest Research Institute, USA

Johannes Benkhoff[1]
Institute for Planetary Research, DLR-Berlin, Germany

Maria-Teresa Capria, Angioletta Coradini, Christina De Sanctis, Roberto Orosei
Istituto di Astrofisica Spaziale, Italy

Dina Prialnik
Tel Aviv University, Israel

August 8, 2006

[1]Presently with Research and Scientific Support Department, ESA-ESTEC, The Netherlands

Contents

List of Figures

List of Tables

Foreword

Modern comet research focuses on the nucleus, its composition and internal structure. The aim is to gain an understanding of the origin of the nucleus and to trace the history of cometary materials. The only regions of the comet that are accessible to remote observation and in-situ measurements are the surface of the nucleus and the coma. In order to draw conclusions about the interior of the nucleus, models must be used that describe the transport of gases and solids to the surface and that simulate the dynamical and chemical processes in the coma. The present volume offers models for gas and heat transport inside the nucleus and for the release of gas and dust from the nucleus.

The model results contained in the book are complemented by chapters about the nucleus in general. This gives the volume the character of a handbook on comet nuclei that should be useful for the experimenters of future comet missions. The comet models will not only support the data interpretation, but will also help in developing measurement strategies and will be useful in the operations of the Rosetta spacecraft while in orbit around Comet Churyumov-Gerasimenko.

It was in 2002 that Walter F. Huebner formed the “Comet Nucleus-Coma Boundary Layer Model ISSI Team” for studying the transport of gas and heat inside the porous nuclei of comets. Team members had previously developed several independent models that gave divergent results. The methods and algorithms used in these models have been analyzed by the team and are presented here together with a reference model in which physico-chemical parameters are discussed and also the coupling of spatial zoning to the attitude of a spinning nucleus. This issue is of importance for the correct calculation of radial gradients at the surface of the nucleus.

The Solar System was probably formed by collapse from an interstellar molecular cloud. Some molecules survived, until 4.5 Gyr later they were released from the nucleus when the comet approached the Sun. Other interstellar molecules were altered in the protosolar cloud, where also new molecules were formed. The Rosetta experiments are expected to identify hundreds of isotopically and chemically different molecules and radicals in the coma of Comet Churyumov-Gerasimenko. The results on the transport of gas and dust in the nucleus presented here - combined with models that mimic the processes in the coma - will be essential to decide whether molecules or radicals were synthesized in the interstellar medium, the protosolar cloud or inside the nucleus, or whether they are just secondary products of photo-dissociation and chemical processes in the coma.

The content of this book should not only be applied to and tested against future cometary data, but it can also be used for improving the interpretation of available data. In this way, for example, one could perhaps decide whether formaldehyde, found in abundance in the coma of Comet Halley, was stored in the nucleus as POM, the formaldehyde polymer. Another open question concerns molecular nitrogen. In the coma of Comet Halley the abundance of N2 is very low relative to CO, although in the solar nebula both these molecules were major constituents.

The work of the "Comet Nucleus-Coma Boundary Layer Model Team" has been an important part of ISSI's activity in the field of cometary research. It should be seen as continuation of the earlier Workshop on the Composition and Origin of Cometary Materials held in September 1998 and published as Volume 8 of the Space Science Series of ISSI. Another volume on comets is in preparation for this series. The present book will be followed by another ISSI Scientific Report on interactive comet coma modelling.

Roger-Maurice Bonnet Johannes Geiss

Preface

The discussions in this book are primarily about comet nuclei; however, links to some related topics, including comet comae, tails, and dust trails are briefly mentioned. In our discussions we distinguish between well understood and established facts, less certain causes for some observed phenomena, inferred phenomena and processes, and speculative features.

Among the well understood and established facts we list orbit determinations, non-gravitational forces, that comet nuclei are the sources for the development of comet comae and tails, that small comet nuclei have a non-spherical shape, and that they are composed of frozen gases and dust. It is also well established that comet nuclei have active and less active (inactive) surface areas. The less active areas are surface regions covered by layers of dust that quench the gas production, i.e. the sublimation of ices. Dust is entrained by gases escaping from very low gravity nuclei. Every active comet has water ice and usually also CO and CO_2. Other species are often present, but their relative abundances can vary widely.

Comets can show sporadic activity (outbursts) and their nuclei are known to split. Several reasons for the outbursts and splitting have been proposed, but the causes are less certain. Among possible causes are temperature gradients in the nucleus leading to differential internal pressures or an exothermic phase transition from amorphous to crystalline ice, gravitational force gradients produced by close approaches to the Sun or another planet, and internal stresses produced by changes of moments of inertia and changes in spin angular momentum. Changes in the moments of inertia may be caused by uneven outgassing.

The causes for dust mantle development are also less certain. Several different processes have been proposed. Among them are differential entrainment by size sorting and surface topography in which hilly areas lead to divergent gas (and dust) flow while valleys lead to jet-like features in which dust is more easily entrained.

The structure of dust particles, probably composed of smaller interstellar grains, is an inferred property. However, results from the Stardust mission may bring new insights.

The presence of amorphous water ice in comet nuclei has been proposed widely. Low temperatures are a necessary but not a sufficient condition for the formation of amorphous water ice. Amorphous water ice is formed when water molecules condense at low temperatures but rapidly so that they do not have the opportunity to reorient themselves, i.e. their dipoles, to form crystalline ice. Amorphous ice has been made in the laboratory and several properties, notably its ability to trap other gases, have been well established. However, amorphous ice has not been detected in interstellar clouds, star-forming regions, or the outer Solar System. This may not be surprising, because amorphous ice may not be able to survive for long on a surface exposed to photon and particle radiations. Several processes suggest indirectly the presence of amorphous water ice in comets. Among them are the release of gases, such as CO, approximately proportional to the rate of sublimation of water ice at certain heliocentric distances of a comet and exothermic phase transitions to crystalline ice, causing outbursts of comet activity. Even though all of these processes are physically possible, the existence of amorphous water ice in comet nuclei should be considered speculative until it can be proven more directly. Proving the existence of amorphous water ice remains one of the goals of comet missions.

Also speculative is the flow of dust particles in the porous comet nucleus. Even when a dust particle is released from the ice and dust matrix in a pore in the nucleus, its path of travel in the highly tortuous pores must be very short.

Finally, even if the presence of ^{26}Mg could be firmly established in comet nuclei, it does not prove that ^{26}Al decayed and heated a nucleus. Since the half-life of ^{26}Al is 730,000 years, it may have decayed before the nucleus formed, but its decay products may nevertheless have been incorporated in comet nuclei. Thus, models that assume heating of the nucleus by the decay of ^{26}Al shortly after the comet nucleus assembled, must be viewed as speculative, although very interesting.

A major goal for comet nucleus modeling is to provide the mixing ratio of species in the nucleus. These ratios can be directly linked to the composition of the solar nebula. In this respect, coma observations are insufficient, since the abundances of volatiles in the nucleus are not mirrored directly by the observed mixing ratios in the coma, since this ratio changes with heliocentric distance of the comet.

At the start of this investigation, comet nucleus models gave widely different Results (Huebner et al., 1999). Thus, the most important goal for the team was to understand the physical and mathematical sources of these differences.

We concentrate on modeling techniques that enable us to understand the reality of the physical processes occurring in comet nuclei. We do not divert our attention to more complex issues, such as multi-dimensional geometries, the nucleus/coma boundary layer, mechanically restricted outgassing, such as dust layers and complicated mixtures. These would require many additional assumptions and uncertain free parameters.

We consider several different numerical computational procedures, with their intrinsic advantages and disadvantages, and compare them. We also consider different implementations of boundary conditions. Our aim is to assess the accuracy of numerical models and to identify the main factors that will affect it.

We are deeply indebted to Prof. Johannes Geiss for his encouragement, interest, and participation in our team effort and ISSI for repeatedly hosting the team.

At the start of these investigations, Dr. Achim Enzian was an active member of this team. We lost him when he accepted a position in industry not related to comet science. We wish to express our appreciation for his many contributions to the team effort. References to his computational algorithms are marked by the letter A throughout the text.

We benefited from discussions with many short-term visitors participating in our team meetings. Among them were Dr. E. Kührt and Dr. D. Möhlmann, who discussed their models for heat and gas diffusion in comet nuclei; Dr. J. Klinger, who discussed thermal conductivity and other properties of amorphous ice; Dr. Celine Reylé, who discussed the fluorescence of S_2 in the inner coma; and Dr. K. Seiferlin, who described thermal conductivity experiments.

Various sections of the manuscript have been reviewed by many colleagues. We hope that these reviews made this volume relatively free of errors. Any remaining errors are entirely our responsibility.

June 2006

Walter F. Huebner
Johannes Benkhoff
Maria-Teresa Capria
Angioletta Coradini
Christina De Sanctis
Roberto Orosei
Dina Prialnik

Table 1: List of Symbols (see also List of Constants)

Symbol	**Meaning**	**Units (SI)**
$\mathcal{A}$	Albedo	–
A	Area	m^2
a	Semimajor axis of comet orbit	AU
a_J	Semimajor axis of Jupiter's orbit	AU
$\hat{a}$	Acceleration of dust particle	m s^{-2}
$\mathcal{C}$	Compressive strength	Pa
C_D	Drag coefficient	
c	Specific heat	J kg^{-1} K^{-1}
d	Molecular diameter	m
E	Eccentric anomaly	–
$\dot{E}_{rad}$	Rate of heat release by radioactive decay	W kg^{-1}
e	Eccentricity	–
$\mathcal{F}$	Force	N
F	Energy flux	W m^{-2}
$\tilde{f}_n$	n-dimensional Maxwell distribution	
f_r	Nr. of excited rotational degrees of freedom	–
f_H	Hertz factor	–
$\mathcal{G}$	Gas diffusion coefficient	s
g	Gravitational acceleration	m s^{-2}
H	Height	m
ΔH_{crys}	Crystallization enthalpy (amorphous H_2O)	J kg^{-1}
ΔH_n	Enthalpy of sublimation of species n	J kg^{-1}
i_{orb}	Angle of orbit plane relative to ecliptic	$^\circ$
i_{spin}	Angle of spin axis relative to orbit plane	$^\circ$
J	Mass flux of volatile	kg m^{-2} s^{-1}
$\hat{J}$	Mass flux of dust particles	kg m^{-2} s^{-1}
j	Gas mass flow	kg s^{-1}
$\mathcal{K}$	Thermal diffusivity	m^2 s^{-1}
Kn	Knudsen number	–
L	Length	m
ℓ	Mean free path	m
M	Mass of comet nucleus	kg
m	Mass of molecule	kg
m_r	Mass enclosed in sphere of radius r	kg
$\hat{m}$	Mass of dust particle	kg

Symbol	Meaning	Units (SI)
N	Number (total)	m^{-3}
n	Number density	m^{-3}
$\hat{n}$	Dust particle number density	m^{-3}
$\mathcal{P}_n$	Saturation vapour pressure of species n	Pa
P_n	Gas pressure of species n	Pa
P_{orb}	Orbital period	yr
P_{spin}	Nucleus spin period	s
Q_n	Surface mass sublimation flux of species n	kg m^{-2} s^{-1}
Q	Aphelion distance	AU
q	Perihelion distance	AU
q_n	Mass sublimation rate of species n	kg m^{-3} s^{-1}
$\mathcal{R}_{\mathrm{g}}$	Universal gas constant	J g-mol^{-1} K^{-1}
R	Radius of comet nucleus	m
r	Distance from nucleus centre	m
r_{p}	Pore radius	m
r_{H}	Heliocentric distance	AU
$\hat{r}$	Dust particle radius	m
$\hat{r}^*$	Critical dust particle radius	m
S	Surface to volume ratio in porous medium	m^{-1}
$\mathcal{T}$	Tensile strength	N m^{-2}
T	Temperature	K
T_{s}	Surface temperature	K
T_{J}	Tisserand invariant	–
t	Time	s
u	Energy per unit mass	J kg^{-1}
V	Volume	m^3
$\hat{V}$	Volume of a dust particle	m^3
v	Velocity of gas	m s^{-1}
$\hat{v}$	Velocity of dust particle	m s^{-1}
v'_{oz}	Centre of mass speed	m s^{-1}
v_s	Speed of sound	m s^{-1}
v_{th}	Thermal speed	m s^{-1}
X_n	Mass fraction of species n	–
Z	Gas production rate per unit area	m^{-2} s^{-1}
z	Depth	m

Symbol	**Meaning**	**Units (SI)**
α	Latitude	$^\circ$
α_{p}	Polarizability	F m^2
ϵ	Emissivity	
ζ	Angle of insolation	$^\circ$
θ	Cometocentric latitude	rad
κ	Thermal conductivity	W m^{-1} K^{-1}
Λ	Coupling constant between molecules	J m^6
λ	Crystallization rate	s^{-1}
μ_n	Molar mass of species n	kg g-mol^{-1}
ν	Viscosity	kg m^{-1} s^{-1}
Ξ	Specific surface in porous medium	m^{-1}
ξ	Tortuosity	–
ρ	Total density	kg m^{-3}
ρ_{N}	Density of comet nucleus	kg m^{-3}
ρ_{g}	Gas density	kg m^{-3}
$\hat{\rho}$	Density of dust particle	kg m^{-3}
ρ_n	Partial density of species n (ice phase)	kg m^{-3}
$\tilde{\rho}_n$	Partial density of species n (gas phase)	kg m^{-3}
ϱ_n	Solid density of species n	kg m^{-3}
σ_n	Cross section of species (or element) n	m^2
$\hat{\sigma}$	Cross section of dust particle	m^2
σ_θ	Tangential stress	N m^2
σ_r	Radial stress	N m^2
τ_{cond}	Characteristic heat diffusion time	s
τ_{crys}	Characteristic crystallization time	s
τ_{diff}	Characteristic gas diffusion time	s
τ_{subl}	Characteristic sublimation time	s
υ	Poisson ratio	
Ψ	Porosity	
$\psi\hat{r}$	Dust size distribution function	
$\psi(r_{\mathrm{p}})$	Pore size distribution function	
Φ	Particle flux	molecules m^{-2} s^{-1}
ϕ	Azimuth angle	$^\circ$
φ	Permeability	
Ω	Hour angle	rad
ω	Nucleus spin rate	rad s^{-1}

Table 2: List of Constants

Constant	**Symbol**	**Value**	**Units**
Speed of light	c	2.99792458×10^{8}	m s^{-1}
Gravitational constant	G	6.67259×10^{-11}	m^3 kg^{-1} s^{-2}
Planck constant	h	$6.6260755 \times 10^{-34}$	J s
Boltzmann constant	k	1.380658×10^{-23}	J K^{-1}
Stefan-Boltzmann	σ	5.67051×10^{-8}	W m^{-2} K^{-4}
Avogadro number	N_A	6.0221367×10^{23}	g-mol^{-1}
Universal gas constant	$\mathcal{R}_{\mathrm{g}}$	8.314510×10^{3}	J g-mol^{-1} K^{-1}
Solar constant	$F_{\odot}$	1.3695×10^{3}	W m^{-2}
Solar mass	$M_{\odot}$	1.9891×10^{30}	kg
Solar radius	$R_{\odot}$	6.9598×10^{8}	m
Solar luminosity	$L_{\odot}$	3.8515×10^{26}	W
Year (solar)	yr	3.1558×10^{7}	s
Astronomical Unit	AU	1.496×10^{11}	m
Earth mass	$M_{\oplus}$	5.976×10^{24}	kg
Earth radius	$R_{\oplus}$	6.378×10^{6}	m
Permittivity of free space	ε_{o}	$8.854187817 \times 10^{12}$	F m^{-1}

— 1 —

Introduction - Observational Overview

> "...In order to see the nucleus as small as it really is, we should look at it a long while, that the eye may gradually lose the impression of the bright coma which surrounds it. ..."
>
> William Herschel, LL.D.F.R.S., *Philosophical Transactions*, 1808.

This book is about modeling the nuclei of comets. We concentrate on heat and gas diffusion, but also touch on other properties and effects such as the evolution of comet nuclei. From the outset, we want to emphasize that these models are not restricted to comet nuclei. They can also be applied to icy satellites and asteroids. Since sublimation of ices and diffusion of gases are not essential elements for asteroids, some simplifications apply.

It is appropriate to start with a definition of a comet and a comet nucleus. A *comet* is a *phenomenon* in the sky. It has a diffuse appearance because of its outstreaming gases entraining dust and usually has one or more tails. A comet becomes visible through induced fluorescence of its gases and scattering of sunlight by its dust. Comets have been observed for centuries. Kronk (1999) lists comets going back to the year -674. This most ancient reference to a comet was found on Babylonian cuneiform stone tablets. There are records of even more ancient observations of possible comets. The most ancient of these uncertain observations is that of -1193, the year Troy fell to the Greeks (Kronk, 1999). While the word "comet" is based on Greek ($\kappa o \mu \eta \tau \eta$), meaning longhaired, the Chinese referred to comets as "broom stars," "sparkling stars," "guest stars," "tangle stars," or even as "celestial magnolia trees." For more detail and a historical overview, see Keller (1990) and Kronk (1999).

The comet *nucleus* is composed of a mixture of frozen (and possibly some trapped) gases and particles of refractory silicates and complex organic molecules. It is the source of all comet activity, which includes the coma (the continuously escaping atmosphere) composed of gas, plasma, and dust, and three types of tails: a dust tail, a plasma tail, and a tail composed of neutral atoms and molecules. Everything we know about the composition of a comet nucleus is based on ground- and space-based observations of the coma and (to a lesser degree) the tails. Its activity is initiated by intense sunlight when a comet nucleus approaches the inner planetary system in its orbit around the Sun. The icy conglomerate nucleus was first proposed in a more rudimentary form by Whipple (1950).

The coma and subsequently the gas, plasma, and dust tails, develop during the approach to the Sun. They subside and disappear in reverse order after perihelion passage. Since the nucleus is of low density and generally only about ten kilometres in size, it has insufficient mass to bind its atmosphere gravitationally, contrary to what is typically the case for planets. The escape speed is of the order of 1 m/s, depending somewhat on the size of the nucleus. The escaping dusty atmosphere causes the ephemeral, visually observable effects that define a comet.

Comet nuclei lose matter when exposed to heat. Their fragility associated with the progressive mass loss suggests that nuclei have not been heated significantly during formation or during their existence before they enter the inner Solar System. However, the frozen gases in the surface layer of a nucleus have been altered by ultraviolet (UV) radiation and cosmic rays during the 4.5 Gy that a nucleus is part of a distant comet cloud. The interior may have undergone similar changes from residual radioactivity, from the conversion of kinetic energy to energy of deformation in collisions during the aggregation phase, and, if comets contain amorphous ice, from the release of energy during the phase change from amorphous to crystalline water ice. Once a comet enters the inner Solar System, it progressively decays with each orbit. Although unlikely, this could lead to complete sublimation of the ices and disintegration, but it is more likely to lead to a dead, asteroid-like body.

The mass of a comet nucleus is less than 10^{-10} times that of the Earth; hence planets can perturb the orbits of comets, but the reverse effect is negligible. Because of its low mass, gravity on its surface is only about 10^{-6} times that on Earth, which makes it comparable to the residual acceleration (caused by atmospheric drag) on the Space Shuttle and on the Space Station. Thus, these space platforms are suitable for experiments simulating conditions on asteroids and comet nuclei. Figure 1.1 illustrates comet nuclei from the first four flyby missions to comets.

Comets play an important role in cosmogony. We study their origin within the framework of a particular cosmogonical model that is closely linked to the origin of the Solar System. The physical details for formation of the Solar System and the sequence of formation of comet nuclei in it are active areas of research. There now are a number of hypotheses linking the study of interstellar clouds as precursors for the solar or presolar nebula and the physics, chemistry, and orbital dynamics of comets.

There are two reservoirs of comet nuclei: the Kuiper belt and the Oort cloud. The primary source, the Kuiper belt, extends outward from the

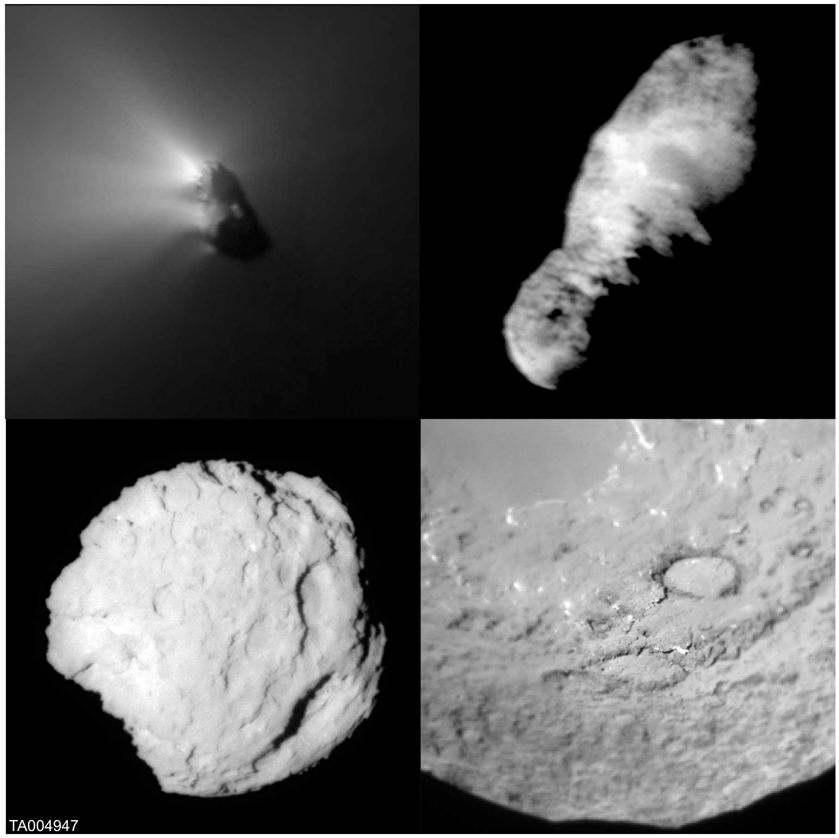

Figure 1.1: Four comet nuclei visited by spacecraft. Top left: The nucleus of Comet 1P/Halley is about $15.5 \times 8.5 \times 8$ km in size. The best spatial resolution (2 pixels) is about 100 m at the top part of the image as obtained by the Halley Multicolour Camera on the Giotto spacecraft (Courtesy H.U. Keller; copyright 1986 MPAE). Top right: The nucleus of Comet 19P/Borrelly is about $16 \times 8 \times 8$ km in size. Spatial resolution (2 pixels) over most of the image is about 90 m. The image was obtained with the Miniature Imaging Camera and Spectrometer (Courtesy L. Soderblom). Bottom left: The nucleus of Comet 81P/Wild is about $5.5 \times 4.0 \times 3.3$ km in size. The spatial resolution (2 pixels) is about 20 m as obtained by the Stardust mission (Courtesy R. Newburn). Bottom right: A composite of many images from the Impactor Targeting Sensor of the Deep Impact mission on approach to the nucleus of 9P/Tempel 1. The nucleus is about 6.2×4.6 km in size. Highest resolution, approximately 2-3 metres, is in the area near the impact site, where small, sub-frame, close-up images were obtained. The resolution gradually degrades toward the edges of the frame (Courtesy Deep Impact Project. Image processing by A. Delamere and D. Stern).

orbit of Neptune in a disk centered on the ecliptic. It is thought that comet nuclei were the planetesimals from which the giant planets formed. As these planets formed, they scattered the remaining comet nuclei from the inner part of the Kuiper belt (and possibly some asteroids) into the Oort cloud.

The Oort cloud forms the boundary between the Solar System and the galaxy beyond. This cloud of comet nuclei is arranged in a spherical distribution with mean radius of about 30,000 AU around the Sun, as deduced by Oort (1950) from aphelia positions of long-period comets, and serves as a reservoir for the dynamically new long-period comets that visit the inner Solar System for the first time. The orbits of these comets differ from those of the planets and the asteroids not only by their large aphelia and hence long period of revolution of several million years, but also in that they are not confined to the region of the ecliptic. When they are gravitationally perturbed by a passing star in such a way that they come into the inner Solar System, their elliptic orbits are so long that they are referred to as "nearly parabolic". Aside from some clustering, caused by perturbations from passing stars or interstellar clouds, and depletion in a narrow band along the galactic equator, apparently caused by galactic tide effects, their aphelia distribution on the sky is isotropic. Although comet nuclei have been expelled from the Solar System into interstellar space, the chance that an interstellar comet from another Solar System passes close to the Sun is extremely small. This may explain why no interstellar comets have been observed with certainty.

Comets are primordial, physico-chemically primitive, and unconsolidated objects from times before the formation of the planetary system. They most closely reflect the original structure of accretion of bodies that formed in the outer regions of the solar nebula from interstellar matter that survived the accretion shock and from gases condensable at the local temperature. Minor constituents may be molecular radicals and highly volatile gases that were trapped during the processes of condensation and accretion. Comet nuclei therefore provide clues about the composition and thermodynamic conditions in the solar nebula before and during formation of the planetary system.

Comets can be classified according to dynamical or compositional properties. From the aspect of dynamical properties we distinguish between two major groups: the long-period comets with periods of revolution around the Sun $P_{\mathrm{orb}} > 200$ years and short-period comets with $P_{\mathrm{orb}} < 200$ years. The long-period comets can be further divided into subgroups according to their energy, which is measured in terms of $1/a$, where a is their orbital semi-major axis. A period of 200 years corresponds to $1/a \approx 0.03$ AU^{-1}. The dynamically new comets, probably coming for the first time from the Oort cloud into the inner Solar System, have $1/a \approx 3 \times 10^{-5}$ AU^{-1}. Their period is about 2×10^6 years. Dynamically young long-period comets, which have entered the inner Solar System only a few times, have $1/a \approx 3 \times 10^{-4}$ AU^{-1} . For example, Comet Hyakutake (C/1996 B2) is a young long-period comet. Dynamically old long-period comets have $1/a \approx 3 \times 10^{-3}$ AU^{-1}. Comet Hale-Bopp (C/1995 O1), for example, is an old long-period comet.

At the other extreme are the short-period comets ($P_{\mathrm{orb}} < 200$ years). They have been captured by planets, mostly Jupiter, into orbits that prevalently lie close to the ecliptic, or they had their origin in an 'inner' cloud in the ecliptic trans-Neptunian region. Short-period comets are classified into two subgroups based on the value of the Tisserand invariant

$$T_{\mathrm{J}} = \frac{a_{\mathrm{J}}}{a} + (1-e)\left(\frac{a}{a_{\mathrm{J}}}\right)^{1/2} \cos i_{\mathrm{orb}} \,. \tag{1.1}$$

Here a_{J} is the semimajor axis of the orbit of Jupiter and i_{orb} is the inclination of the comet's orbit with respect to the ecliptic. According to this classification, introduced by Carusi and Valsecchi (1987) [and immediately adopted by Levison and Duncan (1987)], Jupiter family comets are defined by $T_{\mathrm{J}} > 2$ and Halley family comets by $T_{\mathrm{J}} < 2$.

In addition to the orbital classification, comets have also been classified by their dust content based on continuum emission in the visible range of the spectrum. There are dust-rich and dust-poor comets. This classification refers to the dust observed in the coma. It is a measure of the amount of dust entrained by the escaping coma gas and does not necessarily reflect the amount of dust in the nucleus. It must also be remembered that there can be no dust-free comets. Dust particles are needed as condensation nuclei for the ices before comet formation.

A'Hearn et al. (1995) attempted a further classification based on compositional differences. One of their main conclusions was that a significant number of short-period comets (mostly Jupiter family comets) are depleted in carbon-chain molecules. This depletion is usually recognized by the ratio of $C_2/CN < 2/3$. However, it must be kept in mind that this ratio may be a function of the heliocentric distance of a comet.

When a comet traverses the inner planetary system during its orbit around the Sun, solar visible radiation provides most of the energy for sublimation of ices from the comet nucleus and of the organic polycondensate components in the coma dust (giving rise to a *distributed* source of coma gases). The comet dust is entrained into the coma by the gases escaping from the nucleus. We identify three sources for the coma gas (de Almeida et al., 1996): (1) the nucleus surface, which is the main source and furnishes mostly H_2O, (2) dust distributed throughout the coma (the distributed source), giving rise to some organic species and possibly water trapped in particle aggregates, and (3) the interior of the nucleus, which provides gases that diffuse through the pores in the nucleus after being liberated by heat conducted to ices more volatile than water (e.g. CO, CO_2, CH_3OH, NH_3, etc.) or to amorphous water ice in which other volatiles (and possibly some molecular radicals) are trapped.

Until about a decade ago, the origin and evolution of observed, minor species in the coma of a comet were not understood. The space missions to Comet 1P/Halley in 1986 changed that. The identification of the CHON particles (polycondensates of organic materials associated with dust particles) led to the identification of the distributed sources of some minor species.

The identification of a third source of coma gas was based on the realization that comets have a low density and must therefore be porous, on laboratory experiments (e.g. the KOSI experiments as summarized by Sears et al., 1999), and on comet nucleus modeling. The fraction of the solar heat that is not reflected, reradiated, or used for sublimation of water ice from the surface, is conducted into the nucleus. When this heat reaches layers where ices more volatile than water ice are admixed or adsorbed in amorphous water ice, they sublimate or are desorbed during crystallization of the amorphous ice. Above the sublimation or crystallization front, the radial gradient of the partial pressure is negative, and below it it is positive. This pressure gradient causes vapours to flow outward (above the sublimation or crystallization front) and inward (below the sublimation or crystallization front). The vapours in the nucleus diffuse through pores. The inward flowing vapours reach colder regions in the deeper interior where they recondense and constrict the pores. The outward flowing vapours change the heat flow in the ice - dust matrix and escape into the coma. This leads to chemical differentiation of surface layers of the nucleus and to a change in the mixing ratios of vapours in the coma as a function of heliocentric distance. As a comet moves in its orbit around the Sun, the insolation changes inversely with the square of the heliocentric distance (except at heliocentric distances of just a few solar radii, where the Sun cannot be considered as a point source). The sublimation of water ice from the surface of the nucleus changes accordingly, but more rapidly for distances $r_{\mathrm{H}} > 2.5$ AU. For example, as a comet recedes from the Sun, the insolation and the sublimation of water ice decrease. However, although less heat is available to sublimate water ice, there is still enough heat to diffuse into the nucleus to sublimate volatile ices that have a change of enthalpy of sublimation less than that of water ice. As these gases diffuse out of the nucleus into the coma, the mixing ratio of the gases in the coma changes with heliocentric distance.

Therefore, the abundance of volatiles in the nucleus is not mirrored directly by the observed mixing ratios in the coma (Huebner and Benkhoff, 1999). However, the mixing ratio of species in the *nucleus* provides the important clues about the composition of the solar nebula. Thus, it becomes important to relate the observed mixing ratios in the coma to those in the nucleus. *This is a major goal for modeling comet nuclei.*

Besides the composition, the physical structure of comet nuclei plays an important role. There are several reasons why it is thought that comet nuclei must be porous:

- The analyses of nongravitational forces acting on Comet 1P/Halley by Sagdeev et al. (1988) and Rickman (1989) indicated that the mass of the comet nucleus must be less than the mass of that body if it consisted of compacted material. While Rickman and Sagdeev did not agree in detail on values for the density, they both agreed that the density indicates that the nucleus is porous.

- It is difficult to sustain continuous sublimation of volatile ices if only the volatile component of the surface sublimates. However, Comet Hale-Bopp (C/1995 O1) showed continuous vapourisation of CO from distances of 7 AU inward. This required a source of CO much larger than could be provided by a thin surface layer.

- The material for the KOSI experiments (Grün et al., 1993) showed high porosity, even though these materials were prepared in the environment of Earth's gravity and on a much shorter timescale than it takes for a comet nucleus to form. Carbon dioxide gas was released from under the surface and diffused through the pores into the vacuum surrounding the experiment.

- Comet nucleus models based on heat and gas diffusion through pores indicate that vapourisation can be sustained for times corresponding to the observations of Comet Hale-Bopp (C/1995 O1).

Our more detailed knowledge about comets is based on the spacecraft investigations of Comet 1P/Halley in 1986. The data from these investigations have been supplemented by observations of two unusually active recent comets: Hale-Bopp (C/1995 O1) and Hyakutake (1996 B2). The analysis assumes that there is no difference between a Halley family short-period comet, an old long-period comet, or a young long-period comet.

All of the properties of comets listed above form the basis for comet models. The ultimate goal is to develop reliable multi-dimensional and time-dependent models for comet nuclei. Various investigators consider different approaches. It is not always clear what the relative importance is of various effects that are being modeled. Thus, to gain confidence in the procedures of the different numerical codes, the first step is to compare results of simple, one-dimensional codes from five independent groups based on predetermined orbit and spin parameters, composition, and some other physical conditions. Comparisons are focused on understanding the differences in the implementation of the physics and mathematical procedures in the computer codes.

Here we do not direct our attention to more complex issues and new ideas such as complicated mixtures, multi-dimensional geometries, mechanically restricted and unrestricted outgassing (dust mantle evolution), different states of matter (amorphous vs. crystalline ice, trapped vs. frozen volatile components), long-period vs. short-period comets, the nucleus – coma boundary layer, etc. *Instead, we concentrate on modeling techniques to understand the reality of the physical processes occurring in comet nuclei.*

— 2 —

The Structure of Comet Nuclei from Observations and Experiments

"It has been stated that within the head of a comet there is usually a bright point termed the nucleus. This is the only part of its structure which excites any suspicion of a solid substance."

Robert Grant, *History of Physical Astronomy*, 1852.

2.1 Size and Composition

Only the nuclei of Comets 1P/Halley, 19P/Borrelly, and 81P/Wild 2 have been measured with some accuracy from the Giotto, Vega 1 and 2, Deep Space 1 (DS1), and Stardust spacecraft investigations. Dimensions of Comet 1P/Halley are about 15.5 km $\times$ 8.5 km $\times$ 8 km (Keller et al., 1986; Keller, 1990). Dimensions of Comet 19P/Borrelly are about 8 km $\times$ 4 km $\times$ 4 km, while those of Comet 81P/Wild 2 are about 5.5 km $\times$ 4.0 km $\times$ 3.3 km. From ground-based observations of nuclei of several other comets, the aspect ratio of Comet 1P/Halley's dimensions of about $2:1:1$ appears to be typical.

Determining the size of a comet nucleus from ground-based observations is difficult. When the comet is close to the Earth, its gas and dust coma conceal the nucleus. At large heliocentric and therefore large geocentric distances, it is difficult to spatially resolve the nucleus. Measurements that are made are a product of the cross section of the nucleus and the albedo of its surface. To separately determine these two quantities, measurements must also be made in the infrared. This has been done for several comets, including Comet 46P/Wirtanen. This nucleus diameter appears to be only about 800 m. It is one of the smaller comet nuclei. Comet Hale-Bopp (C/1995 O1) on the other hand appears to have a very large nucleus. Estimates are that its diameter is about 40 km. 2060 Chiron may be one of the biggest nuclei with a diameter of about 150 to 200 km. At the other extreme are the Kreutz group of comets. These comets appear to be fragments of a large comet that broke up during a close encounter with the Sun. Comet Ikeya-Seki (C/1965 S1) is one of the larger fragments of this group. It passed through the Sun's corona in October 1965 and survived. Many of the smaller fragments, which have almost the same orbital parameters, do

Table 2.1: Relative atomic element abundances of the gas and dust released by Comet 1P/Halley. The results of a study by Geiss (1988) renormalized to Mg with the solar Mg/Si-ratio and the abundances in the primordial Solar System and in CI-chondrites are listed (Anders and Ebihara, 1982) for comparison.

	Geiss (1988)	Grün & Jessberger (1990)	Solar System	CI
H/Mg	39.	31.	25200.	4.9
C/Mg	12.	11.3	11.3	0.71
N/Mg	0.4 - 0.8	0.7	2.3	0.06
O/Mg	22.3	15.	18.5	7.1
N/C	0.03 - 0.06	0.06	0.2	0.08
O/C	1.8	1.3	1.6	10.0

not survive their passage through the corona. We know that many of these fragments have small nuclei because they remain undetected until shortly before they enter the Sun's corona.

Data from Comet 1P/Halley has been analyzed by Geiss (1988) and by Grün and Jessberger (1990). Grün and Jessberger suggested that since the ratio of C to Mg in the dust is almost, but not quite, as high as the solar ratio, the missing carbon must be in the ice. Making this assumption, the results of the analyses are given in Table 2.1. Combining the known gas composition (Krankowsky and Eberhardt, 1990) with that of the dust, the bulk composition of 1P/Halley can be derived. This composition can be compared to the composition of the Sun and CI chondrites. Compared to solar composition, nitrogen is underabundant by a factor of about 3 and hydrogen is deficient by more than a factor of 700. However, the ratios of the other elements are very similar to the solar values, but differ significantly from CI values. This finding corroborates the contention that comets are only slightly altered relics from the solar nebula. The dust to gas mass ratio, resulting from the above argument, is 1 :1 with an uncertainty of a factor of two. This value is well within the much wider range of values derived from direct measurements in the coma.

One can approximate the abundances of *molecular* species in comets by making the following assumptions: (1) Only molecules that are condensable at about 25 to 30 K exist in comet nuclei, (2) the elemental number abundances of C, O, Mg, Si, S, and Fe are solar, (3) N is depleted by a factor of about 3, and (4) the abundance of H is determined by its ability to chemically bind with other available species. We assume that the silicate abundances are adjusted such that all Si is consumed in silicates, all iron is in Fe_2SiO_4 and all magnesium is in Mg_2SiO_4. Then the amount

Table 2.2: Molecular distribution of elements in condensable molecules assuming solar abundances (except for H) with N depleted by a factor of 3.

Elmt.	Solar number abund.	Comet number abund.	Silic.	Rem 1	H_2O	HCO Comp	Rem 2	HCNS Comp
C	305	305	0	305	0	72	233	232
N	84	28	0	28	0	0	28	28
O	608	608	122	486	401	84	0	0
Mg	24	24	24	0	0	0	0	0
Si	31	31	31	0	0	0	0	0
S	16	16	0	16	0	0	16	16
Fe	37	37	37	0	0	0	0	0
H					802	80		464

of oxygen contained in silicates can be determined from $18.5[Fe_2SiO_4] + 12.1[Mg_2SiO_4]$, which exhausts the available Si, Mg, and Fe. We further assume that the remainder of the oxygen (labeled Rem 1 in Table 2.2) is in H_2O, with 5% (relative to H_2O) in CO, 3% in CO_2 (including a small amount of CH_3OH), and 10% in H_2CO (the most likely distributed source for CO in the coma). The fractions of CO, CO_2, and H_2CO relative to H_2O are based on Comet 1P/Halley measurements. The result is a mixture of H-, C-, and O-bearing molecules that is equivalent to the hypothetical compound $H_{20}C_{18}O_{21}$ (labeled HCO Comp in Table 2.2). This results in the abundance ratio of 118% of $H_{20}C_{18}O_{21}$ with respect to H_2O (100%) and exhausts the remainder of the available oxygen (Huebner, 2002). We can assume that the remainder (labeled Rem 2 in Table 2.2) of the carbon, nitrogen, and sulphur is in CH_2-type polycondensates (i.e. an organic dust component without oxygen). The result is a mixture of H-, C-, N-, and S-bearing molecules equivalent to a molecule of the hypothetical compound $C_{58}H_{116}N_7S_4$ (labeled HCNS Comp in Table 2.2). The resulting mass fractions are summarized in Table 2.2.

The last line in Table 2.2 determines the relative number of H atoms in a comet: 1346 relative to 31 atoms of Si. The total number of H atoms relative to the number bound in water is 1.68, and the total number of O atoms relative to the number bound in water is 1.52. This means that only about 3/5 of all hydrogen and 2/3 of all oxygen in a comet are in H_2O.

Table 2.3 summarizes the results in terms of mass fractions. We have separated the HCO compounds into the refractory organic forms (simply labeled H_2CO) and the icy form (approximately 5 CO and 3 CO_2, labeled as C_8O_{11}). Further, we assume that half of the HCNS compound is icy and half is refractory organic. We note that H_2O is about 38% and silicates

Table 2.3: Mass fractions of the components discussed in Table 2.2

Molecule	Total	Ice	Dust	% Ice	% Dust
H_2O	7218	7218	0	38.3	0.0
H_2CO	1203	0	1203	0.0	6.4
C_8O_{11}	1091	1091	0	5.8	0.0
$C_{58}H_{116}N_7S_4$	3896	1948	1948	10.3	10.3
Silicates	5454	0	5454	0.0	28.9
Totals	18862	10257	8605	54.4	45.6

about 29% by mass of the comet nucleus. Greenberg (1998) obtains similar values (31% and 26%, respectively). Greenberg's values are based in part on laboratory results of organic fractions, while the fractions used here are based on analyses of measurements from Comet 1P/Halley made by spacecraft. It is also apparent from Table 2.3 that the mass ratio of dust to ice is about 1 : 1, very similar to Greenberg's result. This ratio does not depend strongly on how the organics are distributed between the ice and the dust phases. The analysis again points out that the abundances in the coma may change significantly from dust rich to dust poor, but this may be the result of outgassing and mantle development, not necessarily an innate property.

The observed chemical composition in the coma is characterized by chemical disequilibrium including high abundance ratios of isomeric pairs such as HNC/HCN and of deuterated-to-normal abundances for many simple molecules. The deuterium enrichment is reminiscent of the analogous isotopic anomaly found in certain organic fractions of carbonaceous chondrites, and has led to the suggestion that some interstellar material has survived the accretion shock in molecular form to be incorporated into primitive objects such as carbonaceous meteorites and comets. Table 2.4 lists the currently identified molecules in interstellar clouds and extended circumstellar envelopes (excluding photospheric molecules). In addition, some molecular ices present on interstellar grains, such as CO_2, have been identified by IR spectroscopy.

Studies of the HNC/HCN abundance ratios (Biver et al., 1997; Irvine et al., 1998, 1999) and HCO^+ (Lovell et al., 1999; Irvine et al., 1998) in the coma of Comet Hale-Bopp (C/1995 O1) suggest an important role for superthermal hydrogen atoms and ion-molecule reactions in the coma (Rodgers and Charnley, 1998). Thus the HNC/HCN ratio must not be construed to mean that the chemical species detected in comets are of interstellar origin, even if there are still some discrepancies in accounting for the observed ratio in Comet Hyakutake (C/1996 B2). More work is needed in this area.

The entries for gas-phase species that have been detected in protostars

Table 2.4: Comparison of identified cometary and interstellar neutral molecules

Molecule	Comets	ISM	Disc	Molecule	Comets	ISM	Disc
Diatomic				HNCS		$\surd$	
H_2		$\surd$	$\surd$	c-SiC_3		$\surd$	
CH	$\surd$	$\surd$	$\surd$	C_3S		$\surd$	$\surd$
NH	$\surd$	$\surd$		Pentatomic			
OH	$\surd$	$\surd$	$\surd$	CH_4*	$\surd$	$\surd$	
HF		?		CH_2NH		$\surd$	
C_2	$\surd$	$\surd$	$\surd$	SiH_4*		$\surd$	
CN	$\surd$	$\surd$	$\surd$	l-C_3H_2		$\surd$	$\surd$
CO	$\surd$	$\surd$	$\surd$	c-C_3H_2		$\surd$	$\surd$
N_2	$\surd$			CH_2CN		$\surd$	$\surd$
NO		$\surd$	$\surd$	NH_2CN		$\surd$	
SiH		?		CH_2CO		$\surd$	$\surd$
SH		$\surd$		HCOOH	$\surd$	$\surd$	$\surd$
HCl		$\surd$		C_4H	$\surd$	$\surd$	$\surd$
SiC*		$\surd$		HC_3N	$\surd$	$\surd$	$\surd$
SiN		$\surd$		HCCNC		$\surd$	
CP*		$\surd$	?	HNCCC		$\surd$	
CS	$\surd$	$\surd$	$\surd$	C_5*		$\surd$	
PN		$\surd$		C_4Si*		$\surd$	
SiO		$\surd$		Hexatomic			
AlF*		$\surd$		$H_2C_2H_2$*		$\surd$	
NS	$\surd$	$\surd$		CH_3OH	$\surd$	$\surd$	$\surd$
SO	$\surd$	$\surd$	$\surd$	CH_3CN	$\surd$	$\surd$	$\surd$
NaCl*		$\surd$		CH_3NC		$\surd$	
AlCl*		$\surd$		CH_2CHO	$\surd$	$\surd$	
SiS		$\surd$		NH_2CHO	$\surd$	$\surd$	
S_2	$\surd$			H_2CCCC		$\surd$	$\surd$
FeO		?		CH_3SH		$\surd$	
KCl*		$\surd$		HC_4H*		$\surd$	
Triatomic				HC_2CHO		$\surd$	$\surd$
CH_2	$\surd$	$\surd$		C_5H		$\surd$	$\surd$
NH_2	$\surd$	$\surd$		HC_4N		$\surd$	
H_2O	$\surd$	$\surd$		C_5N		$\surd$	
C_2H		$\surd$	$\surd$	C_5O		$\surd$	
HCN	$\surd$	$\surd$	$\surd$	C_5S		$\surd$	
HNC	$\surd$	$\surd$	$\surd$	Septatomic			
HCO	$\surd$	$\surd$		CH_3NH_2		$\surd$	

Molecule	Comet	ISM	Disc	Molecule	Comet	ISM	Disc
HNO		√		CH_3CCH		√	√
H_2S	√	√	√	CH_3CHO		√	√
C_3*	√	√		c-CH_2OCH_2		√	
C_2O		√	√	CH_2CHOH		√	√
CO_2	√	√		CH_2CHCN		√	√
N_2O		√		C_6H		√	√
NaCN*		√		HC_5N		√	√
MgCN*		√		Octatomics			
MgNC*		√		C_2H_6	√		
AlNC*		√		CH_3OCHO	√	√	
c-SiC_2		√		CH_3COOH		√	
SiCN*		√		CH_2OHCHO		√	
SiNC*		√		$OH(CH)_2OH$	√	√	
C_2S		√	√	CH_3C_2CN		√	√
OCS	√	√	√	H_2C_6		√	
SO_2	√	√	√	HC_6H*		√	
CS_2	√			C_7H*		√	
Tetra				Supraoctatomic			
CH_3		√		CH_3CH_2OH		√	
NH_3	√	√	√	CH_3OCH_3		√	
HC_2H	√	√		CH_3CH_2CN		√	
H_2CN		√		CH_3C_4H		√	√
H_2CO	√	√	√	C_8H		√	
l-C_3H		√	√	HC_7N		√	√
c-C_3H		√	√	CH_3COCH_3		√	
HCCN		√		NH_2CH_2COOH		?	
HNCO	√	√	√	CH_3C_4CN		?	?
H_2CS	√	√	√	HC_9N		√	√
C_4		√		$C_2H_5OCH_3$		√	
C_3N		√		C_6H_6*		√	
C_3O		√	√	$HC_{11}N$		√	√

* Only in envelopes of evolved stars ? Tentative identification
c- Cyclic molecule l- Linear molecule

(PS) and in dark interstellar clouds (DISC) in Table 2.4 are based on data originally assembled by Dickens et al (2001). Ions are not presented in this table because the differences of the interstellar radiation field and that of the Sun are too large to make such a comparison meaningful. The same argument might be used for radicals as photodissociation products. However, in this case it is difficult to decide which radical is the result of photodissociation and which is a product of chemical reactions. Species are listed according to increasing number of atoms per molecule (diatomic, triatomic, etc.) and then, within each group, according to the sum of atomic numbers of the elements in each molecule. Elements (mostly metals) derived from dust of Sun-grazing comets are not listed. More appropriate for the comparison would be abundances of molecular species condensed on interstellar grains. Work such as that by Ehrenfreund et al. (1997a, b) will be important in such analyses in the future.

2.2 Some Physical Properties

Two types of forces act on a comet nucleus: forces that tend to pull it apart, such as tidal forces and centrifugal forces, and forces that tend to hold it together, such as self-gravity, cohesion, and adhesion of dust and ice components. Here we investigate some of these properties.

Comet nucleus spin periods are poorly known and the few determinations that have been made are debatable. The most powerful methods are those based on the analyses of light-curves of inactive nuclei. In these cases the approach is the same as for asteroid spin studies. Light-curve analyses can be used also to search for precession and multi-axes spin of a comet nucleus. Anisotropy in the mass loss produces forces acting on the nucleus that result in nongravitational acceleration and possibly in change of spin. For smaller nuclei, spin-up processes are more effective than for large nuclei such as 2060 Chiron. We can expect that comet nuclei will, in general, precess.

Thermal conduction in a comet nucleus is an important aspect for its tensile strength because it induces ice sintering. The equilibrium vapour pressure over concave areas is higher than over convex areas. This is particularly true if the radii of curvature are very small. Thus, volatiles will tend to sublimate from convex particle surfaces and tend to recondense on concave areas where particles are in contact with each other. The recondensation forms sintering necks that strengthen the contacts between particles. This is particularly true for ices on the surface of a nucleus. Sintering may also occur in the dust mantle where the temperature is higher. In the dust mantle some organic compounds may sublimate and recondense to form sintering necks between dust grains making larger aggregates, which we will call dust particles. Thus, submicron grains can aggregate into micrometre- and millimetre-sized dust particles that are entrained and observed in the coma. The largest particles may acquire a mass to area $\approx 4\pi\hat{r}^3\rho/3\pi\hat{r}^2 = 4\hat{r}\rho/3$ that is too large for particles to be entrained by escaping gases. Consequently they remain on, or fall back to, the surface to form a semipermanent mantle. Particles that are entrained will be exposed to full sunlight and heat up. The heat may disintegrate these particles into their constituent grains as was observed in 1P/Comet Halley (Simpson et al., 1987; Vaisberg et al., 1987). Other mechanisms of their disintegration may be rapid spin or electric charging. Observed changes in the size distribution of dust particles are consistent with fragmentation effects (McDonnell et al., 1987).

We will now discuss thermal conduction, compressibility, and tensile strength of the nucleus based on Greenberg's aggregated interstellar dust model of comets. This model assumes a homogeneous nucleus composed of submicrometre-sized ice-coated dust particles with pores of comparable size. Layering, such as a dust mantle, fissures, and other structural changes from internal rearrangements are ignored. Thus, this model needs further development.

If we let the effective radii of the different components be $\hat{r}_\mathrm{s}$ for the silicate core, $\hat{r}_\mathrm{o}$ for the intermediate organic refractory mantle, and $\hat{r}_\mathrm{i}$ for the outer ice mantle, then we can approximate the thermal conductivity of the core mantle structure by the Maxwell-Garnet approximation as used for dielectrics (Haruyama et al., 1993). Here, $\hat{r}_\mathrm{s} < \hat{r}_\mathrm{o} < \hat{r}_\mathrm{i}$. The effective thermal conductivity of the silicate core-organic refractory mantle grains is then given by

$$\kappa_\mathrm{s,o} = \kappa_\mathrm{o}[1 + \frac{3f^3_\mathrm{s,o}(\kappa_\mathrm{s} - \kappa_\mathrm{o})}{\kappa_\mathrm{s} + 2\kappa_\mathrm{o} - f^3_\mathrm{s,o}(\kappa_\mathrm{s} - \kappa_\mathrm{o})}] \tag{2.1}$$

where $f_\mathrm{s,o} = \hat{r}_\mathrm{s}/\hat{r}_\mathrm{o} < 1$. If we use this silicate core-organic mantle grain to define the refractory "core" of radius $\hat{r}_\mathrm{o}$ for an ice mantle of radius $\hat{r}_\mathrm{i}$, the effective thermal conductivity of the three component grain is

$$\kappa_\mathrm{s,o,i} = \kappa_\mathrm{i}[1 + \frac{3f^3_\mathrm{o,i}(\kappa_\mathrm{s,o} - \kappa_\mathrm{i})}{\kappa_\mathrm{s,o} + 2\kappa_\mathrm{i} - f^3_\mathrm{o,i}(\kappa_\mathrm{s,o} - \kappa_\mathrm{i})}] \tag{2.2}$$

where $f_\mathrm{o,i} = \hat{r}_\mathrm{o}/\hat{r}_\mathrm{i}$.

As noted by Haruyama et al. (1993), the above is strictly valid only when $f_\mathrm{s,o}, f_\mathrm{o,i} << 1$. When $\kappa_\mathrm{i} << \kappa_\mathrm{s,o}$, as is true for amorphous ice mantles, Eq. (2.2) reduces to $\kappa_\mathrm{s,o,i} = \kappa_\mathrm{i}$ within a factor ~ 1, so that the thermal conductivity of a grain is dominated by its ice mantle if the ice is amorphous. Taking into account the effects of aggregation leads to a correction factor,

Table 2.5: Thermal conductivity of representative grain materials

Material	Estimated Thermal Conductivity $[\mathrm{W\,m^{-1}\,K^{-1}}]$	Reference
H_2O (amorphous)	$7.1 \times 10^{-8} T$	Kouchi et al. (1994)
H_2O (crystalline)	$567/T$ $(T > 25\,\mathrm{K})$	Klinger (1975)
Glass, Silica	1	Handbook Chem. Phys.
Fused Quartz	100	Horai and Susaki (1989)
Organic (paraffin)	≤ 0.1	Handbook Chem. Phys.

f_H (commonly referred to as the Hertz factor), which reduces the effective conductivity by the ratio of the contact area, A_c, between grains to the mean cross section of a grain. A value for $f_\mathrm{H} = A_\mathrm{c}/A_\mathrm{s}$ has been calculated to be $\sim 2-7\times 10^{-4}$ for grains of a few tens of micrometres in a high porosity ($\Psi = 0.7 - 0.8$) structure (Greenberg et al., 1995; Sirono and Yamamoto, 1997). The grain – grain contact area, A_c, changes with the amount of sintering. In Table 2.5 are shown some representative values for thermal conductivities of various materials.

Compressibility and tensile strength of the materials in the nucleus depend on the amount and type of sintering. Sintering is governed by the interactions between its microscopic components. We expect that comets will be fragile and compressible relative to compact material because of their high porosity. Mathematical modeling of the tensile strength of materials in a comet nucleus has led to two alternative values. One of these is very simply based on the average molecular energy of interaction between grains, which depends on the effective surface energy. The other is based on the cutting of contacts connected in a cubic lattice. Perhaps something between the two will be a useful compromise value. Figure 6 in Sirono and Greenberg (2000) gives a comparison between tensile strengths calculated on different bases. They differ, at porosity $\Psi = 0.8$, by a factor of at most 30. A nominal value would probably be $T = 5 \times 10^3\,\mathrm{Pa}$ to $10^4\,\mathrm{Pa}$. However, with a lower value for the water intermolecular force, it could be as low as $T \approx 5 \times 10^2\,\mathrm{Pa}$ (Greenberg et al., 1995).

The compressive strength of a grain aggregate is shown in Fig. 5 of Sirono and Greenberg (2000). It is $\mathcal{C} \approx 5 \times 10^3\,\mathrm{Pa}$ at porosity $\Psi = 0.8$. In conclusion, it can be stated that because of these values collisions between cometesimals in a protoplanetary nebula must have resulted in compaction and deformation at the contact areas, but that the colliding pieces are bound by tensile forces that exceed gravitational binding by at least two orders of magnitude (Sirono and Greenberg, 2000).

Table 2.6: Some generic physical parameters for comet nuclei based on the interstellar dust model

Quantity	Value
Bulk density ($\Psi = 0.7 - 0.8$)	$300 - 500\,\mathrm{kg\,m^{-3}}$
Tensile strength ($\Psi = 0.8$)	$5 - 10 \times 10^3\,\mathrm{Pa}$
Compressibility ($\Psi = 0.8$)	$\sim 5 \times 10^3\,\mathrm{Pa}$
Dust thermal conductivity	
Silicates	$10\,\mathrm{W\,m^{-1}\;K^{-1}}$
Silic. + organic mantle	$0.2\;\mathrm{W\,m^{-1}\;K^{-1}}$
Silic. + organic + amorph. ice mantle	$1.5 \times 10^{-7} T\;\;\mathrm{W\,m^{-1}\;K^{-1}}$
Silic. + organic + cryst. ice mantle	
(< 100 K)	$1.9 \times 10^2/T\;\;\mathrm{W\,m^{-1}\;K^{-1}}$
Aggregate reduction factor ($\Psi = 0.8$)	
(Hertz factor)	5×10^{-4}
Bulk thermal conductivity ($\Psi = 0.8$)	
Amorphous ice mantle	$0.75 \times 10^{-10} T\;\;\mathrm{W\,m^{-1}\;K^{-1}}$
Crystalline ice mantle	$0.4 - 1.5 \times 10^{-3}/T\;\;\mathrm{W\,m^{-1}\,K^{-1}}$
Pore radius	$1\,\mu\mathrm{m}$
Chemical composition (by mass)	
Sil : org : carb : ices	0.26 : 0.23 : 0.086 : 0.426
Bond albedo	0.04

In Table 2.6, we summarize the physical parameters for materials in comet nuclei as derived from the aggregated interstellar dust model. The unit (fully accreted) interstellar grains in the comet nucleus when considered as spheres, can be described as silicate and organic refractory cores, with icy material (including the small carbonaceous and PAH particles) as mantles. The radii are respectively $\hat{r}_\mathrm{s} = 0.07\,\mu\mathrm{m}$, $\hat{r}_\mathrm{o} = 0.101\,\mu\mathrm{m}$, $\hat{r}_\mathrm{i} = 0.139\,\mu\mathrm{m}$. The volume proportions used to provide these radii have been obtained from the chemical proportions (by mass) given by:

$$\begin{aligned}&\mathrm{Sil : Carb : Org.\ Refr. : H_2O : CO : CO_2 : CH_3OH : H_2CO : Other}\\ &\quad = 0.26 : 0.086 : 0.23 : 0.31 : 0.024 : 0.030 : \; 0.017 : 0.005 : 0.04.\end{aligned}$$

When different theories give different results, we choose nominal values rather than presenting a range. A similar set can be readily derived for a range of porosities.

While the bond albedo is a consensus of observations, it is not much lower than what was predicted from the interstellar dust model based on the very porous character of the surface (Greenberg, 1998). We note that the value of the pore radius is taken as $1\,\mu$m because it can be shown that the pore size must be of the same order as particle size for a mean density of $500\,\mathrm{kg\,m^{-3}}$.

2.3 Comet – Asteroid Transitions

The distinction between asteroids and comets is becoming less clear and the existence of a strict relation between these bodies, first suggested by Öpik (1963), is now widely accepted. A comet nucleus is a body that formed in the outer Solar System. It can be *active, dormant*, or *extinct*, while an asteroid is a body formed in a region between Mars and Jupiter (McFadden et al., 1993). These definitions point out the relationship between the two classes of objects and the volatile content that was originally present in the different zones of the protosolar disk.

It is believed that in the primordial phases of Solar System formation the volatile content increased from the inner to the outer parts of the Solar System and the bodies that formed in these regions reflect the local composition of the nebula. In this respect, the above distinction between comet nuclei and asteroids can be accepted mainly on a statistical basis, because it cannot be excluded that bodies with intermediate volatile content were present in the original population. This simplified scenario describes only the primordial phase in the history of minor bodies because the formation of giant planets perturbed the original spatial distribution. Therefore, if only the physical aspects of these bodies are considered, it is difficult to establish where the boundary between comet nuclei and asteroids lies.

From the dynamical point of view it is also difficult to use an unequivocal criterion to distinguish between comet nuclei and asteroids: Long-term dynamical evolution of Jupiter family comets, Mars crossing asteroids, and near-Earth objects (NEOs) have shown that, in terms of orbital stability, transitions between "a comet-like" orbit – in the sense that Jupiter perturbations affect this motion – and "an asteroid-like" orbit – in the sense that the Jupiter perturbations do not dramatically affect the evolution – can be possible.

The dynamical evolution strongly influences a comet's thermal history and differentiation. Extinct or dormant comet nuclei can be classified easily as asteroids, if only their appearance is considered, and an inconsistent classification can result if only the dynamical aspects are taken into account.

Generally speaking, a comet is considered active when it is loosing volatiles in a detectable coma, and inactive when the coma is not detectable. The inactivity can be caused by low insolation at large heliocentric distance, so that the sublimation of ices is thermodynamically not possible. A comet nucleus can become dormant or extinct, when the coma is not detectable in any part of the orbit. In this case, a comet can be lost, since it is not observable. An example is Comet 107P/Wilson-Harrington that was lost in 1942. Comets can become dormant or extinct because all ices in the nucleus have been consumed. In that case a comet becomes less active, or the activity stops because a stable dust mantle forms that inhibits any detectable activity, making the comet unobservable. Giotto measurements (Keller et al., 1986) indicate that active areas are limited to a small fraction of the surface of short-period comets.

Many comets show an extremely low activity; this is usually interpreted as a sign of volatile depletion in the outer layers of the nucleus, and is thus expected that over time, activity would decline to the point of being negligible. Comet nuclei become in this way dormant or extinct, and they may assume an asteroidal appearance that makes them indistinguishable from true asteroids. It is not necessary that the body has no emission at all: there may be bodies with a level of cometary activity below the threshold of detectability (Luu and Jewitt, 1992). This hypothesis is especially important in the study of the origin of NEOs: it seems that from dynamical evidence and statistical considerations, a fraction of NEOs may be of cometary origin (Wetherill, 1988; Binzel et al., 1992; Harris and Bailey, 1998).

From an observational point of view, the distinction between asteroids and comets is not as clear as it was in the past. While there are only two objects (2060 Chiron and 4015 Wilson-Harrington) with IAU double designations, there is a list of objects classified as asteroids that are suspected to be extinct or dormant comets on the basis of dynamical and observational considerations, among them 2201 Oljato (McFadden et al., 1993). Oljato had been singled out as an unusual asteroid because of its orbital elements and the possible relation with the Orionid meteor shower. The UV photometric data, modeled as fluorescent emissions of neutral species, seem to indicate a plausible gas production of OH and CN. The previous characteristics, together with the anomalous excess of UV in the reflectance spectra, have been regarded as an indication that Oljato can be an extinct comet (McFadden et al., 1993).

On the other hand, there are bodies for which a cometary origin appears very unlikely, yet they exhibit fluorescent emission, such as 1862 Apollo, 1566 Icarus, and 1 Ceres (Bockelée-Morvan and Crovisier, 1992). There are many examples of small bodies first designated as comets, which later have been classified as asteroids. Recent cases are 119P/Parker-Hartley that was named 1986 TF, 137P/Shoemaker-Levy 2 known as 1990 UL3, and 107P/Wilson-Harrington that had been lost and was then found again as an asteroid named 4015 1979 VA, before being definitively named 4015 Wilson-Harrington.

2.4 Laboratory Simulations

The physical and chemical properties of comet nucleus materials are basically unknown and their structure may range from nearly compact ice-dust mixtures to very fluffy dust-dominated loose agglomerates. The density ranges from about 0.2 kg m^{-3} to 2 kg m^{-3}. Until cometary matter can be studied in situ, or until comet nucleus samples are brought back to Earth for analysis, theoretical models and laboratory studies remain the only tools for estimating its nature.

From space-based and ground-based observatories a few constraints on the nature of the primordial material are available. The structure of the ice in the nucleus, which may have coexisting amorphous and crystalline phases and which may include trapped gases, strongly influences a comet's outgassing properties. To better understand these processes, studies on the thermal processing of ices and their implications for the structural changes and subsequent release of volatile ices are essential. For some time laboratory experiments relevant to comets were performed by Kajmakov und Sharkov (1972) and Ibadinov et al. (1991). They irradiated and electrically heated small probes of water ice and ice-dust mixtures. Experiments with ice-dust samples in vacuum were performed by Saunders et al. (1986).

In the post-Halley era from 1987 until 1993, comet simulation experiments were carried out under conditions simulating space (very low pressure and low temperature) known as the KOSI-project (Grün et al., 1991a). Recent laboratory results on volatile compounds allow us to investigate the link with small bodies in the Solar System. Until a space probe lands on a comet nucleus and studies its composition directly, laboratory measurements of ice and refractory analogues will – together with the analysis of meteorites and interplanetary dust particles (IDPs) – significantly improve our knowledge on the origin and structure of comets.

2.4.1 KOSI Experiments

Eleven comet simulation experiments (KOSI) were carried out in a big (walk-in) vacuum chamber at the German Research Institute DLR (Deutsches Zentrum für Luft- und Raumfahrt) in Cologne by an international team of scientists (Grün et al., 1991a). The experiments were designed to study sublimation and heat transfer processes in porous ice and dust mixtures to better understand comet nuclei. An overview of the experimental equipment was given by Seidensticker and Kochan (1992).

The thermal histories of the samples showed that the contribution of energy transport to the power balance by water vapour was very important. It was found that the sublimation of volatile ices causes a chemical differentiation of the samples. The sublimated gas escapes from the surface of the sample and also diffuses into the interior where it recondenses. Smoluchowski (1982) was the first to recognize the importance of heat transport via to the vapour phase in a porous comet nucleus. This idea was verified during the KOSI experiments (Spohn and Benkhoff, 1990; Benkhoff and Spohn, 1991a,b). Benkhoff and Spohn (1991a,b) showed that in a porous matrix heat transport into the interior by the vapour phase is more effective than heat conduction by the matrix. The dominant heat mechanism is transfer of latent heat. This strongly influences the gaseous diffusion of the volatile ices and the temperature profile within the body. Convex shapes of the temperature profiles below energy sinks (sublimation fronts) were observed as a result of the heat-carrying, inward-flowing vapour and subsequent freeing of latent heat after condensation of the gas at cooler, deeper layers.

The main differences between the various simulation experiments were the duration of the insolation period, the intensity of the insolation, the time profile of the insolation, and the composition of the samples. In ten of the experiments, porous water-ice and dust samples together with one or two volatile ices (CO_2, CH_3OH) were used. The experiments were aimed at investigating the influence of the sample material on the sublimation, the formation of a dust layer (mantle) attenuating the gas flux, the dust mantle erosion through entrainment by the escaping gas, and the thermal history of the sample. Most of the comet nucleus material was a porous mixture of water ice and dust; therefore the physics of sublimation of water ice from the porous samples was an important process.

In order to investigate the contribution of the gas diffusion to the coma as well as to the heat transport into the interior in more detail, a simulation experiment with a pure, porous water ice sample (KOSI-8) was performed (Benkhoff et al., 1995). The thermal behaviour, the sublimation, and the thermal infrared emission of this sample were investigated in response to irradiation by an artificial Sun.

The theoretical model, which described the thermal evolution of the laboratory samples, became the basis of the thermal comet nucleus model of Benkhoff and Huebner (1995). An energy analysis for an ice and dust sample given by Grün et al. (1991b) shows that the main contributions to the power balance are radiative input, reflected light, thermal reradiation, energy consumed for gas sublimation and diffusion, increase of the internal energy of the sample, and energy flow through the walls of the sample container.

2.4.2 Cometary Materials: the Effects of Bombardment with Energetic Charged Particles

Many surfaces in the Solar System, including comet nuclei and asteroids, are continuously bombarded by energetic particles. Investigations of this bombardment are important because these processes may modify the composition and other properties of the surface. Almost all of the studies of these effects have been based on laboratory experiments. Ices of water and some organic compounds dominate the surfaces of planets and small bodies in the outer Solar System, where comet nuclei might have been formed. These materials are exposed to a flux of energetic ions during their evolution from presolar grains to planetesimals and further to the entire object (see, e.g. Strazzulla and Johnson, 1991). Energetic ions penetrating solids deposit energy in the target by elastic collisions with target nuclei and by inelastic (electronic) interactions causing ionization and excitation. Many ion irradiation experiments have been performed during the last 25 years on relevant ices and their mixtures. Physico-chemical effects such as structural modification, textural changes, formation of new molecular species, and erosion of material from the target were investigated. A number of review papers have been published describing in great detail the experimental procedures, the results of the investigations, and their astrophysical relevance (e.g. Johnson, 1998; Strazzulla 1997, 1998; Moore et al., 2001; Strazzulla et al., 2001; Johnson et al., 2003).

In the case of ices, chemical modifications induce a formation of species both more volatile and less volatile than the original ices. If ices contain or are composed of simple organics, a refractory residue is formed that is stable after warming. Such a residue has a complex structure and after long-term exposure to irradiation evolves to hydrogenated amorphous carbon with a neutral colour. Strazzulla and Johnson (1991) suggested that in the Oort cloud the external 0.1 to 0.5 m thick layer of comet nuclei were exposed for a long time to the flux of galactic cosmic rays equivalent to an irradiation dose of 600 eV/molecule. Such a dose is sufficient to produce a substantial "crust" of nonvolatile material. Other experiments demonstrated that the organic crust has already been formed during bombardment at low temperature (Strazzulla et al., 1991). This gives credence to the hypothesis that the crust might already have formed in the Oort cloud and its development does not require a first passage (heating) through the inner Solar System (Strazzulla et al., 1991).

The disproportionation of CO into CO_2 on condensation in the presence of cosmic or UV radiation may be a key in the chemistry of comet formation. Although laboratory experiments confirm that this process occurs (Sandford et al., 1988), its efficiency is not well established. Laboratory experiments by Pirronello et al. (1982) show that an icy mixture of CO_2 and H_2O irradiated by energetic ions, simulating cosmic rays, leads to formation of H_2CO. Exposure of H_2CO to UV radiation or to energetic ions even at very low temperatures of about 10 K (Gol'dyanskii, 1977) leads to polymerization. The existence of polymerized H_2CO (polyoxymethylene or POM) in interstellar dust had been suggested by Wickramasinghe (1974, 1975) and in comets by Vanýsek and Wickramasinghe (1975) and Mendis and Wickramasinghe (1975). POM had been identified in Comet 1P/Halley through the work by Huebner (1987), Huebner and Boice (1989), and Meier et al. (1993). POM begins to disintegrate at temperatures of about 400 K and totally disintegrates at 440 K; particles that reach that temperature in the coma of a comet (even higher particle temperatures were measured in 1P/Halley) appear to disintegrate at about that temperature, indicating that POM, or related substances, may be the agents that cement grains into particle aggregates. Since it is thought that CHON particles formed before comet nuclei formed, particle aggregation must have started in the early stages of collapse of the protosolar nebula.

Some experiments demonstrate that proton implantation of highly carbonized materials such as graphite may cause hydrogenization of the surface layer (e.g. Wright et al., 1976) and synthesis of polycyclic aromatic hydrocarbons (PAHs) (Starukhina et al., 1995). Moroz et al. (2003a, b) reported on results from ion irradiation experiments performed on complex natural hydrocarbons. The experiments were accompanied by spectral reflectance measurements before and after each irradiation step on well characterized natural solid oil bitumens (asphaltite and kerite, see Nikolaeva et al., 1991; Moroz et al., 1998) as the target samples.

Note that chemical alteration by ion irradiation of frozen material can be a relevant process for icy objects such as comets. However, the experimental results must be applied with caution to the different astrophysical environment. In fact, in laboratory simulations some parameters can be reproduced quite well, but others cannot be simulated. For example, it is impossible to reproduce the total energy spectra or to know the total ion fluorescence in a particular astrophysical environment.

2.4.3 Experiments on Gas Trapping

Experiments on the ability of amorphous water ice to trap gases have been carried out since the work of Ghormley (1968). Ghormley observed that oxygen trapped in amorphous ice was not released continuously, but at fixed temperatures of 90, 160, and 214 K. Similar behaviour was reported for other gases trapped in amorphous ice, such as argon, nitrogen, and methane. Bar-Nun et al. (1985) established a "Comet Simulation Laboratory" in which water vapour mixed with different gases is passed over a plate at 18-140 K in a vacuum chamber with the aim of freezing the water and trapping the gases in amorphous ice. Bar-Nun et al. (1985) reported the trapping of CO, CH_4, N_2, and Ar and the release of each gas from the ice at different temperatures. Between 30-60 K the gas frozen at the amorphous water ice surface sublimated; between 135-155 K the trapped gas was released during the transformation of amorphous ice to cubic ice; gas was also released between 160-175 K, during the transformation of cubic ice into hexagonal ice; and between 165-190 K, when gas and water are released simultaneously.

In another experiment, the trapping and release of argon by water ice was used to understand the structure of the water ice (Bar-Nun et al., 1986). The argon was trapped at about 20 K and was found to be released at different temperatures (23, 35, 44, 80, 136, 160, and 180 K). Hudson and Donn (1991) reported that Ar and CO release from amorphous water ice occurred in five temperature regions.

The amorphous ice is able to trap gases probably because of the open structure of this phase of ice. The trapping mechanism depends on different parameters such as the size of the molecules of the trapped gas, the polarizability of the gas, and mechanical blocking of the channels by overlaying ice accumulated during the deposition. The main parameter, however, seems to be the sublimation temperature of the gas to be trapped. This can explain why different gases have different efficiencies in the ability to be trapped in amorphous water ice. Some gases, such as methanol, hexane, and hydrogen cyanide, are trapped in ice even at 140 K (Notesco and Bar-Nun, 1996). Gas trapping above 130 K suggests that also crystalline ice has the ability to trap gas. This may be due to the presence of channels and cracks into which gas can penetrate, or to the presence of a small fraction of amorphous ice within the crystalline ice. The main results of laboratory experiments on gas trapping show that gases are not only frozen among water ice and evaporate when the sublimation temperature is reached, but they can also be trapped in amorphous water ice, and some gases with high sublimation temperatures may be trapped also in crystalline ice (Bar-Nun and Owen, 1998).

It has been suggested that comet activity at large heliocentric distances may be explained by release of trapped gases when a heat wave reaches the amorphous ice layers.

2.4.4 Measurements of Thermal Conductivity

Modeling of comet-analogue material associated with the KOSI heat and gas diffusion experiments resulted in the realization that the transfer of heat into the interior of a comet nucleus or a laboratory sample is dominated by diffusion of the vapour phases of volatile ices such as H_2O, CH_3OH, and CO_2 through the pores. The thermal conductivity of the matrix is generally assumed to be small, homogeneously distributed and constant in time, based on the assumption that the ice matrix is only loosely bound by the very small gravity of comet nuclei. It is apparent that the texture of such a loosely bound ice matrix is not in thermal equilibrium and will evolve on timescales that are relevant for thermal evolution models. These texture modifications will increase the thermal conductivity and the compressive strength of the matrix and may influence the overall behaviour of comets.

The main differences between KOSI samples and a comet nucleus are the physical dimensions and the value of gravity. In the KOSI experiments very steep temperature gradients were imposed on the entire sample, whereas in a comet nucleus steep gradients exist only very close to the surface. As a result of the transport of vapour and associated latent heat into the interior the ice component is enriched and the temperature increased by the freezing of the ice. This results in the observed convex shape of the temperature profiles in the KOSI experiments. In a comet nucleus, these convex shaped temperature profiles can be expected only near the sublimation front of minor volatile ices. Because of the grid spacing in the calculations and the time step needed for a spinning nucleus, these effects are not recognized at the water ice sublimation front close to the surface. It appears that the resublimation of water vapour is a very local process that happens only in a very thin layer. On the other hand, the enrichment of material in deeper layers – one major result of the KOSI experiments – can be recognized in the modeling results of comet nuclei and it may be an important factor in the observed gas flux of minor volatiles in comets. It also has some importance for the sublimation of water in the interior and the formation of a crust below the dust mantle. Some of the KOSI results can be confirmed in a comet nucleus only by measuring the temperature gradient below the surface. The first such measurements will be made by the MUPUS instrument suite that is part of the Lander of the European Rosetta mission.

The KOSI comet simulation experiments (Grün et al., 1993) have provided experimental evidence for significant texture modifications. These experiments were aimed at a study of the behaviour of porous ice-mineral-mixtures under space conditions and under insolation. Thin sections of the sample material were studied by Stöffler et al. (1991). They showed that recrystallization occurred in the entire sample, but much more so in the upper layer that became the crust, just below the dust mantle. The recrystallization resulted mainly in particle growth and in the growth of bonds between single ice aggregates. It is also possible that sintering caused the texture modifications. However, while sintering is a process that seems to dominate at or near thermal equilibrium (Colbeck, 1983), recrystallization, including crystallization from the vapour flowing through the pores, seems to be more important under large temperature and vapour pressure gradients. Samples that were stored isothermally for some tens of hours at temperatures around 250 K have also undergone significant texture modifications that resulted in increased compressive strength, and thermal conductivity (Spohn et al., 1989). Similar processes may occur in comet nuclei.

Cometary particles most likely aggregated through condensation of water and other volatiles in cold (30-90 K) and highly diluted regions in the protosolar nebula (Taylor, 1992). The grains may have been loosely packed after accretion, but bonds between individual grains most likely grew even at these low temperatures during the passage of time. Similar effects, although at significantly higher temperatures, are well known from snow. In near surface layers of comet nuclei that come sufficiently close to the Sun, recrystallization and bond growth may proceed at much higher rates as the temperature increases. The relevance of the results of the KOSI experiments to comets must also consider that always fresh samples were investigated. Therefore, significant changes in the physical parameters of these samples were occuring during the experiments and the behaviour of these samples does not represent the behaviour of an almost evolved sample or even a comet nucleus. Thus, in contrast to most comet nucleus models, we believe that the thermal conductivity of at least the uppermost layers that were heated repeatedly in numerous perihelia is much higher than expected. The heat will penetrate the interior much more quickly and volatiles such as CO_2 and CO, which are observed in the coma, will be released in deeper regions of the nucleus.

It is also important to note that conventional models with heat transfer by vapour diffusion will fail when the matrix of the studied material is dominated by the mineral phase (simulating a dust mantle), where the water content is small (5-30%). The dark surface of 1P/Halley and the activity from only a small fraction of its surface imply such mineral-dominated mixtures. Nevertheless, the bonds between mineral grains may still be formed by water ice, and will therefore still dominate the thermal behaviour, which is fully compatible with our model. Similar effects are well known from the surface of Mars, where optically identical regolith reveals thermal inertia that is almost two orders of magnitude different, and shows seasonal variations. This effect is believed to be a consequence of seasonally growing and disappearing interstitial ice crystals, connecting the dust particles in the regolith.

Measurements of the thermal conductivity in the uppermost layers of the Rosetta target comet could supply valuable confirmation of or challenges to our theory and might help (or not help) to confirm whether comets really offer access to "pristine matter." Seiferlin et al. (1996) reported measurements of the thermal conductivity of porous loose minerals, porous H_2O ice, and porous CO_2 ice samples at low temperatures (77 K $< T <$ 300 K) and pressures (10^{-5} Pa $< P < 10^{-4}$ Pa). These samples were selected to be representative of possible comet nucleus compositions and the ambient conditions were chosen to investigate the samples under space conditions. The method used to measure the thermal conductivity is based on the line heat-source technique: a thin internally heated cylindrical sensor is inserted into the sample material. The thermal conductivity is derived from the observed temperature rise in the sensor and the heating power applied. This method should be accurate, fast, and well suited for an application in the laboratory as well as in situ.

Seiferlin et al. (1995b) studied the thermal conductivity of the loose dunite sample as a function of gas pressure. They show that at low pressures it is almost constant and close to 0.03 $\mathrm{Wm^{-1}\ K^{-1}}$. At atmospheric pressure, the thermal conductivity is about one order of magnitude higher. A pressure dependency of the thermal conductivity is evident. Moreover, Seiferlin et al. (1996) investigated three porous water ice samples with different pore sizes. The results are in agreement with theoretical predictions (Steiner and Kömle, 1991a) revealing a strong increase in the thermal conductivity at temperatures close to the sublimation temperature of water ice. The increase seems to be caused by heat transport by vapour in pores, which is more effective in samples with large pore radii. The measured matrix conductivity is close to 0.02 $\mathrm{Wm^{-1}K^{-1}}$, while maximum values for the effective (matrix + vapour) thermal conductivity at high temperatures exceed 0.25 $\mathrm{Wm^{-1}K^{-1}}$. Similar results are obtained for a porous CO_2 ice sample.

2.4.5 Other Laboratory Measurements

A question that has not yet been answered by the comet simulation (KOSI) experiments performed so far is that of the influence of organic matter on the physical properties of the sublimation residues. Therefore, a number of experiments performed in a small vacuum chamber cooled by liquid nitrogen were carried out by Kömle et al. (1996), which were dedicated to studying the influence of organic materials on the thermal properties of a comet analogue sample. They used aliphatic hydrocarbons of low volatility (paraffin) as model substances for organic compounds. They observed the formation of a several centimetres thick cohesive residuum in response to heating of the sample. In particular, in one of the experiments the evolution from an originally homogeneous multi-component sample (containing water ice, organic material, and minerals) to a residuum containing only minerals and organics was investigated. They reported that during this evolution the thermal properties changed dramatically. The heat conductivity of the cohesive residuum was found to be at least an order of magnitude larger than the typical value for a loose dust mantle containing no organic material. These results have been interpreted in terms of a comet's thermal evolution: a comet with the same thermal history containing a considerable amount of organics might be quite different from that of a comet consisting only of ices and minerals.

— 3 —

Physical Processes in Comet Nuclei

"...It seems to be pretty well established that the more tumultuous changes usually take place during the period when the comet is approaching the Sun. Those which occur after the passage of the perihelion appear to be of a more quiescent nature, indicating the gradual relapse of the body into the condition in which it was after returning from aphelion. This circumstance clearly points to the Sun as the exciting cause of these wonderful changes in the constitution of comets, whatever be the nature of the forces which are called into operation by his agency."

Robert Grant, *History of Physical Astronomy*, 1852.

The physical processes taking place in a comet nucleus are driven by solar energy reaching its surface. Another energy source within the comet nucleus may have been radiogenic heating, mainly by ^{26}Al (see, e.g. Prialnik and Podolak, 1995; De Sanctis et al., 2001) but, as will be discussed in Chapter 5, it affects mainly the long-term evolution taking place before the comet nucleus enters the inner Solar System. Finally, crystallization of amorphous ice within the nucleus is a sporadic source of energy release.

Since the comet nucleus is a porous aggregate of ices and dust, sublimation of ices can take place deep in the nucleus. As ice sublimates, some gas will reach the surface and contribute to the overall cometary gas production. Because of this complex phenomenology, in which ices of different volatility are able to sublimate at the same time at different temperatures in different parts of the nucleus, inference of the nucleus chemical composition from the abundances observed in the coma has spurred the development and use of numerical models, solving the nonlinear partial differential equations that describe the physical processes in the nucleus. Several models have been developed, both for the interpretation of observations, and for studies connected with space missions. Although they are characterized by different assumptions, it is generally agreed that the most important processes determining the observed cometary phenomenology are limited to the following (see, e.g. Rickman, 1994):

- Radiative heat input and heat retention by the nucleus.
- Heat and gas diffusion in the nucleus.

- Sublimation and condensation of volatile ices in the nucleus.
- Dust mantle formation and dust entrainment by escaping gases.
- Crystallization of amorphous H_2O ice (if present).
- Fracture of the nucleus caused by internal gas pressure and flexing of the nucleus.

3.1 Sublimation of Ices

Sublimation of ices causes erosion of comet nuclei, the production of comet comae, entrainment of dust (sometimes in jet-like features), and chemical differentiation of the nucleus. Incident solar and retained energy influences the flux of H_2O and minor volatiles from the surface. The flux of an ice component from the interior depends strongly on the amount of energy transported to the sublimation front of the corresponding ice. The gas fluxes from sublimation fronts in the interior of the nucleus vary only slightly as long as the mean surface temperature is higher than the sublimation temperature of water ice, which is almost always the case for a Jupiter family comet.[1] The process is complicated by the presence of one or more mineral phases and other organic refractory components, by uncertainties about the structure of the ices, and by the heat and gas diffusion properties of the surface layers of the sublimating body. Furthermore, the unknown microstructure of the ices influences material parameters, such as thermal conductivity and porosity. How variations of the material parameters influence sublimation processes of the ices in the nucleus is still not fully understood.

The mass release rate of water from a surface is (Huebner, 1965; Delsemme and Miller, 1971)

$$Q_{\mathrm{H_2O}} = \mathcal{P}_{\mathrm{H_2O}}(T)\sqrt{\frac{\mu_{\mathrm{H_2O}}}{2\pi\mathcal{R}_{\mathrm{g}}T}} \tag{3.1}$$

The change in enthalpy of sublimation, $\Delta H_{\mathrm{H_2O}}$, must be obtained consistently from the saturation vapour pressure, $\mathcal{P}_{\mathrm{H_2O}}$, through the use of the Clausius-Clapeyron equation

$$\frac{1}{\mathcal{P}_{\mathrm{H_2O}}(T)}\frac{\partial\mathcal{P}_{\mathrm{H_2O}}(T)}{\partial T} = \frac{\Delta H_{\mathrm{H_2O}}(T)\mu_{\mathrm{H_2O}}}{T^2\mathcal{R}_{\mathrm{g}}} \tag{3.2}$$

An empirical form for the *equilibrium* water vapour pressure over crystalline ice is (Gibbins, 1990)

$$\log[\mathcal{P}_{\mathrm{H_2O}}(T)] = 4.07023 - 2484.986/T + 3.56654\log(T) - 0.00320981T \tag{3.3}$$

[1] A class of short-period comets with orbits close to the ecliptic and approaching the orbit of Jupiter at their aphelion.

The erosion rate of the surface, dR/dt, is given by

$$(\rho - \tilde{\rho}_{H_2O})\frac{dR}{dt} = Q_{H_2O} \tag{3.4}$$

Near the surface the ice is almost depleted of all components more volatile than water, thus we use $\tilde{\rho}_{H_2O}$.[2]

3.2 The Phase Transition of Amorphous Ice

Depending on temperature and pressure, water ice can be in different phases. On Earth it occurs only in the crystalline phase, but in the astrophysical domain it may occur in a metastable state called the amorphous phase. At low temperature (below about 120 K) water ice can occur in the amorphous phase if the rate of condensation is sufficiently fast that the H_2O molecules do not have time to reorient themselves into crystals. Kouchi et al. (1994) point out that for this reason ice that formed in dense interstellar clouds may be in the amorphous form, while ice that formed in circumstellar envelopes of late type stars or in the solar nebula may be in the crystalline form. Amorphous water ice can persist for timescales comparable to the age of the Solar System because an activation energy barrier prevents its transition into crystalline ice. Crystallization of amorphous water ice is an exothermic and irreversible process. When warmed to about 150 K, amorphous ice transforms into a cubic crystalline form and then under confinement pressure and at temperatures of 195-223 K, into the stable hexagonal crystalline form. The heat released during the transformation, found by Ghormley (1968), is 9×10^4 J/kg. The rate of phase transition as a function of temperature is determined from an activation law found experimentally by Schmitt et al. (1989)

$$\lambda = 1.05 \times 10^{13} \mathrm{e}^{-5370/T} \ \mathrm{s}^{-1} \tag{3.5}$$

From differential thermal analysis measurements performed by Jenniskens et al. (1998), it seems that the behaviour of impure ices is different. For sufficiently high impurity content the phase transition to crystalline ice can be endothermic. The reversal of energy balance may be caused by the energy

[2] ρ_n (the partial density of species n in the ice phase) is the mass of that species per unit volume of cometary material at a particular place and time; it depends, for example, on the local porosity and changes with sublimation and condensation; i.e. $\rho_n = \rho_n(r,t)$. For example, if X_n is the mass fraction of species n, then $\rho_n = X_n \rho$, where ρ is the total local density. ϱ_n (the solid density of species n), on the other hand, is a material property. It is the specific density of that material in solid form, regardless of its circumstances (e.g. 917 kg/m^3 for ice).

required to expel the guest molecules from the water lattice. Amorphous water ice has physical properties that are different from those of crystalline ice. It also has the ability to trap molecules of low sublimation temperature that are later expelled during the crystallization process. What we know about the physical properties of amorphous ice and its behaviour upon warming comes from laboratory experiments by Bar-Nun et al. (1985, 1987), Hudson and Donn (1991), Jenniskens and Blake (1994), Bar-Nun and Owen (1998), and Jenniskens et al. (1998). In these experiments, water vapour and gases such as CO, CO_2, and Ar are codeposited at low temperatures, and amorphous water ice is obtained trapping the other gases inside. Once the gas is trapped, in decreasing amounts with increasing deposition temperature, its release depends only on changes in the ice structure related to temperature changes. A major release occurs when ice transforms into cubic ice (at about 145 K). Some gas is held so tightly that it is released only when the ice sublimates.

The thermal conductivity of amorphous ice is much lower than that of crystalline ice. Klinger (1980) derived a theoretical expression from the classical phonon theory

$$\kappa = \frac{1}{4} v_s \ell_{ph} c_{\mathrm{H_2O}} \rho_{\mathrm{H_2O}} \tag{3.6}$$

where $v_s = 2.5 \times 10^3$ m/s is the speed of sound in ice, $\ell_{\mathrm{ph}} = 5 \times 10^{-10}$ m is the phonon mean free path, $c_{\mathrm{H_2O}}$ is the specific heat, and $\rho_{\mathrm{H_2O}}$ the density of H_2O. Kouchi et al. (1992) measured in their laboratory experiments a much lower conductivity of $\kappa = 0.6 \times 10^{-5}$ to 4.1×10^{-5} W m^{-1} K^{-1} in the range $T = 125$ K to 135 K. Haruyama et al. (1993) in their work of radiogenic heating of comet nuclei in the Oort cloud, adopted the values from Kouchi et al. (1992), assuming that the heat conductivity is proportional to temperature $\kappa = 7.1 \times 10^{-5} T$ W m^{-1} K^{-1}. Tancredi et al. (1994) in their nucleus models used a geometric mean between the values of Klinger and Kouchi. In another experiment, Kouchi and coworkers confirmed their earlier values and found that the phase transition from amorphous to crystalline ice is endothermic if the water ice has other gases trapped. Andersson and Suga (1994) found an experimental value for the conductivity of nonporous, low density, amorphous water ice that is similar to the value derived by Klinger $\kappa \approx 0.6$ W m^{-1} K^{-1} in the temperature range $T = 70$ K to 135 K. See also Appendix B.

3.3 Gas Diffusion in Pores

The porous structure of a comet nucleus permits two processes: sublimation of ice from the pore walls or condensation onto them and gas (vapour) diffusion through the pores. Both processes affect not only the structure and composition of cometary material, but also its thermal evolution. Sublimation of ice and condensation of vapour constitute a heat sink and a heat source, respectively, while gas diffusion contributes to the transport of heat through the medium and the composition of the coma. The property of the porous structure that influences sublimation is the *surface-to-volume ratio*, or the related *specific surface*, and the property that influences gas diffusion, or gas flow, is the *permeability.* The evaluation of each requires some model of the porous configuration.

3.3.1 Comments on Porosity

The *porosity* of a material is defined as

$$\Psi = V_{\mathrm{p}}/V \tag{3.7}$$

where V_{p} is the pore volume within a volume V of material. We illustrate determination of porosity from a given material structure with a few simple examples. In the following discussion, we will always assume the same total volume for a cube of porous material. The side of the cube is $2r_{\mathrm{p}}n$, where r_{p} is a constant radial pore dimension (either spherical or cylindrical), and n is the number of just-touching pores along a straight line on one edge of the cube. The volume of the cube is therefore always $V = 8r_{\mathrm{p}}^3n^3$, or $V = 8r_{\mathrm{p}}^3N$, where $N = n^3$ is the total number of spheres.

- Case 1: *Cubic packing of spheres.* Consider n spheres of radius r_{p} arranged in a line so that they just touch. The next line of spheres is parallel to the first line at a distance $2r_{\mathrm{p}}$ centre to centre of just touching spheres. There are n^2 spheres in a plane. In the next layer of spheres their centres are exactly above the centres of the spheres in the lower layer. Thus, the volume occupied by the spheres is $V_{\mathrm{s}} = (4\pi/3)r_{\mathrm{p}}^3N$. If the spheres are vacuum and are surrounded by solid material, then the porosity is $\Psi = V_{\mathrm{s}}/V = \pi/6 = 0.5236$. Conversely, if the spheres are solid material and are surrounded by vacuum, then the porosity is $\Psi = 1 - V_{\mathrm{s}}/V = 1 - \pi/6 = 0.4764$.

- Case 2: *Cubic close packing of spheres.*[3] We start out with the same arrangement of the first layer as in case 1. However, the second layer

[3] Known as the Kepler conjecture - the most efficient way of stacking cannon balls (in the shape of a pyramid).

(and each successive layer) is displaced so that each sphere rests in the geometric middle of four spheres of the lower layer. Thus, the height of two successive layers is $\sqrt{2}r_{\rm p}$ and the number of layers in a volume of height $2r_{\rm p}n$ is $2r_{\rm p}n/(\sqrt{2}r_{\rm p}) = n\sqrt{2}$. The volume occupied by the spheres is

$$V_{\rm s} = n \times n \times \sqrt{2}n \times (4\pi/3)r_{\rm p}^3 = (4\pi/3)2^{1/2}r_{\rm p}^3 N$$

If the spheres are vacuum and are surrounded by solid material, then the porosity is

$$\Psi = V_{\rm s}/V = \pi 2^{1/2}/6 = 0.7405$$

Conversely, if the spheres are solid material and are surrounded by vacuum, then the porosity is

$$\Psi = 1 - V_{\rm s}/V = 1 - \pi/6 = 0.2595$$

- Case 3: *Hexagonal close packing of spheres.* Consider again n spheres of radius $r_{\rm p}$ arranged in a line so that they just touch. Each row of spheres in, say, the x-direction is of the same length, but the centres of the spheres in alternating rows are always displaced by $r_{\rm p}$. In this way, the centres of the spheres of any 3 closest neighbours form an equilateral triangle. The spacing (in the y-direction) between the centres of the spheres in any two adjacent rows is now $3^{1/2}r_{\rm p}$ instead of $2r_{\rm p}$, as was the case for cubic packing. Thus, the number of spheres in a plane of dimensions $2r_{\rm p}n \times 2r_{\rm p}n$ is now $n \times n/(3^{1/2}/2)$. The next layer of spheres is arranged in the same way, but it is shifted, so that the spheres of each successive layer are closest to those of the previous layer. In this arrangement, the centres of any 4 closest neighbours form a tetrahedron. This means that the centre of a sphere in one layer is displaced from the centre of any of the closest spheres in the layer below by $2r_{\rm p}/3^{1/2}$ (as projected on the plane below), as shown in Fig. 3.1. The height of the tetrahedron is

$$[(2r_{\rm p})^2 - (2r_{\rm p}/3^{1/2})^2]^{1/2} = (8/3)^{1/2}r_{\rm p}$$

  Thus in a height of $2r_{\rm p}n$ there are $2n/(8/3)^{1/2}$ layers of spheres. The volume of the hexagonally close-packed spheres is

$$V_{\rm s} = n \times n \times (2/3^{1/2}) \times n \times [2/(8/3)^{1/2}] \times (4\pi/3)r_{\rm p}^3 = (4\pi/3)2^{1/2}r_{\rm p}^3 N$$

  This is the same as for the cubic close packing (case 2). Thus, if the spheres are in vacuum and are surrounded by solid material, then the porosity is again $\Psi = 0.7405$. Conversely, if the spheres are solid material and are surrounded by vacuum, then the porosity is $\Psi = 0.2595$.

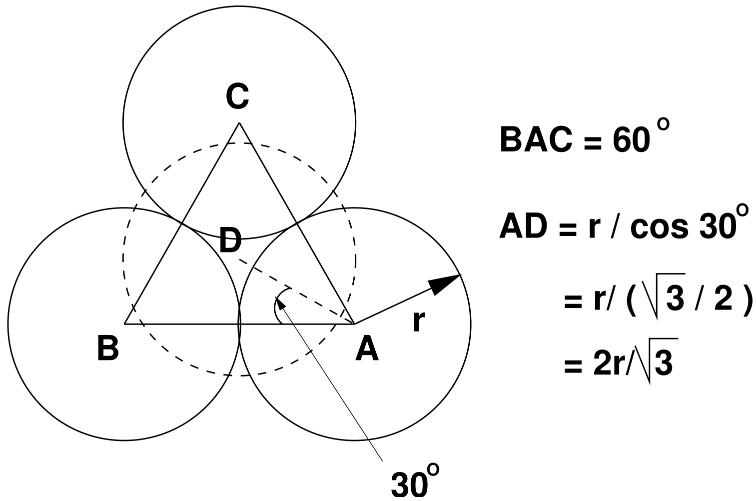

Figure 3.1: Hexagonal packing of spheres

- Case 4: *Straight parallel tubes on a square mesh.* Consider $N = n^2$ tubes of radius r_p and length $2r_\mathrm{p}n$. The volume of the tubes is $V_\mathrm{p} = \pi r_\mathrm{p}^2 \times 2r_\mathrm{p}n \times n^2$. If the tubes are vacuum surrounded by solid material, then the porosity is $\Psi = V_\mathrm{t}/V = \pi/4 = 0.7852$; if the tubes are solid material surrounded by vacuum, then $\Psi = 1 - V_\mathrm{t}/V = 0.2148$.

- Case 5: *Straight parallel tubes on a hexagonal mesh.* From case 3 above, the number of tubes is now $n \times n/(3^{1/2}/2)$. The volume of the tubes is $V_\mathrm{t} = \pi r_\mathrm{p}^2 \times 2r_\mathrm{p}n \times n \times n \times 2/3^{1/2}$. If the tubes are vacuum surrounded by solid material, then the porosity is $\Psi = V_\mathrm{t}/V = \pi/(2 \times 3^{1/2}) = 0.9069$ and conversely, $\Psi = 1 - V_\mathrm{t}/V = 0.0931$. These cases yield the highest and lowest porosity values among the simple cases considered here.

3.3.2 The Surface-to-Volume Ratio

The *surface-to-volume ratio* of a porous material is defined as the total interstitial surface area of the pores, A_p, per given bulk volume V

$$S = A_\mathrm{p}/V \tag{3.8}$$

and the related *specific surface*, Ξ, is defined as the total surface area of the pores divided by the volume of solid, $V(1 - \Psi)$,

$$\Xi = S/(1 - \Psi) \tag{3.9}$$

Here, $\Psi = V_\mathrm{p}/V$ is the porosity, where V_p is the pore volume.

As a simple example, consider the specific surface of a porous material made of identical spheres of radius r_s in a cubical packing. In this case $A_\mathrm{s} = 4\pi r_\mathrm{s}^2 N$, where N is the number of spheres in the given volume V. The volume is $V = (2r_\mathrm{s})^3 N$, which yields $S = \pi/(2r_\mathrm{s})$ and $\Xi = \pi/[2r_\mathrm{s}(1 - \Psi)]$. If the solid spheres are replaced by spherical pores, the result is the same. Clearly, fine materials have a much larger specific surface than coarse materials.

Consider now a more realistic case of a granular medium of spherical particles of n different sizes, where the number of particles of radius r_i $(1 \le i \le n)$ is N_i. The total area and volume of these spheres are

$$A_\mathrm{s} = \sum_{i=1}^{n} 4\pi r_i^2 N_i \qquad V_\mathrm{s} = \sum_{i=1}^{n} \tfrac{4}{3}\pi r_i^3 N_i \tag{3.10}$$

respectively. By definition, $V = V_\mathrm{s}/(1 - \Psi)$, whence

$$S = \sum_{i=1}^{n} 4\pi r_i^2 N_i \Big/ \left[\sum_{i=1}^{n} \tfrac{4}{3}\pi r_i^3 N_i/(1 - \Psi)\right] = 3(1 - \Psi)\sum_{i=1}^{n} f_i/r_i = 3(1 - \Psi)/\bar{r} \tag{3.11}$$

where $\bar{r}$ is the harmonic mean radius weighted by f_i, the volume fraction occupied by spheres of radius r_i. For a unique particle radius r_s, $\bar{r} = r_\mathrm{s}$. As before, pores and particles may be interchanged.

Another case, often used in comet nucleus modeling, is that of a bundle of cylindrical tortuous capillary tubes that do not cross each other (Mekler et al., 1990). [The requirement that tubes do not cross is not important to the geometry considered here, but it is important when gas flow through such a medium is considered.] The *tortuosity*, ξ, is defined as the ratio of the capillary length to the sample thickness. For a given length L and unit cross-sectional area, we have

$$A_\mathrm{p} = \sum_{i=1}^{n} 2\pi r_i N_i \xi L \qquad V = 1 \times L \tag{3.12}$$

where r_i is the capillary radius $(1 \le i \le n)$, N_i is the number of capillaries of radius r_i crossing unit area. Thus

$$S = \sum_{i=1}^{n} 2\pi r_i N_i \xi \tag{3.13}$$

On the other hand,

$$\Psi = \sum_{i=1}^{n} \pi r_i^2 N_i \xi \tag{3.14}$$

which leads to

$$S = 2\Psi \sum_{i=1}^{n} f_i/r_i = 2\Psi/\bar{r}_{\mathrm{p}} \tag{3.15}$$

where $\bar{r}_{\mathrm{p}}$ is the harmonic mean radius weighted by f_i, the volume fraction occupied by capillaries of radius r_i.

We note that the two models behave differently with changing porosity: as Ψ decreases, the surface to volume ratio of capillaries tends to zero, while that of spheres increases to a maximum. Towards high porosities, on the other hand, the surface to volume ratio of spheres tends to zero. It is, however, difficult to visualize a low porosity medium made of a bundle of individual capillaries, as much as a high porosity one made of widely separated spheres. Therefore, in numerical modeling that allows for a changing porosity – due, for example, to vigorous sublimation or condensation – it would be advisable to change from one model to the other as the porosity changes. The models yield equal values of S for $\Psi = 0.6$.

3.3.3 Gas Flow

We now turn to evaluate the flow of gas through a porous medium. For this purpose we visualize the porous medium as a network of channels. The flow regime is assumed to be laminar caused by pressure. If the network is sufficiently dense and interconnected, we may still assume homogeneity on a scale larger than the characteristic pore size and we are allowed to define and use average gradients of pressure, density, etc., regardless of the local pore geometry.

Consider a tube of radius r_{p} in a medium of porous water ice. The mean free path of a water molecule in a pore is given by

$$\ell \approx \frac{kT}{\sqrt{2}\sigma_{\mathrm{H_2O}}\mathcal{P}_{\mathrm{H_2O}}(T)} \tag{3.16}$$

where $\sigma_{\mathrm{H_2O}} \approx 2.5 \times 10^{-19}$ m^2 is the kinetic cross section of a water molecule. The highest temperature attained in the ice of comet nuclei is of the order of 200 K; substitution in Eq. (3.16) yields $\ell \approx 0.05$ m. Hence, as long as the average pore size is less than 1 mm, the Knudsen number

$$\mathrm{Kn} \equiv \ell/(2r_{\mathrm{p}}) \gg 1 \tag{3.17}$$

meaning that the flow of gas through the pores is free molecular, or *Knudsen flow.*

The steady gas flux through a porous medium in the free molecular regime depends (aside from structural parameters) only on the pressure and temperature at the two boundaries, and can be written as (see, e.g. Steiner et al., 1990)

$$\mathbf{J} = -f_\varepsilon r_\mathrm{p} \sqrt{\frac{\mu}{2\pi\mathcal{R}_\mathrm{g}}} \frac{\Delta\left(P/T^{1/2}\right)}{L} \tag{3.18}$$

Here, L is the length of the system, and f_ε is a structural parameter characterising the material. In the simple case where the porous medium is a cylindrical tube, Eq. (3.18) becomes (Gombosi, 1994, p. 149)

$$j = -\frac{8r_\mathrm{p}^3}{3\xi} \sqrt{\frac{\pi\mu}{2\mathcal{R}_\mathrm{g}}} \frac{d\left(P/T^{1/2}\right)}{dx} \tag{3.19}$$

where j is the amount of mass of gas flowing through the tube per unit time, x is the linear distance through the medium. By introducing differentiation to describe a continuously varying medium, and in the case in which temperature variations can be neglected in comparison with pressure variations, Eq. (3.18) can be written as

$$\mathbf{J} = -\mathcal{G}\nabla P \tag{3.20}$$

where $\mathcal{G}$ is called the gas diffusion coefficient. In the case of a bundle of cylindrical capillaries with unit tortuosity, $\mathcal{G}$ can be derived from Eq. (3.19), once it has been scaled for the fraction of a unit section of the porous material occupied by pores:

$$\mathcal{G} = \Psi\, r_\mathrm{p} \sqrt{\frac{\pi}{2\mu\mathcal{R}_\mathrm{g}T}} \tag{3.21}$$

Reintroducing tortuosity and temperature dependence into the model of a bundle of capillaries and defining $j' = j\xi/r_\mathrm{p}^3$, the mass flux can be written as

$$J = \sum_{i=1}^{n} N_i j_i = j' \sum_{i=1}^{n} N_i r_i^3/\xi = \frac{\Psi j'}{\pi} \sum_{i=1}^{n} f_i \frac{r_i}{\xi^2} \tag{3.22}$$

where we have used Eq. (3.14) and the same weighting function as in the calculation of S for the same model [Eq. (3.15)]. We define the *permeability*, φ, by

$$J = -\frac{8}{3}\varphi \sqrt{\frac{\mu}{2\pi\mathcal{R}_\mathrm{g}}} \frac{d}{dx}\left(\frac{P}{\sqrt{T}}\right) \tag{3.23}$$

so that in our case,

$$\varphi = \Psi\bar{r}_\mathrm{p}/\xi^2 \tag{3.24}$$

It is sometimes useful to relate the permeability to the specific surface, rather than to the capillary radius. For capillaries,

$$\varphi = \frac{\Psi^2}{(1-\Psi)\xi^2\Xi} \tag{3.25}$$

A similar relation between permeability and specific surface is obtained in the case of viscous flows and is known as the "Kozeny equation". Since all the parameters can be measured independently, the relation was tested experimentally and was found to be in good agreement with theoretical results. It is therefore reasonable to assume that a relation of the form (3.25) is less model-dependent than one that explicitly includes the pore size. In numerical modeling the theoretical relation (3.24) is the one generally used.

3.4 The Coma/Nucleus Boundary Layer

The boundary layer consists of two parts: the coma gas just above the surface of the nucleus and the topography of the nucleus surface. Both are currently active areas of research. We provide an overview of these topics.

3.4.1 The Knudsen Layer in the Coma

Gas sublimating from a surface can be modeled by assuming that the molecules liberated from the solid matrix have a Maxwell speed distribution (below the sublimating surface) at the temperature T of the matrix. They then effuse, i.e. flow through small holes in the surface. Molecules flowing through small holes into a near vacuum have only velocities with components in the $+z$ direction (away from the hole). They obey only that half of the Maxwell speed distribution function (at temperature T of the sublimating material) for which $v_z > 0$. Thus, gas sublimating from or through the surface of a comet nucleus into a near vacuum is not in thermodynamic equilibrium and the temperature of the gas cannot be defined. Only after many collisions of fast molecules overtaking slow molecules, many collision mean free paths away from the surface, will the gas again obey a full (but drifting) Maxwell velocity distribution with a definable temperature (T'). To better understand the physics, we derive an analytical solution from mass, momentum, and energy conservation in the limiting case of a negligible return flux to the surface. Here we follow the procedure discussed by Huebner and Markiewicz (1993, 2000). A detailed description of this Knudsen boundary layer requires solving the Boltzmann equation. Such solutions are usually based on computer-intensive Monte Carlo procedures (see, e.g. Skorov and Rickman, 1999).

If we assume a gas with number density n and pressure P in thermodynamic equilibrium at temperature T on one side of a surface that divides space into two parts, then the one-dimensional Maxwell distribution in the direction normal to the surface ($+z$ direction), is

$$\tilde{f}_1(v_z)\,dv_z = \left(\frac{m}{2\pi kT}\right)^{1/2} \exp\left(-\frac{mv_z^2}{2kT}\right) dv_z \tag{3.26}$$

Here v_z occurs only in the exponent, i.e. the function is symmetric about its most likely value at $v_z = 0$. The function $\tilde{f}_1(v_z)$ is normalized so that the integral from minus to plus infinity equals 1 and therefore, since gas only flows away from the surface,

$$\int_0^\infty \tilde{f}_1(v_z)\,dv_z = \frac{1}{2} \tag{3.27}$$

The gas particle flux striking a surface is

$$\Phi = n\int_0^\infty v_z\tilde{f}_1(v_z)\,dv_z = n\frac{v_{\mathrm{th}}}{4} \tag{3.28}$$

where

$$v_{\mathrm{th}} = \sqrt{\frac{8kT}{\pi m}} \tag{3.29}$$

is the mean thermal gas speed of the Maxwell distribution function at temperature T. Thus, the number of molecules with mean free path large compared to the dimensions of the small hole with area, A, escaping per unit time into a near vacuum is $Anv_{\mathrm{th}}/4$.

The momentum of the gas in the direction away from the surface must be conserved. This will result in a centre of mass speed v'_{0z} (the bulk or drift motion) and velocities relative to v'_{0z} that obey the (drifting) Maxwell distribution function. (We label quantities after re-establishment of equilibrium with a prime.) The temperature, T', of molecules obeying this Maxwell distribution far downstream can be determined from the conservation of energy.

The most abundant speed group of molecules with a $+z$ component of their velocity in or near the hole are those with $v_z = 0$; but they will not move through the hole. The number of molecules moving through the hole is proportional to the *abundance* of molecules with a velocity component in the $+z$ direction as well as to their *speeds* v_z, as already implicitly stated in Eq. (3.28). To express this, using a three-dimensional Maxwell distribution ($\tilde{f}_3$), we assume a spherical coordinate system with origin in (or just below) the hole and the angle θ measured from the outward normal to the surface

($+z$ direction). Thus, the flux through the hole is also proportional to $v_z = v\cos\theta$, resulting in the (three-dimensional) Maxwell *transmission* (or flux) distribution function (Loeb, 1934; Kittel and Kroemer, 1980)

$$\begin{aligned} \tilde{f}_3^{(t)}(v)\,dv &= \frac{1}{\mathcal{N}}\left(\frac{m}{2\pi kT}\right)^{3/2}\int_0^{2\pi}\int_0^{\pi/2} v^3 \exp\left(-\frac{mv^2}{2kT}\right)\cos\theta\sin\theta\,d\theta\,d\phi\,dv \\ &= 2\left(\frac{m}{2kT}\right)^2 v^3 \exp\left(-\frac{mv^2}{2kT}\right)dv \end{aligned} \tag{3.30}$$

where

$$\mathcal{N} = \left(\frac{m}{2\pi kT}\right)^{3/2}\int_0^{\infty}\int_0^{2\pi}\int_0^{\pi/2} v^3 \exp\left(-\frac{mv^2}{2kT}\right)\cos\theta\sin\theta\,d\theta\,d\phi\,dv \tag{3.31}$$

provides the normalization. Viewing this in a one-dimensional distribution, we obtain

$$\tilde{f}_1^{(t)}(v_z)\,dv_z = \frac{mv_z}{kT}\exp\left(-\frac{mv_z^2}{2kT}\right)dv_z \tag{3.32}$$

which is normalized such that $\int_0^\infty f_1^{(t)}(v_z)\,dv_z = 1$.

The most likely speed, i.e. the speed at the maximum of the Maxwell *transmission* distribution function, Eq. (3.32), is

$$v_{z,\max} = \left(\frac{kT}{m}\right)^{1/2} \tag{3.33}$$

The corresponding quantity in a thermal Maxwell distribution is 0!

Using the three-dimensional Maxwell distribution, Eq. (3.30), the mean speed of the gas passing through the hole of the surface is

$$\langle v\rangle = \int_0^\infty v\tilde{f}_3^{(t)}(v)\,dv = \frac{3\pi}{8}v_{\rm th} \tag{3.34}$$

which is somewhat larger than the mean speed $v_{\rm th}$, as expected.

We now investigate the conservation of momentum and kinetic energy as the gas passes through the hole (unprimed quantities). After many collisions it equilibrates into a Maxwell distribution at temperature T', drifting with the centre-of-mass speed v'_{0z}. The equation for conservation of momentum (per molecule and mass, nm) is

$$\langle v_z\rangle = \int_0^\infty v_z\tilde{f}_1^{(t)}(v_z)\,dv_z = \frac{\pi}{4}v_{\rm th} = \int_{-\infty}^{\infty} v'_z\tilde{f}_1\left(v'_z - v'_{0z}\right)dv'_z = v'_{0z} \tag{3.35}$$

and the corresponding equation for conservation of energy is

$$\begin{aligned}\left\langle v^2\right\rangle &= \int_0^\infty v^2 \tilde{f}_3^{(t)}(v)\,dv = \frac{4kT}{m} \\ &= \sum_{i=x,y}\int_{-\infty}^{\infty} v_i'^2 \tilde{f}_1\left(v_i'\right) dv_i' + \int v_z'^2 \tilde{f}_1\left(v_z' - v_{0z}'\right) dv_z' \\ &= \frac{3kT'}{m} + \left(\frac{\pi v_{\mathrm{th}}}{4}\right)^2 \end{aligned} \tag{3.36}$$

where we have used the results of Eq. (3.35) in the last term of Eq. (3.36) assuming no change in the terms of the internal energy (e.g. for a monatomic gas). As pointed out above, the centre-of-mass speed $v_{0z}' = \langle v_z \rangle = (\pi/4)v_{\mathrm{th}}$, which is the speed of the gas as it passes through the hole. In some applications it has been assumed that $v_{\mathrm{th}}/4$, or some other value between $v_{\mathrm{th}}/2$ and $2v_{\mathrm{th}}/3$ (see, e.g. Delsemme and Miller, 1971) is the speed of the escaping gas, but as can be seen from Eq. (3.35), all of these speeds are too small for dust-free outgassing. Dust entrainment will reduce this speed. Skorov and Rickman (1999) investigated dust entrainment.

Solving for the temperature of the drifting Maxwell distribution for a monatomic gas [using Eq. (3.29)] gives

$$T' = \frac{4}{3}T - \left(\frac{\pi v_{\mathrm{th}}}{4}\right)^2 \frac{m}{3k} = \frac{4}{3}T - \left(\frac{\pi}{4}\right)^2 \frac{m}{3k}\frac{8kT}{\pi m} = \frac{8-\pi}{6}T = 0.8097T \tag{3.37}$$

Now we assume that the number of excited rotational degrees of freedom in the gas before it moves through the hole is f_{r}. Vibrational degrees of freedom are not excited in a cold cometary gas. Then, based on equipartition among the excited degrees of freedom, the rotation energy is $f_{\mathrm{r}}nkT/2$. If the same number of degrees of freedom remain excited and the total energy is conserved (e.g. no radiation losses) until the gas equilibrates, then (after equipartition among all excited degrees of freedom)

$$\frac{1}{2}nm\left\langle v^2\right\rangle + \frac{f_{\mathrm{r}}}{2}nkT = 2nkT + \frac{f_{\mathrm{r}}}{2}nkT = \frac{3}{2}nkT' + \frac{nm}{2}\left(\frac{\pi v_{\mathrm{th}}}{4}\right)^2 + \frac{f_{\mathrm{r}}}{2}nkT' \tag{3.38}$$

This leads to

$$T' = \frac{8 + 2f_{\mathrm{r}} - \pi}{2\left(f_{\mathrm{r}} + 3\right)}T \tag{3.39}$$

The fraction of energy in bulk motion relative to the total (kinetic and thermal) energy is obtained from the ratio of

$$\frac{1}{2}mv_{0z}'^2 / \left(\frac{1}{2}mv_{0z}'^2 + \frac{f_{\mathrm{r}}+3}{2}T'\right) \tag{3.40}$$

Table 3.1: Results for some values of f_r. M' is the Mach number

f_r	T'/T	v'_{0z}/v'_{th}	M'	Energy in Bulk Motion/ Total Energy
0	0.8097	0.8728	1.079	0.3927
2	0.8858	0.8345	1.125	0.2795
3	0.9049	0.8257	1.141	0.2443

Table 3.1 summarizes results for internal degrees of freedom $f_r = 0$ (monatomic gas), $f_r = 2$ (diatomic gas with two rotational degrees of freedom excited), and $f_r = 3$ (polyatomic gas with three rotational degrees of freedom excited).

The processes for vapourisation and sublimation are similar to those of effusion, except for the number of molecules in the vapour phase, and thus the gas flux, is restricted by the vapour pressure as determined from the Clausius-Clapeyron equation. No such restriction applies for effusion. The pressure of gas produced in the interior of the nucleus is also determined by the Clausius-Clapeyron equation at the appropriate temperature, but the gas may be heated in the pores of the matrix material as it escapes.

As gas effuses through or sublimates from the nucleus surface into vacuum, its final temperature can be as low as about 0.81 of its original temperature, T, (depending on the level of internal excitation) and its bulk speed will be $\pi v_{th}/4$ [see Eq. (3.35)]. After re-establishment of the Maxwell velocity distribution, up to about 40% of the energy of the gas is in bulk motion, i.e. the drift speed of the Maxwellian (depending on the level of excitation of rotational degrees of freedom) and the rest is in thermal energy.

The thickness of the coma boundary layer depends on the gas production rate per unit surface area of the comet nucleus. At large heliocentric distances, the rate of gas production is small and the thickness of the boundary layer can be very large. In the extreme case, when the mean free path for collisions between gas molecules approaches infinity, a Maxwell distribution will never be established and the gas remains in free molecular flow. When a comet nucleus is close to the Sun, the gas production rate per unit surface area can be large. As discussed in Section 3.3.3, the collision mean free path is $\ell \approx 0.05$ m close to the surface of the nucleus. Thus, the Knudsen boundary layer is of the order of 10 m on the subsolar side of the nucleus. It will be much larger on the night side of the nucleus.

The discussions of this section are part of an ongoing investigation and for this reason are not fully and consistently applied in this book.

3.4.2 Effects of Nucleus Surface Topography

Gutiérrez et al. (2000) developed a model for water vapour production of a spinning, irregularly shaped nucleus with topography that can be tailored to specific, observed features. Such a model is best applied to heat and gas diffusion in a comet nucleus for which detailed topographic features are available. Here we describe a simpler model (Huebner, 2006) that can include scales for topography smaller than the currently best resolved features (40 m for two pixels on the surface of Comet 81P/Wild 2).

The topography of the surface of a comet nucleus appears to be rough at all scales smaller than the mean effective radius. Thus, models for topographic features must be simple, flexible, and scalable. Surface topography can increase or decrease the gas release rate. For example, a small decrease may be encountered if a hill is near the subsolar point of insolation. This decrease is the result of the increased surface area relative to the original area where the Sun was incident at an angle close to the normal to the surface. Topography may also influence development of a permanent dust mantle. Finally, it can simulate the heterogeneity of comet nuclei. The model described here does not apply when one surface feature shadows another surface feature, i.e. it works best when the distribution of topographic features is sparse. However, self-shadowing (the night-side of a topographic feature) is taken into account.

We model surface roughness by placing hemispheres of different sizes on the smooth surface of a simulated comet nucleus. Positive values for the topography radius, R_{Top}, represent hills, while negative values represent valleys. We choose hemispheres because general model calculations for spherical nuclei are already available. The additions due to topography must be corrected by subtracting the contributions of the base of the topographic feature on the nucleus. Calculations for valleys can be based on the work of Colwell et al. (1990), who investigated crater-like features.

The hemispherical topography model has many advantages: hills and cavities can have their own physical properties such as radius of curvature (positive for hills and negative for cavities), albedo, IR emissivity, composition such as different ices, different dust-to-gas ratios, etc. Thus, the surface can be inhomogeneous, leading to different rates of gas production or having different dust mantle thicknesses. Much of the surface of a nucleus can be covered with bumps and cavities. There are some limitations to the model: topographic features cannot overlap and the shadow of one feature cannot be cast on another feature. If this occurs, the model of Gutiérrez et al. (2000) should be used.

If the topographic feature is a hill, the cap of the hill pointing towards the Sun is illuminated all around, i.e. over an azimuth angle $2\phi_{\max} = 2\pi$.

However, over the part of the hemispherical hill that intersects the nucleus, $\phi_{\max}$ must be calculated from the equations determining the intersection. The equation of a plane bisecting the sphere to make a hemispherical topographic feature is

$$x/\tan\zeta_{\mathrm{Top}} + z = z_0 \tag{3.41}$$

The equation for the spherical nucleus of radius R is

$$x^2 + y^2 + z^2 = R^2 \tag{3.42}$$

The intersection of the plane with the sphere is defined when the coordinates of the plane and the sphere are the same. Expressing the equations in spherical coordinates, where ζ is the angle of insolation on the hemispherical feature and ζ_{Top} is the polar angle that locates the feature on the nucleus,

$$z = R\sin\zeta\cos\phi \tag{3.43}$$

$$y = R\sin\zeta\sin\phi \tag{3.44}$$

$$z_0\sin\zeta_{\mathrm{Top}} = (R^2 - R_{\mathrm{Top}}^2)^{1/2} \tag{3.45}$$

Combining these equations and solving for $\phi = \phi_{\max}$ gives

$$\phi_{\max} = \arccos\left[\frac{-\cos\zeta\cos\zeta_{\mathrm{Top}} + \left(1 - R_{\mathrm{Top}}^2/R^2\right)^{1/2}}{\sin\zeta\sin\zeta_{\mathrm{Top}}}\right] \tag{3.46}$$

It should be noted that the hemispherical feature has its centre of curvature at a distance from the centre of the nucleus at $(R^2 - R_{\mathrm{Top}}^2)^{1/2}$, as indicated by Eq. (3.46). There is no insolation for angles $\zeta > \pi/2$ (self-shadowing). Adding the effects of insolation, re-radiation, sublimation, etc. from the topographic features requires the subtraction of the corresponding effects for the spherical caps of the nucleus covered by the topographic features.

The sizes of the topographic features are limited. If they are much smaller than ~ 10 m, they will erode at heliocentric distances of $r_{\mathrm{H}} \lesssim 1$ AU and are not very relevant for the present discussions. The maximum effective size for a hill is $R_{\mathrm{Top}} = R/\sqrt{2}$. Features larger than this should be modeled by an ellipsoidal nucleus.

Crater-like features can be included in a similar way as shown by Colwell et al. (1990). The model has many additional advantages: it can incorporate effects of shadowing and changes in physical properties such as albedo, emissivity, composition, etc. For hills, one has to consider three types of shadows: (1) The night side of the topographic feature itself (self-shadowing). This is fully taken into account. (2) Shadowing on the featureless parts of the nucleus (i.e. surrounding areas not covered by topographic features), and (3) Shadowing of one topographic feature by another. The second of the effects mentioned depends strongly on the size of the hemispherical hills. Near the subsolar area, such shadows are very small or may not exist at all. At an angle a little further from the subsolar point, the shadows are short, but should be taken into account. This will be done in future models. Shadows become longer near the terminator, but there the large angle of insolation has little effect on sublimation, so that considering shadows there does not improve the model. The third type of shadowing is much more difficult to take into account and requires detailed knowledge of topographic features, which is beyond the objectives of the simple model considered here. Such shadows require detailed knowledge of the surface topography, which is usually not available. If it is available, the model of Gutiérrez et al. (2000) should be used. Shadowing is most important for valleys, but self-shadowing has already been taken into account.

3.5 Dust Entrainment and Dust Mantling

Dust, the refractory component of cometary material, is very important to the thermal evolution of the nucleus. Accounting for it is essential for modeling a “realistic” comet nucleus. There are two major processes for dust mantle development: a primordial process, caused by cosmic ray bombardment, and devolatilization of surface layers caused by ices sublimating. In the first case, the cosmic ray bombardment of a nucleus may lead to the formation of refractory surface layers up to about a metre thick (Strazzulla et al., 1991; Baratta et al., 1994). It is usually assumed that this kind of primordial mantle does not survive the first entry into the inner Solar System. In the second case, gas activity of a nucleus close to the Sun can form a layer of refractory particles that are too heavy relative to their cross section to be entrained by gas outflow.

The fraction of active area on a nucleus appears to be very different from comet to comet, varying from about 10% for 1P/Halley to about 0.1% for 49P/Arend-Rigaux (Weissman et al., 1989). These large differences, together with the evidence of brightness changes during different periods of a comet’s life, may be explained by the cyclic formation and destruction of a dust mantle.

When ice on the surface of a comet nucleus sublimates, it leaves behind the dust that was embedded within the ice. If the dust particles are sufficiently light, they can be entrained by the escaping gas. However, above a critical value of their mass relative to their effective cross section, they will fall slowly back to the surface in the comet’s weak gravitational field.

3.5.1 The Critical Dust Particle Size

The eventual formation of a dust mantle on the surface of a comet nucleus may be modeled in different ways, the essential parameter being the critical dust particle size (mass/cross section), which represents the heaviest particle that can leave the nucleus, as determined by the balance of forces acting on the particle.

The gravitational force of the nucleus of mass M on a dust particle of mass $\hat{m}$ at the surface is

$$\mathcal{F}_{\mathrm{g}} = \left(\frac{MG}{R^2} - \omega^2 R \cos^2\theta\right)\hat{m} \tag{3.47}$$

where G is the universal gravitational constant, ω is the angular speed of the nucleus, and θ is the latitude of the dust particle on the nucleus. The mass of a spherical dust particle is $\hat{m} = 4\pi\hat{r}^3\hat{\rho}/3$ and the mass of the spherical comet nucleus is $M = 4\pi R\rho_{\mathrm{N}}/3$, where $\hat{\rho}$ and ρ_{N} are the densities of the dust particle and the nucleus, respectively, while ρ is the mass density of the gas. The acceleration of a dust particle is

$$\hat{a} = \frac{1}{2}C_{\mathrm{D}}\frac{\hat{\sigma}}{\hat{m}}\rho\,(v - \hat{v})\,|v - \hat{v}| - \left(\frac{MG}{R^2} - \omega^2 R\cos^2\theta\right)$$

where C_{D} is the drag coefficient, $\hat{\sigma}$ is the effective cross section of the dust particle, and v and $\hat{v}$ are the gas and dust speeds, respectively. The critical size of a particle that can be entrained by gas drag from the surface has $\hat{a} = \hat{v} = 0$. This results in a minimum dust particle cross section per unit mass, the "critical" particle size

$$\frac{\hat{\sigma}}{\hat{m}} = 2R\frac{4\pi\rho_{\mathrm{N}}G - 3\omega^2\cos\theta}{3C_{\mathrm{D}}\rho v^2} \tag{3.48}$$

For spherical particles this reduces to

$$\hat{r}^* = \frac{3C_{\mathrm{D}}}{8}\frac{\rho v^2}{\hat{\rho}[MG/R^2 - \omega^2 R\cos^2\theta]} \tag{3.49}$$

Topography leads to depletion of ice on hills and mountains because some part of a convex surface is more effectively exposed to insolation for a longer period than a flat surface. In addition, the gas flux above a convex surface diverges more strongly than over a flatter surface. Dust is entrained, but decouples from the rapidly diluting gas flow a short distance above the surface causing it to fall back onto the nucleus.

3.5.2 Models of Dust Mantle Formation

The problem of dust mantle formation was first studied by Brin and Mendis (1979). They related the mantle thickness at a particular point in the orbit to its thickness at an earlier point taking into consideration the fraction of dust released from ice and carried away by the sublimating gas, and the part of the mantle removed by the increased gas flux as a comet approaches the Sun. However, this simple approach deals only with the *mass* of the mantle.

A different approach to modeling the structure of the dust mantle is to assume that the ice sublimates freely at the nucleus surface, carrying with it the smaller than critical size dust particles, while the larger particles are left behind. At the beginning, these large dust particles are isolated from each other, but as more and more particles accumulate, the surface becomes evenly covered and starts interfering with the escape of smaller and smaller particles. The porosity of the dust mantle decreases and, eventually, drops *below* that of the nucleus. This idea of trapping and compaction, introduced by Shul'man (1972) before the first model of a dust mantle was developed, was adopted by several authors, including, for example, Rickman et al. (1990).

The gas flow through such a mantle can be modeled by considering gas diffusion through the porous medium. If the gas pressure is high enough, the dust mantle may be blown off and the process will start anew. The process depends on latitude and on the inclination of the spin axis. A dust mantle will inhibit gas sublimation when most of the surface is covered by particles (e.g. Prialnik and Bar-Nun, 1988), a result that was observed in the KOSI experiments described in Section 2.4.1 (Grün et al., 1993).

Eventually, the pore size of the dust mantle may become too small to allow particles to escape and a large number of small particles may become permanently trapped. This may lead to a very stable and efficient dust mantle, with a high cohesive strength that may surpass the vapour pressure building up below the mantle (Kührt and Keller, 1994). As a consequence, the gas is driven toward the interior and refreezes, forming an ice layer (crust) of increased density and strength (Prialnik and Mekler, 1991). This effect had been observed earlier in the KOSI comet simulation experiments by Spohn et al. (1989).

The difficulty with all of these models is that they predict uniform and homogeneous dust mantles that either choke all gas production or are periodically blown off. This prompted Huebner (2006) to propose a model for an inhomogeneous and irregular surface structure. In such a model the divergence of the gas flow above a hill is larger than above a smooth surface. Thus, the gas density, ρ_{g}, decreases faster above a hill, which means that only particles with large values for $\hat{\sigma}/\hat{m}$ remain entrained by the gas flow. Particles with small values of $\hat{\sigma}/\hat{m}$, i.e. massive or compacted particles, fall back to the surface between hills. This favours dust mantle development near hills.

On the other hand, some parts of concave surface areas spend a larger part of their time in shadows. Thus, they will outgas more slowly. However, in these areas the gas flow from sublimating ice converges, making dust entrainment more efficient, i.e. the dust is carried further into the coma.

The ice-depleted areas near hills and mountains will not be cooled by sublimation. This favours creation of temperature patches on the surface and is thus a mechanism that may cause inert surface areas. We may conclude that the dust-to-gas ratios observed in comet comae are a result of comet nucleus evolution. This is consistent with at least one of the conclusions by A'Hearn et al. (1995) that dynamically new comets display gas production rates with a very shallow dependence on heliocentric distance on their in-bound legs of their orbits.

3.5.3 Porosity of the Dust Mantle

We follow Podolak and Prialnik (1996) to estimate the porosity of the dust mantle. If $\hat{n}$ is the number density of dust particles (assumed to be spherical), and $\hat{r}$ is their average radius, then the mean free path, ℓ, for dust–dust collisions [see also Eq. (3.29)] is given by

$$\ell \approx \frac{1}{\sqrt{2}\hat{n}\pi\hat{r}^2} \tag{3.50}$$

The number density of dust particles that will produce a given mean free path is then $\hat{n} = (\sqrt{2}\pi\hat{r}^2\ell)^{-1}$. The actual volume occupied by the dust is $\hat{V} = (4/3)\pi\hat{r}^3\hat{n}$, where $\hat{n}$ is the number of dust particles in the volume, V, under consideration. Thus, the porosity for a given mean free path is then

$$\Psi = 1 - \frac{\hat{V}}{V} = 1 - \frac{4\hat{r}}{3\ell\sqrt{2}} \tag{3.51}$$

For a mean free path of $2\hat{r}$, this gives a porosity of about 0.5. Such a mean free path implies that the particles are touching each other, and so this should be the porosity of a medium like sand. In fact, a porosity of about 0.5 for sand is a reasonable value. If we take a mean free path of $4\hat{r}$, so that there is a space of one particle diameter between the surfaces of adjacent particles on average, the porosity increases to about 0.75. This is a typical value for a high-porosity material.

In the microgravity environment of the comet nucleus, it is possible that the cohesive forces between particles can exceed the gravitational force (see, e.g. Section 2.2) and particles might stick together to form "fairy castle" structures of even higher porosity. In the following we estimate the relative strengths of these two forces. The calculation follows that of Debye in his Baker Lectures (Chu, 1967). The energy of interaction between two atoms or molecules due to London forces is

$$\epsilon = -\frac{\Lambda}{d_m^6} \tag{3.52}$$

where d_m is the distance between the molecules and Λ is a coupling constant that depends on the properties of the two molecules. Several expressions have been proposed to describe Λ. One of these is the London-van der Waals constant:

$$\Lambda = \frac{3}{4} E_{\text{ion}} \left(\frac{\alpha_{\text{p}}}{4\pi\varepsilon_{\text{o}}} \right)^2 \tag{3.53}$$

where E_{ion} is the ionization energy of the atom or molecule, α_{p} is the polarizability, and ε_{o} is the permmittivity of free space. From integration over the volumes of the two particles, the total energy of interaction can be computed. If both particles have a radius $\hat{r}$ and their centres are a distance $2\hat{r} + s$ apart, then the energy of interaction is

$$\epsilon \approx -\frac{E_{\text{o}}\hat{r}}{12s} \tag{3.54}$$

where $E_{\text{o}} = n^2\pi^2\Lambda$ and n is the number of atoms or molecules per unit volume in the particles. This implies that the interaction energy diverges when the two particles touch. However, the two atoms or molecules never approach each other to closer than an atomic diameter, or about 2×10^{-10} m. We take this to be the value of s. Similarly, we take typical values $n \approx 10^{27}$ m^{-3} for the average number density of $(Mg, Fe)_2SiO_4$ and $(Mg, Fe)SiO_3$ molecules in the particles, $E_{\text{o}} \approx 10$ eV for the ionization energy, and $\alpha_{\text{p}}/(4\pi\varepsilon_{\text{o}}) \approx 10^{-29}$ m^3. For these values, $\Lambda \approx 10^{-76}$ J m^6, $E_{\text{o}} \approx 5 \times 10^{-21}$ J, and the energy of attraction between two 1 μm particles will therefore be $\epsilon \approx 10^{-18}$ J. For a comet with a 2 km radius and a mean density of 500 kg m^{-3}, the gravitational energy is $E_{\text{g}} \approx 3.5 \times 10^{-20}$ J. The exact values depend on the values of the parameters chosen, but it is entirely possible that the cohesive energy will dominate, and "fairy castle" structures may be expected.

Dust structures consistent with the above model have been observed in experiments performed by Hapke and Van Horn (1963). They shook small particles of dark powder through a sieve and obtained structures with a porosity of 0.85 - 0.9. Computer simulations of the fall of spherical particles that stick on contact (Cameron and Schneck, 1965) give a porosity of 0.86

for uniform spheres vertically incident, and a porosity of 0.83 for irregular spheres vertically incident. There is little difference between true spheres and spheroids. Isotropic incidence tends to increase the porosity slightly. On the basis of this it seems reasonable to expect that the porosity of the dust layer on a comet nucleus is about 0.85, which is probably *higher* than the porosity of the interior. Such high values have been inferred for the surface ice layer on icy satellites such as Rhea (Domingue et al., 1995).

Although the unperturbed mantle may have a higher porosity than the average value for the bulk material in the nucleus, blocking of pores as discussed in Section 3.5.2 may ultimately result in a lower porosity. The details of mantle formation remain an area of active research.

3.6 Fracturing, Splitting, and Outbursts

Comparison between tidally and nontidally split comets indicates that on average tidal-disruption events generate a significantly larger number of fragments. In many cases breakup of the nucleus is associated with outbursts of activity. Sekanina et al. (2002) inferred that the temporal gap between outburst and splitting may be explained by sustained activity that is required in order to overcome the resistance to fracture by cohesion forces and provides strong evidence against strengthless 'rubble-pile' models of comet nuclei. The breakup mechanism for the nontidally split comets is unknown, but it probably results from buildup of internal stresses. These may be caused by mechanical effects, such as flexing induced by changes in the moments of inertia and angular momentum or by thermodynamic effects, such as high thermal or pressure gradients.

Porosity in general and pore size in particular may influence internal gas pressure in the nucleus. The highest gas pressure is obtained for pores of the smallest size that impede the flow of gas. However, since the gas density is proportional to the bulk density, the pressure is also affected by the porosity. High pressures may develop in dense, fine-grained nuclei. The peak pressure always occurs near the source of the gas, be it sublimation or gas released from crystallization of amorphous ice, provided this source is sufficiently deep. Near the surface the pressure is low since the comet's environment is practically a vacuum. When the pressure is exerted by gas released from crystallization, the peak occurs near the boundary between crystalline and amorphous ice, at a depth of a few tens of metres, typically, declining gradually toward the surface and toward the centre. We may estimate the stresses generated by a given gas pressure profile, in the elastic approximation. The gas pressure gradient constitutes a body force acting in a spherical shell that extends from an inner boundary R_1 to the surface of the nucleus of radius R. The pressure is negligible at R_1 (chosen as the radius where the gas pressure becomes smaller than the hydrostatic pressure) and vanishes, by definition, at R. For a spherically symmetric configuration, there are only two non-vanishing components of the stress tensor: the radial stress σ_r and the tangential stress σ_θ. Assuming the boundaries to be free of loads, these stresses are given by

$$\sigma_r = P(r) - \frac{2(1-2\nu)}{1-\nu}\frac{1}{r^3}\left(\int_{R_1}^{r} P(r)\,r^2 dr - \frac{r^3 - R_1^3}{R^3 - R_1^3}\int_{R_1}^{R} P(r)\,r^2 dr\right) \tag{3.55}$$

$$\sigma_\theta = \frac{\nu}{1-\nu}P(r) + \frac{1-2\nu}{1-\nu}\frac{1}{r^3}\left(\int_{R_1}^{r} P(r)\,r^2 dr + \frac{2r^3 + R_1^3}{R^3 - R_1^3}\int_{R_1}^{R} P(r)\,r^2 dr\right) \tag{3.56}$$

(Luré et al., 1964) where ν is Poisson's ratio (0.33 for water ice at 200 K, Miller, 1982). They should be compared to the compressive strength of cometary material, which – according to estimates derived from tidal splitting of comets, as well as from the KOSI laboratory simulations of cometary ice – is found to be of the order of 10^4 N m^{-2}. An example is given by Prialnik and Bar-Nun (1990), showing that pressure induced stresses can surpass the tensile strength in a more than 10 m thick layer, at a depth Δr of several tens of metres. This calculation also shows that for a given pore size, the maximal depth at which the internal pressure exceeds the tensile strength increases by a factor of 3, as the bulk density increases by a factor of 4. For a given bulk density, an increase in pore size by a factor of 100 causes this depth to decrease by a factor of 2. Thus, the precise properties of cometary material will determine the depth of potential instability.

The build-up of high internal pressure may result in cracking of the ice and opening of channels, through which the gas could flow and release the high pressure. It may also result in an explosion, or outburst of gas. The outcome is largely determined by the competition between two timescales, the timescale of gas release and pressure build-up, which is the same as the crystallization timescale $\tau_{\rm crys}$, on the one hand, and the time of pressure release, which is the gas diffusion timescale $\tau_{\rm diff}$, on the other. If $\tau_{\rm crys} > \tau_{\rm diff}$, the pressure is released rapidly enough to prevent an instability; if $\tau_{\rm crys} < \tau_{\rm diff}$, gas will accumulate more rapidly than it is removed and large stresses may result from pressure buildup. The borderline obtained by equating the timescales divides the $(\Delta r, T)$ plane into two zones, a stable and an unstable one (see Prialnik and Bar-Nun, 1990). Clearly, pore enlargement may arrest the development of an instability. If, however, the temperature should rise as a result of heat release and poor heat conduction, then pore enlargement may continue in a runaway process that may

Table 3.2: Nontidally split comets (from Sekanina (1997) and Boehnhardt (2002))

1846 II, 1852 III,	3D/Biela
C/1860 D1	Liais
C/1888 D1	Sawerthal
C/1889 O1	Davidson
D/1896 R2	D/Giacobini
C/1899 E1	Swift
C/1906 E1	Kopff
C/1914 S1	Campbell
C/1915 C1	Mellish
1915 W1	69P/Taylor
C/1942 X1	Whipple-Fedtke
C/1947 X1	Southern Comet
C/1955 O1	Honda
C/1956 F1	Wirtanen
C/1968 U1	Wild
C/1969 O1	Kohoutek
C/1969 T1	Tago-Sato-Kosaka
C/1975 V1	West
1982 C1	79P/du Toit-Hartley
1985 V1	108P/Ciffreo
C/1986 P1	Wilson
1991 L1	101P/Chernykh
C/1994 G1	Takamizawa-Levy
1994 P1	141P/Machholz 2
1994g	51P/Harrington
1994w	73P/Schwassmann-Wachmann 3
C/1995 O1	Hale-Bopp
C/1996 J1	Evans-Drinkwater
C/1999 S4	LINEAR
C/2001 A2	LINEAR
C/2002 A1+2	LINEAR

Table 3.3: Tidally split comets (from Sekanina (1997) and Boehnhardt (2002))

C/1882 R1	Great September Comet	at Sun
1889 N1	16P/Brooks 2	at Jupiter
C/1963 R1	Pereyra (possibly split)	at Sun
C/1965 S1	Ikeya-Seki	at Sun
D/1993 F2	D/Shoemaker-Levy 9	at Jupiter

be interpreted as an explosion. The creation of large pores does not necessarily entail a change in porosity; it may occur at the expense of small pores, which may shrink by the compression of material between the large pores. This implies an increase in strength of the pore walls (similar to the effect known as *strain hardening*, a property of materials that is usually determined experimentally). All these features complicate the simulation of a changing porous structure under pressure-induced stress (cf. Prialnik et al., 1993), but as a rule we should expect cracking and explosions to accompany crystallization and gas release.

If cometary ice is not an elastic material, it may yield to *continuous* application of internal pressure. In this case, the time factor becomes important. The rate of relaxation of the pressure, when crystallization and gas release have ceased, has a time constant of the order of months, i.e. much longer than the time constant of the crystallization process, but much shorter than the time span between bursts of phase transitions. Thus, the state of stress is not a permanent but a transient one, allowing the nucleus ample time to relax between crystallization episodes. This is significant for the role of crystallization in explaining sudden, sporadic eruptions. The frequency of outbursts, as well as the heliocentric distances at which they predominantly occur, are functions of the density of the comet nucleus. In a low-density nucleus, phase transition episodes are frequent and set in at small heliocentric distances. In a high-density nucleus, on the other hand, phase transition episodes are infrequent, occur farther away from the Sun and extend to greater depths. Thus, the frequency of observed outbursts of a comet may provide an indication of the nucleus density.

Differential outgassing from active areas changes the mass distribution on the surface, which in turn leads to changes in the moment of inertia of the spinning nucleus. The readjustment of the spin energy and angular momentum leads to internal friction. As a result, the nucleus may fragment at its weakest structural parts.

— 4 —

Basic Equations

> "As we are now in a great measure acquainted with the physical construction of the different parts of the ... comet, and have seen many successive alterations that have happened in their arrangement, it may possibly be within our reach to assign the probable manner in which the action of such agents as we are acquainted with has produced the phenomena we have observed."
>
> William Herschel, LL.D.F.R.S., *Philosophical Transactions*, 1812.

Numerical models of the evolution of comet nuclei are based on the solution of equations expressing conservation of energy to describe heat diffusion, and conservation of mass to describe gas diffusion. The conservation laws are expressed by means of time-dependent, partial differential equations having the following general form:

$$\frac{\partial \rho}{\partial t} + \nabla \cdot \mathbf{J} = q \tag{4.1}$$

where ρ is the density of the considered quantity, $\mathbf{J}$ is its flux, and q its source term, accounting for all processes, other than transport, that cause a variation of the considered quantity in a unit volume. Conservation of momentum is usually replaced by a steady flow assumption, which results in an expression for gas fluxes similar in form to Fourier's law for the heat flux. Thus, the second term on the left side of Eq. (4.1) becomes a second-order spatial derivative.

Once suitable mathematical expressions for the terms in Eq. (4.1) have been devised for the different quantities considered in the model, the resulting system of partial differential equations is solved numerically in discrete time steps on a discrete grid.

4.1 Mass Balance

The most general composition of a comet nucleus includes crystalline (or amorphous and crystalline) water ice, water vapour, siliceous and carbonaceous dust, and other volatiles (e.g. CO, CO_2, etc.) that may be frozen, free, or trapped in the amorphous water ice. Let ρ denote the bulk mass density, and let the density of the various components be denoted by $\rho_{\rm a}$ (amorphous ice), $\rho_{\rm c}$ (crystalline ice), $\rho_{\rm v}$ (water vapour), $\hat{\rho}$ (all forms of dust), ρ_i and $\tilde{\rho}_i$, where the index i indicates the different species of volatiles other than H_2O (such as CO, CO_2, etc.), in solid (ρ_i) and gaseous ($\tilde{\rho}_i$) phases, respectively. The amorphous ice includes (small) mass fractions f_i of trapped gases. Thus,

$$\rho = \rho_{\rm a} + \rho_{\rm c} + \rho_{\rm v} + \hat{\rho} + \sum_i (\rho_i + \tilde{\rho}_i) \tag{4.2}$$

and the porosity Ψ is given by

$$\Psi = 1 - (\rho_{\rm a} + \rho_{\rm c})/\varrho_{\rm ice} - \sum_i \rho_i/\varrho_i - \hat{\rho}/\hat{\varrho} \tag{4.3}$$

where ϱ denotes the characteristic density of the non-porous solid phase (e.g. $\varrho_{\rm ice} = 917$ kg m^{-3} at 0°C; see also footnote in Section 3.2).

For gas diffusion, we showed in Chapter 3 that thermodynamic conditions within the nucleus result in very low gas densities. This allows the solution of Eq. (4.1) separately for each gas. The partial density of the i-th gas is obtained as a function of pressure from the ideal gas law, by assuming that the pore walls and the gas temperatures are the same due to the negligible thermal inertia of the gas, and by considering that only a fraction of the unit volume equal to the porosity Ψ can be occupied by gas.

Denoting by $\mathbf{J}_i$ the gas fluxes (with $\mathbf{J}_{\rm v}$, the flux of water vapour), by q_i the rates of sublimation (condensation) of the volatile ices, and by $\lambda(T)$ the temperature dependent rate of crystallization of the amorphous ice, we may write the set of mass balance equations as

$$\frac{\partial \rho_{\rm a}}{\partial t} = -\lambda(T)\rho_{\rm a} \tag{4.4}$$

$$\frac{\partial \rho_{\rm c}}{\partial t} = (1 - \sum_i f_i)\lambda(T)\rho_{\rm a} - q_{\rm v} \tag{4.5}$$

$$\frac{\partial \rho_{\rm v}}{\partial t} + \nabla \cdot \mathbf{J}_{\rm v} = q_{\rm v} \tag{4.6}$$

where $q_{\rm v}$ is the rate of sublimation (condensation) of water ice (vapour). Sublimation of amorphous ice may be neglected, since this ice exists only at very low temperatures. For the other volatiles we have

$$\frac{\partial \rho_i}{\partial t} = -q_i \tag{4.7}$$

$$\frac{\partial \tilde{\rho}_i}{\partial t} + \nabla \cdot \mathbf{J}_i = q_i + f_i\lambda(T)\rho_{\rm a} \tag{4.8}$$

Summation of these equations yields the mass conservation law:

$$\frac{\partial \rho}{\partial t} + \nabla \cdot (\mathbf{J}_{\mathrm{v}} + \sum_i \mathbf{J}_i) = 0 \tag{4.9}$$

The evolution of the porosity is obtained, locally, from Eq. (4.3). The evolution of the pore sizes (or the average pore radius, r_{p}) may be expressed symbolically as

$$\frac{\partial r_{\mathrm{p}}}{\partial t} = f(q_{\mathrm{v}}, q_n, P) \tag{4.10}$$

where the index n runs over *all* volatile species, and P represents the total local gas pressure.

4.2 Energy Balance

There are several sources and sinks of energy present in a comet nucleus. The energy balance of the nucleus depends strongly on the material and nature of the matrix in the interior and on the nature and morphology of its surface. Up to now there are no measured data available for the interior of the nucleus. Only a few data for the surface of the nucleus have been obtained. These are mostly from Giotto and DS1 spacecraft measurements. However, one can reasonably expect an irregular shape and probably a dark surface for most comet nuclei.

Internal energy sources include energy released by the decay of radionuclides and energy released by the phase transition from amorphous to crystalline water ice. The phase transition is a highly exothermic and irreversible reaction (see Section 3.2). The heat released is about 1620 J/g-mol (Ghormley, 1968) and is also a function of time (Schmitt et al., 1989). If some minor amount of a volatile ice such as CO is trapped in amorphous water ice, it will also influence the energy release. For a short-period comet, this energy source is probably negligible because the nucleus may have warmed up above the transition temperature during its many passages through the inner Solar System. Energy released by the decay of radionuclides in the nucleus is negligible for present comet observations, but may play a role in the thermal history of comets. Energy may also be released by condensation of vapours within the nucleus. This energy source plays a dominant role in porous, icy bodies and is a function of the change in enthalpy of sublimation and the rate of condensation. Such energy release is a fraction of the energy that has been conducted into the interior of the nucleus.

In porous, icy bodies heat is transferred into the interior of the body not only by solid state heat conduction in the icy matrix but also by vapour flowing through the porous material, the flow being driven by vapour pressure gradients. The transport mechanism is diffusion. There are two processes transferring energy by inward flowing gas into the body. The first process is energy transport of sensible heat and heat exchange to the matrix, because the inward flowing gas is warmer than the solid matrix. In the second, process energy is transferred to the matrix at several depths in the body through latent heat liberated by condensation of the inward flowing gases. However, this energy transfer is only over a very small distance below the sublimation front. The energy conservation equation for a multi-component system of ideal gases is

$$\frac{\partial}{\partial t}(\rho u)+\nabla\cdot(\mathbf{F}+\sum_n u_n\mathbf{J}_n) = -\sum_n q_n\Delta H_n+\lambda(T)\rho_{\mathrm{a}}(1-\sum_i f_i)\Delta H_{\mathrm{crys}}+\hat{\rho}\dot{E}_{\mathrm{rad}} \tag{4.11}$$

where ΔH denotes change in enthalpy of sublimation and ΔH_{crys} is the energy released in the exoergic phase transition of ice. The implicit assumption is that all the components of the nucleus are locally in thermal equilibrium and hence a unique local temperature may be defined. The energy per unit mass, u, is given by

$$\rho u = \sum_n \rho_n u_n + \hat{\rho}\hat{u} \tag{4.12}$$

The specific energies, u_n, may be obtained as functions of temperature, T, by means of heat capacities, c_n, $u_n = \int c_n dT + const.$ Also described through a source term in Eq. (4.11) is radiogenic heating, $\dot{E}_{\mathrm{rad}}$, usually by ^{26}Al, which may be released during the early evolution of comet nuclei. Formulations of source terms describing this process can be found, for example, in Prialnik and Podolak (1995) and De Sanctis et al. (2001). A discussion of the effects of radiogenic heating on the evolution of a comet nucleus can be found in Chapter 5.

Finally, Eq. (4.11) combined with Eqs. (4.9) leads to the heat transfer equation :

$$\begin{aligned}\rho c\frac{\partial T}{\partial t} - \nabla\cdot(\kappa\nabla T) \quad &+ \quad \sum_n c_n\mathbf{J}_n\cdot\nabla T \\ &= \quad -\sum_n q_n\Delta H_n + \lambda\rho_{\mathrm{a}}(1-f)\Delta H_{\mathrm{crys}} + \hat{\rho}\dot{E}_{\mathrm{rad}}\end{aligned} \tag{4.13}$$

where ρc is defined in a manner similar to Eq. 4.12. The value of κ for the porous matrix is computed by means of various models for the effective Thermal conductivity of an inhomogeneous medium; some of the formulae used by different authors will be listed in Section 4.9.

We note that Eq. (4.13) implies local thermodynamic equilibrium (LTE), meaning that, locally, all components have the same temperature; the temperature of the gas conforms almost instantaneously to that of the solid matrix. Some models do not include terms describing heat transport by the gases flowing through the pores because the heat capacity of the solid phase is much larger than that of the gases. This simplification is often justified (see, however, Prialnik 1992). Equation (4.13) shows that heat transfer and gas diffusion are not independent processes. Thus, the corresponding equations are coupled.

4.3 Momentum Balance

From kinetic gas theory (e.g. Kittel and Kroemer, 1980) the speed from the equation of motion for an ideal gas flowing through a porous medium in the Knudsen regime in which the mean free path of the gas molecules is much larger then the pore radius, is

$$\boldsymbol{v}_n = -C\left(\sqrt{T}\nabla \ln \rho_n + \nabla\sqrt{T}\right) \tag{4.14}$$

The constant C in Eq. (4.14) depends strongly on the model assumed for the porous medium. If the ice matrix can be described by a large number of parallel tubes (e.g. Mekler et al., 1990), one obtains, assuming diffuse reflection of the molecules on the walls of the tubes,

$$C = \frac{8\Psi}{3\xi^2}\, r_{\mathrm{p}}\sqrt{\frac{\mathcal{R}_{\mathrm{g}}}{2\pi\mu}} \tag{4.15}$$

Here ξ is the tortuosity (ratio of the length of the tubes to the thickness of the porous layer) characteristic of the porous medium structure, $\mathcal{R}_{\mathrm{g}}$ the universal gas constant, and μ the molecular mass of the gas molecules. The porosity for the tube model can be described by

$$\Psi = 1 - \frac{\rho}{\rho_{\mathrm{o}}} \tag{4.16}$$

where ρ_{o} is the bulk density of the homogeneously mixed material of dust and ice and ρ the bulk density of the porous ice body. Its density changes as a function of depth because of sublimation of ices and condensation of vapours.

4.4 Boundary Conditions

The set of evolution equations must be supplemented by initial and boundary conditions. In the following, we again assume a spherical nucleus. For the heat transfer equation, the boundary conditions refer to the flux. The flux is given by

$$F(r) = -\kappa \frac{dT}{dr} \tag{4.17}$$

on the open interval $r_0 < r < R$, where $r_0 = 0$ when the entire comet is considered, or $0 < r_0 < R$, when only an outer layer is considered in a plane parallel calculation. At the ends of this interval we have

$$F(r_0) = 0 \tag{4.18}$$

$$F(R) = \epsilon\sigma T^4(R,t) + Q\Delta H - (1-\mathcal{A})\frac{F_\odot}{r_{\mathrm{H}}^2(t)}\cos\zeta \tag{4.19}$$

where $\mathcal{A}$ is the albedo, $F_\odot$ is the solar flux at 1 AU from the Sun, $r_{\mathrm{H}}(t)$ is the heliocentric distance (in AU), ϵ is the emissivity, σ is the Stefan-Boltzmann constant, and Q is given by Eq. (3.1). The local solar zenith angle, ζ, which also depends on t through the spin of the nucleus, is given by

$$\cos\zeta = \cos\theta\cos\Omega\cos\delta + \sin\theta\sin\delta \tag{4.20}$$

where δ is the declination (see, e.g. Sekanina 1979a, Fanale and Salvail 1984). The function $r_{\mathrm{H}}(t)$ is given in terms of the changing eccentric anomaly, E, by the familiar celestial mechanics equations

$$t = \sqrt{a^3/(GM_\odot)}\,(E - e\sin E) \tag{4.21}$$

$$r_{\mathrm{H}} = a(1 - e\cos E) \tag{4.22}$$

Similarly, the boundary conditions for the mass equations assume that the gas fluxes vanish at $r = r_0$. At the surface $r = R$ the partial pressures are those exerted by the coma gases. In the lowest approximation, they may be assumed to vanish, i.e. $P_n(R,t) = 0$. We note that when the entire comet is considered, mass and heat fluxes must vanish at the centre. However, at the lower boundary of a finite layer other boundary conditions may be assumed (for example, a fixed temperature and the corresponding vapour pressures), but only by adopting vanishing fluxes, are energy and mass conservation secured.

In a porous medium the surface is not well defined and a surface layer of finite (rather than vanishing) thickness provides the outflowing vapour. Mekler et al. (1990) have shown that the surface layer, where most of the vapour is generated, is just the thermal skin depth, i.e. considerably thinner than the layer of ice that is lost by a comet nucleus during a perihelion passage. We are thus faced with two vastly different length scales – for the surface layer and for the interior – with different timescales. On the evolutionary timescale of the comet, the thin boundary layer may be assumed to be in quasi steady-state. Its ice may be assumed to have crystallized. The gas fluxes from the interior may be taken as constant and their contribution to heat conduction may be neglected. In addition, plane parallel geometry is justified in this case and hence the equations that have to be solved near the surface as a function of depth, z, are

$$dJ_n(T, P_n)/dz = q_n \tag{4.23}$$

$$dF(T)/dz = -q_n(T, P_n)\Delta H(T) \tag{4.24}$$

The boundary conditions for this layer at R are given by Eq. (4.19) and at the lower boundary by a temperature. This procedure, suggested by Prialnik (1992), was also adopted by Tancredi et al. (1994).

If the left side of Eq. (4.19) is replaced by $-\kappa\frac{dT}{dr}\mid_R$, the familiar power balance equation at the surface is recovered

$$(1-\mathcal{A})\frac{F_\odot}{r_{\rm H}^2(t)}\cos\zeta = \kappa\frac{dT}{dr}\mid_R + \epsilon\sigma T^4(R,t) + Q\Delta H\,. \tag{4.25}$$

For the differential equation, this makes no difference. In a difference scheme, however, the two formulations lead to different formulations of the boundary condition. The best solution for a numerical scheme is to adopt a very fine mesh near the surface, or use the boundary layer procedure described above.

The initial conditions must be guessed. Since below a depth of the order of metres to several tens of metres, the comet nucleus as a whole never reaches a steady state, the initial conditions play an important role. This is the reason for the importance attached to the early evolution of comet nuclei at large distances from the Sun, which determines the interior conditions of comet nuclei when they enter the inner planetary system and become active.

4.5 Initial Structure and Parameters

In order to follow the evolution of the material structure of a comet nucleus by means of the equations displayed in earlier sections of this chapter, including the physical processes described in Chapter 3, we still need to specify several parameters:

- *Defining parameters.* These identify a comet and include orbital parameters (semimajor axis, a, and eccentricity, e), the nucleus size, given by an effective radius, R, its mass, M, or bulk density and its spin period, $P_{\rm spin}$. All of these quantities may be determined observationally.

- *Initial parameters.* These are required for the solution of the time-dependent equations and reflect the previous history of the comet nucleus. They include the initial temperature, T, or temperature profile, compositional parameters, such as the mass fractions of the different ices and dust, and structural parameters, such as porosity, Ψ average pore size, r_{p}, or pore size distribution, as well as the nature of the water ice, whether it is crystalline or amorphous. In fact, one of the main goals of modeling is to determine these properties by comparing their predicted behaviour to actual observations. Regardless of details, initial homogeneity is adopted as a rule.

- *Physical parameters.* These are parameters related to the various physical processes discussed in Chapter 3. They supplement the parameters in the above groups and, in principle, should have been investigated in them, had the detailed structure of comet nuclei been better understood. Among them are albedo, $\mathcal{A}$, emissivity, ϵ, thermal conductivity coefficients, κ, tensile strength, and so on. These parameters can be determined by laboratory experiments.

Most of the parameters in the second and third categories are not directly known, but are only inferred from observations and laboratory experiments. Some of the parameters are based on common sense or "tradition." Various comet modelers assume similar values. For other parameters, however, the range of values adopted by different modelers can be quite large.

Gas and dust release rates and the dust particle indexDust particle mass distribution measured in the coma are not directly linked to the nucleus composition (see, e.g. Huebner and Benkhoff, 1999). A few relevant laboratory experiments have been carried out on analogue materials. However, the behaviour of complex cometary mixture at extreme conditions of temperature and pressure are still largely unknown and can only be extrapolated or inferred.

For values such as albedo, density, and dust-to-ice mass ratio, it is possible to use Giotto mission findings from Comet 1P/Halley as well as ground-based observational data. Initial temperature, porosity, and mean pore radius depend on hypotheses for the characteristics of comet matter, its origin, and its evolution. As for the amount of various ices present in the starting composition, modelers still refer to coma observations or derive their initial composition from studies on Solar System formation and evolution (see, e.g. Crovisier, 1999). Experimental results exist about the amount of gas that can be trapped in amorphous ice (Bar-Nun and Owen, 1998). The phase (amorphous or crystalline) in which water ice can be found at different depths is still very uncertain and much debated. It depends on many assumptions: the formation zone in the Solar System, formation processes, hypotheses about the nature of the material and also nucleus size, age, and history of evolution. While typical Jupiter family comets could be completely crystalline, the presence of amorphous ice close to the surface may be possible on a 'new' long-period comet such as Hale-Bopp (C/1995 O1) (Bockelée-Morvan and Rickman, 1998).

The dust size distributions observed in comet tails will be different from that in the nucleus: the larger particles, when ejected from the nucleus, can undergo destructive processes such as fragmentation and interaction with the escaping gases and plasma, producing a distribution having an excess mass in smaller particles with a power law distribution (Brin and Mendis, 1979). Particles observed in the visual and IR ranges of the spectrum are the smaller ones; larger particles are observed only by radar (Harmon et al., 1999).

The particles sampled by the instruments on board the Giotto and Vega spacecraft are not representative of bulk distribution in the nucleus, because dust impact analyzers were sensitive only to small particles. The size distribution was poorly constrained by such experiments, which can only be representative of emitted dust properties and not of nucleus bulk properties. There is evidence that there are some large particles in comets. The Dust Impact Detection System (DIDSY) on board the Giotto spacecraft measured particle sizes of about 10^{-4} g; particles as large as 10^{-2} g perturbed the spacecraft. In comet trails discovered by the IRAS satellite, most of the infrared flux is contributed by millimetre-sized particles (Sykes et al., 1986, 1990). Radar observations show that comets such as IRAS-Araki-Alcock, 1P/Halley, and Hyakutake emitted centimetre-sized particles (Harmon et al., 1999). In contrast, the coma of Comet Hale-Bopp (C/1995 O1) was dominated by very small dust particles.

For all of these reasons, the size distributions of dust particles in the nucleus cannot be the same as those measured by observers in the comae of comets. The large particles may be the result of sintering in the outer layers of a comet nucleus, i.e. they do *not* represent the original particle size distribution; they are more likely the result of comet nucleus evolution, consistent with laboratory experiments such as KOSI.

The temperature-dependent thermal conductivity coefficient of the porous mixture in comet nuclei is usually derived from the conductivities of the different components taking into account the porosity of the medium. As for the conductivity of crystalline ice, most modelers agree with the value introduced by Klinger (1980). For the amorphous ice, Klinger (1980) derived an expression using the classical phonon model for solids. However, experimental data published by Kouchi et al. (1992) give a value four to five orders of magnitude lower. Experimental data about low density amorphous ice published by Andersson and Suga (1994) give values higher than those published by Kouchi et al. and by Klinger. The thermal conductivity appears to also depend on the density of the amorphous ice. As can be inferred, there is a wide range of uncertainty.

Comet dust parameters are deduced from the inferred composition (silicates and organic refractories) and by analogy with terrestrial and lunar materials. The range of conductivities adopted for dust in comet models varies over a wide range, reflecting the uncertainty about the real nature of refractory materials and their structure in comets.

4.6 Flow Regimes and their Transitions

The flow regime for a gas in a porous medium is determined by the *Knudsen* number [see Eq. (3.17)]. In the hard-sphere approximation it is given by

$$\mathrm{Kn} = \frac{m}{\sqrt{2}\rho\pi d^2 2r_\mathrm{p}} \tag{4.26}$$

where m is the average mass of gas molecules, ρ the gas density, d the molecular diameter, and r_p the pore radius. When the pore size is small, Kn is larger than unity and the flow of gas is free molecular (Knudsen) flow, given by

$$\mathbf{J}_\mathrm{Kn} = -\frac{8}{3} f_\phi \left(\frac{m}{2\pi k}\right)^{1/2} \nabla(P/\sqrt{T}) \tag{4.27}$$

For a porous structure of tortuous cylindrical capillaries (Mekler et al., 1990), $f_\phi = \Psi r_\mathrm{p}/\xi^2$, where r_p is the average capillary radius and ξ is the tortuosity. Hence the flux of each gas is given by

$$\mathbf{J}_\mathrm{Kn} = -\frac{8}{3}\frac{\Psi r_\mathrm{p}}{\xi^2} \left(\frac{m}{2\pi k}\right)^{1/2} \nabla(P/\sqrt{T}) \tag{4.28}$$

where P is the partial pressure. However, when the pore size is increased, the condition $\mathrm{Kn} < 1$ applies and the flow becomes a continuum (Poiseuille) flow

$$\mathbf{J}_\mathrm{Po} = -\frac{3}{32}\Psi r_\mathrm{p}^2 d^2 \left(\frac{m\pi^3}{2k^3}\right)^{1/2} \frac{P}{T^{3/2}} \nabla P \tag{4.29}$$

For the intermediate regime, $\mathrm{Kn} \approx 1$, slip-flow applies and semiempirical interpolation formulae are commonly used

$$\mathbf{J} = a_1 \mathbf{J}_\mathrm{Kn} + a_2 \mathbf{J}_\mathrm{Po} \tag{4.30}$$

known as the Adzumi equation (see Scheidegger, 1963, for a detailed discussion), with *fixed* (empirically determined) coefficients a_1 and a_2. Each of the Eqs. (4.28)–(4.30) is suitable for a set of given conditions. However, when Kn is neither uniform nor constant, as in the case of an evolving comet nucleus, the above formulae do not ensure a smooth transition between the two flow regimes as the Knudsen number changes from $\mathrm{Kn} \gg 1$ to $\mathrm{Kn} \ll 1$. Therefore, we have to adopt a slightly modified approach. We note that the gas released upon crystallization flows through an almost isothermal medium (Prialnik, 1992). Thus the Knudsen flow equation reduces to

$$\mathbf{J}_{\mathrm{Kn}} \approx -\frac{8}{3}\frac{\Psi r_{\mathrm{p}}}{\xi^2}\left(\frac{m}{2\pi kT}\right)^{1/2} \nabla P \tag{4.31}$$

By substituting Eq. (3.17) and Eq. (4.31), into Eq. (4.29), we obtain

$$\mathbf{J}_{\mathrm{Po}} = \frac{9\pi\xi^2}{512}\frac{1}{\mathrm{Kn}}\mathbf{J}_{\mathrm{Kn}} \tag{4.32}$$

We now use an interpolation similar in form to Eq. (4.30)

$$\mathbf{J} = \left(1 + \frac{9\pi\xi^2}{512}\frac{1}{\mathrm{Kn}}\right)\mathbf{J}_{\mathrm{Kn}} \tag{4.33}$$

which varies continuously from $\mathbf{J}_{\mathrm{Kn}}$ for $\mathrm{Kn} \gg 1$ to $\mathbf{J}_{\mathrm{Po}}$ for $\mathrm{Kn} \ll 1$.

When two gases (say H_2O and CO) are flowing through the same medium, they are treated independently; namely each flux is computed according to Eq. (4.33). This is strictly correct in the Knudsen regime, and in the case of immiscible flows. Fortunately, the flux of initially trapped gas dominates in the interior of the nucleus, while the H_2O flux becomes dominant in a very thin outer layer of the nucleus, where most of the sublimation occurs. The interaction between gases may therefore be neglected. At high flow rates, turbulence may arise and Eq. (4.33) may no longer hold (Scheidegger, 1963). This is indicated by the Reynolds number exceeding a critical value of order 1000. When the Reynolds number is routinely evaluated during calculations of comet nucleus evolution, it is always found to remain smaller than 100. Therefore Eq. (4.33) may be safely applied.

Finally, we note that the evolution equations are coupled through the source terms and the gas fluxes, which are functions of both temperature and pressure. A great simplification for calculating gas densities and fluxes may be achieved by replacing the gas pressures by their saturation values, which are functions of the temperature. This is an excellent approximation for the interior of the nucleus where the pressures are close to saturation values; it implies, however, that there is sufficient material in both phases to allow instantaneous adjustment and may not be applicable to traces of volatiles. With this approximation, only the heat transfer equation remains to be solved for the evolution of the temperature distribution, where the mass conservation equations are regarded as temperature-dependent expressions for the source terms.

4.7 Dust Flow and Mantling

In this section we discuss a very rudimentary and oversimplified model assuming spherical, nonfragmenting dust particles flowing in straight tubes in the nucleus of a comet. In a more realistic model with tortuous and interconnecting tubes, dust particles cannot manœuvre curves and kinks. Since voids in the matrix material are of about the same size as dust particles, they cannot travel further than a few particle radii before they collide with the tube wall and are stopped. Every time a particle is stopped, the process described here will have to start afresh. Also, particles are nonspherical and a more realistic treatment of their entrainment by gas should consider their ratio of cross section per unit mass (see Section 3.5.1). Dust entrainment in the coma has been considered by Huebner (1970).

In this very simple model, as ice sublimates from the porous matrix of the nucleus, either near the surface or in the interior, dust particles are released into the gas (vapour) stream and entrained by it. The flow of dust within and out of the nucleus must, therefore, be considered. The problem is twofold: first, one has to model the rate of dust release, which may be positive – when dust particles are loosened from the solid matrix – or negative – when particles stick to the pore walls or block the pores. Secondly, the flow speed of dust particles has to be assessed. Since it is expected to depend on the particle size, one may have to consider a differential flow. The results expected from any dust flow model are the particle size distribution of the ejected dust and the changing pore structure of the medium through which the dust flows. For example, the large dust particles left behind on the nucleus surface form a dust mantle, which, in turn, affects the rate of heat and gas flow at the surface.

Different models and approximations have been suggested over the years to deal with the problem of dust flow and dust mantling [see Rickman et al. (1990) and references therein]. In the following we only consider different possible approximations to the dust flux that fit into the general scheme of comet nucleus evolution. The basic assumption will be that the volatiles are everywhere in thermal equilibrium with the dust (see Horanyi et al., 1984). We thus have to determine $\hat{\mathbf{J}} = \hat{\rho}\hat{\mathbf{v}}$ and the source term $\hat{q}$.

We proceed by considering the dust velocity. As we have seen, the flow of gas through porous comet nuclei is, typically, a free molecular (Knudsen) flow, the collision mean free path of the gas exceeding the average pore size. The drag force on a dust particle of radius $\hat{r}$ in the Knudsen regime is

$$\mathcal{F} = \frac{2\pi\hat{r}^2\rho v_{\mathrm{th}}}{\tilde{\psi}}(v - \hat{v}) \tag{4.34}$$

where v is the gas velocity, $\hat{v}$ is the dust particle velocity, $\tilde{\psi}$ is a dimensionless coefficient that depends on the drag coefficient, the accommodation coefficient, the particle shape, and other quantities. For $\hat{r}/\ell \to 0$, $\tilde{\psi} \to 1.154$ (Öpik, 1958), and v_{th} is the thermal velocity of the gas molecules. Substituting these relations in Eq. (4.34) and dividing by the mass of the compacted, spherical dust particle, we obtain the particle's acceleration

$$\frac{d\hat{v}}{dt} = \frac{1}{\tau(\hat{r})}(v - \hat{v}) \tag{4.35}$$

where $\hat{\varrho}$ is the density of the particle and the characteristic time τ, a function of the dust particle radius for given flow conditions, is

$$\tau \approx \frac{\hat{\varrho}}{\rho}\sqrt{\frac{m}{kT}}\;\hat{r} \tag{4.36}$$

The dust particle velocity (assuming a constant gas velocity) is thus

$$\hat{v} = v(1 - \mathrm{e}^{-t/\tau}) \tag{4.37}$$

For conditions that are typical of cometary interiors (a few metres to a few tens of metres below the surface), where crystallization of amorphous ice takes place and trapped gas is released, or where volatile species (such as CO) sublimate, we find $\tau \approx 0.5(\hat{r}/1\mu\mathrm{m}$ s, so that even 10 μm particles can reach 90% of the gas speed in about 10 s. For gas speeds typical of such conditions, the particle will have traveled during that time interval a distance of much less than 1 m. This length scale is considerably smaller than the typical length scale over which conditions change in the interior of the nucleus. Near the surface, where the main driving force is provided by water vapour sublimating from the pore walls, conditions are much more favourable.

So far we have neglected the effect of gravity. A gravitational acceleration g would change the speed, Eq. (4.37), to

$$\hat{v} = (v - g\tau)(1 - \mathrm{e}^{-t/\tau}) \tag{4.38}$$

assuming the positive direction to be radially outward. Hence the effect is negligible as long as $g\tau \ll v$. For a constant nucleus density ρ_{N}, we have

$g = (4\pi/3)G\rho_{\rm N}R$, where R is the radius of the nucleus (since we deal with depths that are much smaller than R). Thus the condition for a negligible effect of gravity is

$$R\hat{r} \ll \frac{3}{4\pi G\rho_{\rm N}\hat{\varrho}} v\rho\sqrt{\frac{kT}{m}}$$

For conditions typical for interiors of comet nuclei (resulting in the above estimate of τ), assuming a nucleus density of 500 kg m^{-3}, we obtain

$$\left(\frac{R}{1\mathrm{km}}\right)\left(\frac{\hat{r}}{1\mu\mathrm{m}}\right) \ll 2\times 10^4$$

a condition that is amply satisfied, unless we deal with very large dust particles or very large comets.

Thus, as a first approximation, we may assume the dust velocity to be (approximately) equal to the gas velocity. Nevertheless, because of the size of dust particles, their trajectories may be different from that of the gas. Large dust particles may "get caught" in the pores or may drift away in a different directions until they find a sufficiently wide path to accommodate them. Different models, based on statistical approaches, that account for the interaction between pores and particles of comparable sizes have been considered by Podolak and Prialnik (1996) and by Shoshani et al. (1997). As the effective rate of flow of dust particles depends on the particle size, we may assume in numerical calculations, that the dust particle radii are distributed over a discrete range $\hat{r}_1$, $\hat{r}_2$, $\ldots \hat{r}_N$, according to some distribution function $\psi(\hat{r})$ (such as a power law). The mass density of dust particles of radius $\hat{r}_i$ is then given by

$$\hat{\rho}_i = \hat{\rho}\frac{\psi(\hat{r}_i)\hat{r}_i^3}{\sum_{m=1}^N \psi(\hat{r}_m)\hat{r}_m^3}$$

where $\sum\hat{\rho}_i = \hat{\rho}$. If the size of dust particles remains unchanged (i.e. ignoring possible fragmentation or coalescence of dust particles), particles in each size category may be treated as independent species. Dust fragmentation has been modeled by Konno and Huebner (1990, 1991).

The local flux of dust particles of radius $\hat{r}_i$ is therefore given by

$$\hat{\mathbf{J}}_i = \beta_i\hat{\rho}_i\mathbf{v}$$

where the coefficient β_i remains to be determined by the flow model ($\hat{\mathbf{J}} = \sum_i \hat{\mathbf{J}}i$). For example, Podolak and Prialnik (1996) adopt

$$\beta_i \propto \log\left[1-\psi(\hat{r}_i)\right]/\log\left[(1-\psi(\hat{r}_i))\psi(\hat{r}_i)\right]$$

The mass conservation equation for these particles is

$$\frac{\partial \hat{\rho}_i}{\partial t} + \nabla \cdot \hat{\mathbf{J}}_i = 0 \tag{4.39}$$

The approximation of equal (or proportional) velocities for the gas and the dust is valid only for particles with radii smaller than the critical radius determined by the balance of the drag force and local gravitational force, Eqs. (3.48, 3.49). We may thus assume larger particles to be effectively blocked. The local size distribution is changed by the different rates of flow of particles of different sizes. Similarly, the size distribution of the ejected particles differs from the original one in the nucleus and is apt to change following the internal rate of gas release. Note that there is no source term in Eq. (4.39); the implicit assumption in this simple approximation is that any dust particle that can be entrained (allowance being made for the critical radius and the local average pore radius) is entrained by the gas. The effect of a source term is artificially included in the factor β_i, allowing only a small fraction of the dust to be carried away by the gas.

Dust mantle formation may be modeled in a similar way (see Capria et al., 1996; Coradini et al., 1997a; De Sanctis et al., 1999; Capria et al., 2001). The particles are initially embedded in the porous ice matrix and as the ice sublimates from the surface, the embedded particles become progressively free and subject to the drag exerted by the escaping gas. They can be ejected from the surface or can accumulate to form a mantle. As a first approximation it may be assumed that all particles with radii smaller than the critical radius (Eq. 3.49), or cross section per mass (Eq. 3.48), are blown off and contribute to the dust flux, while those larger than the critical size accumulate on the surface to form the dust mantle. Given a dust particle size distribution and dust density, the amount of mass ejected at each time step may be calculated. One may keep track of the particle size distribution in the mantle, or else assume that particles are redistributed according to the prescribed law. When the surface layer is completely depleted of ice, the dust mantle is composed of particles of different sizes. This mantle layer is porous and the gases sublimating from the interior of the comet can flow through the pores.

The criterion for mantle formation may be refined by introducing a trapping mechanism (Shul'man, 1972; De Sanctis et al., 1999). On the surface, the interstices between them become too small to allow the escape of particles with smaller radii, even if these are smaller than the critical radius. In this way a large amount of small particles are trapped as well and contribute to the formation of the mantle. This effect may be important for small, fast-spinning nuclei, where the simple condition $\hat{r} < \hat{r}^*$ may not lead to mantle formation.

More advanced models, taking into account particle fragmentation (Konno et al., 1993) and nucleus surface topography are under investigation (Huebner, 2006).

4.8 Sublimation and Condensation in Pores

In the simple case of a single (average) pore size, we can calculate the changes in porosity and pore size caused by sublimation of water ice and condensation of water vapour (neglecting other volatiles). Adopting a model of tortuous capillaries, where N is the number of capillaries crossing a unit area, we have for the porosity

$$\Psi = N\xi\pi r_{\mathrm{p}}^2 \tag{4.40}$$

and for the surface area of the capillaries

$$S = N\xi 2\pi r_{\mathrm{p}} \tag{4.41}$$

(Mekler et al., 1990). Since

$$\dot{\Psi} = \frac{q_{\mathrm{v}}}{\varrho_{\mathrm{ice}}} \tag{4.42}$$

we have

$$\dot{\Psi} = N\xi 2\pi r_{\mathrm{p}}\dot{r}_{\mathrm{p}} = S\dot{r}_{\mathrm{p}} \tag{4.43}$$

which, when combined with Eqs. (4.41) and (3.1), yields

$$\dot{r}_{\mathrm{p}} = \frac{\mathcal{P}_n - P_n}{\rho_n}\sqrt{\frac{\mu_n}{2\pi\mathcal{R}_{\mathrm{g}}T}} \tag{4.44}$$

To obtain a more realistic description of the porous structure, we may assume the *initial* pore radii to be distributed over a discrete range $r_{\mathrm{p},1}$, $r_{\mathrm{p},2}$, $\ldots r_{\mathrm{p,M}}$, according to some distribution function $\psi(r_{\mathrm{p}})$, as in the case of the dust particles considered previously. If pores were to grow or shrink as a result of sublimation or condensation on their walls, the pore sizes in each category ($r_{\mathrm{p},i}$) would subsequently change, but the *relative* number of pores in each category could remain the same. Thus

$$\psi(r_{\mathrm{p}}) = \sum_i \psi_i \xi\pi r_{\mathrm{p},i}^2 \tag{4.45}$$

$$S = \sum_i \psi_i \xi 2\pi r_{\mathrm{p},i} \tag{4.46}$$

$$\dot{\Psi} = \sum_i \psi_i \xi 2\pi r_{\mathrm{p},i}\dot{r}_{\mathrm{p},i} \tag{4.47}$$

but since according to Eq. (4.44) $\dot{r}_\mathrm{p}$ is independent of r_p, $\dot{r}_{\mathrm{p},i}$ is the same for all i, and the relation $\dot{\Psi} = S\dot{r}_\mathrm{p}$ still holds. Hence Eq. (4.44) is still applicable for each i, meaning that narrow capillaries will tend to close before wide ones.

Cracking or fracture of the nucleus due to internal pressure could be modeled as an increase in the *number* of large pores at the expense of small ones (see Prialnik et al., 1993). Blocking of small pores by dust particles could be modeled similarly to narrowing of pores by condensation. Models of the changing pore structure during the evolution of comet nuclei are still an active area of research.

4.9 Effective Thermal Conductivity

When heat is transferred by conduction, Fourier's law applies

$$F = -\kappa \nabla T \tag{4.48}$$

where F is the heat flux, T is the temperature and κ is the proportionality factor called the *thermal conductivity*. Thermal conductivities of common materials (at standard temperature and pressure) range from 4×10^2 W/m/K (copper and silver) to 10^{-2} W/m/K (plastic foams). Heat is transported by electrons in metals and by lattice vibrations in crystalline solids. From a theoretical point of view, heat conduction can be considered as the diffusion of a phonon gas from a hot region, in which phonons are more numerous, to a cold region, in which phonons are less numerous. This is because the internal energy of a solid can be modeled as lattice vibrations and can be analyzed using the theory of harmonic oscillators. For practical applications, conduction can be considered as a problem of conductance or resistance, which leads to the electric analogy of a network of resistors in series and in parallel. The applied electric potential corresponds to the temperature and the electric current represents the heat flux. Parallel paths represent heat flows in mixtures of conductors and resistors simulating heat flux limiting processes.

Cometary material may be considered a heterogeneous porous mixture on various scales. The evaluation of the thermal conductivity for such a material is always a complicated problem, mainly because it depends on the microstructure. In the case of comets, this structure is not known. However, in order to obtain an analytical expression for the thermal conductivity of a heterogeneous material, one must adopt a model for its microstructure. In general, it may be shown that the *effective* conductivity of the mixture has an intermediate value between those of the single components and depends on the volume and distribution of each component. The thermal conductivity of low temperature ice, as found in comet nuclei, has been determined both experimentally and from theoretical considerations. The formulae provided by Klinger (1980, 1981) have gained widespread use.

Cometary material is highly porous. Porosity lowers the thermal conductivity, but it is unclear to what extent and in what way the correction depends on porosity and on the pore size distribution. It is important to note that pore structure (whether the pores are closed or interconnected) is important in the evaluation of thermal conductivity.

Generally, a porous medium may be regarded as a homogeneous two-phase material – one occupying a volume fraction Ψ and the other $1-\Psi$ – with two characteristic conductivities, κ_1 and κ_2, respectively. At large Knudsen numbers the effective conductivity in pores resulting from energy transferred by radiation may be derived as follows: consider two planes of material separated by a distance Δx, having temperatures T and $T+\Delta T$, respectively. Assuming the planes radiate as black bodies, the net flux passing from one to the other is

$$\Delta F = -[\epsilon\sigma(T+\Delta T)^4 - \epsilon\sigma T^4] \approx -4\epsilon\sigma T^3 \Delta T \tag{4.49}$$

Multiplying and dividing by Δx, and substituting the pore size for Δx on the right side, we obtain an expression similar to Fourier's law, with an effective conductivity of the pores

$$\kappa_\mathrm{p} = 4\epsilon\sigma r_\mathrm{p} T^3 \tag{4.50}$$

Let κ_p be the conductivity in a pore and κ_s the conductivity of the solid around the pores. Generally, $\kappa_\mathrm{p} \ll \kappa_\mathrm{s}$, the conductivity of the solid matrix material. Simple analytical approximations for the effective conductivity of a two-phase medium, expressed as $f_\phi \kappa_\mathrm{s}$ in terms of the ratio of the conductivities of the two phases, $f_\mathrm{ps} = \kappa_\mathrm{p}/\kappa_\mathrm{s}$, include: an arithmetic mean, $f_\phi = 1 + f_\mathrm{ps}$, which is inappropriate at high values of Ψ, if $f_\mathrm{ps} \ll 1$ (such as in the case when pores are one of the phases); a weighted geometric mean

$$f_\phi = f_\mathrm{ps}^\Psi \tag{4.51}$$

a parallel combination of the two phases

$$f_\phi = \Psi f_\mathrm{ps} + (1-\Psi) \tag{4.52}$$

or a series combination

$$f_\phi = \left[\frac{\Psi}{f_\mathrm{ps}} + (1-\Psi)\right]^{-1} \tag{4.53}$$

(Horai, 1991, and references therein).

The first to supply a formula for the Thermal conductivity of a *structured* mixed medium – a packed-sphere bed – was Maxwell (1873), based on an analogy between thermal and electrical conductivities. In fact, this approach provides upper and lower limits for the conductivity, obtained by exchanging the roles of the two phases. In terms of the ratio f_{ps} of the pore conductivity to that of the solid, the conductivity of the medium normalized to that of the solid varies between the lower limit

$$f_{\phi_L} = f_{\mathrm{ps}} \frac{2\Psi f_{\mathrm{ps}} + (3 - 2\Psi)}{(3 - \Psi) f_{\mathrm{ps}} + \Psi} \tag{4.54}$$

and the upper limit

$$f_{\phi_U} = \frac{(2 - 2\Psi) + (1 + 2\Psi) f_{\mathrm{ps}}}{(2 + \Psi) + (1 - \Psi) f_{\mathrm{ps}}} \tag{4.55}$$

These formulae are valid, however, only at low porosities, where $f_\phi \sim f_{\phi_U}$ and at high porosities, where $f_\phi \sim f_{\phi_L}$. It is noteworthy that for $f_{\mathrm{ps}} \ll 1$, the upper limit yields results that are very close to the correction suggested by Smoluchowski (1981) for the conductivity of a porous medium, $f_\phi = 1 - \Psi^{2/3}$, which was based on geometrical considerations. The restricted applicability of Maxwell's formula was discussed by Steiner and Kömle (1991b). An extension of Maxwell's formulae, valid to higher orders of the solid concentration $1 - \Psi$, was later provided by Rayleigh (1882). A similar approach, based on an analogy between thermal and electrical conductivity, was adopted by Russel (1935), leading to a formula similar to Maxwell's:

$$f_\phi = \frac{\Psi^{2/3} f_{\mathrm{ps}} + (1 - \Psi^{2/3})}{\Psi - \Psi^{2/3} + 1 - \Psi^{2/3}(\Psi^{1/3} - 1) f_{\mathrm{ps}}} \tag{4.56}$$

Russel's formula gives approximate results if the two media have very similar conductivities. Numerous other formulae followed, based on different assumptions regarding the structure of the porous medium in two or three dimensions (see, e.g. Cheng and Hsu, 1999). All of these formulae share the property that the effective conductivity is extremely sensitive to porosity either near $\Psi = 0$ or near $\Psi = 1$. The structures considered are simple if the sizes of the voids are fixed (although their shapes may vary) and the two phases may be interchanged.

A different correction to the conductivity of a porous medium results from consideration of the reduced area of contact between grains, approximated by the Hertz factor, f_{H}. However, this correction, which can be substantial (Squyres et al., 1985; Kossacki et al., 1994), should be included as a correction to $K_{\rm ice}$ itself, before the latter is modified to take account of the porous structure. Thus the effective conductivity is given by $\kappa_{\rm s} f_{\rm H} f_\phi(\Psi)$. Attempts to determine the Hertz factor by fitting laboratory data yielded a rather wide range of values, between 0.1 and 0.001. Similarly, if the solid material is composed of a mixture of ices or ices and dust, the conductivity of the mixture must be determined independently of the porosity.

The thermal conductivity of porous ice relevant to comet nuclei was considered by Steiner and Kömle (1991b), who use a similar, albeit more elaborate, version of Maxwell's procedure and arrive at a formula for the effective thermal conductivity of a mixture (ice and void) in terms of the individual conductivities of the components,

$$f_\phi = (1-\sqrt{1-\Psi})\Psi f_{\rm ps} + \sqrt{1-\Psi}\left[f_{\rm H} + (1-f_{\rm H})\frac{B+1}{B}\frac{f_{\rm ps}}{1+f_{\rm ps}}\right] \tag{4.57}$$

where B is a "deformation factor", which controls particle shape and is related to porosity, $B = 1.25[(1-\Psi)/\Psi]^{10/9}$.

Sirono and Yamamoto (1997) derive formulae both for the effective conductivity of porous ice and for a mixture of amorphous and crystalline ice, based on the effective medium theory. First $\kappa_{\rm H_2O}$ is derived taking into account amorphous and crystalline ice, then the conductivity of a particle with a silicate core $\hat\kappa(\kappa_{\rm H_2O})$ is calculated following Haruyama et al. (1993), and finally, the effective conductivity is obtained as

$$\kappa = \tfrac{3}{2}[\Psi - \tfrac{1}{3}] f_{\rm H} \hat\kappa \tag{4.58}$$

See also Section 2.2.

None of these studies consider a distribution of pore sizes. A porous medium, however, is characterized by at least two parameters: the porosity and the pore size, or the pore size distribution. How, if at all, does the latter influence the conductivity? This question was recently investigated by Shoshany et al. (2002) by means of a 3-D fractal, hierarchical model of a porous medium. They find that the thermal conductivity is lowered by several orders of magnitude at high porosities. The temperature dependence of the ice conductivity is preserved – the conductivity decreases with increasing temperature – so much so that, to a good approximation, the correction factor is temperature independent. They also find that, for a given basic porosity, the correction factor is the same when one passes from one medium to the next. Thus as larger and larger pores are added, the conductivity decreases by an increasing power of the basic correction factor. At very high porosities, $\Psi > 0.7$, below the *percolation limit* of the solid through the porous medium, the low radiative conduction through the pores becomes dominant. If the pores were filled with a perfect insulator, the conductivity would tend to zero under these circumstances.

The fractal medium considered corresponds to a power law pore size distribution with a power close to 3. A normal distribution of pore sizes is not well described by the model of a porous medium and the results may not apply there. However, it is rather well established that comets are made of an aggregation of grains and that the particle size distribution follows a power law with a power of order 3.5. We should, therefore expect the voids between the particles, that is the pores, to have a similar size distribution. As a simple example, if pores and particles are randomly distributed and their mean sizes are r_p and $\hat{r}$, respectively, then $\frac{1}{2} \lesssim r_\mathrm{p}/\hat{r} = [\Psi/(1-\Psi)]^{1/3} \lesssim 2$, if $\Psi \leq 0.9$. Hence, the fractal model is well suited for cometary material. The problem is to find a correspondence between a real porous material and the schematic fractal model, in order for the results to be applicable to realistic configurations. To this end, physical characteristics of a porous medium have been identified that can be translated into the model parameters used. If only the porosity is known, the model provides lower and upper limits to the correction factor by which the conductivity of the solid material should be multiplied,

$$(1-\Psi/\Psi_\mathrm{c})^{n(\Psi)} \leq f_\phi(\Psi) \leq (1-\Psi_\mathrm{min}/\Psi_\mathrm{c})^{n(\Psi_\mathrm{min})\ln(1-\Psi)/\ln(1-\Psi_\mathrm{min})} \tag{4.59}$$

where $n(\Psi) = 4.1\Psi + 0.22$, $\Psi_\mathrm{c} = 0.7$ is the percolation limit of the solid through the porous medium, and Ψ_min is the minimal fractal porosity allowed. The range is quite large at high porosity values. It may be reduced, however, if the minimal possible fractal porosity for the material can be estimated, as the upper limit in Eq. (4.59) decreases with increasing Ψ_min. For example, if $\Psi = 0.5$, the correction factor varies between a lower limit of 5.8% of the solid conductivity and an upper limit of $\sim 50\%$ for $\Psi_\mathrm{min} = 0.1$ and $\sim 20\%$ for $\Psi_\mathrm{min} = 0.3$.

If any two parameters of the pore size distribution are known, then a unique correction factor can be derived (provided the distribution may be described by a power law). Correction factors span several orders of magnitude, meaning that porosity has a very significant effect on the thermal conductivity and hence on the behaviour (evolution and activity) of comets.

To summarize, the simplest way to deal with the thermal conductivity problem in models of comet nuclei is to consider heterogeneity and porosity separately. Regarding cometary matter as a heterogeneous mixture in which the various components are arranged as parallel layers and heat is flowing along a direction perpendicular to the layers, we have for the solid matrix $\kappa = \Sigma\varphi_i\kappa_i$, where φ_i are the respective volume fractions. This should be corrected by one of the methods discussed above, which amounts to a correction factor usually varying between 0.1 and 0.01. To this one may add the radiative transfer through pores, although this would be a second order correction. In case that advection is neglected in the energy equation, another small correction may be introduced to account for heat conduction by the flowing gas (Steiner and Kömle, 1991b). One should bear in mind, however, that this effect may be significant under particular circumstances.

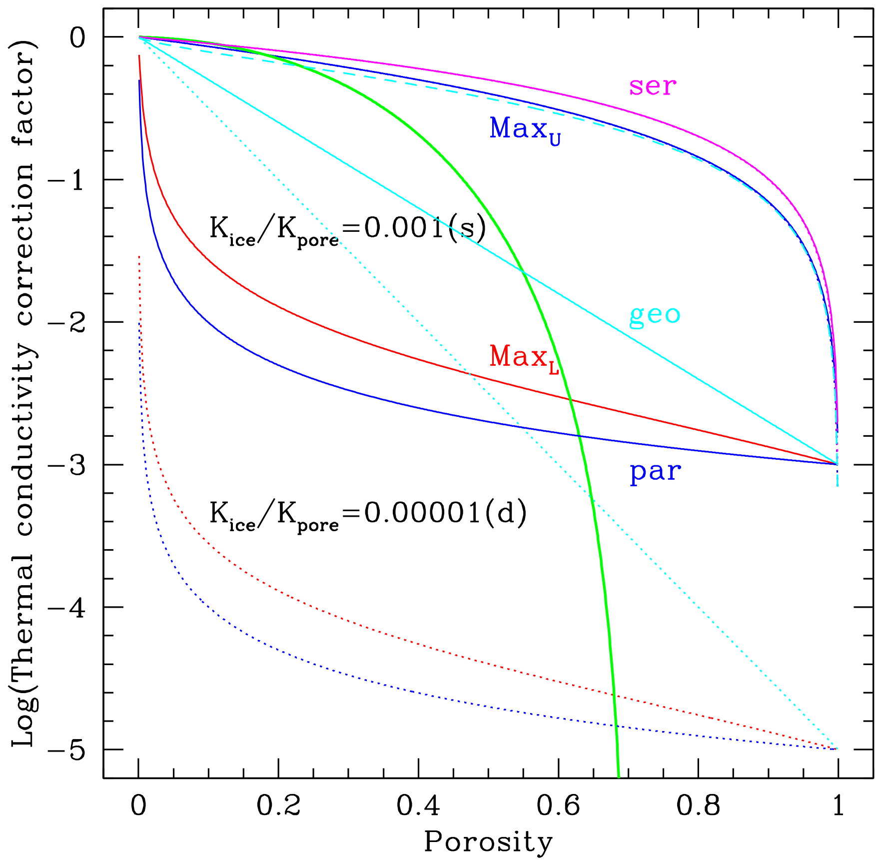

Figure 4.1: Thermal conductivity correction formulae: parallel combination (par), series combination (ser), geometrical mean (geo), Maxwell upper limit (Max$_U$) and lower limit (Max$_L$). Results are given for two ice to pore ratios: solid lines for the higher ratio(s), and dotted lines for the lower one (d). The green line represents the Monte Carlo fractal model.

— 5 —

Analytical Considerations

> "My opinion that there are unseen comets is disputed by many. One asks how I could know this. But I do not say that I know it, I only think it is probable. You believe that one should see them if they exist. I deny this. For, if they follow their course far away from the Earth, it is quite possible, if they are small, that one does not see them."
>
> Johannes Kepler, *Letter to J. G. Brengger*, Prague, 1608.

5.1 Early Models

The simplest models for gas production from a comet nucleus assume sublimation of ice from the surface of a spherical body and neglect heat diffusion into its interior. Levin (1943a,b) had proposed that the gas production in comets is caused by desorption of gases from dust on the surface of the nucleus. After Whipple (1950, 1951) proposed the icy conglomerate model for the comet nucleus, the first quantitative discussion of gas production from ices was by Squires and Beard (1961). Their main effort was to calculate the nongravitational forces on the nucleus from the outgassing in the solar direction only. Since parts of the nucleus surface are not normal to the incident radiation, the surface temperatures of these parts are lower and the rate of sublimation from them is smaller. Thus, Squires and Beard assumed that the comet nucleus was only a two-dimensional disk normal to the direction of the Sun. They equated the instantaneous solar insolation of the nucleus with the reradiation from the surface and the sublimation of the ices on the nucleus. Whipple (1963) ruled out gas production in a comet by desorption of gas from dust, because it would require a high degree of multilayer adsorption to explain the observed gas-to-dust ratio. Huebner (1965) made the first calculations assuming the incident solar energy is distributed uniformly over the surface of a spherical nucleus composed of a mixture of ices with an appropriately effective change in the enthalpy for sublimation and compared the results with the brightness of twenty comets. This provided the initial clues about the *real* rate of gas production from a comet nucleus and finalized the demise of the model for gas production by desorption from dust.

Improvements to this model were made by Delsemme and Miller (1971), who introduced a temperature-dependent change in the enthalpy of sublimation, and by Cowan and A'Hearn (1979), who considered the specific angular dependence of the surface elements with respect to the Sun. Delsemme and Miller (1971) also corrected the change in enthalpy of sublimation for vacuum conditions that are more appropriate for comets. Unfortunately, it appears that they made the correction twice and Cowan and A'Hearn (1979) made a fit to this over-corrected change in enthalpy of sublimation for water (see Fig 5.1). Appendix B gives a modern fit for the vapour pressure and the internally consistent change in enthalpy for sublimation into vacuum.

The instantaneous energy balance on a unit of area at solar zenith angle, ζ, on the surface of a comet nucleus, neglecting heat transport into the interior, is

$$\frac{F_{\odot}(1-\mathcal{A})\cos\zeta}{r_{\mathrm{H}}^2} = \epsilon\sigma T^4 + Q_i \Delta H_i \tag{5.1}$$

Here, ϵ is the IR emissivity (usually set equal to $1-\mathcal{A}$, where $\mathcal{A}$ is the visual albedo) and Q is the mass gas production rate per unit area and per unit time. The gas production rate is $Z_i = m_i^{-1} Q_i$, where m_i is the mass of a gas molecule of species i. The observed gas production rate for a comet is $Z = \sum_i Z_i$ times the effective (active) area on the nucleus. The flux of molecules at number density n_i striking unit surface area is

$$Z_i = n_i \frac{v_{\mathrm{th}}}{4} \tag{5.2}$$

where v_{th} is the thermal speed (mean gas speed of the Maxwell speed distribution function) at temperature T. It is *not* the mean (centre of mass) speed of the escaping gas. The mean gas speed radially away from the surface is (Huebner and Markiewicz, 1993, 2000; see also Section 3.4.1)

$$\langle v_{\mathrm{r}} \rangle = \frac{\pi}{4} v_{\mathrm{th}} \tag{5.3}$$

Thus, the surface temperature and the gas production rate are related through the vapour pressure

$$Z_i = v_{\mathrm{th}} \frac{P_i}{4kT} = \frac{P_i}{\sqrt{2\pi m_i kT}} \tag{5.4}$$

With the aid of Eqs. (5.2) and (5.3), Eqs. (5.1) and (5.4) can be solved simultaneously for Z_i and T, if the vapour pressure is known as a function of temperature. The species i of prime interest on the surface of the nucleus is H_2O. In early work, starting with Huebner (1965) until Cowan and A'Hearn

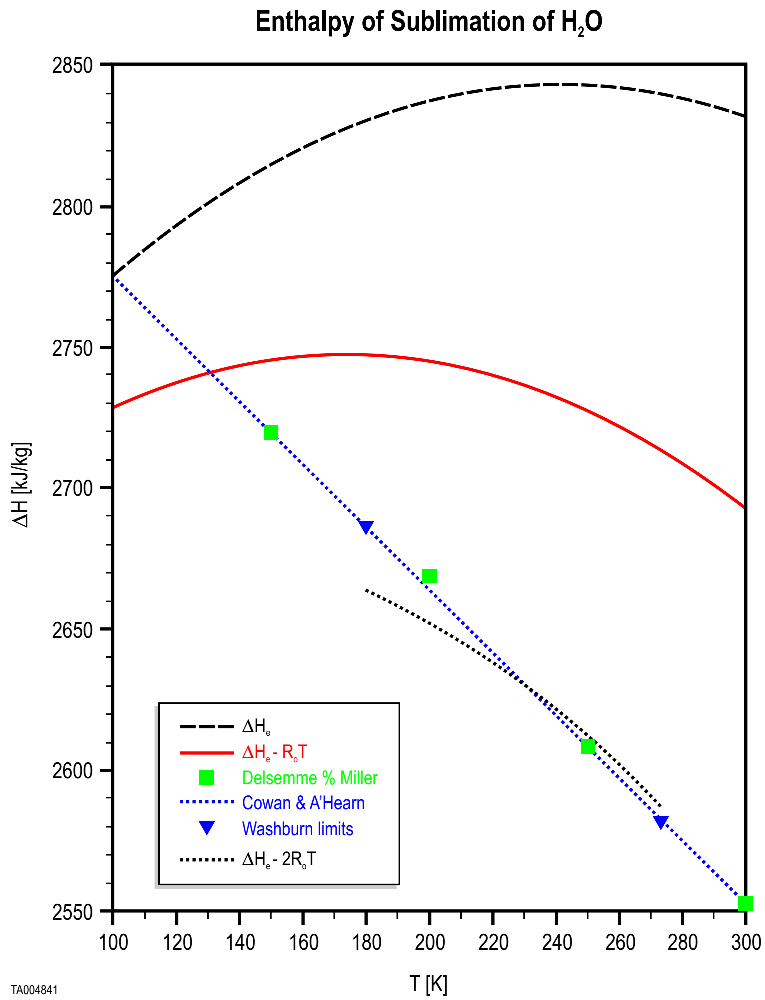

Figure 5.1: Change in enthalpy of sublimation of water ice. The black dashed curve is the change in enthalpy of sublimation of water ice under equilibrium conditions (Gibbins, 1990). The solid red curve presents this correct change in enthalpy of sublimation into vacuum. The green squares represent the change in enthalpy for sublimation into vacuum as obtained by Delsemme and Miller (1971) based on data from Washburn (1928). Note that two points are outside the limits of validity of the Washburn data, indicated by blue triangles. The blue dashed curve is the fit by Cowan and A'Hearn (1979) to the data of Delsemme and Miller. The black dotted curve has been corrected twice for sublimation into vacuum using the data of Gibbins. The similarity between the blue and black dotted curves leads us to believe that Delsemme and Miller made the correction twice.

(1979) the "fast rotator" ("spherical average") approximation was in vogue.[1] It assumes that the incident solar energy is distributed uniformly over the spherical surface of the nucleus, i.e. that $\cos\zeta = \pi R^2/\left(4\pi R^2\right) = 1/4$. This corresponds to $\zeta \approx 75°$. This angle is usually too large to be representative for the average gas production rate, $Z_{\mathrm{H_2O}}$. Assuming that the solar energy is distributed uniformly over a *hemisphere* ($\cos\zeta = 1/2$) results in a much better approximation. It corresponds to $\zeta = 60°$ and agrees very well with the value obtained by integrating $Z_{\mathrm{H_2O}}$ over the hemisphere for values of $r_{\mathrm{H}} < 2$ AU. It starts to deviate significantly for $r_{\mathrm{H}} > 3$ AU, giving results that are too low by a factor of about 100 for $r_{\mathrm{H}} > 6$ AU. The hemispherical approximation also agrees well with results presented in this book for small values of r_{H}, which include heat conduction into the nucleus, because the heat conduction at small r_{H} is small compared to the energy used for sublimation of water ice. Although the "spherical average" approximation is still applied in some models, it clearly should not be used except possibly for icy particles in the coma. The first model for an icy particle halo was developed by Huebner and Weigert (1966). Figure 5.2 displays universal solutions of Eqs. (5.1) and (5.4) for $Z_{\mathrm{H_2O}}$ and T as a function of $x = r_{\mathrm{H}}/\sqrt{(1-\mathcal{A})\cos\zeta}$. The equation

$$\frac{(1-\mathcal{A})F_{\odot}\cos\zeta}{r_{\mathrm{H}}^2} = \epsilon\sigma T^4 + \mathcal{P}\sqrt{m_{\mathrm{H_2O}}/2\pi kT}\,\Delta H_{\mathrm{H_2O}} \tag{5.5}$$

which considers the energy balance (actually the power balance) at a unit area, is sometimes referred to as a "standard model" for comets, equivalent to the "standard model" commonly used for asteroids. The total gas production of a comet, i.e. the integral of $Z_{\mathrm{H_2O}}(\zeta)$ over the active surface area of a comet nucleus (ignoring heat conduction into the nucleus), gives excellent results for heliocentric distances $r_{\mathrm{H}} < 3$ AU. The reason for this is that the energy conducted into the nucleus at small heliocentric distances is only a small fraction of the energy used for the sublimation of ice.

One of the earliest models of heat diffusion into the nucleus of a comet resulting in a temperature profile is the work by Kuehrt (1984). He assumed a spherical nucleus of water ice with an isothermal surface and calculated the heat diffusion into the nucleus numerically. He concluded that heat conduction leads to thermal hysteresis of the surface temperature and a gradual warming of the interior as a comet as a comet approaches the Sun and over many orbits around the Sun. He also estimated the thermal

[1] The term "fast rotator" is a misnomer. If the spin axis points to the Sun, then only one half of the sphere is illuminated. If the spin axis is perpendicular to the direction to the Sun, then the poles are not illuminated. There is no way that the Sun can illuminate the nucleus over 4π of the sky. "Spherical average" is a better descriptor of the approximation.

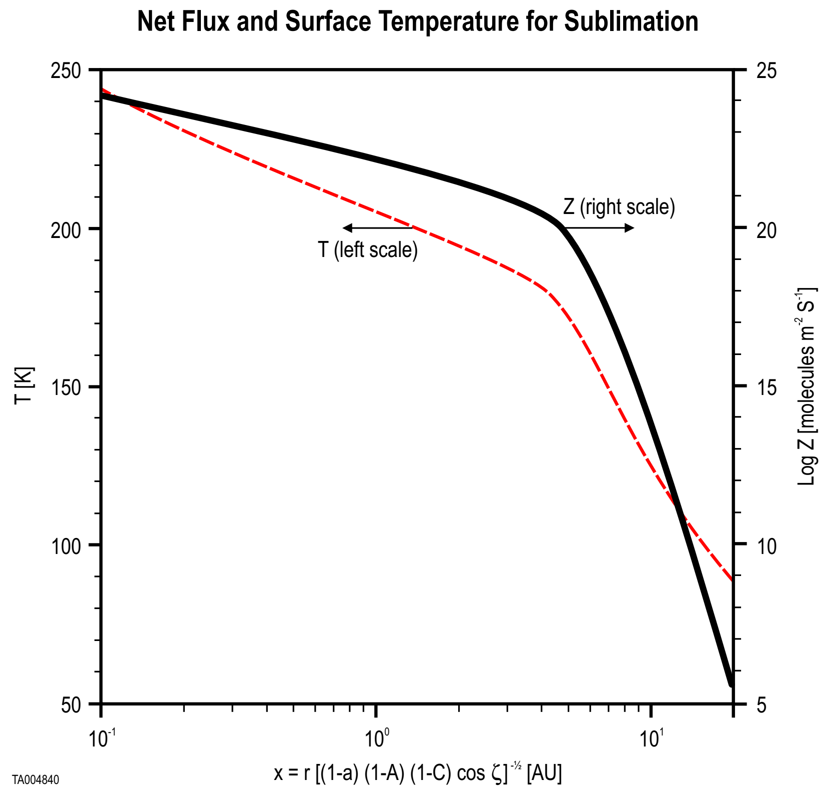

Figure 5.2: Net flux and surface temperature for sublimation of H_2O ice, in terms of the molecular flux, $Z_{H_2O} = Q_{H_2O}/m_{H_2O}$, where m_{H_2O} is the mass of a water molecule.

stresses associated with the temperature gradients and the rising temperature in the interior. At about the same time Weissman and Kieffer (1984) considered heat diffusion into the nucleus. Fanale and Salvail (1985) developed a heat and gas diffusion model for comet nuclei. It included the dust mantle development and effects of latitude, spin period, and spin axis orientation. They concluded that an initially homogeneous nucleus would develop a thin, less than 1 mm thick, dust mantle. They applied their model to Comet 2P/Encke. McKay et al. (1985) discussed methods of computing core temperatures in comet nuclei, and Squyres et al. (1985) also investigated thermal profiles in comet nuclei taking into account variations in latitude and spin axis orientation. Herman and Podolak (1985) considered the nucleus interior as a heat reservoir, while Herman and Weissman (1987) solved the one-dimensional thermal diffusion equation to obtain temperature profiles into the comet nucleus. Prialnik and Bar-Nun (1987) examined the thermal evolution of a spherical comet nucleus composed initially of amorphous ice in the orbit of 1P/Halley. They pointed out that the phase transition from amorphous to crystalline ice was an important heat source in a comet nucleus.

5.2 Characteristic Properties of the Nucleus

Adopting typical values for the physical properties of cometary material in general, simple estimates may be derived for the characteristics of the nucleus structure and evolution, in terms of the defining parameters, as shown in Table 5.1. These provide insight into the nature of comet nuclei, as well as instructive guidelines for building numerical models of their structure and evolution. For example, the skin depth associated with a periodically varying heat source – caused by spin or orbital motion, for example – is obtained from the heat diffusion equation

$$\delta r_{\mathrm{s}} = \sqrt{(\kappa P_{\mathrm{rot}}/\pi\rho_{\mathrm{n}} c)} \tag{5.6}$$

where $P_{\mathrm{rot}} = P_{\mathrm{spin}}$ for the diurnal skin depth, while for the orbital skin depth $P_{\mathrm{rot}} = 2\pi a^{3/2}/\sqrt{GM_{\odot}}$. The thermal timescale for the entire nucleus is obtained in a similar way. These estimates help in defining an adequate numerical grid, in space and time, while the mass loss rate and life span indicate what the size of such a grid should be. The total amount of solar energy absorbed by the nucleus during one orbital revolution is estimated by integrating the left side of Eq. (5.5)

$$\pi R^2 \int_t^{t+P_{\mathrm{orb}}} \frac{F_{\odot}}{r_{\mathrm{H}}^2} dt$$

neglecting the albedo. Dividing it by $4\pi R^2 \rho_{\mathrm{n}} \Delta H_{\mathrm{H_2O}}$ yields an upper limit to the average thickness of the ice layer that is sublimated during one orbital revolution

$$\Delta R_{\mathrm{orb}} < \frac{\pi}{2\Delta H_{\mathrm{H_2O}}} \frac{F_{\odot}}{\sqrt{GM_{\odot}}} \frac{1}{\sqrt{a(1-e^2)}} \tag{5.7}$$

The life span of an active comet is then approximately given by $R/\Delta R_{\mathrm{orb}}$. The maximal temperature (calculated from Eq. (5.5) for the sub-solar point) indicates what thermochemical processes are to be expected.

These, however, are only crude estimates. The detailed behaviour of comet nuclei is obtained by applying the full set of equations given in Chapter 4, including complex input physics, as discussed in Chapter 3. The resulting numerical evolution codes will be described in the next chapter.

Table 5.1: Estimates for characteristic properties of comets

Property	Dependence on parameters	Value
Orbital skin depth	$\left(\frac{2\kappa a^{3/2}}{\sqrt{GM_\odot}\rho_\mathrm{n}c}\right)^{1/2}$	18 m
Diurnal skin depth	$\left(\frac{P_\mathrm{spin}\kappa}{\pi\rho_\mathrm{n}c}\right)^{1/2}$	0.1 m
Thermal timescale	$\frac{R^2\rho_\mathrm{n}c}{\pi^2\kappa}$	8×10^4 yr
Insolation per orbit	$\frac{\pi L_\odot}{2\sqrt{GM_\odot}}\frac{R^2}{\sqrt{a(1-e^2)}}$	10^{18} J
Production rate at perihelion	$\frac{L_\odot}{4\mu\Delta H_{\mathrm{H_2O}}}\left(\frac{R}{a(1-e)}\right)^2$	1.3×10^{30}/s
Erosion per orbit	$\frac{L_\odot}{8\sqrt{GM_\odot}\Delta H_{\mathrm{H_2O}}\rho_\mathrm{n}}\frac{1}{\sqrt{a(1-e^2)}}$	1.7 m
Max. temperature	$\frac{4\pi a^2(1-e)^2Q\Delta H_{\mathrm{H_2O}}}{L_\odot}=1$	205 K
Day-night range at perihelion	$\int_{T_n}^{T_d}\sqrt{\frac{\rho_\mathrm{n}c\kappa}{\pi P_\mathrm{spin}}}\frac{dT}{Q\Delta H_{\mathrm{H_2O}}}=\frac{1}{2}$	23 K
Life-time	$\frac{8\sqrt{GM_\odot}R\rho_\mathrm{n}\Delta H_{\mathrm{H_2O}}\sqrt{a(1-e^2)}}{L_\odot}$	3×10^3 yr

Note: $\sqrt{GM_\odot}=1.152\times10^{10}$ m$^{3/2}$ s^{-1}.
Values listed in the last column were obtained using the following parameters: $a=10$ AU, $e=0.9$, resulting in a perihelion distance of 1 AU, $R=5$ km, $\rho_\mathrm{n}=7\times10^2$ kg/m^3, $P_\mathrm{spin}=10$ hr, $\kappa=0.6$ W/(m K), $c=8\times10^2$ J/(kg K).

Since the evolution of nuclei, as already indicated by the crude estimates, is largely determined by their *defining* parameters, numerical models are mostly applied to individual comets, rather than to comets in general. Even then the results may diverge, as compositional and structural parameters vary.

5.3 Characteristic Timescales

In this section it is assumed that amorphous ice exists in comet nuclei. Such an assumption is reasonable, based on laboratory results for the fast, low-temperature condensation of water vapour (but amorphous ice has not yet been identified in the interstellar medium). The evolution of a comet is characterized by several different timescales:

- *The thermal timescale*, obtained from the energy balance equation, which in its simplest form without sources and advection, is a heat diffusion equation. Distinction must be made between the thermal timescale of amorphous ice τ_{a}, crystalline ice τ_{c}, and dust $\hat{\tau}$.
- The *timescale of gas diffusion* (say, for some representative gas component) τ_{gas}, which is also the timescale of pressure release, obtained from the mass conservation equation, which (without sources) can be regarded as a diffusion-type equation for the release of gas pressure.
- The *timescale of crystallization* $\tau_{\mathrm{a-c}}$, which is also the timescale of gas-release and pressure build-up.
- The *timescales of sublimation* of different volatiles, $\tau_{\mathrm{subl-H_2O}}$ for water, $\tau_{\mathrm{subl-CO}}$ for CO, $\tau_{\mathrm{subl-CO_2}}$ for CO_2, and so forth.
- The *timescale of heating by absorption of solar radiation*, $\tau_{\odot}$, which concerns the *skin* of the comet nucleus that depends on the spin period.

To these, the constant characteristic *times of decay* of the radioactive species may be added; the only relevant one would be that of ^{26}Al, whose decay time $\tau_{^{26}\mathrm{Al}}$ is relatively short.

For a layer of thickness Δr and temperature T,

$$\tau_{\mathrm{a-ice}} = (\Delta r)^2 \rho_{\mathrm{a}} c_a(T)/\kappa_a(T)$$

Similar expressions are obtained for crystalline ice $\tau_{\mathrm{c-ice}}$ and for dust $\hat{\tau}$; as a rule, $\tau_{c-ice} < \tau_{a-ice} < \hat{\tau}$. Porosity may increase all these timescales considerably. In addition,

$$\tau_{\rm gas} = \frac{3}{4}\frac{(\Delta r)^2}{\Psi r_{\rm p}}\left(\frac{2\pi m}{kT}\right)^{1/2}$$

$$\tau_{\rm c} = \lambda^{-1}(T) = 9.54\times 10^{-14}{\rm e}^{5370/T}\ [{\rm s}]$$

$$\tau_{\rm subl-H_2O} = \frac{\rho_{\rm c}}{S\mathcal{P}_{\rm H_2O}\sqrt{m_{\rm H_2O}/2\pi kT}}$$

with similar expressions for $\tau_{\rm subl-CO}$, $\tau_{\rm subl-CO_2}$, and so forth. Assuming the ice near the nucleus surface to be crystalline, the insolation timescale at a given heliocentric distance $r_{\rm H}$ is given by

$$\tau_\odot = \sqrt{(\kappa_{\rm c}P_{\rm spin}/\pi\rho_{\rm c}c)}\rho_{\rm c}cT\frac{4\pi r_{\rm H}^2}{L_\odot}$$

with a typical nucleus spin period $P_{\rm spin} \sim 1$ day.

The relationships between these timescales will determine to a large extent the evolutionary pattern of the comet nucleus. Since the diffusion timescales (for heat and gas) depend on depth, we consider three different situations, as illustrated in Fig. 5.3, where timescales are plotted against temperature, assuming an average pore size of 10μm and a porosity of 0.65. One case applies to the nucleus surface, involving a subsurface layer of 1 m, which is relevant close to the Sun, say, at $r_{\rm H} = 1$ AU. Another case concerns internal processes – such as crystallization – which are particularly important at relatively large heliocentric distances, say, $r_{\rm H} = 10$ AU, and occur at depths of the order of 10 m. A third case concerns evolution of the central part of the nucleus (a typical depth of 1 km), due to energy released by radioactive decay, which is important during the early evolution of comet nuclei, very far from the Sun (say, $r_{\rm H} = 1000$ AU).

5.3.1 The Surface Temperature

Starting with subsurface activity close to the Sun (Fig. 5.3 *top*), we note that the timescale of solar heating intersects the sublimation timescales for CO at temperatures of about 25 K, for CO_2 at about 80 K, and for H_2O at about 60 K. If such ices are found near the surface at these temperatures, the solar energy will be used for sublimation and the rate of surface heating will decrease. We note that in all cases conduction to the interior is almost negligible. A steady state will be reached at slightly higher temperatures, when the timescale of gas diffusion for a thin subsurface layer (the dotted line in Fig. 5.3 *top* corresponds to a thickness of about 5 cm) intersects the sublimation timescales for CO at about 30 K, for CO_2 at about 100 K, and

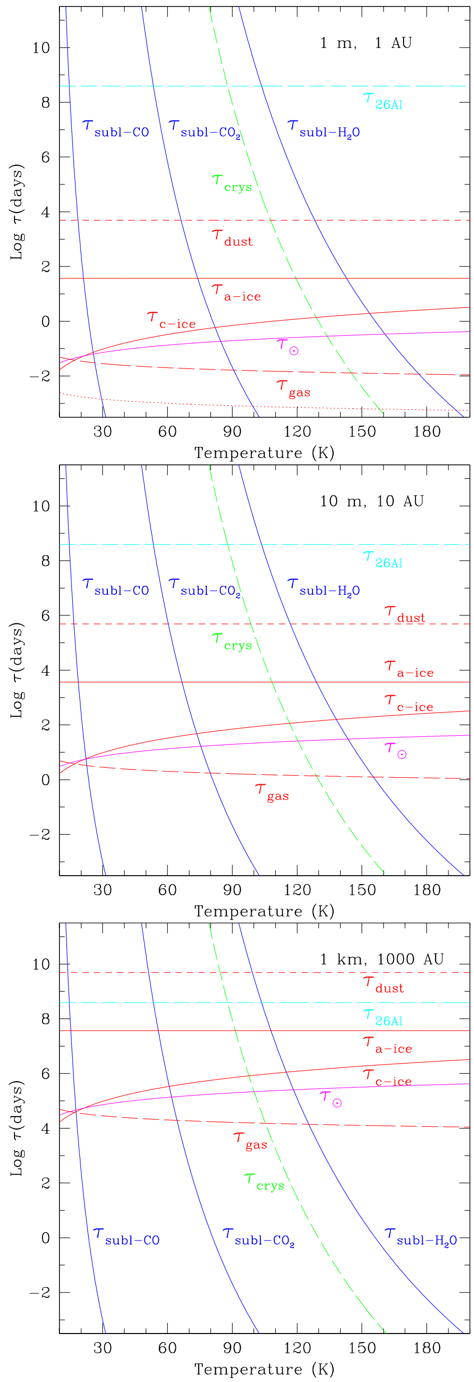

Figure 5.3: Timescales of different evolutionary processes (see text) as a function of temperature for different cases: (*top*) 1 m at 1 AU; (*middle*) 10 m at 10 AU; (*bottom*) 1000 m at 1000 AU.

for H_2O at about 200 K. These are the expected surface temperatures of comet nuclei near $r_\mathrm{H} \approx 1$ AU, when the corresponding ices are exposed. If a mixture of ices is present, the temperature will be determined by the most volatile component.

5.3.2 The Onset of Crystallization

What determines the onset of crystallization? Considering the timescales of crystallization, heat conduction, and sublimation, we find that at very low temperatures conduction dominates. This means that heat released by a local source will be efficiently removed. Crystalline ice is a much better heat conductor than amorphous ice, and hence heat will predominantly flow to the surface through the growing outer crystalline layer. Thus, as long as the temperature of the outer layer of the nucleus is below the critical temperature where τ_c intersects τ_{c-ice} (see Fig. 5.3 *middle*), the rate of heating by crystallization will be very slow. Since the crystallization rate is much more sensitive to temperature than the conduction rate of crystalline ice, it will eventually surpass the rate of heat conduction. For a 1 m thick layer, the conduction timescale exceeds the crystallization timescale at $T \approx 120$ K, and at $T \approx 110$ K at a depth of 10 m. When, due to insolation, the temperature at the crystallization front reaches this critical value of $T_\mathrm{c} \approx 120$ K, the local heat release causes it to rise still further. The higher temperature causes crystallization to proceed even faster and thus a runaway process develops. As the temperature rises, sublimation of the ice from the pore walls becomes important and since it absorbs a large amount of energy per unit mass, the outburst is arrested and proceeds at a controlled steady state rate (see, e.g. Prialnik et al., 1993). This occurs at the intersection between τ_c and τ_gas (see Fig. 5.3 *middle*), which indicates the temperature in the crystallization zone. The point of the orbit where runaway crystallization sets in is

$$r_\mathrm{H} = \sqrt{\frac{L_\odot}{16\pi\sigma}}\sqrt{\frac{1-\mathcal{A}}{e}}\,\frac{1}{T_\mathrm{c}^2} = 7.8\sqrt{\frac{1-\mathcal{A}}{e}}\,\left(\frac{100\mathrm{K}}{T_\mathrm{c}}\right)^2 \quad \mathrm{AU}$$

and thus depends on the factor $\sqrt{(1-\mathcal{A})/e}$, which is always of the order of unity. Hence, as a rule, comets that have an outer amorphous ice layer can be expected to exhibit high activity at heliocentric distances of 7 ± 1 AU. The rise time and the timescale of fluctuations should be of the order of $\tau_\mathrm{c-ice}(T_\mathrm{c}) = \tau_\mathrm{c}(T_\mathrm{c})$. According to Fig. 5.3 *top, middle* it is about 100 days for crystallization at a depth of 10 m, and about 1 day for a depth of 1 m. This means that fluctuations (and outbursts) at small heliocentric distances should occur on much shorter timescales than at large heliocentric distances.

Observations appear to confirm this conclusion. It should be noted that for old, periodic comets that have undergone crystallization and, as a result, the amorphous ice boundary is found at some depth below the surface, the temperature at this boundary is not directly correlated with heliocentric distance. Because of the thermal lag, a new burst of crystallization may start in such comets at any point in the orbit.

5.3.3 Fracture Instability

The competition between $\tau_{\rm c}$ and $\tau_{\rm gas}$ should indicate when an instability is likely to occur. We recall that the crystallization timescale is also the timescale of gas release and pressure build-up (assuming gas is occluded in the amorphous ice), while the diffusion timescale of the gas is also the timescale of pressure relaxation. If $\tau_{\rm c} > \tau_{\rm gas}$, the pressure is released sufficiently rapidly to prevent mechanical instability; however, if $\tau_{\rm gas} \gg \tau_{\rm c}$, gas would accumulate more rapidly than it is removed and large stresses may result from pressure build-up. We may regard the borderline, obtained by $\tau_{\rm c} = \tau_{\rm gas}$, as a division of the $(\Delta r, T)$ plane into two zones: a stable and an unstable one. Thus, if the temperature of amorphous ice at a certain depth exceeds a critical value, it could lead to a state of instability. This situation may be avoided either if the temperature decreases, which is possible if the thermal timescale is sufficiently short, or if the pore size increases, thereby reducing $\tau_{\rm gas}$. However, according to Fig. 5.3, the thermal timescales for both amorphous and crystalline ice are longer than $\tau_{\rm gas}$ by 2 to 3 orders of magnitude. Hence, only expansion of the pores may arrest the development of an instability once it occurs. However, the analysis of timescales does not provide clues to the magnitude of the pressure and pressure gradients in relation to the strength of the material, nor to the outcome of unstable conditions. This necessitates detailed numerical modeling, and the establishment of an algorithm for treating fracture (Prialnik et al., 1993).

Because of the complex motion of comet nuclei caused by their elongated shape and simultaneous spin about two axes, alternate flexing and stretching may occur. Loss of material from sublimation of the ices will further change the angular momentum. Thus the complex motion will be further aggravated and cause stresses and strains in a nucleus. Since the mechanical strength of a nucleus does not appear to be large, fractures may develop.

5.3.4 The Effect of Radioactivity

We now consider the possible effect of radioactive heating, mainly by ^{26}Al (see, e.g. Prialnik and Podolak, 1995). At a depth of about 1 km the decay time of ^{26}Al becomes comparable to the thermal timescale of amorphous ice, meaning that the ice might barely be heated; it would certainly be heated at larger depths, of a few km. Eventually, the internal temperature would become sufficiently high for crystallization to set in, thereby providing an additional internal heat source. At the same time, however, the thermal timescale would decrease, crystalline ice being a much better heat conductor than amorphous ice. Hence, only in still larger comet nuclei ($R > 10$ km) would the internal temperature continue to rise. If the internal temperature becomes such that the timescale of sublimation is shorter than the timescale of radiogenic heat release, then most of the released energy will be used for sublimation of ice from the pore walls. If, in addition, the radius is such that the timescale of gas (vapour) diffusion is lower than the timescale of sublimation, then sublimation will consume the radiogenic heat indefinitely (so long as there is ice), since the vapour will be efficiently removed. A steady state will develop, without further heating of the ice matrix.

Since ^{26}Al has a short lifetime (7.2×10^5 yr) its effectiveness in heating comet nuclei depends strongly on its abundance, i.e. on how much of it may have decayed before formation of comet nuclei. Only general conclusions, such as the ones above, may be drawn from the structure and evolution equations of comet nuclei. Results that are more specific require detailed investigations about the nucleus formation processes and timescales and the relative abundance and conductivity values of amorphous ice.

5.4 An Analytical Model for Crystallization and its Implications

Comets are often found to be active at heliocentric distances far beyond the limit of about 3.5 AU, within which the activity may be explained by sublimation of water ice induced by insolation. Well known examples are 2060 Chiron, 29P/Schwassmann-Wachmann 1, 1P/Halley – outburst at 14 AU – and Hale-Bopp (C/1995 O1) – at 7 AU before perihelion. The exothermic transition from amorphous to crystalline ice has long been recognized as a possible mechanism for explaining such activity. Although cometary behaviour is largely determined by the orbit, and hence activity patterns vary widely among comets, it would be extremely useful to assess the possible effect of crystallization in comet nuclei in a general manner, regardless of orbit. We shall show that a quite simple analytical model may be applied to this problem, based on typical properties of cometary ice. On the other hand, it must be remembered that the existence of amorphous water ice in comet nuclei is circumstantial, it has not been proven.

A heat wave propagating through an initially cold, isothermal medium of porous amorphous ice, and generating sublimation, causes a sharp temperature gradient to arise between the regions lying in front and behind it, where the temperatures are almost uniform. The uniform temperature in front of the wave is maintained because the very low thermal conductivity of porous amorphous ice prevents spreading of the heat wave. In other words, the ice properties are such that the thermal timescale is much longer than the timescale of the advance of the heat wave. The uniform, relatively high temperature behind it is caused by the stabilizing effect of sublimation and condensation from the pore walls. A local increase in temperature would lead to sublimation and absorption of heat, resulting in local cooling and lowering of the temperature, and vice versa. This is equivalent to a very high effective thermal conductivity caused by the heat transport of latent heat. It is much more efficient than conduction (see also Section 2.4.1).

In a comet nucleus, such a heat wave may be generated by a crystallization front propagating, say, from the surface inward. Deviations from a uniform temperature distribution throughout the outer crystalline ice zone are confined to a very thin subsurface layer (regardless of the thickness of the entire crystalline layer) and are negligible at relatively large heliocentric distances (beyond about 3 AU). Such a configuration may be modeled as a two-zone medium and studied analytically.

5.4.1 A Two-Zone Model

Consider a surface of discontinuity, S, advancing at constant velocity, $\dot{S}$, perpendicular to the surface, from a medium labeled 1 into a medium labeled 0 (see Fig. 5.4). The discontinuity is caused by a crystallization front propagating through porous ice of uniform bulk density ρ. The ice behind the front (medium 1) is crystalline at a temperature T_1, and in front of it (medium 0) amorphous at a uniform temperature T_0. The bulk density of the highly porous cometary ice is not affected by crystallization, which might only change the microdensity of the ice particles. The heat capacity of the ice is given by $c(T) = \alpha T + \beta$, with the same coefficients for both ice phases, and hence $u(T)$ – the energy per unit mass – is given by $u = 0.5\alpha T^2 + \beta T$ plus a constant. The constants for the two phases are chosen so that the enthalpy difference is equal to the heat released in the process of crystallization $\Delta H_{\mathrm{crys}} = 9 \times 10^4$ J/kg (Ghormley, 1968). Medium 1 loses energy by thermal emission and sublimation at its free outer surface at a rate

$$F_S = \epsilon\sigma T_1^4 + \mathcal{P}(T_1)\sqrt{m/(2\pi k T_1)}\Delta H \tag{5.8}$$

(all physical and thermal properties in what follows refer to water and thus, for clarity, indices have been deleted.) The saturation vapour pressure may

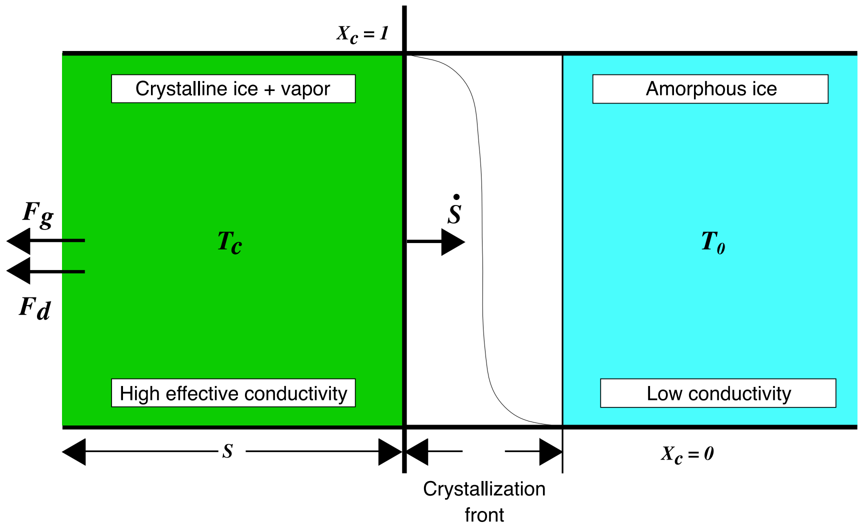

Figure 5.4: Schematic representation of the two-zone model

be approximated by

$$\mathcal{P}(T) = A\mathrm{e}^{-B/T}$$

where A and B are constants. Assuming crystallization is instantaneous (in reality it can be slow or incomplete), continuity of the energy flux at S requires

$$\rho\dot{S}[\Delta H_{\mathrm{crys}} - (u_1 - u_0)] = F_S \tag{5.9}$$

The assumption of a constant temperature throughout medium 1, in spite of the heat loss at its free surface, is based on the high effective thermal conductivity of porous ice with vapour filled pores, κ_{eff}. In steady state, the temperature behind the front, at a distance x_1 from S, is obtained from the solution of the heat conduction equation, where $\partial/\partial t = -\dot{S}\partial/\partial x_1$,

$$-\rho c\dot{S}\frac{dT}{dx_1} = \kappa_{\mathrm{eff}}\frac{d^2T}{dx_1^2}$$

If T_1 is the temperature at S,

$$T(x_1) = T_1\mathrm{e}^{-\rho c\dot{S}x_1/\kappa_{\mathrm{eff}}} \tag{5.10}$$

and the deviation $|T(x_1) - T_1|$ becomes vanishingly small for large κ_{eff}.

The surface of discontinuity S is a thin layer of finite thickness δ, where amorphous ice is transformed into crystalline ice. Denoting by X_c the mass fraction of crystalline ice, the boundaries of this layer are $x = 0$, where $X_c = 1$ and $x = \delta$, where $X_c = 0$. The rate of crystallization, λ, is a function of temperature, determined experimentally as

$$\lambda(T) = a\mathrm{e}^{-b/T}$$

with a and b constants. Between $x = 0$ and $x = \delta$ the temperature changes from T_1 to T_0 and X_c changes from 1 to 0, according to

$$\dot{X}_c = \lambda[T(x)](1 - X_c)$$

where $\lambda(T_0)$ is negligible. In a *steady state* this leads to

$$-\dot{S}\frac{dX_c}{dx} = \lambda(1 - X_c) \tag{5.11}$$

Integrating over x, we obtain the velocity of the front

$$\dot{S} = \int_0^\delta \lambda(x)[1 - X_c(x)]dx \tag{5.12}$$

We now define a temperature, θ, such that

$$\lambda(\theta) = \frac{1}{\delta}\int_0^\delta \lambda(1 - X_c)dx \tag{5.13}$$

as an effective temperature of the reaction front.

The thickness δ of the reaction front may be estimated according to the thermal diffusivity $\mathcal{K} = \kappa/(\rho c_a)$ of the amorphous ice (medium 0) into which the front propagates and the time constant $\tau = \lambda^{-1}$ of the reaction, in the form

$$\delta = \sqrt{\mathcal{K}\tau} = \sqrt{\mathcal{K}/a}\,\mathrm{e}^{b/2\theta} \tag{5.14}$$

The diffusivity of amorphous ice is experimentally determined as constant – independent of temperature – and very low. Combining Eqs. (5.12), (5.13), and (5.14), the velocity of the front is given by

$$\dot{S}(\theta) = \delta(\theta)\lambda(\theta) = \sqrt{\mathcal{K}a}\,\mathrm{e}^{-b/2\theta} \tag{5.15}$$

For a given set of parameters ρ, ϵ, and T_0, the conservation Eq. (5.9) can be solved to obtain $T_1(\theta)$,

$$\mathrm{e}^{-b/2\theta}\rho\sqrt{\mathcal{K}a}[\Delta H_{\mathrm{crys}} - \tfrac{1}{2}\alpha(T_1^2 - T_0^2) - \beta(T_1 - T_0)] = \epsilon\sigma T_1^4 + \mathcal{P}(T_1)\sqrt{\tfrac{m}{2\pi kT_1}}\Delta H \tag{5.16}$$

This solution describes a steady state, where the rate of energy gain by crystallization is exactly balanced by the rate of loss at the outer surface. The steady state is stable. For example, consider a perturbation that would decrease the energy loss rate at the surface, F_S: more energy would then be released by the reaction front than required at steady state conditions; as a result, T_1 would increase, which in turn would raise F_S back to the steady state value (the argument applies as well in the opposite direction). Although in principle θ may surpass T_1, only solutions corresponding to $\theta < T_1$ are compatible with the assumptions of the model. Physical solutions of Eq. (5.16) are possible only when the term in parentheses on the left side (i.e. the net energy gain) is positive, $\Delta H_{\rm crys} - 0.5\alpha(T_1^2 - T_0^2) - \beta(T_1 - T_0) > 0$. This condition imposes an upper limit on T_1, determined by T_0, as a solution of $\Delta H_{\rm crys} - 0.5\alpha(T_{1,\rm max}^2 - T_0^2) - \beta(T_{1,\rm max} - T_0) = 0$. Thus,

$$T_1 < T_{1,\rm max}(T_0) \tag{5.17}$$

Indeed, it can be shown that the solutions of Eq. (5.16) tend asymptotically to $T_{1,\rm max}$ as θ increases.

5.4.2 Implications for the Onset of Cometary Activity

The temperature T_1 represents the surface temperature of a comet nucleus (or other icy body) undergoing crystallization and determines the rate of sublimation and hence the level of activity of the comet. The steady state solutions obtained demonstrate that icy bodies that are devoid of any external energy source may reach quite high surface temperatures and levels of activity, powered solely by ongoing crystallization in the interior. In the case of high T_1 values, this energy source would soon be exhausted, but a steady state involving moderate temperatures may last for a considerable time. The time span of such a phase in a given object is directly proportional to the object's size. Typical front velocities, as obtained from Eq. (5.15), range from 1 to 100 m yr^{-1}.

It is instructive to compare this internal energy source with the external source provided by solar radiation. Instantaneous energy balance at the subsolar point on the surface of a comet nucleus, neglecting albedo effects and the heat conducted into the interior, implies $F_S = L_\odot/(4\pi r_{\rm H}^2)$, with F_S given by Eq. (5.8) and $r_{\rm H}$ in metres. This relation yields a reasonable approximation for the surface temperature $T_{\rm s}(r_{\rm H})$ at a given heliocentric distance $r_{\rm H}$, which can be regarded as a measure of the irradiation power. The relevant question is: Beyond what distances would crystallization be more significant than solar radiation? This should be determined by the competition between $T_{\rm s}(r_{\rm H})$ and $T_1(T_0)$. By equating $T_{\rm s}(r_{\rm H})$ with $T_{1,\rm max}(T_0)$, we obtain a curve $T_0(r_{\rm H})$, as shown in Fig. 5.5, which divides the $(r_{\rm H}, T_0)$ plane into two zones: one – above the curve – in which crystallization provides the major energy source, and another – below it – where solar energy is dominant. The division is particularly sensitive to the emissivity assumed, as illustrated by the three examples shown in Fig. 5.5. The interpretation is as follows: for a comet of initial temperature, say the internal temperature of 1P/Halley is 60 K, reaching steady-state crystallization, the internal energy source would surpass the external one at heliocentric distances beyond 5 AU (for an emissivity $\epsilon \approx 0.5$), closer for a higher emissivity, and further out for a lower one. The steady-state model could only be applied beyond this distance.

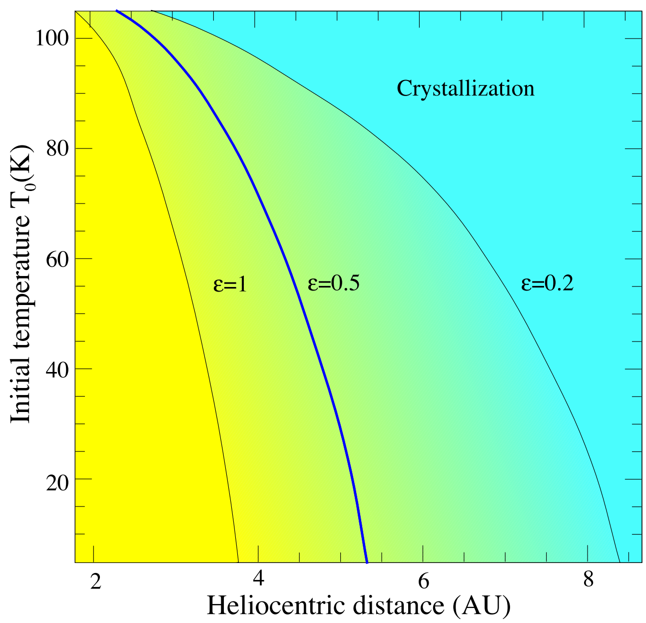

Figure 5.5: Regions of dominance of the two energy sources: insolation and crystallization of amorphous ice, as a function of initial comet temperature T_0 and heliocentric distance, r_H; ϵ is the emissivity.

In conclusion, distant comets ($r_\mathrm{H} > 5$ AU, typically) may have much warmer and more active surfaces than predicted by absorption and reflection of solar radiation, lasting for long periods of time, provided crystallization has been triggered and has reached a steady-state. (Crystallization may be induced by an inward propagating heat wave, generated by insolation, or by chemical reactions, such as polymerization of HCN.) In such cases the activity level should *not* be significantly affected by orbital position, as in the case of sublimation in comets with eccentric orbits.

5.4.3 The Intermittent Progress of Crystallization

We have shown that a steady state solution for the advance of the crystallization wave is not always possible. What would happen if crystallization were triggered, but a steady state could not be established? Imagine a large mass of amorphous ice at temperature T_0 and assume the temperature threshold for crystallization to be T_1 (this is approximately the temperature for which the rate of crystallization surpasses the rate of heat conduction, or $\tau_{crys} < \tau_{\mathrm{cond}}$, and hence most of the released heat is absorbed locally). Suppose a mass element Δm_1 has just crystallized, liberating an amount of heat $\Delta H_{\mathrm{crys}} \Delta m_1$. Assume now that a fraction η of this heat is absorbed by an adjacent mass element Δm_2, raising its temperature to T_1, so that it will, in turn, undergo crystallization; the rest, $1-\eta$, of the released energy will be 'wasted', that is, it will be dissipated, causing a slight temperature rise over a more extended region. Thus $\eta \Delta H_{\mathrm{crys}} \Delta m_1 = (u_1 - u_0)\Delta m_2$, where $u_1 = u(T_1)$ and $u_0 = u(T_0)$, and heat is again released in an amount $\Delta H_{\mathrm{crys}} \Delta m_2$. A fraction $\eta \Delta H_{\mathrm{crys}} \Delta m_2$ will eventually be absorbed by a mass element Δm_3 that will crystallize, and so forth. The total amount of mass ΔM that will ultimately crystallize (starting spontaneously with the crystallization of Δm_1) is given by the sum

$$\Delta m_1 + \Delta m_2 + \Delta m_3 + \ldots = \Delta m_1 \left[1 + \frac{\eta \Delta H_{\mathrm{crys}}}{u_1 - u_0} + \left(\frac{\eta \Delta H_{\mathrm{crys}}}{u_1 - u_0} \right)^2 + \ldots \right] \tag{5.18}$$

reducing to $\Delta M = \Delta m_1 \mathcal{S}_q$, where $\mathcal{S}_q$ is the sum of a geometric series with the factor

$$q = \frac{\eta \Delta H_{\mathrm{crys}}}{u_1 - u_0}$$

If $q \geq 1$, the sum diverges, meaning that crystallization will continue indefinitely. In fact, for $\eta = 1$, we return to the earlier, steady state, model of crystallization, for Eq. (5.17) is satisfied. On the other hand, if $q < 1$, the sum converges to $\mathcal{S}_q = (1-q)^{-1}$, that is,

$$\Delta M = \Delta m_1 \frac{u_1 - u_0}{\eta \Delta H_{\mathrm{crys}} - (u_1 - u_0)} \tag{5.19}$$

and crystallization will stop. We may define a critical initial temperature of the ice, T_{crit}, corresponding to $q = 1$, and $u_{\mathrm{crit}} \equiv u(T_{\mathrm{crit}})$. Accordingly,

$$q = \frac{u_1 - u_{\mathrm{crit}}}{u_1 - u_0}$$

and hence, if $T_0 \geq T_{\mathrm{crit}}$, crystallization will proceed continuously, feeding on its own energy (and all the more so, if other internal energy sources are available). Otherwise ($T_0 < T_{\rm crit}$), it will stop and will need to be triggered again.

Crystallization may be initiated by the heat wave propagating inward from the insolated comet nucleus surface to the crystalline/amorphous ice boundary, provided that on reaching this boundary it still carries sufficient energy for raising the local temperature to T_1. However, once this has occurred and the boundary has moved deeper into the nucleus, later heat waves originating at the surface will be too weak when reaching the boundary to rekindle crystallization. A quiescent period would thus ensue, until the surface recedes by sublimation to a sufficiently short distance from the crystalline/amorphous ice boundary. At this point, a new spurt of crystallization may take place. Since in the meantime the interior temperature of the ice has risen to some extent, crystallization will advance deeper into the nucleus than at the previous spurt. This will, in turn, affect the time span to the next spurt of crystallization, since the rate of surface recession for a given comet is constant. In conclusion, crystallization appears to be triggered sporadically, even at large heliocentric distances, where comets spend most of their time. This might explain the distant activity including outbursts and possibly splitting of comets.

— 6 —

Numerical Methods

> "...if the worth of the arts were measured by the matter with which they deal, this art – which some call astronomy ..., and many of the ancients the consummation of mathematics – would be by far the most outstanding. This art which is as it were the head of all the liberal arts and the one most worthy of a free man leans upon all the other branches of mathematics. Arithmetic, geometry, optics, geodesy, mechanics, and whatever others, all offer themselves in its service. And since a property of all good arts is to draw the mind of man away from the vices and direct it to better things, these arts can do that more plentifully, over and above the unbelievable pleasure of mind (which they furnish)."
>
> Nicolaus Copernicus *De Revolutionibus*, Book 1, 1543.[1]

6.1 1-D Difference Schemes

Let us consider a 1-D time-dependent, boundary-value problem of heat transport in a finite region $0 \leq r \leq R$, subject to a boundary condition of the second kind at one end and a boundary condition of the third kind at the other. We assume, for simplicity, that the diffusivity is constant and that there are no internal heat sources. Then,

$$\frac{\partial T}{\partial t} = \mathcal{K}\frac{\partial^2 T}{\partial r^2} \qquad \text{for} \quad 0 \leq r \leq R,\ t \geq 0 \tag{6.1}$$

$$\frac{\partial T}{\partial r} = 0 \qquad \text{at} \quad r = 0 \tag{6.2}$$

$$\frac{\partial T}{\partial r} + h(T) = f(t) \qquad \text{at} \quad r = R \tag{6.3}$$

where $h(T)$ is some prescribed function of the temperature. In order to complete the definition of the problem, we assume a given initial temperature distribution,

$$T = T(r) \qquad \text{for} \quad 0 \leq r \leq R \quad \text{at} \quad t = 0 \tag{6.4}$$

[1]Translation by Charles Glen Wallis, *On the Revolutions of Heavenly Spheres*, St. John's Bookstore, Annapolis, 1939.

Let the time and space domains be divided into finite intervals $\delta t_n = t_n - t_{n-1}$ and $\Delta r_i = r_i - r_{i-1}$, where I runs from 0 at the centre to I at the surface such that $t_0 = 0$, $r_0 = 0$ and $r_I = R$. Since we are dealing with a physical problem, not a purely mathematical one, it is appropriate to associate the values of temperature, as well as other thermodynamic quantities, with volumes (or masses), such as are represented by the space *intervals*, rather than to points or surfaces, represented by the *interfaces* r_i. A heat flux, on the other hand, may be taken as one crossing an interface, as shown in Fig. 6.1.

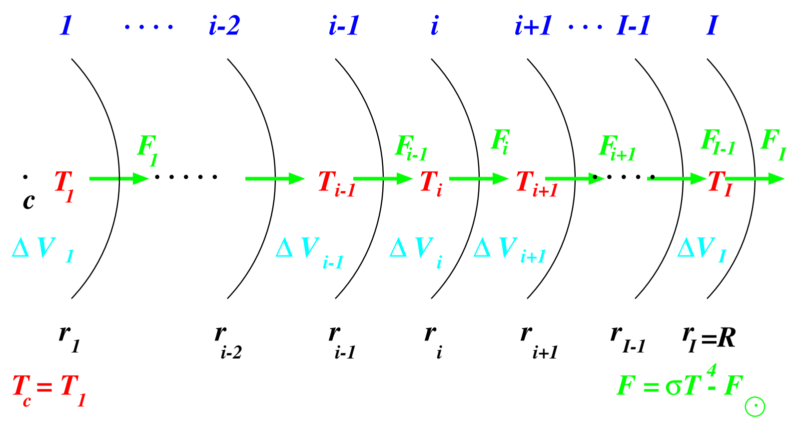

Figure 6.1: Numerical grid. T_c is the central temperature, which corresponds to T_0 in the text. The F_i are the fluxes crossing boundaries.

Thus, the solution for the change of the temperature profile is represented by a series of stepped functions T_i^n, where T_i is the temperature within the interval Δr_i, and $T_0 = T_1$ by the lower boundary condition Eq. (6.3). Using forward differences in time, we have

$$\frac{\partial T}{\partial t} = \frac{T_i^n - T_i^{n-1}}{\delta t^n} \tag{6.5}$$

The space derivative of the temperature, proportional to the heat flux through the interface r_i, is

$$\frac{\partial T}{\partial r} = \frac{T_{i+1} - T_i}{0.5(\Delta r_{i+1} + \Delta r_i)} \tag{6.6}$$

The second derivative of the temperature (or the flux derivative) is then given by

$$\frac{\partial^2 T}{\partial r^2} = \frac{1}{\Delta r_i}\left[\frac{T_{i+1} - T_i}{0.5(\Delta r_{i+1} + \Delta r_i)} - \frac{T_i - T_{i-1}}{0.5(\Delta r_i + \Delta r_{i-1})}\right] \tag{6.7}$$

We note that for equally spaced intervals, Eq. (6.7) reduces to the more familiar

$$\frac{\partial^2 T}{\partial r^2} = \frac{T_{i+1} - 2T_i + T_{i-1}}{(\Delta r_i)^2} \tag{6.8}$$

There are several possibilities for combining the space and time derivatives into a difference equation for Eq. (6.7): the *explicit* scheme, the *fully implicit* scheme, and a modified implicit form, known as the *Crank-Nicholson* scheme. They differ in form with regard to the superscript of T on the right side of (6.7), whether it is $n-1$, that is, the known values of T at the beginning of the time-step, or n, that is, the unknown values of T at the end of the time-step. Using the simplified form Eq. (6.8) for illustration, we have

$$\frac{T_i^n - T_i^{n-1}}{\delta t^n} = \mathcal{K}\frac{T_{i+1}^{n-1} - 2T_i^{n-1} + T_{i-1}^{n-1}}{(\Delta r_i)^2} \tag{6.9}$$

for the explicit scheme, which can be solved directly, and

$$\frac{T_i^n - T_i^{n-1}}{\delta t^n} = \mathcal{K}\frac{T_{i+1}^{n} - 2T_i^{n} + T_{i-1}^{n}}{(\Delta r_i)^2} \tag{6.10}$$

for the fully implicit scheme, which, upon rearranging terms, results in a system of I linear equations, whose solution requires the inversion of a *tridiagonal* matrix. Finally,

$$\frac{T_i^n - T_i^{n-1}}{\delta t^n} = \frac{1}{2}\mathcal{K}\left[\frac{T_{i+1}^{n} - 2T_i^{n} + T_{i-1}^{n}}{(\Delta r_i)^2} + \frac{T_{i+1}^{n-1} - 2T_i^{n-1} + T_{i-1}^{n-1}}{(\Delta r_i)^2}\right] \tag{6.11}$$

for the Crank-Nicholson scheme, which requires the inversion of a tridiagonal matrix as well. The explicit scheme has the disadvantage that time-steps are restricted by the Courant-Friedrichs-Levy condition (Courant condition, for brevity),

$$\delta t \, \leq \, \frac{(\Delta r)^2}{2\mathcal{K}} \tag{6.12}$$

for a given space discretisation; thus time-steps may become prohibitively small when a fine mesh is required in order to resolve sharp temperature gradients. The implicit schemes, on the other hand, are unconditionally stable for all values of the time-step. However, they require a far larger amount of computations for each time-step, prohibitively large in the case of a large spatial grid, or in the two- or three-dimensional cases. The Crank-Nicholson scheme has the advantage of being second-order accurate in time, whereas the fully implicit and the explicit schemes are only first-order accurate in time. The fully implicit scheme, on the other hand, is best suited for *stiff* equations, that is, when there are two or more very different timescales on which the temperature is changing (as is the case in comets). The reason is that the implicit scheme converges to the steady-state solution for large time-steps.

The same methods apply to the more complicated case when the heat capacity and thermal conductivity are functions of the temperature, and there is also a temperature-dependent source term,

$$\rho c(T)\frac{\partial T}{\partial t} = \frac{\partial}{\partial r}\left[\kappa(T)\frac{\partial T}{\partial r}\right] + q(T) \tag{6.13}$$

In this case, the difference equations of the implicit schemes must be linearized and solved iteratively. Thus, the vector

$$\mathbf{T}^n \equiv (T_0^n, \ldots T_{i-1}^n, T_i^n, T_{i+1}^n, \ldots T_I^n)$$

is obtained from $\mathbf{T}^{n-1}$ by "relaxation," through a series of vectors $\mathbf{T}^{(m)}$, where $\mathbf{T}^{(1)} = \mathbf{T}^{n-1}$ and $\mathbf{T}^{(m)} = \mathbf{T}^{(m-1)} + \mathbf{X}^{(m)}$. Any function of T is expanded,

$$[\mathbf{f}(T)]^{(m)} = \mathbf{f}(T^{(m-1)}) + \left(\frac{d\mathbf{f}}{dT}\right)^{(m-1)} \cdot \mathbf{X}^{(m)} \tag{6.14}$$

and second-order terms in $\mathbf{X}$ are neglected. The resulting set of difference equations – now linear in the unknowns $X_i^{(m)}$ – is solved successively, and when the norm of $\mathbf{X}^{(m)}$ becomes smaller than the norm of $\mathbf{T}^{(m)}$ by a prescribed factor ϵ, $\mathbf{T}^{(m)}$ is regarded as the solution, that is, $\mathbf{T}^n = \mathbf{T}^{(m)}$ are the temperatures at the end of the time-step δt^n.

It is important to point out that implementation of the convergence criterion may be achieved in many different ways. In principle, the solution should not be affected by the application of the criterion, but this is not always the case. For example, if the norm is defined as the absolute value of the vector of differences $\mathbf{X}^{(m)}$ and changes are confined to a very small part of the grid, then a solution may be accepted even though the convergence accuracy will be poorer than the nominal requirement in that part of the grid where large changes have occurred. This may be circumvented by defining the norm as the maximum relative change over the grid, which ensures that at each point of the grid convergence accuracy is better than ϵ. The problem in this case is that if almost no change occurs at some place, then convergence may be altogether prevented by the accuracy of the computing machine (truncation error). Thus devising an acceptable and working convergence criterion becomes more of an art.

In order to ensure energy conservation in the numerical scheme, the time derivative on the left side of Eq. (6.13) should now be taken as

$$\rho c(T)\frac{\partial T}{\partial t} = \rho\frac{\partial u}{\partial t} = \rho\frac{u(T_i)^n - u(T_i)^{n-1}}{\delta t^n} \tag{6.15}$$

In the case of a 1-D spherical coordinate system, it is convenient to choose the volume V enclosed within a sphere of radius r for the space variable, rather than r, because then the equation retains the form of the plane-parallel one. From the physical point of view, it would be even better to adopt the mass enclosed within a sphere of radius r as space variable, but if the mass is allowed to change during evolution as a result of internal sublimation and gas flow, the volume is a better choice. In this case the flux through r must be replaced by the energy crossing the spherical surface of radius r per unit time, $F' = 4\pi r^2 F$, given by $F' = -\kappa' \partial T/\partial V$. As an example, the fully implicit difference scheme is

$$\rho_i \frac{u_i^n - u_i^{n-1}}{\delta t^n} = \frac{1}{\Delta V_i}\left[\bar{\kappa}_i' \frac{T_{i+1}^n - T_i^n}{\frac{1}{2}(\Delta V_{i+1} + \Delta V_i)} - \bar{\kappa}_{i-1}' \frac{T_i^n - T_{i-1}^n}{\frac{1}{2}(\Delta V_I + \Delta V_{i-1})}\right] + q(T_i^n) \tag{6.16}$$

where

$$\bar{\kappa}_i' = (4\pi)^{2/3}(3V_i)^{4/3}\,\frac{\kappa(T_i^n)\Delta V_i + \kappa(T_{i+1}^n)\Delta V_{i+1}}{(\Delta V_{i+1} + \Delta V_i)}$$

Another numerical method of solution of the non-linear heat equation is the *predictor-corrector* method, essentially a two-step iterative procedure. The advance from $\mathbf{T}^{n-1}$ to $\mathbf{T}^n$ is performed through an intermediate step $\mathbf{T}^{n-1/2}$ in the following way. First, $\mathbf{T}^{n-1/2}$ is obtained by taking the coefficients $c(T)$, $\kappa(T)$ and $q(T)$ at time t^{n-1}, that is, as functions of the known values $\mathbf{T}^{n-1}$. This is the *predictor* step, which requires the solution of a *linear* set of equations, involving the inversion of a tridiagonal matrix. In the next step, the *corrector* step, the coefficients are taken at time $t^{n-1/2}$, that is, as functions of the newly found $\mathbf{T}^{n-1/2}$, in order to obtain $\mathbf{T}^n$. Once again by solving a linear system of equations involving a tridiagonal matrix.

It is noteworthy that in the comparison of computational results to be presented in Chapter 7, all four methods of solution (explicit, predictor-corrector, Crank-Nicholson, and fully implicit) will be considered.

6.2 Treatment of Boundary Conditions

The 1-D Heat transfer equation in finite difference form is, essentially,

$$\rho_i \frac{(u_i - u_i^0)}{\delta t} = -\frac{1}{\Delta \mathcal{X}_i}(F_{i+1} - F_i) + q_i \Delta H \tag{6.17}$$

where a zero superscript denotes values at the beginning of the time step δt. Whether the variables on the right side are taken at the beginning or the end of a time step, or between them, is immaterial for the following discussion. In a plane-parallel calculation, $\Delta \mathcal{X}$ stands for distance and F for energy flux, while for a spherical volume, $\Delta\mathcal{X} \equiv \Delta V$ is the volume enclosed in a spherical surface around the centre, and $F \equiv F'$ is the energy crossing such a surface per unit time. In either case, we may multiply Eq. (6.17) by $\Delta\mathcal{X}_i \delta t$ and sum over the entire system, to obtain

$$U - U^0 = \delta t(F_0 - F_I + \sum_i q_i \Delta\mathcal{X}_i) \tag{6.18}$$

where the left side is the change in the total internal energy of the system over the time interval and the right side is the total contribution of all energy sources and sinks. This, in fact, is the energy conservation law in difference form. In this way the boundary conditions of the heat transfer equation, as formulated in Chapter 4, Eqs. (4.18) and (4.19), become obvious. But, whereas the inner boundary condition may be immediately implemented, $F_0 = 0$, the outer one requires some caution, because of the dependence of F_I on temperature.

By identifying U with the total energy of the system, it is implied that u_i is uniform over the volume (distance) of a grid shell. The straightforward approach will then be to express F_I by means of T_I of the outermost grid shell. This, however, requires very fine zoning near the surface of the nucleus, where temperature gradients may be very steep. Otherwise, since the surface flux is the main energy source of a comet, serious errors can result.

Another approach is to use the outer boundary condition in the form of Eqs. (4.25), or (6.3). This means adding a new variable T_s, the temperature at the very surface of the nucleus, different from T_I. Thus another difference equation must be added as well, the difference form of Eq. (4.25), which links T_s and T_I. Even in this case, fine zoning near the surface is still required, for this approach assumes a linear temperature gradient over half of the outermost mass shell, which may still be far from accurate.

To better illustrate the problem, a concrete example follows, in which a comparison between the two different formulations of the heat transfer boundary condition at the surface is attempted. Consider the uppermost grid layer, between I (the surface) and $I-1$ and assume it is sufficiently thin so that the change in temperature from its centre to the surface is negligible. In this case we may apply Eq. (6.17) to this layer, with the heat flux crossing the surface of the nucleus given by

$$F_I = \epsilon\sigma T_I^4 - (1-\mathcal{A})\frac{F_\odot}{r_\mathrm{H}^2(t)}\cos\zeta \tag{6.19}$$

Thus,

$$\Delta\mathcal{X}_I \rho_I \frac{\delta u_I}{\delta t} = -\epsilon\sigma T_I^4 - (1-\mathcal{A})\frac{F_\odot}{r_\mathrm{H}^2(t)}\cos\zeta + F_{I-1} + \Delta\mathcal{X}_I q_I(T_I)\Delta H \tag{6.20}$$

where the heat flux crossing the inner surface of the layer is

$$F_{I-1} = -\kappa \frac{T_I - T_{I-1}}{\Delta \mathcal{X}_I} \tag{6.21}$$

We thus take into account the thermal inertia of the thin upper layer (cf. Carslaw and Jaeger, 1986) and assume the *surface* sublimation to be produced within the volume of this layer.

The other approach is to adopt the surface boundary condition Eq. (4.25), which implies a surface boundary layer of vanishing thickness. To compare the two boundary conditions, two runs of the same 1-D comet nucleus model described in Section 7.2 were performed (see also Orosei et al., 1999). The model parameters were the same as those of Model 1 in Chapter 7. It was found that, while surface temperatures computed at perihelion were the same for both Eqs. (4.25) and (6.20), aphelion surface temperatures at noon differed by almost 20 K. It was also found that the agreement between perihelion temperatures is caused by the surface sublimation term, which becomes dominant at perihelion because it increases exponentially with temperature, and is the same for both Eqs. (4.25) and (6.20).

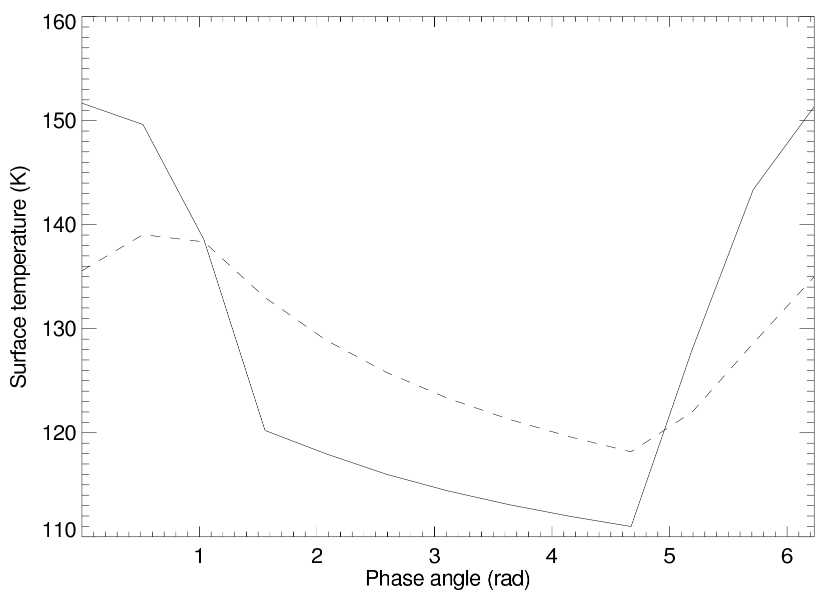

Figure 6.2: Daily variation of surface temperature at aphelion as a function of the phase angle from the local meridian, for the temperature surface boundary conditions Eq. (4.25) (solid line) and Eq. (6.20) (dashed line).

The difference in surface temperatures at aphelion is not limited to their values, but involves also the shape of the temperature variation during a single complete spin of the nucleus. Figure 6.2 shows that, for Eq. (6.20), the temperature peak is delayed and that the daily temperature variation is smaller. The difference in aphelion temperatures is caused by the term that accounts for the thermal inertia of the layer in Eq. (6.20).

The difference between the results obtained by adding or neglecting the term including the time derivative of the surface temperature questions the validity of the approximations used to obtain Eqs. (4.25) and (6.20): as said, Eq. (4.25) can be solved exactly only if the thickness of the outermost layer is zero, while on the other hand one may doubt that the temperature used to compute the internal energy of the surface layer in (6.20) can be the same as the surface temperature.

The first test was to estimate the timescale for heat diffusion across the surface layer, and to compare it with the duration of the discrete time step used in the computations: if the time step is significantly longer than the heat diffusion timescale across the layer, then the assumption of thermal equilibrium implied by Eq. (4.25) is correct. The timescale τ_{cond} for heat diffusion across a layer of thickness Δr is

$$\tau_{\mathrm{cond}} = \frac{\rho c (\Delta r)^2}{\kappa} \tag{6.22}$$

The values of physical parameters used in the model are the same as those of Model 1 in Chapter 7. For a temperature of 110 K, giving a minimum value of τ_d, and for a given layer thickness of 0.05 m, one obtains $\tau_d \approx 2 \times 10^4$ s, while the time step used in the computations is of the order of 7×10^3 s. This means that the assumption of thermal equilibrium is not valid for a layer 5 cm thick, and that the use of Eq. (4.25) for the computation of surface temperature is inappropriate. The comparison between the two surface boundary conditions shown in Fig. 6.2 is thus not significant.

In Fig. 6.3 the daily variation of surface temperature at aphelion is shown, computed for a 5 mm thickness of the first layer (yielding $\tau_d \approx 2 \times 10^2$ s); for comparison, the curves of Fig. 6.2 are shown as dotted lines: it can be seen that now the two boundary conditions produce results that are almost identical, and are similar to those obtained with Eq. (6.20) for a 5 cm thickness of the surface layer.

The comparison between different boundary conditions favours the inclusion of the thermal inertia term, even if it produces no effect on the results for an adequately thin surface layer. It seems to make the surface temperature computation more robust with respect to mismatches between the duration of the discrete time step used in the model and the boundary layer thickness. This is shown by the fact that the results in Fig. 6.3 converge close to the lower temperatures obtained for a thicker surface layer with Eq. (6.20).

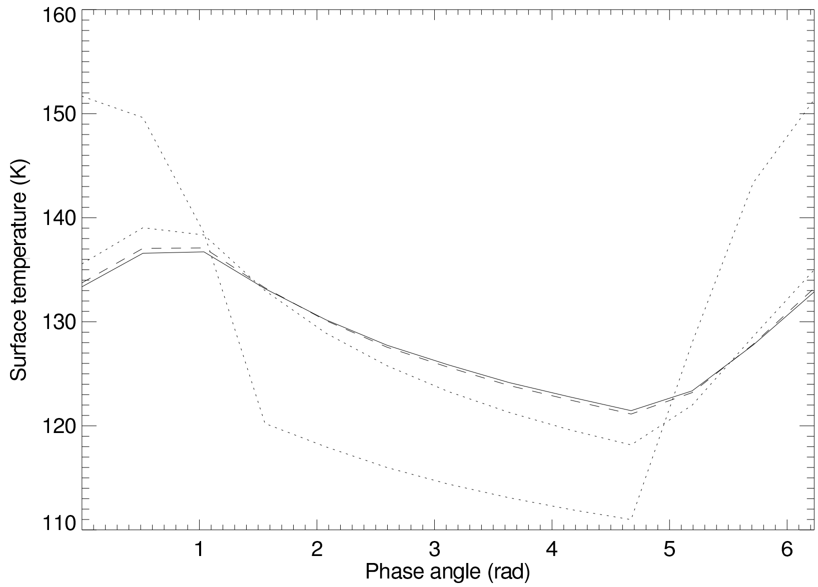

Figure 6.3: Daily variation of surface temperature at aphelion as a function of the phase angle from the local meridian, for the temperature surface boundary conditions Eq. (4.25) (solid line) and Eq. (6.20) (dashed line) and for a surface layer thickness of 5 mm. The curves of Fig. 6.2 are shown as dotted lines for reference.

6.3 From 1-D to Multi-Dimensions

Since comet nuclei are too small for self gravity to be of importance, they are not necessarily spherical. Indeed, the first four nuclei observed at close distance (1P/Halley, 19P/Borrelly, 81P/Wild 2, and 9P/Tempel 1) are clearly non-spherical. However, a non-spherical object is far more difficult to model. In addition, the number of free parameters for an arbitrary shape tends to infinity. The simplest among spherical models are 1-D, i.e. a spherically *symmetric* nucleus. Thus, most of the cometary nucleus thermal models published to date have used the 1-D, evenly heated surface approximation (also known as 'fast rotator') for a spherical nucleus, where the absorbed solar radiation is assumed to be distributed uniformly over the nucleus surface. This approximation has the advantage of simplicity and enables the use of relatively long time steps in evolutionary calculations, thus requiring short computation time.

However, in order to obtain an accurate surface temperature distribution and its diurnal change at any heliocentric distance, one must adopt the so-called 'slow-rotator' approach, which takes into account the diurnal and latitudinal solar flux variations. This type of model requires a far greater amount of computing time, since much smaller time steps – a small fraction of the spin period – must be used in the numerical integration over time.

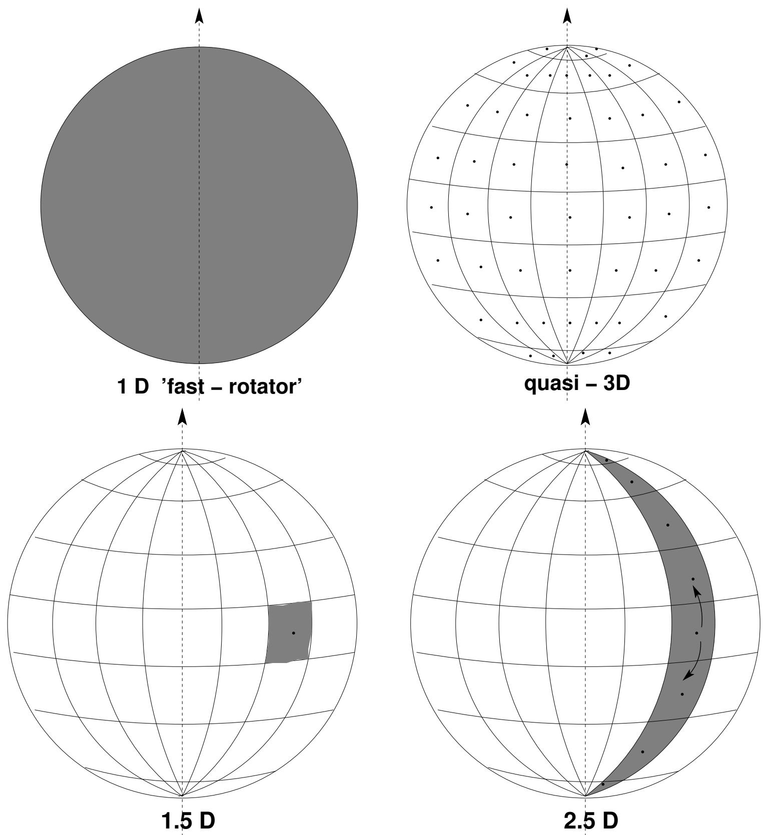

Figure 6.4: Schematic representation of numerical grids for a spinning nucleus, commonly used in model calculations. Dots indicate radial directions along which heat conduction is computed; only in the 2.5-D model is lateral conduction included, and only along the meridian, as shown.

A first attempt in this direction was to consider a point on the equator of a spinning nucleus, and translate the diurnal temperature change obtained into a map of the equatorial temperature at any given time. Such a procedure (Benkhoff and Boice, 1996; Capria et al., 1996; Benkhoff, 1999; De Sanctis et al., 1999) may be described as a 1.5-D model. An upper limit for the production rate is obtained by using the maximum noon flux for the entire surface of the sunlit hemisphere. A more advanced model is achieved by considering a wedge of surface elements aligned along a meridian (Enzian et al., 1997, 1999). Thus the latitudinal effect is taken into account and the total production rate is obtained by summing the contributions of such wedges over one spin period. This is, essentially, a 2.5-dimensional calculation. The next step is to take into account both diurnal and latitudinal solar flux variations (Huebner and Boice, 1992; Gutiérrez et al., 2000; Julian et al., 2000; Cohen et al., 2003, De Sanctis et al., 2005), considering, however, only radial heat conduction, that is, neglecting lateral conduction. This quasi 3-D approach is amply justified by the extremely low heat conductivity of cometary material; the characteristic heat diffusion time between equator and pole (as between surface and centre) is of the order of the life-time of a comet (see Table 5.1 above). The different models are shown schematically in Fig. 6.4; however, calculations use much finer meshes than the ones shown.

6.4 Simultaneous Solution for Transfer of Heat and Mass

We note that the evolution equations are coupled through the source terms and the gas fluxes, which are functions of both temperature and pressure, and hence must be solved simultaneously. A flowchart of an evolution code that uses an implicit numerical scheme is shown in Fig. 6.5; the energy and mass balance equations are solved in an alternating sequence, until they converge. The question marks represent the question whether convergence has been achieved in the corresponding process. The question mark following n or m represents the question whether the number of iterations has exceeded the allowed limit (since there is no point in continuing an iterative process that does not converge).

The simultaneous solution of the heat and mass conservation equations is extremely time consuming, keeping in mind that the equations are strongly nonlinear. Simplifying approximations may be used under special conditions.

If the effective permeability of the medium is sufficiently high, the left side of the mass conservation equation for the gas phases (Eq. 4.9) becomes negligible. Neglecting it is tantamount to a quasi-steady state approximation, where gas densities and production rates change only as far as the temperature distribution changes. Thus Eqs. (4.9 – 4.11) are replaced by

$$\nabla \cdot \mathbf{J}_n = q_n \qquad \frac{\partial \rho_{s,n}}{\partial t} = -q_n \tag{6.23}$$

In this way we have to solve only one time-dependent equation, supplemented by structure (space-dependent) equations. This constitutes a large computational advantage, particularly in a long-term evolution calculation,

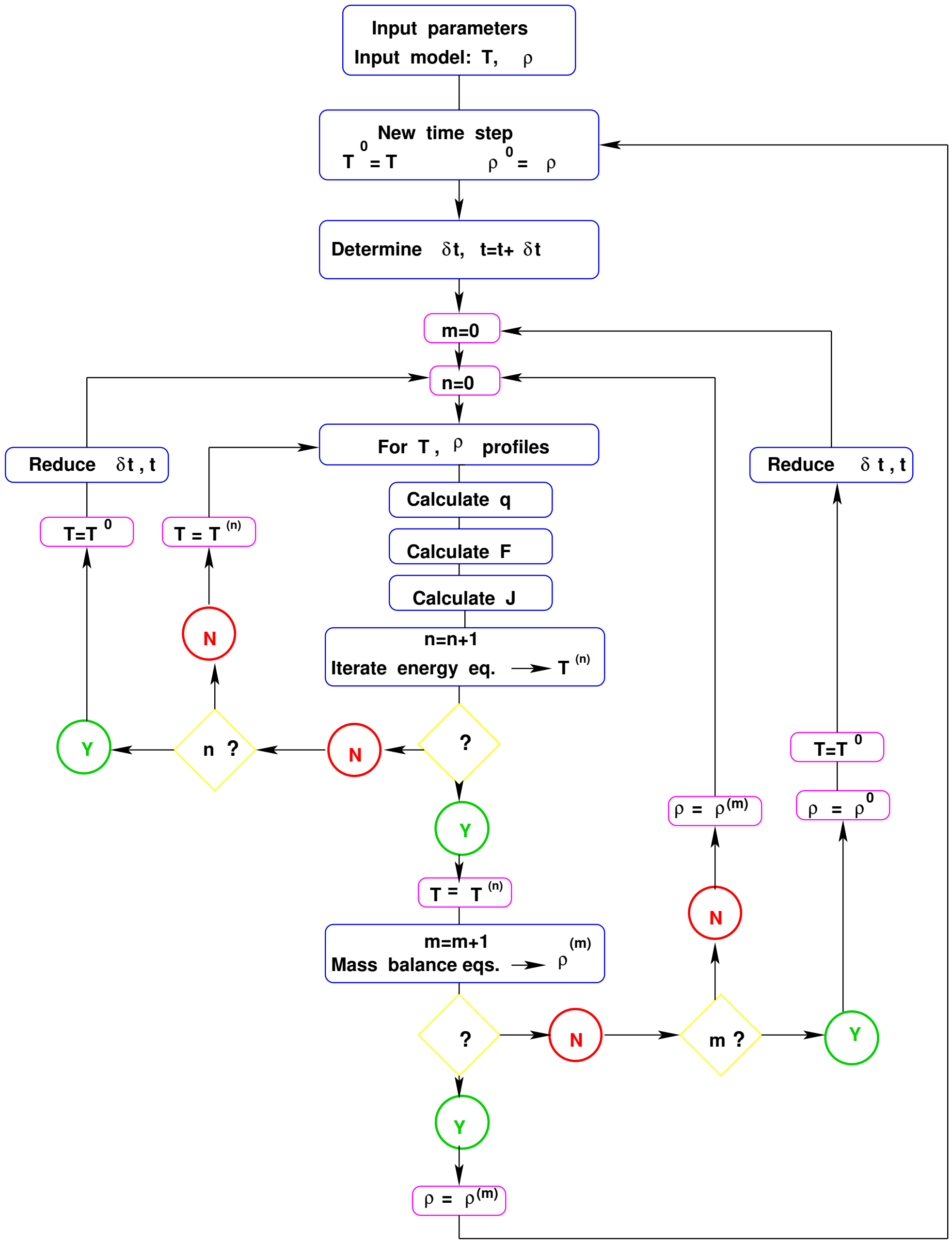

Figure 6.5: Flowchart for an implicit comet nucleus evolution code.

where a detailed account of gas flow through the porous medium, coupled with heat transfer, would require a prohibitively large amount of computing time. Combining Eqs. (6.23) and integrating over the volume, we obtain

$$-\dot{M}_{s,n} = J_n(R,t)4\pi R^2 \tag{6.24}$$

which means that the total mass of gas ejected through the comet's surface per unit time is equal to the total amount of gas sublimated throughout the nucleus per unit time, for each species. This approximation is valid for minor species, for which the bulk density is low. It breaks down when the net gas sublimation rate is negative, that is, when condensation of gases surpasses sublimation of ices. This approach has recently been adopted by Choi et al. (2002) in long-term evolution calculations of Kuiper belt objects. It is also applied for the outermost layer of the nucleus, as already mentioned in Section 6.2.

A different approximation with the same computational advantage – reduction of the number of time-dependent equations – has been used in other studies (e.g. De Sanctis et al., 2001). It assumes that when both the ice and gas phases are present, the gas density is equal to the saturated vapour density, which is a function of temperature. Strictly, this would imply that no sublimation and condensation could take place. However, as the temperature changes, the saturated density (pressure) changes with it, and this change can be translated into a rate of sublimation and condensation. This is an excellent approximation for the interior of the nucleus, where the pressures are found to reach saturation; it implies, however, that there is sufficient material in both phases to allow instantaneous adjustment. It is not valid, therefore, for minor volatile components and fails close to the surface of the nucleus. The two simplifying approximations are thus complementary.

6.5 Stability Problems

Besides being time consuming, the simultaneous solution of the heat and mass transfer equations is bound to encounter numerical stability problems when an explicit difference scheme is used. As discussed by Steiner et al. (1991) and others, a comparison of characteristic times of heat conduction and gas diffusion reveals that mass transport occurs on a much smaller timescale than energy transport, in typical cometary conditions of temperature and pressure, thus making it difficult to solve the two corresponding partial differential equations using the same discrete time step and spatial grid.

Different solutions to this problem have been devised: several models do not solve the time-dependent heat conduction equation and the time-dependent continuity equation for the gas simultaneously, using instead the quasi-stationary continuity equation.

A more sophisticated approach has been attempted by Orosei et al. (1999), in which two different time steps are used to solve the heat conduction and gas diffusion equations over the same spatial grid: one, Δt_e, is used for heat conduction calculations, and it is determined by means of Kepler's equation for a constant discrete increment of the eccentric anomaly of the comet nucleus along its orbit. The other time step, Δt_g, is used for gas diffusion, and it is computed at each heat diffusion equation integration time step, for each gas: in each discrete layer n, between the sublimation interface to surface, an estimate of the velocity v of the gas flow is computed from the ratio of gas flux through the layer and the gas density,

$$v = \frac{\mathbf{J}}{\tilde{\rho}} \tag{6.25}$$

This computation takes place only above the sublimation front of the particular ice considered, because in the model it is assumed that gas pressure is equal to saturated vapour pressure below the interface.

Then, the time t_n needed for the gas flow to cross the n-th discrete layer is computed from the ratio of the layer thickness and the estimate of the gas velocity in that layer

$$t_n = \frac{(\Delta r)_n}{v} \tag{6.26}$$

Finally, the total time, t_{tot}, needed for a variation of the interface pressure to propagate up to the surface is computed as the sum

$$t_{tot} = \sum_n t_n \tag{6.27}$$

If $t_{\text{tot}} \ll \Delta t_e$, it is assumed that the gas flow reaches a steady state condition well within the time duration of the heat equation time step, and thus the quasi-stationary continuity equation is used. Otherwise, the time-dependent continuity equation is solved through an implicit, predictor-corrector scheme with a time step Δt_g given by the minimum of all t_n values from interface to the surface, and the solution is iterated a number of times equal to $\Delta t_e/\Delta t_g$.

Another numerical problem related to the simultaneous solution of the heat and mass transfer equations arises from the coupling between the source terms. As discussed in Section 4.2, it is found that heat conduction and gas diffusion are not independent processes, because of the exchange of latent heat with the solid matrix during sublimation of ice and condensation of gas.

As the timescale for sublimation and condensation is even shorter than that of gas diffusion (see Steiner et al., 1991, for a discussion), it can happen that during the numerical integration of the heat diffusion equation the source term introduces heat to or removes heat from a discrete comet nucleus layer in which ice is present at a much faster rate than heat conduction. This, in turn, can produce numerical instabilities which severely affect computational results.

A change in the mathematical scheme for the numerical solution of the heat diffusion equation was attempted by some authors to overcome this problem. A method originally proposed by Steiner and Kömle (1991a,b) and used also by Orosei et al. (1999) consists of extracting from the gas source term some factors that can contribute to an effective heat diffusion coefficient, which includes the contribution of sublimation of ice and recondensation of gas in the pores. The volume sublimation rate term q_n, to be used in Eq. (4.13) in those layers in which the volatile species n is present, is obtained by inverting Eq. (4.6)

$$q_n = \frac{\partial \tilde{\rho}_n}{\partial t} + \nabla \mathbf{J}_n \tag{6.28}$$

Then, by assuming that gas pressure is equal to the saturation vapour pressure in Eq. (3.20), $\mathbf{J}_n$ is written as

$$\mathbf{J}_n = -\mathcal{G} \frac{\partial \mathcal{P}_n}{\partial T} \frac{\partial T}{\partial r} \tag{6.29}$$

so that the term $\nabla \mathbf{J}_n$ in Eq. (6.28) can be added to $\nabla(\kappa \partial T/\partial r)$ in Eq. (4.13). Equation (6.28) thus reduces to

$$q_n = \frac{\partial \tilde{\rho}_n}{\partial t} \tag{6.30}$$

and, ignoring for the moment all sources and sinks of energy not related to the sublimation of ices, Eq. (4.13) becomes

$$\rho c \frac{\partial T}{\partial t} = \nabla \left[\left(\kappa + \Delta H \mathcal{G} \frac{\partial \mathcal{P}_n}{\partial T} \right) \frac{\partial T}{\partial r} \right] + Q \tag{6.31}$$

Another numerical stability problem arising in the simultaneous solution of the heat and mass transfer equations is caused by the change in the structure of the comet nucleus as ices sublimate and dust is dragged away by escaping gases. The evolution of the stratigraphy is a continuous process, whereas its computation is at discrete points. The most obvious approach to the representation of such process consists of keeping the discrete grid points fixed in space, but the physical properties of the discrete layers are corrected for the gradual change in ice and dust content.

A different scheme has been proposed by Orosei et al. (1999), to prevent those instances in which the change of physical properties of a layer determines an oscillation in the thermal properties propagating through the numerical solution of the heat diffusion equation, and potentially undermining the validity of gas diffusion and dust mantle formation.

To devise a continuous representation for the advance of interfaces toward greater depths as ices sublimate and gas escapes through the porous medium, their erosion rate has been evaluated

$$\frac{\partial R_i}{\partial t} = \frac{\mathbf{J}_i}{\rho_i} \tag{6.32}$$

where R_i is the radius of the i-th volatile interface, $\mathbf{J}_i$ is the gas flux of the i-th gas originating from the interface, and ρ_i is the mass of the i-th volatile species per unit volume at the interface. The volatile interface erosion ΔR_i in the current time step is then computed from

$$\Delta R_i = \frac{\partial R_i}{\partial t}\,\Delta t_e \tag{6.33}$$

Following the computation of the new radii of the interfaces, the discrete grid is redrawn, centreing grid points on the new positions of the interfaces. Temperatures, pressures, and densities are linearly interpolated on the new grid.

— 7 —

Comparison of Algorithms – A Reference Model for Comet Nuclei

> "…by the application of the Newtonian principles at a vast expense of time and labour, Halley laid the foundation upon which cometary astronomy has since risen. We shall endeavour so to arrange our description of this and other comets, that the reader gains an insight into the *kind of interest* attaching to this department of science, and the difficulties with which astronomers have to contend in prosecuting their inquiries respecting these extraordinary bodies."
>
> John Russell Hind, *The Comets: a descriptive treatise upon those bodies*, 1852.

7.1 Rationale

Calculating the heat flow into, and the related vapour flux out of, a porous mixture of ices and dust is a challenging task. Different timescales for heat flow and gas production yield complicated and sometimes very sensitive or unstable numerical schemes. Results are dependent on physico-chemical parameters, zoning, time steps, etc. It was observed that the numerical treatment of heat transport in the matrix may also lead to different results, even though the assumed values of the thermal conductivity were identical. Another numerical stability problem arising in the simultaneous solution of the heat and mass transfer equations is caused by the change in the structure of the comet nucleus as ices sublimate and dust is entrained by escaping gases: the evolution of the stratigraphy is a continuous process, whereas the computational grid is a set of discrete points. To resolve these issues, algorithms and numerical codes from different and independent comet nucleus modeler groups (represented by the authors of this book) were compared in order to gain a better understanding of the physical and chemical behaviour of comets and other icy objects, to develop more reliable tools for data analysis, and to provide better input parameters for the construction and calibration of instruments of future space science missions (Huebner et al., 1999).

The main differences between the models of these different modeler groups are found mostly in the mathematical formulation of the physics, in assumptions adopted for the numerical treatment of properties used in the calculations (e.g. treatment of thermal conductivity), and in parameters used in the calculations. To keep the comparison of our models simple and easy, we agreed on simple models with the following assumptions: one dimensional calculation; simple mixtures consisting of H_2O, CO, and dust only; no amorphous ice; and a set of simple structural parameters, e.g. constant porosity.

Although every code used the same input parameters, we found large discrepancies in the results from the models. Therefore, we also agreed on many technical details, e.g. the treatment of conductivity of the matrix material. Here we report on problems encountered during the comparisons. Reference models are defined and the results of the calculations are presented in this chapter. We hope that this may lead to a simple and transparent standard for the comparison of future models.

To simplify the calculations we assumed that the dust flux from the surface is zero. As a consequence, all dust remains at the surface during the evolution of the model and forms a dust mantle. This mantle is depleted of all volatiles. In the case of a dust and ice mixture, the initially thin dust mantle grows because of inward migration of the sublimation fronts.

The presence of amorphous ice in short-period comets, especially in small ones, is questionable. On the other hand, many nucleus models include amorphous ice and a transition from amorphous to crystalline ice. In this chapter the influence of this transition on gas flux and temperature profiles is ignored.

There are a number of processes by which heat is transferred into the interior of ice and dust samples or comet nuclei. Radiation within the pores is small at or below temperatures of 200 K and can be neglected. It was therefore neglected in all our calculations. The vapour within the pores moves by diffusion along a vapour pressure gradient into the colder interior and transports sensible heat. This effect was taken into account in some codes, but neglected in others. In addition, latent heat is exchanged during sublimation of ice and recondensation processes. This effect was included in all our calculations. Values for the thermal conductivity of dust and ice mixtures vary over a wide range. However, this parameter is very important in determining how fast and how deep the heat wave penetrates a comet nucleus. As seen in previous chapters, the intrinsic thermal conductivity of the ice matrix is smaller than that of compact water ice, because of the reduced contact area between particles. The reduction is usually described by the Hertz factor.

Table 7.1: Numerical treatment of physical quantities in different codes

Code	Effective κ	Gas Production q_i	Gas Flux $j_i/(\nabla P_i)$
A	$f_{\mathrm{H}}\left[\frac{\tilde{\rho}_{\mathrm{H_2O}}}{\rho_{\mathrm{H_2O}}}\kappa_{\mathrm{H_2O}} + \frac{\tilde{\rho}_{\mathrm{CO}}}{\rho_{\mathrm{CO}}}\kappa_{\mathrm{CO}} + \frac{\tilde{\rho}_d}{\rho_d}\kappa_d\right] + \kappa_p$	$\frac{1}{\mathcal{R}_{\mathrm{g}}T}\frac{\partial P_i}{\partial t} - \nabla\left(j_i\right)$	$\frac{1}{3}\frac{\langle \ell\rangle\langle v\rangle}{\tau}$
B	$f_{\mathrm{H}}\left[\frac{\rho_{\mathrm{H_2O}}}{\rho}\kappa_{\mathrm{H_2O}}(T) + \frac{\rho_d}{\rho}\kappa_d(T)\right]$	$\frac{8r_{\mathrm{p}}}{3\xi}\left(\mathcal{P}_i - P_i\right)\sqrt{\frac{\mu_i}{2\pi\mathcal{R}_{\mathrm{g}}T}}$	$-\frac{8\Psi r_{\mathrm{p}}}{3\xi^2}\sqrt{\frac{1}{2\mu_i\pi\mathcal{R}_{\mathrm{g}}}}\left[\frac{1}{\sqrt{T}} + P_i\frac{\nabla\left(1/\sqrt{T}\right)}{\nabla P_i}\right]$
C1, C2	$f_{\mathrm{H}}\left[\frac{\tilde{\rho}_{\mathrm{H_2O}}}{\rho_{\mathrm{H_2O}}}\kappa_{\mathrm{H_2O}} + \frac{\tilde{\rho}_{\mathrm{CO}}}{\rho_{\mathrm{CO}}}\kappa_{\mathrm{CO}} + \frac{\tilde{\rho}_d}{\rho_d}\kappa_d\right]$	$\frac{\partial\tilde{\rho}_i}{\partial t} - \nabla\left(G\frac{\partial\mathcal{P}_i}{\partial T}\nabla T\right)$	$r_{\mathrm{p}}\sqrt{\frac{\pi}{2\mu_i\mathcal{R}_{\mathrm{g}}T}}$
D	$f_{\mathrm{H}}\left[\frac{\rho_{\mathrm{H_2O}}}{\rho}\kappa_{\mathrm{H_2O}}(T) + \frac{\rho_d}{\rho}\kappa_d(T)\right]$	$S\left(\mathcal{P}_i - P_i\right)\sqrt{\frac{\mu_i}{2\pi\mathcal{R}_{\mathrm{g}}T}}$	$-\frac{8\Psi r_{\mathrm{p}}}{3\xi^2}\sqrt{\frac{1}{2\mu_i\pi\mathcal{R}_{\mathrm{g}}}}\left[\frac{1}{\sqrt{T}} + P_i\frac{\nabla\left(1/\sqrt{T}\right)}{\nabla P_i}\right]$

7.2 Thermal Algorithm: Different Formulations

Our 1-D *reference models* assume a porous body, containing in the simplest case only H_2O ice. For more complex models we add CO, dust, or both. The body's porous structure is modeled as a bundle of parallel tubes with a given tortuosity and a pore diameter that changes because of ice-to-gas and gas-to-ice phase changes. Heat transfer into the interior of the body is controlled by solid-state heat conduction of the ice and dust matrix, by vapour flow through the porous matrix (the flow being driven by a vapour pressure gradient), and by sublimation and recondensation. We solve the mass and energy equations for the different volatiles simultaneously. The model includes in- and out-flowing gas within the body, dust mantle build-up if dust is included, depletion of the less volatile ice in outer layers, and recondensation of gas in deeper layers. The details about thermal evolution and chemical differentiation were given in previous chapters.

The outer boundary condition is calculated from the balance between the net incoming solar flux, losses from thermal reradiation, heat needed for sublimation of ices, and heat transport into or out of the nucleus. As a result of our calculations, we obtain the temperature and abundance distribution in the interior, porosity and pore size distribution as a function of depth, the gas flux into the interior, and the gas flux through the surface of the nucleus into the coma for each of the volatiles at various positions of the comet in its orbit around the Sun.

In Table 7.1 we show the different mathematical formulations for gas production, gas flux, and heat flux. All formulations describe the physics in a slightly different way. However, we agreed on using the algorithms unchanged because they were thoroughly tested and we tried to explain differences if they could be related to the formulation of the gas production, gas flux, and heat flux, respectively. In the table $\tilde{\rho}$ is used for the mass per unit volume of porous matter. The total mass density of the matrix material is given by $\rho = \tilde{\rho}_{\mathrm{H_2O}} + \tilde{\rho}_{\mathrm{CO}} + \tilde{\rho}_d$. The heat conductivity of the solid phase is κ_{d} and $\kappa_{\mathrm{p}} = 4\epsilon\sigma r_{\mathrm{p}} T_{\mathrm{s}}^3$ is the effective heat conductivity of the pores. The mean thermal gas velocity is $\langle v \rangle = \sqrt{8\mathcal{R}_{\mathrm{g}} T/(\mu\pi)}$. The mean free path is $\langle \ell \rangle = 4 r_{\mathrm{p}} \Psi/(1-\Psi)$, where Ψ is the porosity of the ice and dust matrix of the nucleus, i.e. the ratio between pore volume and total volume. The partial pressures of the various ices are given by $P_i = \mathcal{R}_{\mathrm{g}} \rho_i T/\mu_i$, where $\mathcal{R}_{\mathrm{g}}$ is the universal gas constant, μ_i is the corresponding molecular weight, and ξ is the tortuosity.

As mentioned earlier, the evolution of a comet is characterized by several different timescales: the thermal timescale, the timescale of gas diffusion, the timescale of crystallization, the timescales of sublimation of the different volatiles, and the timescale of heating by absorption of solar radiation. The relationships between these timescales determine to a large extent the evolutionary pattern for a comet nucleus. The accuracy of the solution of the set of equations depends on the time step and the spatial grid size used to take care of the different timescales. There are several possibilities for combining the space and time derivatives into a difference equation: the *explicit* scheme, the *fully implicit* scheme, and a modified implicit form, known as the *Crank-Nicholson* scheme, as described in Section 6.1. The explicit scheme has the disadvantage that time-steps are restricted by the Courant condition, for a given space discretisation; thus time-steps may become prohibitively small, when a fine mesh is required in order to resolve steep temperature gradients. The fully implicit scheme results in a system of linear equations and is unconditionally stable for all values of the time-step, but requires a far greater amount of computations for each time-step. The Crank-Nicholson scheme has the advantage of being second-order accurate in time, whereas the fully implicit and the explicit schemes are only first-order accurate in time. The fully implicit scheme, on the other hand, is best suited for stiff equations. Finally, the *predictor-corrector* method is a two-step iterative procedure. The scheme used by each code is indicated in Table 7.2.

Table 7.2: Spatial resolution of top layer [mm], time step [s], numerical scheme (e = explicit scheme, i = fully implicit scheme, cn = Crank-Nicholson, pc = predictor-corrector method)

Algorithm	Grid spacing [mm]	Time step [s]	Numerical Scheme	Grid
A			e	Spherical
B	5	900	cn	Plane-par
C1	1 - 5	200 - 300	pc	Spherical
C2 small r_{H}	1	215	pc	Spherical
C2 large r_{H}	1	1025	pc	Spherical
D small r_{H}	1	few	i	Spherical
D large r_{H}	1	1800	i	Spherical

The numerical method adopted for algorithm C1 is called Douglas–Jones. It is a predictor-corrector method in which the predictor computes the solution at $i + 1/2$, while the corrector is a modification of the Cranck–Nicholson method giving the solution at $i + 1$. This method has the advantage of being stable with a time step independent of the spatial grid.

For comparison of the computational results in this chapter, the spatial grid size and time steps are summarized in Table 7.2. These quantities influence — among other things — the accuracy of the temperature gradients at the surface of the nucleus.

7.3 The Models

The ultimate goal of our work was to develop reliable, time-dependent models for heat and gas diffusion in comet nuclei. As pointed out earlier, different approaches are considered by different investigators. Here we show results from comparisons between five different algorithms independently developed by the authors of this book. We agreed on a set of seven models characterized by different compositions and pore sizes (see Table 7.3) and on a set of assumptions. For all the calculations, a spherical comet nucleus in an orbit of a Jupiter family comet with an orbital period of about 5.2 years is assumed. The spin axis is perpendicular to the orbital plane. The results are calculated for a point located on the equator. A spin period of 1/2000 of the orbital period (about 24.0 hrs) is used to obtain easy time steps. The comparison of different numerical algorithms started with a very simple Model 0. For this model we used a "fast rotator" approximation to average the daily energy input instead of calculating the daily variations. Thus, the peak insolation is reduced to 1/4 of its subsolar value and is independent of the spin of the nucleus. We used this Model 0 as a reference calculation. The solar constant is $F_\odot = 1360$ W m^{-2}. Other constants are given in Table 7.4. For the saturation vapour pressures over ice equations given by Fanale and Salvail (1984) are adopted: $\mathcal{P}_{\mathrm{H_2O}} = 3.56 \times 10^{12} \exp(-6141.667/T)$ Pa and $\mathcal{P}_{\mathrm{CO}} = 1.2361 \times 10^{9} \exp(-764.16/T)$ Pa.

Table 7.3: Input parameters used for model calculations

Reference model	0	1	2	3a	3b	4a	4b
X_{dust} (mass %)			50			50	50
$X_{\mathrm{H_2O}}$ (mass %)	100	100	50	95	95	47.5	47.5
X_{CO} (mass %)				5	5	2.5	2.5
pore radius r_{p} [mm]	1	1	1	0.1	10	0.1	10

The model calculations were carried out as follows: we started with a homogeneously mixed body at a uniform initial temperature ($T_0 = 20$ K) and a uniform mass density distribution. Because heating of the body causes higher rates of sublimation of the most volatile components, the initially homogeneous Composition differentiates into a multi-layer body composition (if it contains more than one component), where the deepest layer has the original composition. The layers above are successively depleted of volatiles,

Table 7.4: Physical parameters used in the reference models

Semimajor axis of orbit	3.09 [AU]
Eccentricity of orbit	0.6579
Radius of nucleus	0.6 [km]
Spin period	24 [hours]
Specific heat of H_2O	1610 [J kg^{-1} K^{-1}]
Change in enthalpy of sublimation of H_2O	2.84×10^6 [J kg^{-1}]
Density of H_2O ice	917 [kg m^{-3}]
Thermal conductivity of ice	$5.68/T$ [Wm^{-1}K^{-1}]
Specific heat of CO	2010 [J kg^{-1} K^{-1}]
Change in enthalpy of sublimation of CO	0.227×10^6 [J kg^{-1}]
Density of CO ice	1250 [kg m^{-3}]
Density of dust	3250 [kg m^{-3}]
Specific heat of dust	1300 [J kg^{-1} K^{-1}]
Thermal conductivity of dust	0.1 [Wm^{-1}K^{-1}]
Initial porosity	0.5
Tortuosity	1
Mean albedo	0.04
IR Emissivity	0.96
Initial uniform temperature	20 [K]

with the top layer containing only the dust component. The boundaries between the layers are the sublimation fronts of the corresponding volatiles.

7.4 Results of Different Algorithms for Various Models

We now compare the results obtained for a few models in order to illustrate and understand differences resulting from implementation of the physics and mathematical procedures. Since it is not always clear what the relative importance of various implementations will be, we believe it is useful to isolate and understand the differences between models. This will direct our attention to more complex ideas and also to a reference that may be useful for comparison to other existing or future models. We wish to stress again that the different algorithms were not altered for the purpose of the present calculations. Instead, we used the capabilities of the algorithms to switch off a functionality or to modify equations. Thus, numerical treatment or solution techniques in the algorithms were intentionally not modified. This is the reason why we do not obtain identical results. We will discuss differences within the algorithms in order to understand the results. It is also our goal to point out these differences in order to let the readers decide what kind of numerical treatment fits their needs best.

Starting out with the simple Model 0, we found almost 100% agreement among the results obtained from different algorithms (computer codes). The first deviations between the results from the different algorithms were encountered when we compared the temperature and gas flux obtained for Model 1. In Figs. 7.1 - 7.7 the maximum surface temperature and the surface gas fluxes of H_2O and CO (if applicable) are plotted versus time for five orbits. Each curve corresponds to a different algorithm: A (solid line), B (short broken line), C1 (long broken line), C2 (dash-dot line), and D (dotted line).

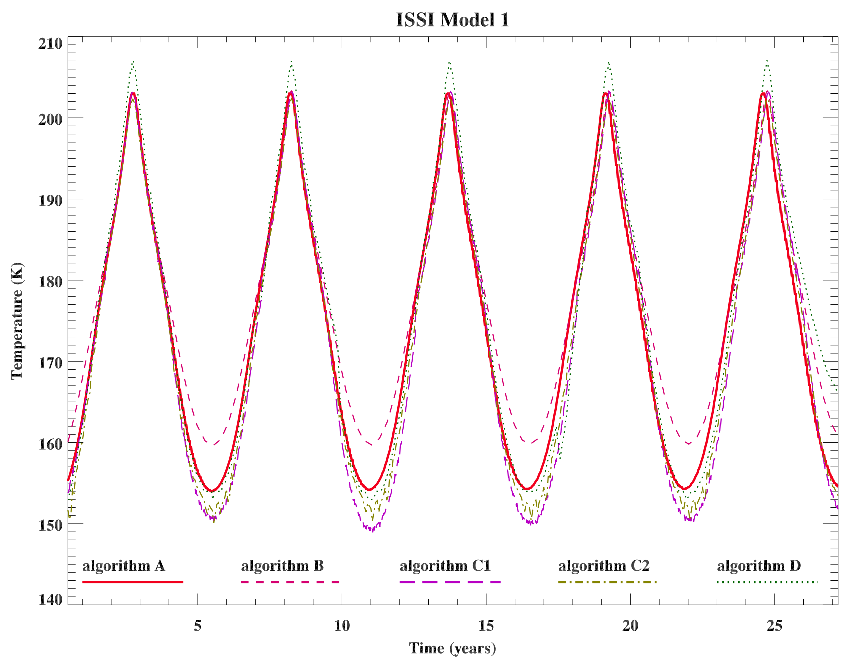

Figure 7.1: Temperature as a function of time. Results obtained from five different algorithms of Model 1: Algorithm A (solid line), algorithm B (short broken line), algorithm C1 (long broken line), algorithm C2 (dash-dot line), and algorithm D (dotted line).

Fig. 7.1 shows the maximum surface temperatures and Fig. 7.2, the surface gas flux of H_2O for Model 1. As can be seen, we obtain good agreement of the results between perihelion and aphelion. At aphelion results vary by ± 5 K for the temperature and about a factor of 10 for the extremes in the gas flux. At perihelion all algorithms but one show the same maximum surface temperature of about 203 K, while one algorithm (D) yields a somewhat higher temperature of about 207 K. The results for perihelion are easy to understand: the entire solar input energy is consumed by the sublimating ice and hence the mass rate of gas production is identical for all calculations, amounting simply to $(1-\mathcal{A})F_{\odot}/[\Delta H_{\mathrm{H_2O}}(1-e)^2a^2]$. The difference in temperature arises from an effort to account for pores on the surface; thus an active area factor $f<1$ multiplying the sublimation rate is assumed in algorithm D. This is compensated by a slightly higher surface temperature, since the sublimation rate depends exponentially on temperature. This effect becomes negligible at larger heleocentric distances, where the other terms in the energy balance equation gain significance. Surface temperatures obtained at aphelion range from about 151 to 154 K, whereas results from algorithm B yield a temperature of about 159 K. The reason for the larger differences obtained at aphelion is that in this case, in contrast to perihelion, energy balance represents a delicate balance of *several small terms*. The result is far more sensitive to differences in algorithms regarding the numerical treatment of heat transported inward (by the water vapour and by matrix heat conduction) at the nucleus boundary.

Thus, differences are related to the numerical treatment, such as zoning, selection of grid size, determination of the heat flux over one grid point, or small variations in the time step of each numerical scheme. In the algorithms that obtain lower surface temperatures, more heat is transferred into the interior, even by using the same value for the heat conductivity, due to a steeper temperature gradient near the surface. One important result of our investigations is that the temperature gradient at the surface is a critical parameter. The gradient itself depends on thermal history and on grid resolution. Moreover, Model 1 is characterized by very strong erosion. Although in reality erosion is a continuous process, it is simulated numerically by rezoning or shell removal at discrete points in time. The rate of erosion may be so rapid that sometimes a layer is removed before the temperature of the next lower layer of the grid has adjusted thermally, resulting numerically in a thermal disequilibrium of the uppermost layers.

Finally, convergence criteria differ between algorithms and these also affect the results. In Section 6.1 we addressed the importance and possible pitfalls of convergence criteria. Here we have an example where differences between these criteria may lead to divergent results. This effect becomes apparent when the same algorithm with exactly the same parameters is used on computers of different specifications. In conclusion, numerical effects cannot be completely avoided. One of the important results of our investigation is that a comparison of different and independent algorithms may be used to provide error bars on the theoretical results, which are otherwise difficult to estimate.

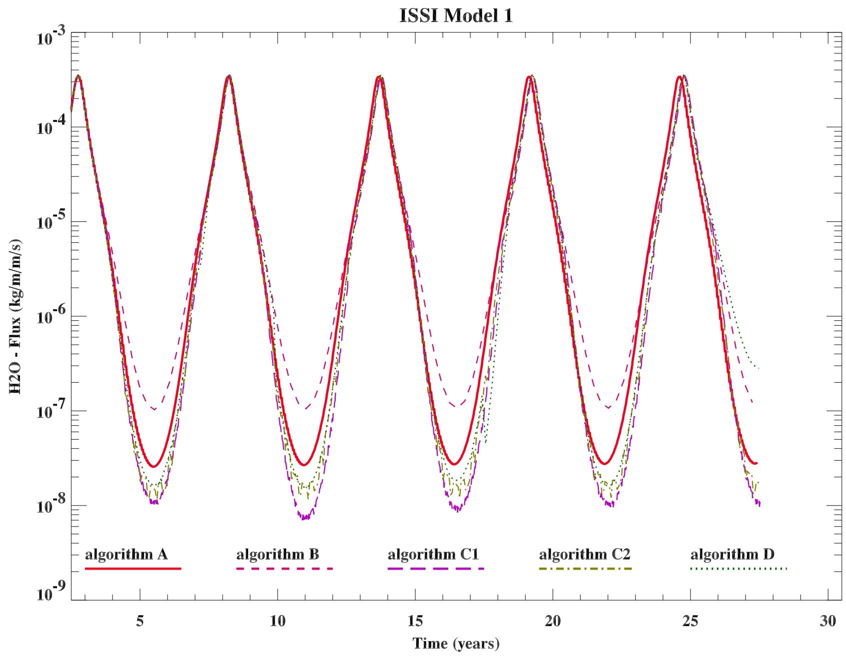

Figure 7.2: Water flux as a function of time. Results from five different algorithms of Model 1 (see Fig. 7.1).

In Fig. 7.2 the maximum water flux from the surface is plotted as a function of time. All algorithms show the same maximum values of about 3.5×10^{-4} kg m^{-2} s^{-1} at perihelion. The results of the different algorithms also show good agreement up to ± 1.5 years around perihelion. At aphelion the results for the water fluxes vary by about a factor of 10 in the extremes. The reason for the strong variation is the same as discussed above. Because of the exponential dependence of the flux on temperature, the variations are much bigger. Nevertheless, absolute values of the flux are extremely small and therefore the results are acceptable.

We now turn to Model 3a, which contains 5% by mass CO in the initial composition. To illustrate the differentiation process that occurs in this case, the depth of erosion of the surface (or H_2O sublimation front) and the sublimation front of CO ice as a function of time are shown in Fig. 7.3.

At the beginning, water ice and CO ice are homogeneously mixed. When the heat from the Sun reaches the nucleus, the CO ice sublimates first from the surface. When all the CO ice at the surface has vanished the CO gas

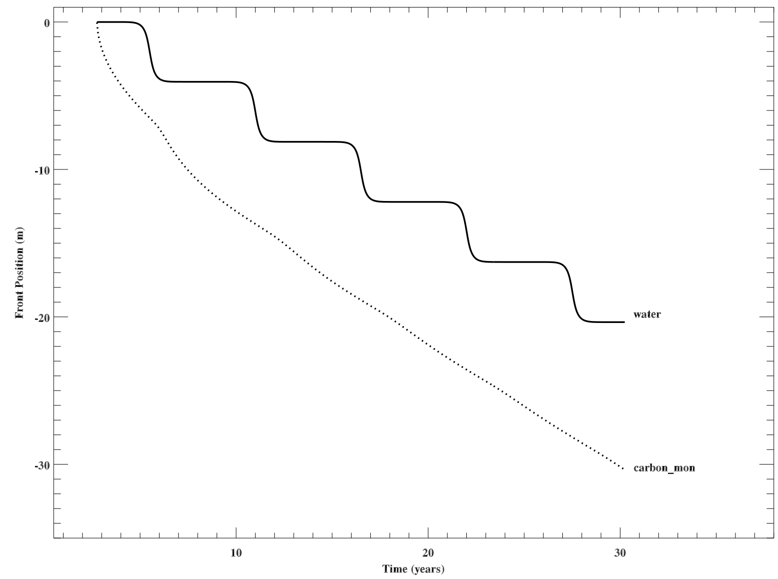

Figure 7.3: Decay of the water ice surface and the location of CO sublimation front as a function of time for Model 3a.

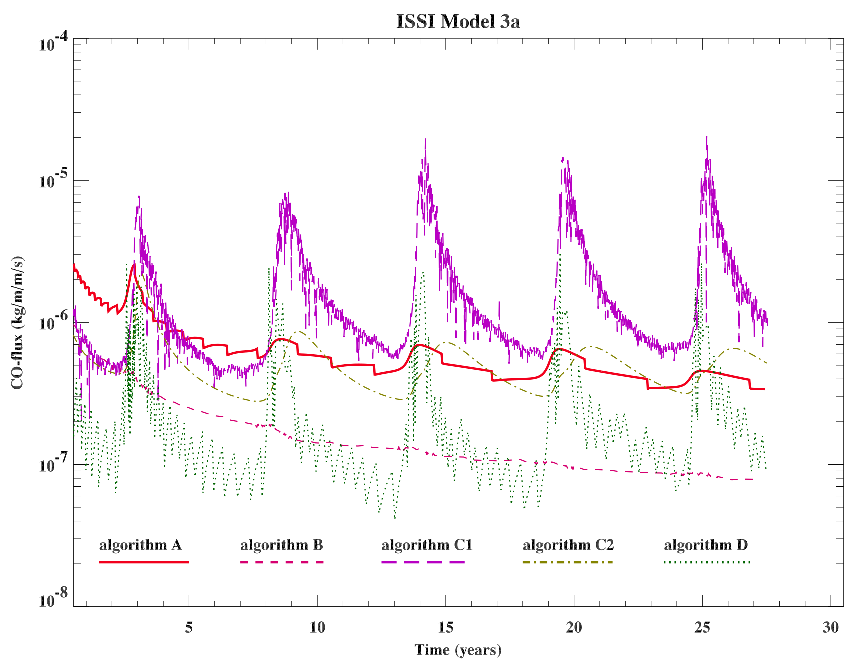

Figure 7.4: CO flux as a function of time. Results from different algorithms of Model 3a (see Fig. 7.1).

flux originates from an inner sublimation front. The CO vapour diffuses through the pores. After a short time the CO sublimation front has moved some distance below the surface, leading to a chemical differentiation of the outer layers of the nucleus. The layer between the surface and the CO sublimation front is depleted of CO. The depth of the CO sublimation front as a function of time depends on the amount of energy transported into the interior. This amount is a strong function of the heat conductivity of the matrix material. The heat conduction is assumed to be that of compact water ice reduced by the Hertz factor to take into account the reduced area of contact in the granular structure of the porous matrix (for our models $f_{\mathrm{H}} = 0.01$ was assumed). After five orbits (approximately 30 years) the CO front has moved about 30 m into the interior of the nucleus compared to its initial position, and is found about 10 m below the actual (eroded) surface of the nucleus.

The surface of the nucleus shrinks by about 4 m each orbit. During perihelion passage the sublimation of water ice is very strong, because it depends exponentially on surface temperature. The flux of water vapour from the surface varies by several orders of magnitude from aphelion to perihelion. This is the reason why the surface stays almost constant at larger heliocentric distances and shrinks significantly only during perihelion passage.

For Model 3a, we obtain excellent agreement among algorithms regarding surface temperature and water production rate for most of the orbit, with differences in temperature of ± 10 K at aphelion and correspondingly larger differences in the H_2O flux, keeping in mind that the flux in all cases is negligibly small near aphelion. Here, however, surface temperature and heat flux *into* the interior strongly influence the flux of CO from the interior. In Fig. 7.4 the mass flux of CO emitted from the surface at the subsolar point is presented for five orbits, as obtained by the different computational algorithms for Model 3a. As can be seen, the results show some significant differences among algorithms. Algorithms C1 and D show significant variations from perihelion to aphelion and possibly a small increase in the minimum CO flux from orbit to orbit (the small oscillations are of numerical nature, being caused by frequent rezoning). Algorithms A and C2 show much smaller fluctuations. In addition, algorithm C2 shows a possible damping of the oscillations and a small increase in the minimum values from orbit to orbit. Results obtained with algorithm B show a slowly decreasing mass flux of CO with no orbital variation.

In order to understand these differences, it is important to note that the energy absorbed in CO sublimation is less than half of a percent of that absorbed in sublimation of H_2O. This results from a factor of 12.5 in the

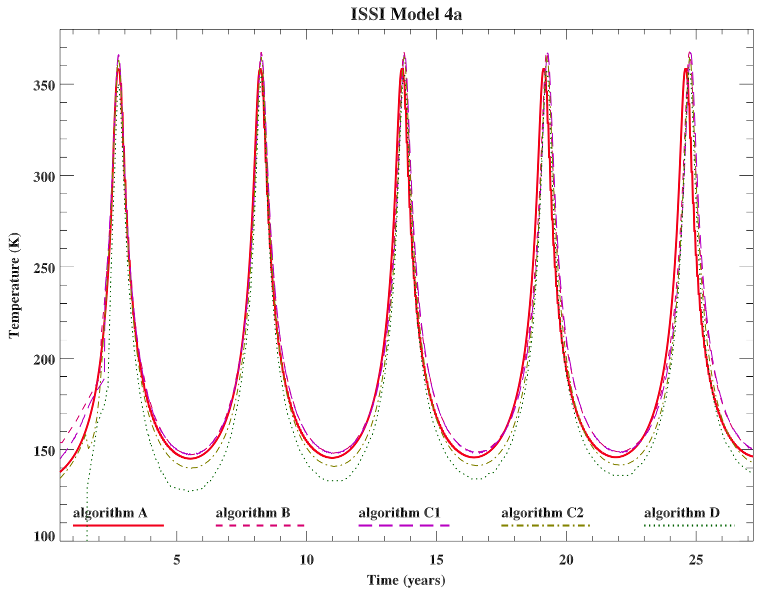

Figure 7.5: Temperature as a function of time. Results from five different algorithms of Model 4a (see Fig. 7.1).

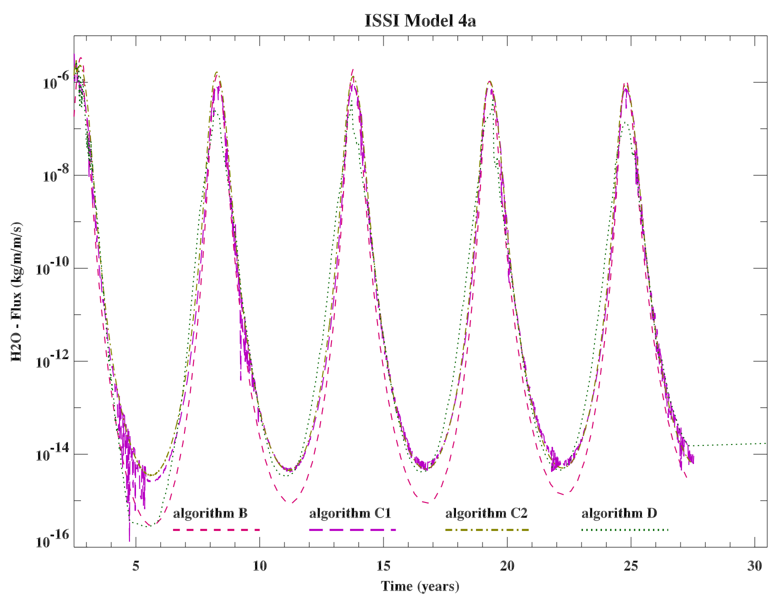

Figure 7.6: Water flux as a function of time. Results from four different algorithms for Model 4a (see Fig. 7.1).

ratio of the respective latent heats and another factor of 19 in the assumed ratio of mass abundances. Thus very small differences in the algorithms, particularly those related to the various mechanisms of heat conduction, may lead to significantly different results for the rate of CO sublimation. We distinguish between two different patterns: cyclic orbital variation (algorithms C1 and D) and an almost monotonic behaviour (algorithms A and B), as well as an intermediate case (algorithm C2). This may be explained by the depth of the CO sublimation front with respect to the orbital skin depth of about $2-3$ m: a CO front within the skin depth will lead to orbital variation in production rate, while a deeper CO front, below the skin depth, will not.

Results may be divided into two groups from yet another point of view. Within a factor of 2, all flux values start with about 10^{-6} kg m^{-2} s^{-1}. Algorithm B reaches the smallest CO flux of about 8×10^{-8} kg m^{-2} s^{-1} after five orbits. This decrease of the CO flux is not accompanied, however, by a slow-down in the inward motion of the CO sublimation front (see Fig. 7.3). This means that not all of the sublimated CO diffuses outward to contribute to the surface flux. A fraction of the CO gas diffuses inward and recondenses in deeper layers. The effect of recondensation is treated differently by the different algorithms: A, C1, and C2 assume that the gas pressure equals the saturated vapour pressure, while B and D do not – they calculate sublimation and condensation rates from the difference between the gas pressure, obtained from the ideal gas law, and the saturated vapour pressure. Indeed, the results of A, C1, and C2 are closer to each other, as are those of B and D. In addition, different expressions for the gas diffusion coefficient in the various algorithms influence the inward and outward fluxes of the CO gas. Clearly, the treatment of volatiles in the porous interior of a comet nucleus needs further examination.

Finally, given that the rate of erosion is about 4 m/orbit (as obtained by all algorithms), a steady state would be reached if the *averaged* CO flux were roughly 5.7×10^{-7} kg m^{-2} s^{-1}. Indeed, in three cases it seems that the average rate converges toward steady state (algorithms A, C2, and D), with C1 above and B below this value.

Next we added dust to the initial composition of our model comet. Models 2 and 4 are both characterized by a dust layer on the surface assuming that dust is not entrained by escaping gas. Results obtained from Model 2 were very similar to the results of Model 4. Thus, to be brief, we comment only on Model 4a. In Fig. 7.5 the temperature and in Figs. 7.6 and 7.7 the surface gas flux of H_2O and CO are plotted versus time for five orbits. Each figure shows again the results obtained by the different computational algorithms. It can be seen that all algorithms give results in good agreement.

In Fig. 7.5 surface temperatures are plotted versus time for five orbits. All algorithms show a similar maximum surface temperature of about 360 K near perihelion. Because we assume a dust mantle on the surface that cannot be entrained by escaping gas, the observed maximum surface temperatures are much higher than in a case of a dust-free surface. The gas flux originates from sublimation below the dust mantle. Thus, the energy input into the dust-water ice boundary controls the gas flux from the interior.

Surface temperatures obtained at aphelion range from about 130 to 150 K. The reason for the difference in the results at aphelion can be understood with the help of Eq. 4.19. If the rate of energy input from the Sun is small, the fraction of the reradiated power ($\varepsilon\sigma T_{\mathrm{s}}^4$) is also small. The fraction of input power for sublimation at the surface is zero because of the dust mantle. As a consequence, the energy input into the nucleus and the surface temperature depend mainly on the power of the heat flux ($\kappa_{\mathrm{d}}\nabla T_{\mathrm{s}}$). All algorithms used a constant value of the emissivity and the heat conductivity. Thus, the only free parameters to be balanced at the surface are the temperature gradient into the interior and the surface temperature itself.

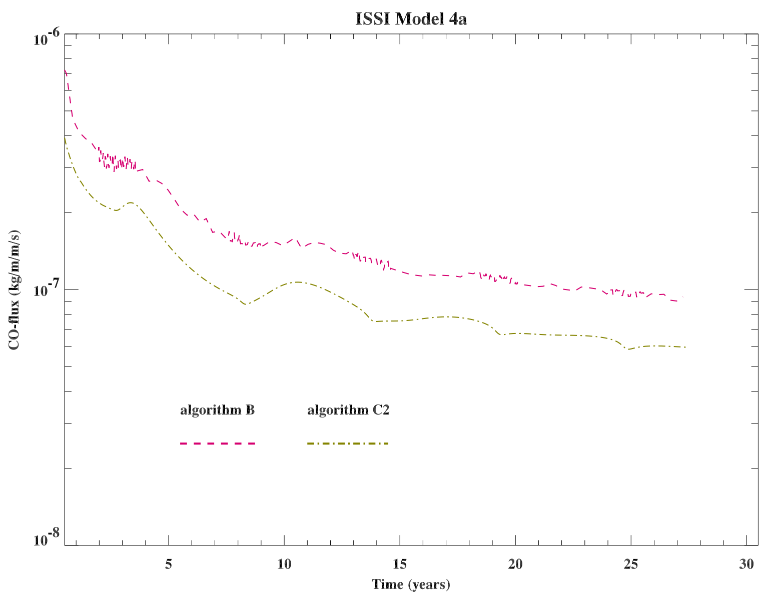

Figure 7.7: CO flux as a function of time. Results of two different algorithms (B and C2) of Model 4a (see Fig. 7.1).

In all algorithms, very steep temperature gradients below the surface were obtained. Because of daily variations of the insolation on the surface for a rapidly spinning nucleus, the gradient changes significantly at every time step of the numerical scheme. In order for the the solution of the difference equation to converge to the exact solution of the differential equation, very fine zonings — both temporal and spatial — are required. This differs among algorithms, as shown in Table 7.2. Even very small differences in temperatures at the subsurface grid points will impact the temperature gradient significantly. After thorough investigations, we concluded that the numerical treatment of the temperature calculations at subsurface grid points caused differences between the results of various algorithms. We found that porosity has only a small influence on the temperature results.

In Fig. 7.6 the maximum water flux from the surface is plotted as a function of time. The H_2O mass flux varies by several orders of magnitude during one orbit. The flux depends strongly on the amount of energy transported to the sublimation front of water ice below the surface. Each curve shows again the results obtained by different numerical algorithms. All algorithms show the same maximum value of about 3×10^{-6} kg m^{-2} s^{-1} at perihelion. This absolute value is about two orders of magnitude smaller than the values obtained in the dust-free case where the ice is sublimating directly from the surface. The overlaying dust mantle quenches the water flux significantly. The flux reductions compared to a free sublimating surface depend mainly on the pore radius of the overlaying dust layer and the depth below the surface of the sublimation front. The results of the different algorithms show also good agreement up to ± 2 years around perihelion. At aphelion the results for the water fluxes vary by about a factor of 10 between the different algorithms. These strong variations are due to the reasons discussed above. Because of the exponential dependence of the flux on temperature, the variations are more prominent. Nevertheless, absolute values of the water flux are very small at aphelion.

In Fig. 7.7 the mass flux of CO from the surface at the subsolar point is plotted for five orbits for Model 4a, as obtained from two algorithms. It can be seen that the results of algorithms B and C2 disagree by about a factor of 2. Results obtained with algorithm B show a slowly decreasing mass flux of CO. It starts at about 7×10^{-7} kg m^{-2} s^{-1} and converges to about 1×10^{-7} kg m^{-2} s^{-1} after five orbits. The reason for the decrease of the CO flux is the inward motion of the sublimation front. Results obtained with algorithm C2 also show a slowly decreasing mass flux of CO, but absolute values are a factor of 2 smaller. CO fluxes started at about 4×10^{-7} kg m^{-2} s^{-1} and after five orbits had decreased to about 6×10^{-8} kg m^{-2} s^{-1}. The sublimation front of these models lies just below the penetration depth of the orbital heat wave. As discussed earlier, not all of the total mass sublimation of CO will diffuse outwards through the pores and contribute to the surface mass flux; a significant fraction of the sublimated gas diffuses inwards and condenses in deeper layers below the sublimation front.

7.5 Conclusions

The results of the calculations presented here are obtained from the 1-D models of five independent modeler groups. Although each group agreed to use an identical set of parameters, we found differences in the results. Our conclusion to explain these differences is that the treatment and calculation of parameters such as thermal conductivity and porosity are different and that these differences, even if they appear to be minor, have significant effects on the results. Therefore, computing the energy flux balance on the nucleus accurately and in detail is essential to understand the results. The effective heat flux into the interior controls the amount of energy available within the body for internal sublimation of ices and internal heating. The fact that the differences are small at perihelion strengthens that conclusion because at perihelion the relative fraction of energy transported via heat conduction is the smallest. Heat transport via thermal conduction of the matrix material depends on the value of the thermal conductivity and the thermal gradient into the interior. Heat transported via the vapour into the interior depends on the porosity and the gas flux into the interior. As a consequence, the number of molecules diffusing through the pores and leaving the surface of the nucleus is strongly dependent on the amount of energy that is available for the sublimation of ices. Temperatures at the surface are proportional to the reradiated energy. The energy flux balance is different for active and inactive surfaces. In the case of an active surface our results show that water vapour flux can be orders of magnitude higher than in the case of an inactive surface, where the vapour flux is quenched by the dust mantle.

Maximum surface temperatures and the surface gas flux of H_2O of Model 1 are in a reasonably good agreement between all results from the different algorithms. At aphelion results vary slightly for the temperature. However, we observed differences of a factor of about 10 for the extreme gas fluxes. One explanation is that the heat transported by the water vapour and by matrix heat conduction into the interior is treated slightly differently in each algorithm. Thus, it is believed that differences are related to the numerical treatment, e.g. zoning, selection of grid size, determination of the heat flux over one grid point, or the small variations in the time step of each numerical scheme. In the models that obtain lower surface temperatures, more heat is transferred into the interior, even by using the same value for the heat conductivity. We have shown that the temperature gradient is the critical parameter. The gradient itself depends on the thermal history, on the grid size, and on the insolation, which varies continually. Because thermal steady state could not be reached in the surface layer, we found that the different algorithms seem to have different convergence values. The results for the water fluxes at aphelion vary by about a factor of 10 in the extremes. Because of the exponential dependence of the flux on the temperature, the variations are much larger. Nevertheless, absolute values of the flux are extremely small and therefore these results are acceptable for most investigations.

In Models 2, 4a, and 4b a dust layer develops on the nucleus because we did not allow dust to be entrained by escaping coma gases. The main effects of dust layer are: (a) the dust layer strongly reduces the surface sublimation and accordingly the temperature rises, (b) a strong differentiation takes place and the sublimation front of CO ice (when present) recedes, (c) the H_2O vapour release follows the seasonal temperature variations, and (d) the CO release exhibits an almost continuous behaviour.

Considerably better agreement in the results is obtained from all algorithms in models with a dust mantle. Because the dust was not allowed to be entrained by the escaping gas, the observed maximum surface temperatures are much higher. The gas flux in these models originates from sublimation below the dust mantle. The crucial parameter is again the temperature gradient into the interior. If the gradient is steep, the surface temperature becomes smaller. In almost all our models very steep temperature gradients below the surface were obtained. We concluded that the numerical treatment of the subsurface temperature gradient causes the observed differences between algorithms. The temperature gradients did not converge to the same values because of non-linearity of the insolation.

We obtained almost identical results for models where the average insolation profile was constant. The maximum water flux in the Models 2, 4a, and 4b depends also on the porosity of the matrix material between the sublimation front and the surface. The maximum H_2O gas flux is about 3×10^{-6} kg m^{-2} s^{-1} at perihelion and about two orders of magnitude smaller than the values obtained in the case of a dust-free surface. The dust mantle quenches the water flux significantly. At aphelion the results for the water fluxes vary by about a factor of 10 in the extreme cases. The reasons for these strong variations are the exponential dependence of the gas flux on the temperature. However, absolute values of the water fluxes are very small at aphelion. The overall behaviour of the gas release is similar in models with small or large pores.

Surface temperature strongly influences the H_2O flux from the surface, and similarly the heat flux into the interior strongly influences the CO flux.

In Model 3a, containing CO, results show a time-dependent decrease of the CO flux. The reason for the decrease is the progressive inward motion of the sublimation front. The CO fluxes show only very small orbital fluctuations. Thus, the depth of the sublimation front must be close to the lower limit of the orbital penetration depth of about 2 - 3 m. Not all of the sublimated CO will diffuse outwards and contribute to the surface gas flux. A significant fraction of the sublimated gas condenses in deeper layers below the sublimation front.

To define a 'real' or an 'absolute standard,' would require devoting a much larger effort to the numerical treatment or to defining a standard algorithm. This was not our goal. We exploited used the capabilities of algorithms used by different groups and switched off certain functionalities. Thus, the numerical treatment of some parameters or the solution techniques in the algorithms were not optimized to obtain a 'real standard.' Our goal was to make the reader sensitive to the problems that may occur. At present, the results are an average of the algorithms and models discussed. They may be used as a reference for other models.

The total gas production of a comet, i.e. the integral of $Z_{\mathrm{H_2O}}(\zeta)$, as obtained from Fig. 5.1, over the active surface area of a comet nucleus (ignoring heat conduction into the nucleus), gives excellent results for heliocentric distances $r_{\mathrm{H}} < 3$ AU.

— 8 —

Orbital Effects

> "Halley produced the Elements of the Calculation of the Motion of the two Comets that appear'd in the Years 1607 and 1682, which are in all respects alike, as to the place of their Nodes and Perihelia, their Inclinations to the plane of the Ecliptick and their distances from the Sun; whence he concluded it was highly probable not to say demonstrative, that these were but one and the same Comet, having a Period of about 75 years; and that it moves in an Elliptick Orb about the Sun, being when at its greatest distance, about 35 times as far off as the Sun from the Earth."
>
> from *Journal Book* of the *Royal Society*, 3 June 1696.

8.1 Inward Heat Flux

The thermal evolution of a comet nucleus is determined by the heat flux into its interior. The calculated heat flux depends on the approximations that were used. It is instructive to compare the slow- and fast-rotator approximations in this respect. These two approximations will give different results since for the slow rotator large diurnal surface temperature variations must be taken into account, while only the averaged values are considered in the fast rotator approximation. However, of greater interest is the long-range timescale of evolution, since we expect the internal thermal evolution to be very slow.

Figure 8.1 shows the heat flux that penetrates the nucleus for the fast and slow rotator (averaged over one spin period) as a function of time, for an entire orbit of Comet 46P/Wirtanen resulting from a quasi 3-D model (Cohen et al., 2003). Along the orbit, the heat flux reverses direction. Starting from a distance of about 2.5 AU post-perihelion until aphelion, the heat flux is directed outwards, which means that the nucleus emits some of the heat gained while it was closer to the Sun and cools off. The fast-rotator approximation yields higher inward heat flux as the comet approaches perihelion, starting at about 3 AU. On the other hand, as the comet approaches aphelion (where the effective heat flux is negative), the fast-rotator model again yields a higher absolute value, i.e. the comet dissipates more heat.

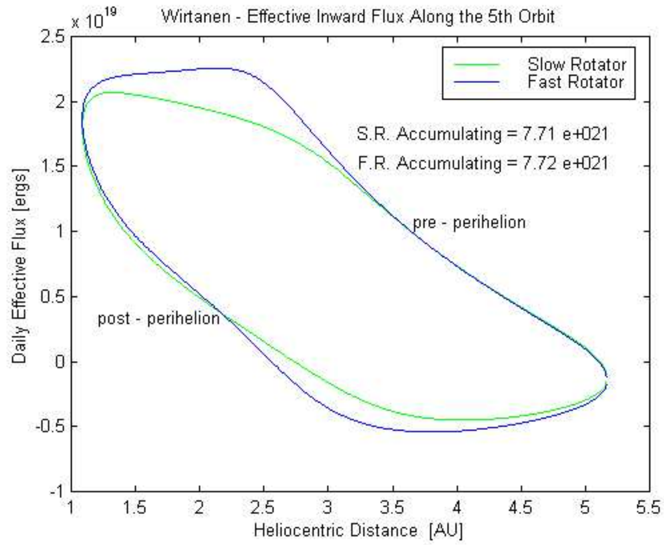

Figure 8.1: Comparison of heat flux for a fast spinning and a slowly spinning comet nucleus in the orbit of 46P/Wirtanen. Negative flux values indicate that the flux is outflowing. (From Cohen et al., 2003.)

Thus, the fast-rotator model's tendency to yield more extreme flux values results in a compensation of energy along the orbit that leads to about equal total net fluxes, when integrated along the entire orbit. This result has important implications for long-term evolution calculations of the interior structure of comet nuclei. It indicates that such calculations – which would be difficult to perform if time steps were limited by the spin period – may adopt the fast-rotator approximation. In view of the significance of this conclusion, it was also tested for the orbit of Comet 1P/Halley, with very similar results: large differences on short timescales that compensate each other and result in almost equal effective heat input over a full orbital revolution. In more general terms, the effect of compensating heat fluxes may be explained as follows. In the lowest approximation, we may assume that the heat flux at the surface (either inward or outward) is about proportional to the surface temperature, since the temperature below the skin depth is about constant by definition. For the slowly spinning comet the daily flux will thus be determined by the daily average temperature, roughly, $T_{\mathrm{day-av}} = 0.5(T_{\max} + T_{\min})$, where $T_{\max}$ and $T_{\min}$ represent temperatures at the sub-solar and anti-solar points, respectively. For the fast spinning nucleus, the surface temperature T_{fast} is uniform and independent of spin; it is calculated from the averaged solar flux. It is interesting to compare

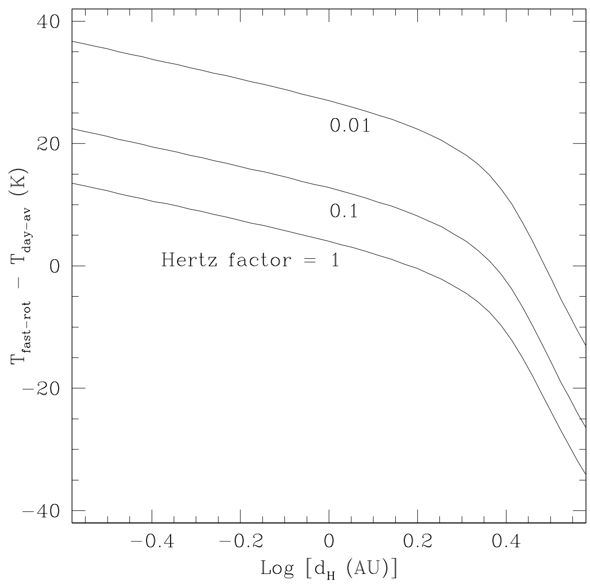

Figure 8.2: Difference between surface temperature of a fast spinning nucleus and daily average of a slowly spinning nucleus versus heliocentric distance, with the Hertz factor as parameter (from Cohen et al., 2003).

these two temperatures as a function of heliocentric distance. This is shown in Fig. 8.2 for different values of thermal conductivity. We note that the difference between these temperatures changes sign as the distance increases, meaning that heat easily gained at smaller $r_{\rm H}$ is also easily dissipated at larger $r_{\rm H}$. We also note that this compensating effect is not perfect, but will depend on thermal conductivity and on the orbital parameters. A systematic investigation on the semimajor axis – eccentricity plane, performed by calculating in each case the averaged difference over one full revolution showed that the smallest difference, amounting to a fraction of a percent, was indeed obtained for short-period orbits (such as Comet 46P/Wirtanen) and low conductivities. This crude approximation breaks down at large distances, but there temperature differences are always small.

8.2 Short-Period vs. Long-Period Comets

8.2.1 Dynamical Evolution

The study of the dynamical evolution of comets can help in establishing relationships between their present status and their origin. The evolutionary paths connecting the comet reservoirs in the outer Solar System and the population of short-period comets involve stellar and planetary perturbations. In the region well outside the planetary system the dynamical evolution is dominated by the vertical component of the galactic tidal potential and by encounters with passing stars and giant molecular clouds. In the inner regions of the Solar System planetary close encounters play a special role, increasing or decreasing the rate of the orbital evolution of a comet depending on its orbital elements at various stages of the evolutionary process (Carusi et al., 1985). As a consequence of these processes, comet orbits are chaotic. A body in a chaotic orbit experiences various regimes of motion and is characterized by orbital variability. For this reason comets can be found over a range of heliocentric distances much greater than those spanned by planets and asteroids.

Reservoirs of long- and short-period comets are thought to exist in the outer Solar System. The Oort cloud seems to be the most probable source of long-period comets. Jan Oort (1950) noticed that no comet had been observed coming from interstellar space. Instead, all long-period comets normally have aphelia that lie at a great distance and their orbits have no preferred direction. For these reasons he deduced the existence of a vast cloud of comet nuclei, now named the Oort cloud, in the shape of a diffuse spherical shell at about 50,000 AU from the Sun (which is about 1/5 of the distance to Alpha Centauri, the nearest star). The statistics imply that this cloud, which surrounds the entire Solar System, could perhaps contain up to 10^{13} objects. In this hypothesis, the Oort cloud may account for a significant fraction of the mass of the planetary system (perhaps even more than Jupiter itself). Unfortunately, since the individual comet nuclei are so small and at such large distances, scientists have very little direct evidence about the Oort cloud. Some of the comet nuclei in the Oort cloud can, from time to time, fall into the inner Solar System and come under the gravitational control of the planets, becoming long-period comets.

Several physical mechanisms have been proposed that remove comet nuclei from the Oort cloud, pulling them into the inner Solar System, or ejecting them to interstellar space. First of all, comet nuclei in the Oort cloud can be perturbed by the gravity of passing stars (Biermann et al., 1983). In fact, all the stars in the disk of the Milky Way share a common motion around the centre of the galaxy, but also move relative to each other. Stars approach from random directions, so the velocity changes are sometimes positive, sometimes negative. The combined effect is a chaotic perturbation of the velocity (or a "random walk") such that, after 10,000 stars have passed by, the original orbits of comet nuclei have been drastically altered. It is important to establish how long this might take. The answer depends on where comets come from in the Oort cloud.

Most comets appear to come from the outer edge of the cloud, where the attraction to the Sun is weakest and passing stars have larger effects. Closer to the Sun, comets are more tightly bound to the Sun. Other perturbations might occur, such as the gravity of the Milky Way disk itself disturbing the orbits of comet nuclei in the Oort cloud, with an effect comparable in size to that of passing stars. Also the Sun may disturb the Oort cloud's objects (on very rare occasions, when passing through a giant molecular cloud) causing a shower of comets to rain on the planetary system. Another possible mechanism to make comets leave the Oort cloud may be the shock wave from an explosive event such as a supernova.

The short-period comets are now believed to come from a closer reservoir named after Kuiper and Edgeworth. Edgeworth (1943, 1949) and Kuiper (1951) were the first to speculate on the existence of matter residing beyond Pluto. However, it was only recently that the Kuiper belt has been proposed as a source region for the low inclination short-period comets (Fernandez, 1980). Kuiper Belt Objects (KBOs) could be a remnant of the formation of the giant planets, because the amount of rocks and ices should not have truncated arbitrarily at Neptune.

The first trans-Neptunian object was discovered in 1992 (Jewitt and Luu, 1993), followed by the discovery of a large number of similar bodies (Weissman and Levison, 1997; Luu et al., 1997). About two thirds of these bodies have semimajor axes between 42 and 47 AU, small eccentricities and a wide range of inclinations; about one third reside in the 3:2 resonance with Neptune at 39.4 AU (the so called Plutinos), but the estimated abundance of the Plutinos can be affected by observational bias. A few objects have large eccentric and inclined orbits with perihelia near 35 AU: these "scattered Kuiper belt objects" may represent a swarm of bodies scattered outward by Neptune. The total scattered population is very uncertain.

The Kuiper belt is probably the source of most short-period comets and Centaurs (Valsecchi and Manara, 1997; Morbidelli, 1999). It is interesting to note that the Kuiper belts existence was postulated on theoretical arguments before its discovery. The main argument in favour of the existence of a disk is that it is difficult to explain the average low inclination of "Jupiter family" comets (orbital periods < 20 yr and Tisserand invariant[1] $T_{\mathrm{J}} > 2$) starting from a spherical distribution, like that of long-period comets. Numerical simulations show that, starting from an isotropic cloud, one can likely produce Halley-type comets (orbital period between 20 and 200 yr and Tisserand invariant $T_{\mathrm{J}} < 2$), while it is difficult to reproduce a flat distribution similar to that of the Jupiter family (Stagg and Bailey, 1989; Quinn et al., 1990).

[1]See Chapter 1.

Many models of the Kuiper belt have been published. Several lines of evidence suggest that the Kuiper belt was once more massive than it is today and that mutual collisions have played a crucial role (Farinella and Davies, 1996). Such collisions provide an extraction mechanism for the short-period comets, but the precise location of the source and details of the extraction process remain undefined (Ip and Fernandez, 1997; Morbidelli, 1997; Duncan and Levison, 1997).

The coupled effect of orbital evolution and loss of volatiles and dust from the nucleus leads to a cometary lifetime in the inner Solar System much shorter than the age of the system itself. It is important to establish the different dynamical channels connecting the proposed reservoirs of comets to short-period comets, because this may allow us to infer their original composition and subsequent physical evolution. We will discuss this in the next section.

8.2.2 Differences between Long- and Short-Period Comets

The chemical composition of long-period and short-period comets is similar, although some differences should be expected. The difference in composition can be related to their formation zone, which in turn is characterized by different compositions of the ices originally present. In fact the protosolar nebula was characterized by the presence of radial gradients in pressure and temperature. What pressure and temperature values characterized the nebula is not yet stated: the application of accretion disk theory to the protosolar nebula can help in giving some reference values, however, and as stated by Wood (1999), most of planetary accretion – including comet formation – took place after gas accretion onto the protosolar disk was already completed. The position of the ice condensation zone in the disk, the so-called "snowline", is model dependent and divides the solar nebula into an inner and an outer region (see Fegley, 1999, and references therein). The position of the snowline moves inwards as the protosolar nebula cools, but never beyond the present position of Jupiter (Stevenson and Lunine, 1988), since ice was probably needed to give rise to the runaway accretion of Jupiter.

The outer part of the nebula is not well described by existing models, particularly the Kuiper belt region. However, the presence of N_2, CO, CH_4 ices in Triton and Pluto and possibly of CH_4 in the Kuiper belt object 1993SC, is an indication that the temperatures there were low enough to condense these ices. Thus, we can expect temperatures below 25 K for the comet nuclei of the Kuiper belt. Oort cloud objects are instead thought to have formed closer to the Sun than the KBOs, but surely beyond the snowline. At the time of giant planet formation the region where Kuiper belt objects originated probably contained a larger amount of material than now. Icy planetesimals not incorporated in giant planets were interacting gravitationally with them. Close encounters of planetesimals with Jupiter were responsible for depletion of the protosolar nebula since the probability to eject bodies into hyperbolic orbits was very high. Other giant planets could have been less effective in the ejection, but much more eff-ective in displacing planetesimals into far, but still gravitationally bound orbits. These objects might then have been ejected from the Solar System by gravitational encounters, and those that didn't totally escape could have formed the distant Oort cloud. The source of long-period comets has been assumed to be primarily the Uranus – Neptune zone, since not only Jupiter but also Saturn was expected to eject most of the icy planetesimals into interstellar space. According to Weissman (1999, and references therein) the efficiency of Uranus and Neptune in placing objects in the Oort cloud exceeds that of Jupiter and Saturn by a factor of about 20. However, recent studies seem to indicate that the entire region of giant planets may be responsible for the ejection in the Oort cloud, thus increasing the probability of objects with different chemical compositions being trapped in the same dynamical reservoir.

How do these differences in origin affect the chemical composition of comets? Clearly, the main composition is water ice in both cases, but the different condensation temperatures can lead to different ice phases. For example, comets that are formed in the Jupiter – Saturn region are possibly formed at temperatures higher than 78 K – where the transition from amorphous to crystalline ice starts (Schmitt et al., 1989) – so probably their ice is in crystalline form, while comets that are formed at much lower temperatures, like those in Kuiper belt region, possibly contain amorphous ice. The origin of amorphous ice is still unclear. It is not observed in the interstellar medium and it is difficult to understand how it might have formed in the solar nebula (Kouchi et al., 1994). The presence of amorphous ice can contribute to trapping of different highly volatile ices, thus making the differences more pronounced. The argument of the snowline can be applied to any volatile. Thus, if models with several volatile species are developed, the stability region of different ices can be defined as a function of distance from the Sun. The ice composition of a comet nucleus will depend on formation temperature, but the trapped volatile content will be related to the composition of the protosolar nebula and to the phase and temperature of the water ice. For example, objects formed in the Jupiter region – at about 170 K – will be unable to retain large amounts of highly volatile gases such as CO, while objects formed at the Neptune distance and beyond will probably incorporate many other molecules. Unfortunately, we do not have compelling observational constraints to discriminate between the two populations in terms of their composition. The only stated difference is in the deficiencies in long-chain carbon molecules as seen among some long-period and short-period comets (A'Hearn et al., 1995). How this is related to the original composition of comet nuclei or how it is related to the overall thermal history of a single body, is not yet understood. Overlap of the different original compositions with the effects of processes in comet nucleus formation should be considered. Among the most important processes, as far as the comet nucleus is concerned, we list the effects of collisions, the formation of irradiation mantles associated with devolatilization of outer layers, and the decay of radioactive elements.

- *Collisions.* Collisions could have affected the thermal evolution of an object provided that the heat is not dissipated in a short time. Small, high velocity impacts can simply deposit energy on the surface of the body and is then rapidly radiated into space. Energetic collisions may involve larger parts of a comet nucleus, thus mixing the material and redistributing the heat in a layer. In this case, the heat generated will not be easily reradiated by the nucleus, but will contribute to the overall warming of the nucleus. However, the temperature increase is very small. For example, if heat is shared uniformly throughout the colliding bodies, heating by inelastic collisions leads to a temperature increase $\Delta T = v_{\mathrm{coll}}^2/(2c)$, where c is the specific heat of the comet nucleus and v_{coll} is the relative speed of collision. For $v_{\mathrm{coll}} = 100$ m/s and ice temperature of 30 K, $c = 230$ J kg^{-1} K^{-1} and the temperature increase $\Delta T \approx 20$ K. At an ice temperature of 50 K, $c = 440$ J kg^{-1} K^{-1} and $\Delta T \approx 10$ K. The effects have been considered in the primordial evolution of terrestrial planets (see, e.g. Coradini et al., 1983) and for the evolution of planetary satellites (see, e.g. Lanciano et al., 1981 and references therein). The problem is the relevance of the small temperature increase, and how frequent collisions in the Oort cloud and in the Kuiper belt are. Davis and Farinella (1997) found that most objects that evolve to short-period comets are fragments of objects collisionally disrupted. Thus, this process may contribute to a rubble pile structure of comet nuclei.

- *Irradiation mantle.* Once formed, comets are exposed for about 4.5×10^9 years to the flux of galactic cosmic rays. Stellar UV photons and cosmic ions deposit their energy on comet nucleus surfaces. In the Oort cloud, which is outside the heliopause, the flux of energetic cosmic radiation is larger than at the Kuiper belt. According to Allamandola et al. (1999), we can expect the production of many new species including organic refractory materials, even from simple ices. Laboratory experiments using particle accelerators show that during irradiation there is preferential escape of hydrogen and an increase in the chemical complexity of the irradiated material. Many complex carbon compounds may be formed resulting in materials that are dark and neutral to red in colour. Cosmic rays of about 1 MeV energy are responsible for most damage in ice to a penetration depth of about 1 m (Strazzulla, 1999). The conclusions of these experiments are mainly based on irradiated ices thicker than the penetration depth of the radiation. Not only are mantles formed, but the mantle is also stable when the underlying ices sublimate. If this mantle is porous and has a high degree cohesion, then it might even survive the first perihelion passage of a "new" comet.

- *Radioactive decay.* The effects of radioactive heating on comet nuclei can be an important process in the early phase of their evolution when the comets are far from the Sun. Whipple and Stefanik (1966), Wallis (1980), Prialnik et al. (1987), Yabushita (1993), Haruyama et al. (1993), Prialnik and Podolak (1995), and De Sanctis et al. (2001) examined thermal evolution of comet nuclei taking into account radiogenic heating using different thermal models and assumptions. Some of these investigations are devoted to the thermal history of comet nuclei during their residence in the Oort cloud, where the thermophysical conditions are somewhat different from those in the Kuiper belt. Radiogenic heating (if it occurs) becomes a substantial source of energy for differentiation. Between 30 and 50 AU, radiogenic heating may be comparable to solar radiation. Radioactive elements, if they exist in sufficient quantity, may modify the original composition of these objects. The results obtained for the internal structure of comet nuclei in the Oort cloud cannot be projected to short-period comets because of their different evolution. From the results of previously quoted simulations, KBOs may be depleted in volatiles. These bodies may have chemically differentiated (compositionally layered) structures. At some depth below the surface, the most volatile ices (e.g. CO) may be completely absent. Simulation results depend on the kind and amount of radiogenic elements considered in the model body and on the physical parameters, such as thermal conductivity, porosity, size of the nucleus, etc., that were assumed.

Thermal evolution calculations for large ($R > 10$ km) porous nuclei in the Oort cloud (Prialnik and Podolak, 1995) show that these bodies can emerge with different internal structures than small nuclei. They may be:

- preserving their pristine stratigraphy,
- almost completely crystallized, or
- with a crystallized core, a layer of condensed volatiles, and outer layers of unaltered materials.

The final structure depends not only on initial conditions, such as radius and composition, but also on thermal conduction, porosity, etc. Haruyama et al. (1993) have studied the combined effects of radiogenic heating and very low thermal conductivity of amorphous ice on the thermal history of comet nuclei during their residence in the Oort cloud. Their models show that nuclei with very low thermal conductivity experience a runaway increase of the internal temperature that leads to the crystallization of the amorphous ice; comet nuclei with a sufficiently large thermal conductivity do not exhibit this temperature increase and the initial amorphous ice is preserved. Haruyama et al. suggest that the volatile molecules are expelled from the ice and, if the diffusion is efficient, the volatiles may be concentrated near the surface where the temperature is lower.

8.3 Changing Orbits

Considering dynamical evolution of the comet and asteroid populations, we note that for comets dynamical evolution strongly affects their thermal history and therefore their chemical differentiation. The study of the dynamical evolution of comet nuclei may help in establishing relationships between their present status and their origin. The paths of evolution connecting the comet nucleus reservoirs in the outer Solar System with the population of comet orbits in the inner Solar System involve stellar and planetary perturbations (see Section 8.2). Because of these processes, comet orbits are chaotic. A body in a chaotic orbit experiences various regimes of motions and is characterized by a large orbital variability. For this reason comet nuclei can be found over a range of distances from the Sun much greater than those spanned by planets and asteroids.

The dynamical link between the outer Solar System reservoirs and the short-period comets is complicated. An old idea, accepted until recently, is that the short-period comets can be grouped in families like the asteroids, on the basis of an apparent clustering of aphelion distances at the orbital radii of the four giant planets. However, a critical analysis of the situation has shown that only the Jupiter family can be recognized on this basis, while the other clusterings are not particularly meaningful from the dynamical and statistical points of view (Carusi and Valsecchi, 1987, 1992). Moreover, Jupiter is the strongest perturber of the whole population of short-period comets. Jupiter family comets differ from Halley family comets because they change the orbit drastically on a timescale of centuries, and sometimes tens of years. An extreme case is that of 39P/Oterma. In less than 30 years it passed from an orbit totally outside of that of Jupiter to one totally inside and then back close to the initial orbit (Carusi et al., 1981).

The dynamical evolution that leads to short-period comets is complex, since the change in their orbital period can be caused by the action of several giant planets. The process is usually described as a multistage capture. It should be stressed that this process can be stopped at any stage and even reversed and that it can end abruptly with the ejection from the Solar System. Everhart (1969) modeled multistage processes and found that a minority of comets reach short-period orbits without being ejected. This process seems to be very inefficient. However, it is not easy to quantify the capture probability because numerical integration depends strongly on the initial conditions. The timescales found by Everhart are of the order of hundreds of millions of years for comets starting with a perihelion at Neptune, millions of years starting with a perihelion at Saturn, and less starting with a perihelion at Jupiter distance. According to this scheme, short-period comets underwent a complex dynamical and thermal evolution that may also have drastically modified their original composition. Unfortunately, an investigation similar to that of Everhart, but starting from the Kuiper belt, has not been performed. A calculation by Quinn et al. (1990) artificially augmented the masses of the giant planets in order to computationally increase the speed of evolution. This, however, modified the dynamical problem unacceptably.

The physico-chemical behaviour of a nucleus when it arrives at a "final," short-period orbit does not change substantially, provided that the depth of the amorphous ice (if it was present) is not reached by the thermal heat wave. Considering the coupling between thermal and dynamical evolution, the "final" stratigraphy of these comet nuclei is such that the external layers protect the internal ones, thereby preserving the pristine composition. When the "final" orbit is such that the surface layers are strongly ablated and the underlying amorphous ice comes to the surface, further evolution may be strongly affected by the energy release in the amorphous–crystalline transition. A nucleus that arrives in a short-period orbit with a large amount of volatiles and still contains amorphous ice, even if it is covered by a dust mantle, may remain dormant only for a few orbits. Re-activation is always possible for several reasons, including disturbances produced by thermal and pressure stresses, mechanical stresses induced by its tumbling motion, or impacts with micro-meteorites. In the case where amorphous ice is not

Table 8.1: Dynamical parameters for a comet that may have an orbit similar to 4015 Wilson-Harrington = 1979 VA

Orbit	a [AU]	e	Q [AU]	q [AU]	P_{orb} [yr]
Stage I	50.000	0.500	75.000	25.000	351.6
Stage II	25.000	0.400	35.000	15.000	124.3
Stage III	8.000	0.500	12.000	4.000	22.5
Stage IV	3.750	0.500	5.625	1.875	7.2
Stage V	2.644	0.622	4.289	0.999	4.3

present or is very deep, rejuvenation is more difficult.

The behaviour of CO is different from that of less volatile gases. The primordial CO may be depleted. CO may be lost continuously during the life of a short-period comet. Emission tends to be continuous because the flux is generated in deep layers remaining at a quasi-constant temperature.

8.4 Multistage or Direct Injection

We will now compare the final structure of a fictitious comet nucleus that is being injected into a short-period orbit by a multistage process. In Table 8.1 we illustrate a typical path that a comet may follow. For each orbit we compute the thermal evolution and establish the associated differentiation characteristics for each orbital modification.

The model of the nucleus that we have used for this illustration is characterized by a mass ratio of dust to ice = 1, an albedo $\mathcal{A} = 0.05$, abundance ratios $CO_2/H_2O = 0.01$, $CO/H_2O = 0.03$, and a porosity $\Psi = 80\%$. The final orbit of the nucleus will be that of 4015 Wilson-Harrington for which an extensive calculation was performed by Coradini et al. (1997a,b). Because of the high volatility of CO, we can expect an orbit-dependent behaviour of its emissions. We may expect some diffuse emission even far from the Sun (Crovisier et al., 1995).

The outer layers of the nucleus are rapidly depleted of CO. The gas will come from deep layers at a quasi-constant temperature. For this reason the overall evolution in this model of an "aging" nucleus is characterized by a continuous CO emission that starts at perihelion of the first orbit at about 25 AU from the Sun. The emission pattern of CO is different from that of CO_2 and H_2O. It is not characterized by the peaks near perihelion. The stratigraphy exhibits a depletion of CO in the first layers, while the other volatiles remain unaltered. Surface erosion becomes strong only in the last two stages of orbit families, where the formation of a transient mantle (in stage IV, see Table 8.1) is followed by its ejection when the last orbital change takes place.

Comparing this model with a model without multistage capture we note that the temperatures of the surfaces are very similar in the two cases, because water ice is the dominant species on the surfaces and the energetics are dominated by free sublimation of water ice. The stratigraphy of the "old" nucleus when it arrives in its final orbit exhibits a remarkably different behaviour when compared with the "new" nucleus. In the "old" nucleus the CO interface sinks to more than hundred metres below the surface, after five orbits, while in the "new" one the CO interface remains very close to the surface, which is progressively ablated. Other, less volatile gas remains close to the surface in both cases. The transition of amorphous ice to crystalline ice behaves similarly to CO. In both cases no dust mantle is formed in the last orbits, while an unstable mantle was formed in stage IV of the "old" nucleus.

The water flux is, as expected, very similar in the two cases, while the CO flux is remarkably different: CO emission from the "old" body is almost ten times less than from the "new" one and its pattern doesn't follow the water emission. From the comparison we can draw the following conclusion: the behaviour of volatile gases can be a diagnostic for earlier evolution. When it is completely decoupled from the orbital behaviour it reveals a long stability in the same orbit. Small variation in the orbit, changing the internal energy distribution, can permit clear modification in the emitted flux. CO emission may be used as an indicator. A sudden outburst of volatile gases can be a diagnostic of a recent orbital change, as has been suggested in the case of 46P/Wirtanen (Jorda and Rickman, 1995). In another example, if amorphous ice is present and is heated, the transition of amorphous to crystalline ice can become more rapid, thus increasing the overall emission of trapped gases.

8.5 Sungrazing Comets

Sungrazing comets have been observed for many years. Kreutz (1891), studying the sungrazing comets that had been observed up to years 1880-1890, found that they move on the same orbit, meaning that they were probably all fragments of a single comet. This group of comets is named the Kreutz group. It is probable that the original comet and even its fragments split repeatedly. The Kreutz sungrazers have perihelion distances of about 0.005 AU, which is within about 50,000 km of the solar photosphere.

Until 1979, only about nine sungrazing comets had been discovered by ground observations. Then, space-based coronagraphs were able to detect more sungrazing comets. The SOLWIND instrument on the P78-1 satellite discovered six sungrazers between 1979 and 1984. The CP coronagraph on the Solar Maximum Mission (SMM) discovered ten sungrazing comets between 1987 and 1989 (St. Cyr et al., 1989). Since 1995, when the Large Angle Spectrometric Coronagraph (LASCO) on the Solar and Heliospheric Observatory (SOHO) was launched, many new sungrazing comets have been discovered. In its first six and a half years of operation since 1996 more than 500 small sungrazing comets (averaging more than one comet per week) have been detected with LASCO. None of them seem to have survived the close approach to the Sun intact. They appear to be associated with or possibly even trigger some solar instabilities or transient phenomena in the photosphere that cause observable effects such as an enrichment of heavier elements and light scattering (Chochol et al., 1983). All of the sungrazing comets undergo disproportionate brightening just before their perihelion passage (Uzzo et al., 2001). It may be a common end-state for comets and is a likely source of interplanetary matter.

Based on observations and dynamical modeling, it has been pointed out that the sungrazing state is common among the population of high inclination long-period comets as well as among Halley family short-period comets (Bailey et al., 1992). They predict the existence of a number of devolatilized cometary cores or fragments that can be considered as a particular class of extinct comets. The same fate seems common also for some members of the NEA (Near-Earth Asteroid) population (Farinella et al., 1994a, 1994b).

Comets such as Ikeya-Seki (C/1965 S1) and the Kreutz group are the most typical representatives of these sungrazing comets. The Kreutz sungrazing group of comets, composed of approximately thirty members with perihelion distances $q < 2$ solar radii, are related to one another. They may have a unique progenitor. Bailey et al. (1992), using long-term integrations, have shown that the Kreutz sungrazing group can be considered an example of orbits that are now close to their minimum perihelion distance. The sungrazing phase is expected to be much more common than had been believed.

Long-term secular perturbations cause correlated changes in the orbital elements, especially the perihelion distance, eccentricity, and inclination, which can lead to a temporary sungrazing state of extremely small perihelion distances. Long-period comets that have initially high inclination orbits and small perihelion distance frequently become sungrazers. This kind of evolution is foreseen in long-term integrations of different objects, both asteroids and comets, such as 161P/Hartley-IRAS, P/Bradfield, P/Levy, 122P/de Vico and the Asteroid 5335 Damocles (1991 DA) (Hahn and Bailey, 1992).

More recently, it has been calculated that six of the known short-period comets can evolve into a sungrazer state on a timescale of 10^5 years (Levison and Duncan, 1994). The number of sungrazers is far higher than would be expected from existing analytical investigations.

Comets undergo temperature variations in their orbits, especially when they pass very close to the Sun. Therefore, we should expect that thermal and pressure stresses influence the evolution of comet nuclei. Nevertheless, the actions of stresses on comet nuclei are poorly studied and the strengths of cometary materials are also poorly known. The main problem concerns the comet nucleus structure, which is known only approximately. Many authors assume that the nucleus is an agglomeration of cometesimals and, therefore, has a friable structure. However, even in such a case thermal and pressure stress can produce fragmentation and outbursts that are rather common events in cometary evolution [Sekanina (1982, 1984) gives overview on comet splitting; see also Section 3.6]. Several different mechanisms have been proposed to explain outburst and fragmentation, such as rotational break up, tidal stress, collisions with minor bodies, phase transitions from amorphous to crystalline ice, and exothermic chemical reactions. Destruction by solar heating or fragmentation could be a common end-state for sungrazing comets. However, some of these bodies seem to survive their close encounters with the Sun. This could indicate the existence of a particular class of extinct comets.

In most astronomical applications field quantities such as radiative energy density and flux density are determined from factors of solid geometry in which the distance of the field point from the source is large compared to the linear dimensions of the source, i.e. the source is considered a point source. To investigate sungrazing comets, however, we must determine energy density and energy flux density as a function of angle close to the surface of the Sun. Specifically, we are interested in heliocentric distances $R_\odot < r_\mathrm{H} < 5R_\odot$, where $R_\odot$ is the radius of the Sun ($R_\odot = 6.9598 \times 10^5$ km), while a comet nucleus has an effective radius $R << R_\odot$. Thus, it is important to realize that sunlight can reach the nucleus even on its backside, the side that at large heliocentric distances is the night side. However, not the full amount of sunlight is available on that side. As seen from the comet nucleus, part of the Sun is below the horizon of the nucleus.

The energy density (a scalar quantity) at small heliocentric distances is

$$u_\nu\left(r_\mathrm{H}\right) = \frac{4}{c}\pi F_\nu \frac{1}{2}\left(1 - \sqrt{1 - \frac{R_\odot^2}{r_\mathrm{H}^2}}\right) \tag{8.1}$$

where $1/2\left(1 - \sqrt{1 - R_\odot^2/r_\mathrm{H}^2}\right)$ is the dilution factor for the radiative energy density and F_ν is the solar radiation at frequency ν (Huebner et al., 2006).

The standard form for calculating the flux density (a vector quantity) is more complicated than calculating the energy density. The evaluation has to be done numerically. However, Huebner et al. (2006) give some limiting results.

— 9 —

Spin Effects

"The motion of comets doth very much imitate not that of the fixed Stars, but that of the Planets, whence they are by some called Pseudo-Planets, and by others Spurious-planets....They dispatch more way by far then the Planets do. That Comet, A.D. 1618 in the space of three Moneths dispatched 180 Degrees. No Planet goeth over so great an arch of the circle in so short a time....comets then are *temporary*, whereas the true Planets are *perpetual*."

Increase Mather, *A Discourse Concerning Comets*, Boston, 1683.

9.1 Diurnal Evolution

The diurnal evolution of a comet nucleus depends on its properties of heat inertia, its spin rate, and on the orientation of its spin axis. In order to understand the effects of spin rate and spin axis orientation better, we will discuss them as separate entities. In this section, we assume the spin axis is normal to the orbit plane. Section 9.4 will discuss the tilt of the spin axis.

For a very slowly spinning nucleus, or a nucleus with very low heat inertia, heating is virtually symmetric for equal angles of longitude from the noon meridian. For a fast spinning nucleus with significant heat inertia, on the other hand, the surface temperature in the early morning hours is colder than in the afternoon hours. In Fig. 9.1 we plot the energy flux at the surface for insolation, reradiation, water sublimation, and conduction into the nucleus at $r_{\mathrm{H}} = 1.1$ AU. The energy fluxes decrease from their noon values towards evening, are nearly flat during night time, and then increase again in the morning hours.

With the exception of insolation, daytime fluxes cannot be approximated by a $\cos\zeta$ dependence as one might expect.

9.2 Gas Emission

The activity of a comet nucleus is controlled by the incident solar energy which varies with nucleus spin. Solar flux absorbed on the surface is partially

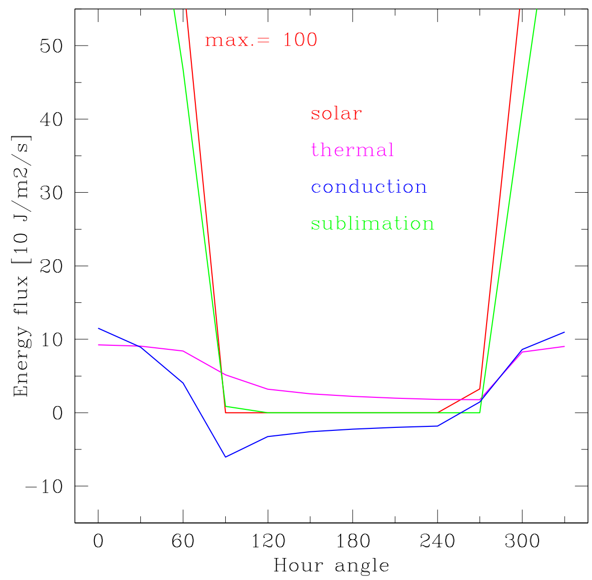

Figure 9.1: Energy flux at the nucleus surface for insolation, reradiation in the infrared, water ice sublimation, and conduction into the interior as a function of subsolar angle ζ, at heliocentric distance $r_H = 1.1$ AU.

reradiated in the infrared, partially spent in sublimation of the water ice at the surface, and partially conducted into the interior of the nucleus. During the night, when the solar flux is not available, comet activity, in terms of gas and dust flux, is strongly reduced. Water ice on the surface is affected the most by the spin of the nucleus, because water ice sublimates from the surface layers (if there is no dust mantle on the nucleus). The species more volatile than water sublimate from the interior of the nucleus. Their behaviour is determined to a large extent by the internal structure and compositional stratification. Therefore, their emission depends on the nucleus internal properties such as porosity, composition, heat capacity, and thermal conductivity. The latter is the key parameter for the penetration of the thermal wave into the nucleus. From the results of nucleus models, we can expect that the nucleus is chemically differentiated and volatile ices continue to sublimate from some depth. In the nucleus, different sublimation fronts can be present. Their depths depend on the thermal properties of the comet nucleus materials and on the volatility of the ice species. Thus, the emissions of the more volatile ices do not depend strongly on the diurnal evolution of the nucleus. We can expect a nearly constant emission over a full nucleus spin. For instance, the CO emission should be independent of the diurnal insolation. Figure 9.2 shows the diurnal evolution of gas emission

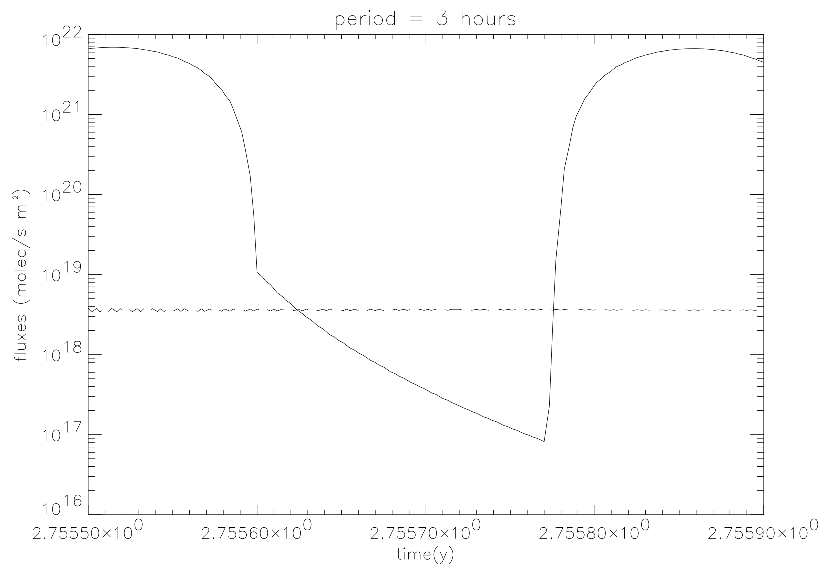

Figure 9.2: Diurnal evolution of gas emissions over a spin period of 3 hours. Water (solid line) and CO (dashed line) fluxes computed from algorithm C1 with parameters given in Table 7.4.

for a typical comet: the water emission follows the diurnal modulation, while the CO emission is constant during the spin of the nucleus.

Less volatile species should be closer to the surface and, consequently, their sublimation should be modulated by the spin period, even if to a lesser extent with respect to water ice. However, if the internal structure of the nucleus is more complex, with volatiles trapped in amorphous ice, then volatiles are released when the transition between amorphous ice and crystalline ice occurs.

9.3 Day – Night Temperature Difference

Two examples of the temperature distribution throughout an outer layer of a spinning nucleus are shown in Fig. 9.3 for a model of a comet in the orbit of 46P/Wirtanen (Cohen et al., 2003) and in Fig. 9.4 for a model of a comet in the orbit of 1P/Halley. The surfaces shown are cuts through the equator and serve to illustrate the diurnal temperature variations at the perihelia and aphelia of the orbits. Only an outer layer of the order of the skin depth is shown, the rest of the nucleus, which is practically isothermal, is shrunk to a point mass. We note in particular the asymmetry with respect to the subsolar point and the negative temperature gradient near the surface on

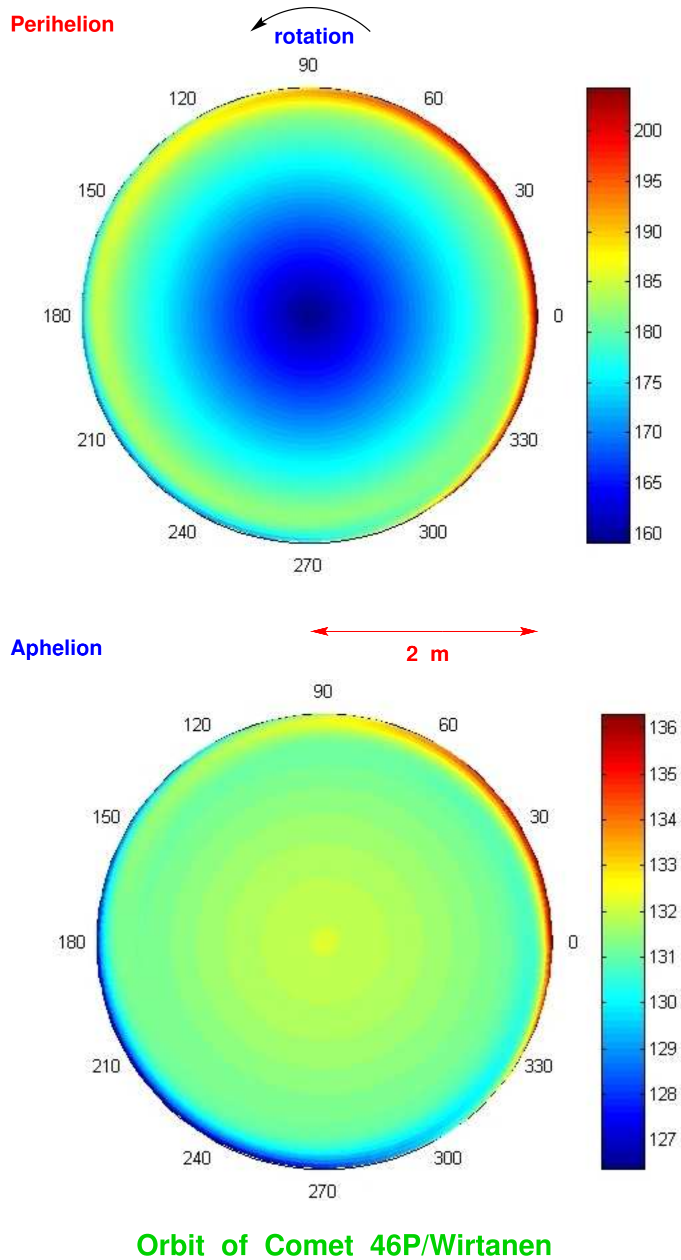

Figure 9.3: Model of 46P/Wirtanen: temperature distribution throughout an outer layer in the equatorial plane of the spinning nucleus ($P_{\rm spin} = 24$ h). The geometry is distorted, as the nucleus bulk is represented by a central, isothermal point mass and only the outermost 2 m around the equator are shown. (Adapted from Cohen et al., 2003.)

the night side. We draw attention to the large temperature variations at perihelion for both orbits, compared to the almost isothermal nucleus at aphelion of the comet in 1P/Halley's orbit.

The diurnal temperature variation may be understood and estimated by the following simple argument. The rate of cooling [i.e. the cooling flux, $F_{\rm cool}(T)$] on the night side is given by setting the solar flux in Eq. (4.19) to zero so that

$$F_{\rm cool}(T) = \epsilon\sigma T^4 + Q\Delta H \tag{9.1}$$

This is balanced by the heat lost from an outer layer to a depth equal to the skin depth corresponding to the spin period of the nucleus, $s = \sqrt{KP/\pi\rho c}$. Thus, over a time interval dt, measured in units of the spin period, the temperature will change by an amount dT given by

$$F_{\rm cool}(T)dt \approx -\rho s c dT \approx -\sqrt{\rho c(T)K(T)/\pi P}dT \tag{9.2}$$

which, integrated over half a spin period, yields

$$\int_{T_{\rm min}}^{T_{\rm max}} \frac{\sqrt{\rho c(T)K(T)/\pi P}}{F_{\rm cool}(T)}dT = \frac{1}{2} \tag{9.3}$$

where $T_{\rm max} - T_{\rm min}$ is the approximate temperature difference between the subsolar and antisolar points. Inserting in Eq. (9.3) the parameter values adopted for the Comet 46P/Wirtanen evolution calculations, Cohen et al. (2003) obtain about 9 K at aphelion and 50 K at perihelion, given the corresponding $T_{\rm max}$, in very good agreement with their numerical results shown in Fig. 9.3.

The day to night temperature difference should be sensitive to the thermal conductivity of the medium. In order to check this effect, $T_{\rm max} - T_{\rm min}$ differences were calculated for the relevant range of subsolar temperatures, adopting three different values for the Hertz factor. The results are shown in Fig. 9.5.

We note that the temperature difference increases as a comet approaches the Sun. At the same heliocentric distance the subsolar temperature increases with decreasing conductivity. A high conductivity has a moderating effect on the surface temperature: it lowers the peak temperature by enhancing the inward heat flux and it raises the minimum temperature by enhancing the outward flux.

9.4 Effect of Spin Axis Inclination

9.4.1 Uneven Distribution of Dust Mantles

The influence of the spin axis inclination on the dust mantle formation has been investigated by Rickman et al. (1990). They computed thermal

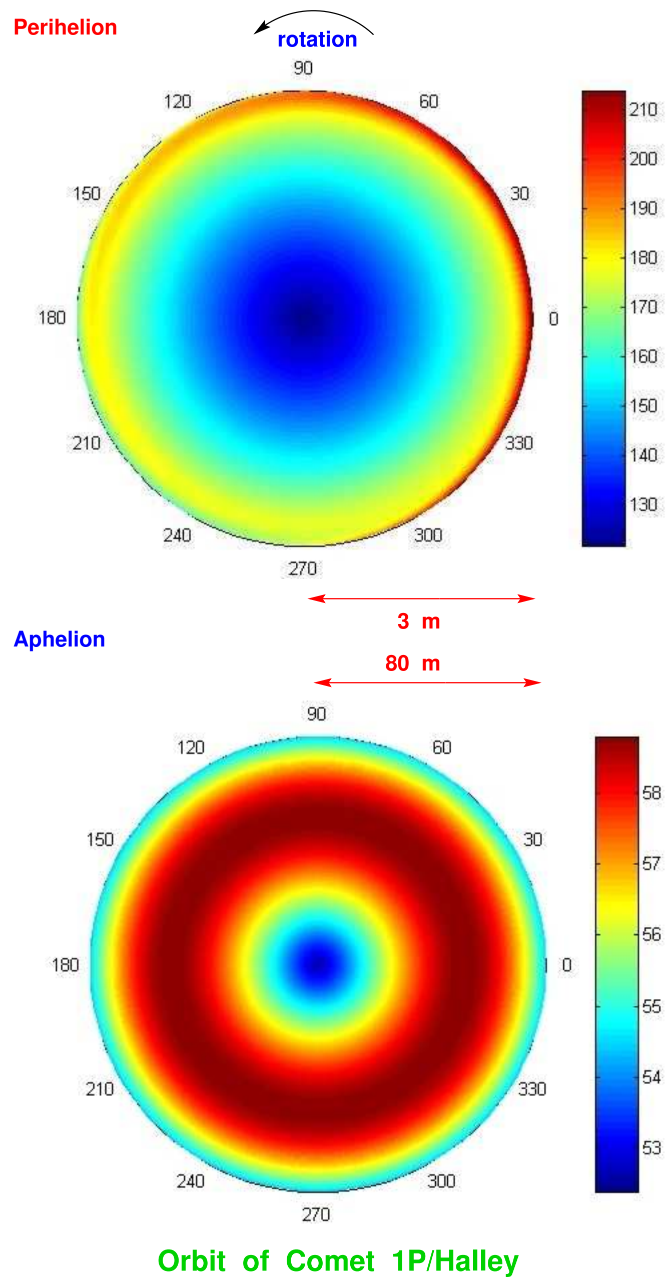

Figure 9.4: Same as Fig. 9.3, for a comet in the orbit of 1P/Halley, with $P_{\rm spin} = 72$ h, with the bulk of the nucleus represented again by a central point mass. Note that the temperature distribution is shown down to a depth of 3 m at perihelion, and 80 m at aphelion.

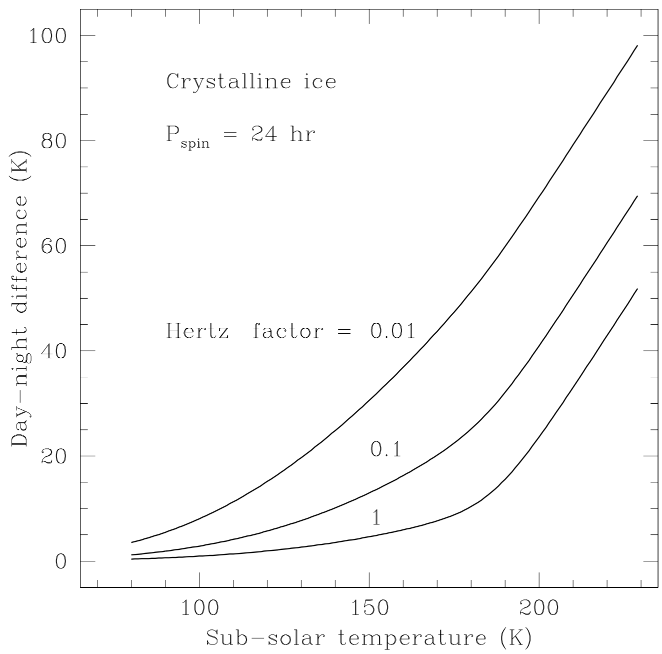

Figure 9.5: Day to night temperature differences vs. subsolar temperature for three different Hertz factors (from Cohen et al., 2003).

evolution models of comet nuclei for different axis inclinations. They used the concept of a critical dust particle radius and a trapping mechanism proposed by Shul'man (1982) to allow for the formation of a dust mantle on a comet nucleus surface. Three different orientations were explored: the first one with the axis perpendicular to the orbital plane (I), the second one with the axis aligned with the apsidal line (II), and the third one with the axis in the orbital plane but perpendicular to the apsidal line (III). They divided the comet surface into ring-like regions covering equal intervals in latitude: polar regions, intermediate regions, and equatorial regions.

All simulations start at aphelion assuming a homogeneous spherical nucleus without a dust mantle on the surface. The nucleus is followed for several orbits. The initial conditions are those of a "new" comet, namely undifferentiated and not aged before it enters the inner Solar System. Their results show that as the comet approaches perihelion, the critical radius of dust particles (see Section 3.5.1) increases and large particles are entrained by the escaping coma gas. The formation of the dust mantle is very difficult in this pre-perihelion phase. When the comet recedes from the Sun, the dust mantle forms. The thickness of the mantle is variable: thicker mantles tend to be more stable than thin mantles but, depending on the orientation of the spin axis, the thin mantles can also be stable. In the case of the spin axis being perpendicular to the orbital plane, Rickman et al. (1990) found that sometimes mantles can form periodically in polar and intermediate regions when the comet is near aphelion. In the case where the spin axis is aligned with the apsidal line, they show that mantle formation is easier: stable mantles cover the hemisphere opposite to the Sun at perihelion. For spin axis orientation III, the mantle forms only on the surface that faces the Sun after perihelion. These models show that we can expect dust-covered inactive areas interlaced with icy active areas on comet surfaces as a function of latitude. However, this simple scenario is not what is observed on comet nuclei. Observations show spots of active areas rather than ring-like active or inactive regions.

If we assume that comet spin axes are oriented randomly, a fraction of comets will have a spin axis orientation that favours retention of a stable mantle. This situation, however, is not stable, it evolves continuously: we may expect a reshaping of the nucleus because of sublimation from active regions. This will cause a torque because of asymmetric outgassing. Reactivation of mantled regions can occur for different reasons: thermal and pressure effects, micro-collisions, small orbital changes, and non-gravitational forces that can act on the nucleus. This leads to changes in the nucleus orientation and, possibly, to excited spin states. In such a situation, different regions of the nucleus are exposed to solar radiation in a "quasi random" way. It is difficult to say how the short-term evolution of such a nucleus will proceed.

9.4.2 Uneven Erosion

Most cometary thermal evolution models still use a spherical nucleus, mostly for numerical convenience, but also in order to limit the number of free parameters. However, observational evidence accumulated over the years clearly indicates that the nucleus is far from spherical. Furthermore, there is no reason for it to be so, since gravity is negligible even compared with the feeble material strength. The clearest evidence is presented by the close images of Comets 1P/Halley and 19P/Borrelly, which reveal irregular, ellipsoidal shaped nuclei. In all probability, comet nuclei formed in complicated shapes. But even if we assume an initially spherical shape, this shape is most likely to change because of uneven temperature distribution over the surface (as illustrated in Fig. 9.3) and because of the strong dependence of sublimation processes on temperature. In about a hundred orbits around the Sun, the highly variable sublimation rate will lead to changes in the moments of inertia and changes in the spin properties.

We now turn to examine the cumulative effect of erosion on the shape of an initially spherical comet nucleus (Cohen et al., 2003). For illustration we assume the orbit of Comet 46P/Wirtanen and a nucleus spin period of 24 hours. Since the spin period is much shorter than the orbital period, the orbital position remains practically unchanged during one day. It is thus sufficient to follow the erosion history of a single meridian and track the latitudinal variations along this meridian. Assuming uniform erosion, the final shape will be the rotational body of the meridian curve. The erosion rate at a given point on the surface, that is for the ith surface element along a meridian, is dr_i/dt, where r_i measures the depth in the direction perpendicular to the surface at the given latitude (initially the radial direction), given by

$$\frac{dr_i}{dt} = \frac{\dot{E}(T_i)}{\rho} \tag{9.4}$$

The erosion of the surface caused by sublimation is calculated for each time step and each point along the meridian. The solar zenith angle, ζ, is given by the cosine law for sides of spherical triangles

$$\cos\zeta = \cos\theta\cos\phi\cos\psi + \sin\theta\sin\phi \tag{9.5}$$

where θ is the latitude, ϕ is the hour angle, and ψ, the cometocentric latitude of the subsolar point, which satisfy

$$\phi_{\text{subsolar}} = 0, \qquad \theta_{\text{subsolar}} = \psi \tag{9.6}$$

The cometocentric latitude of the subsolar point can be expressed as (Sekanina, 1979a)

$$\sin\psi = \sin\delta\sin(\Omega + \alpha) \tag{9.7}$$

where δ is the obliquity, Ω is the angle between the ascending node and the subsolar point, and α the true anomaly. Since the nucleus is no longer regarded as spherical, the normal to the surface no longer coincides with θ and is instead calculated numerically for each surface element.

Calculations were made for 60 orbits around the Sun, for two cases: a simple one, with the spin axis perpendicular to the orbital plane, and a more complicated case, with the angle of inclination of the spin axis at 45° in the plane perpendicular to the orbital plane and containing the apsidal direction. For the second case, the model resolution was improved: the latitudinal intervals were 5°, rather than the 10° used in the perpendicular case. Figure 9.6 *left* shows the final nucleus shape for the simple case. This ellipsoid shape is explained by the sublimation differences and different latitudes: the sublimation rate is higher close to the equator. At the equator, the average erosion rate is 2.1 m yr^{-1}, in contrast to an average of

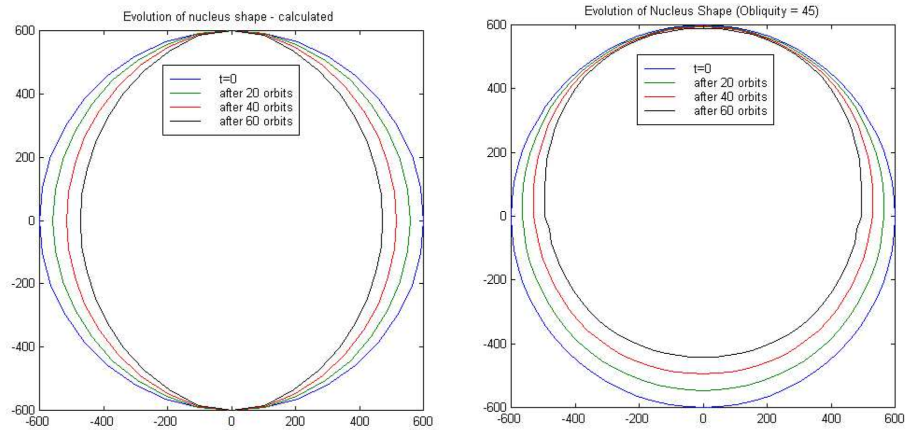

Figure 9.6: Model for the shape evolution of an initially spherical nucleus in the orbit of Comet 46P/Wirtanen (Cohen et al., 2003), assuming uniform erosion, i.e. no inactive areas. The inclination of the spin axis to the orbital plane is: 90° (*left*) and 45° (*right*). In the latter case, the spin axis is in the plane perpendicular to the orbital plane and contains the apsidal direction. The shape of the comet is projected on a 2-dimensional plane. Axis labels are given in metres

10 cm yr^{-1} at latitude 85°. Figure 9.6 *right* shows the final shape for the second, more complicated case, which implies higher sublimation rates at the "southern cap" (extending from 45° south to the southern pole), compared to a negligible erosion rate at the opposite northern cap. These results are not intuitively obvious: the initial conditions were such that at aphelion the northern cap is facing the Sun during the entire comet day. This situation is reversed at perihelion, where the southern cap faces the Sun, while the northern cap is in the dark all day long. However, since most of the sublimation is taking place at perihelion, the southern cap experiences far more surface erosion. The average erosion rate there is 2.6 m yr^{-1}, compared to only 18 cm yr^{-1} at the northern pole. It may be concluded that long-term evolution leads to a marked deviation from the original shape, and this deviation is strongly dependent on the obliquity of the spin axis, its orientation with respect to the apsidal direction, and on the eccentricity of the orbit.

9.5 Effect of Spin Rate

The spin of a nucleus can have observable effects on the photometric and morphological properties of the inner coma of comets. The interrelations between the spin and the properties of the nucleus are very complicated.

Spin affects the temporal and spatial patterns of outgassing of the nucleus (through diurnal and seasonal effects) and is in turn influenced by activity-driven torques. It is very difficult to quantify the interactions between the spin, the outgassing, and the resultant torques on the nucleus, and to understand the role of spin in determining the basic physical properties of the nucleus. Spin properties of comets were reviewed by Sekanina (1981), Whipple (1982), Belton (1991), Jewitt (1997), and Samarasinha and Mueller (2002).

In general, in the absence of external torques, a body spins about the short axis (the so-called "principal spin axis"). A comet nucleus can spin with its angular momentum vector and axis of maximum moment of inertia not aligned in what is called an excited state. Excited states produce periodical stresses in the nucleus, leading to energy dissipation and gradual re-alignment of the principal spin axis depending on the damping timescale (Burns and Safronov, 1973).

Outgassing can create torques that change the angular momentum of the nucleus, either in the magnitude or in direction. It also changes the moments of inertia. The creation of a torque is naturally produced by any asymmetric distribution of active areas on the nucleus. Some other mechanisms have been suggested for modifying the nucleus spin. Wallis (1984) suggested that debris ejected from the polar regions and landing on the equator would constitute an "angular momentum drain," tending to increase the spin period. Comet nuclei split often when far from the Sun and the planets (Whipple and Stefanik, 1966; Chen and Jewitt, 1994). One of the suggested mechanisms is acceleration of the spin above the critical angular velocity, the velocity at which the centripetal acceleration at the surface of the nucleus is equal to gravitational acceleration towards the centre (Whipple, 1961). In such splitting, secondary nuclei can carry mass and angular momentum, and may leave the primary nucleus in an excited spin state. Coradini et al. (1997a) note that a general characteristic of thermal evolution of comet nuclei is that polar regions, in the idealized case of the spin axis being perpendicular to the ecliptic plane, become covered by dust earlier than equatorial regions. This leads to a reshaping of the body that undergoes stronger ablation at the equator. This may result in an intrinsic spin instability that can cause re-activation of dust-covered areas. In the long term, this effect can contribute to the formation of localized activity.

Photometry of bare nuclei can provide the spin period. This technique can be applied either to comets that are weakly active when near the Sun, or to comets that are inactive far from the Sun, but it is difficult to implement.

Aperture photometry of the coma of some very active comets has been used to search for periodicities caused by spin modulation of the outgassing rate (Rodriguez et al., 1997; Millis and Schleicher, 1986). This technique provides a good measure of the temporal variability of the outgassing rate, but it is still not entirely clear how the outgassing rate variability relates to the nucleus spin.

The best-observed short-period comets, such as 2P/Encke, 10P/Tempel 2, 28P/Neujmin 1, and 49P/Arend-Rigaux have lightcurves with a single period, consistent with spin about the principal axis. Photometric evidence for complex spin has occasionally been claimed for 10P/Tempel 2 (Mueller and Ferrin, 1996) and for 29P/Schwassmann-Wachmann 1 (Meech et al., 1993).

To be effective, the timescale for excitation of the spin by jet-like activity must be shorter than the damping time and shorter than the time for devolatilization. Therefore, we might expect that some comet nuclei may be in excited spin states, but evidence for excited spin states in comets is poor. The best known case is that of Comet 1P/Halley. It seems to spin about two axes. The general lack of evidence for non-principal axis spin in comets may be a bias because of the limited data available from most comets, rather than an indication of the absence of excited spin states.

From the thermal point of view, the spin period is a key parameter for the evolution of comet nuclei. It has an influence on the diurnal evolution and on the long-term global thermal history. The effects of different spin periods on active comets may be seen in the figures below, where the results of two test cases are reported. To assess the influence of long and short spin periods on thermal evolution, we computed the same model with two different spin periods: model A with 3 hours, and model B with 3 days (see Table 9.1). In these two models we assume that the spin axes are perpendicular to the orbital plane (Obliquity = 0) and we record the data at the subsolar point on the nucleus equator. The figures illustrate the temperatures and the gas flux obtained when the nucleus is at its perihelion (at about 1.08 AU), over one spin period. The spin periods influence the minimum of the temperatures attained at the surface during the comet night, and consequently the level of water emission at night. The maximum temperatures obtained during the day are the same in the two models, and consequently also the maxima of water fluxes are equal. In the case of the fast rotator, the minimum temperature is about 150 K, while in the case of the slow rotator the temperature goes down to about 100 K. In the case of slow spin, the surface temperature is almost the same as that of the subsurface layers during the night because the thermal wave is completely dissipated.

The effects of spin are most important when the comet nucleus is at small

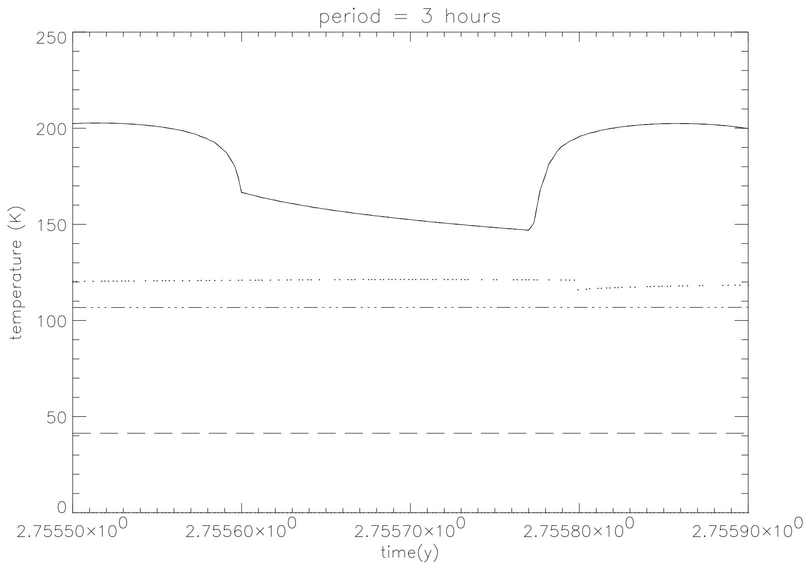

Figure 9.7: Diurnal temperatures for a model with a spin period of 3 hours. Solid line: surface temperature, dotted line: CO_2 ice sublimation front; dash-dotted line: amorphous - crystalline ice interface; dashed line: CO ice sublimation front.

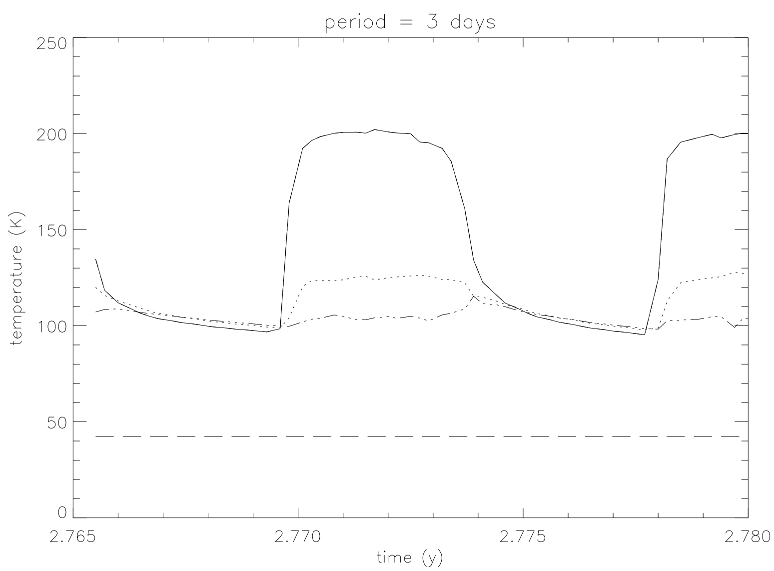

Figure 9.8: Same as Fig. 9.7, except the spin period is 3 days.

Table 9.1: Parameters of the models

Radius	1000 m
Dust/ice ratio	1
CO_2/H_2O	0.01
CO/H_2O	0.01
Porosity	0.8
Albedo	0.4
Emissivity	0.96
Semimajor axes	3.115 AU
Eccentricity	0.652

heliocentric distances, where the energy input for sublimation is strongest. From the point of view of long-term evolution, the spin period may be one of the most important parameters for the formation and stability of a dust mantle on the surface. The day to night fluctuations influence the forces that determine the critical particle radius for entrainment of dust by coma gas (see Section 3.5.1).

Particles with an effective radius $\hat{r} < \hat{r}^*$ (the maximum critical radius of a dust particle that can be entrained by the coma gas) are entrained by the escaping gas and form the dust flux, while those with $\hat{r} > \hat{r}^*$ accumulate on the surface to form the dust mantle. It is clear that comets with a slow spin rate can more easily develop and retain dust mantles on them, because the centrifugal force on dust particles is low. In the case of small but fast spinning nuclei, mantle formation is difficult to explain. The evolution of a Jupiter family comet nucleus of 1 km radius was investigated by Coradini et al. (1997b), considering two different spin periods: 10 hours and 3 days. The results indicate that the evolution changes dramatically: in the case of a slow spin rate the formation of a stable mantle is achieved, and consequently the gas flux is reduced. The presence of a dust mantle tends to inhibit the gas emission. We may expect slowly spinning nuclei to accumulate thicker mantles and be more likely to assume an asteroidal appearance.

— 10 —

Comparison of Models with Observations

> "For the truth of the conclusions of physical science, observation is the supreme Court of Appeal. It does not follow that every item which we confidently accept as physical knowledge has actually been certified by the Court; our confidence is that it would be certified by the Court if it were submitted. But it does follow that every item of physical knowledge is of a form which might be submitted to the Court. It must be such that we can specify (although it may be impracticable to carry out) an observational procedure which would decide whether it is true or not. Clearly a statement cannot be tested by observation unless it is an assertion about the results of observation. *Every item of physical knowledge must therefore be an assertion of what has been or would be the result of carrying out a specified observational procedure.*"
>
> Sir Arthur Eddington, *Philosophy of Physical Science*, 1939.

10.1 Modeling Guided by Observations

10.1.1 Example 1: Comet Hale-Bopp (C/1995 O1)

Comet Hale-Bopp (C/1995 O1) was discovered at a distance of about 7 AU from the Sun, when it already had an unusually bright dust coma. Observations seemed to indicate that the comet was discovered on the rise of its activity. However, during several months after discovery the rising trend subsided. As the gas production rates did not increase as expected with decreasing heliocentric distance, a relatively low perihelion activity was anticipated. Despite these early predictions, Hale-Bopp (C/1995 O1) became one of the brightest comets of the century.

As it turned out, the comet had been active already at $r_{\mathrm{H}} \approx 13$ AU and probably even farther out, at 18–20 AU; CO was detected at $r_{\mathrm{H}} \approx$ 6.6 AU and OH at 4.8 AU. It appears that CO was the dominant driver of comet activity until $r_{\mathrm{H}} \approx$3.5–4 AU pre-perihelion, when water sublimation became significant. A steep increase in CO (and other minor volatiles) gas production was noticed near $r_{\mathrm{H}} = 4.8$ AU, in coincidence with the first detection of OH. While before perihelion the transition from CO-driven

Table 10.1: Model parameters for Comet Hale-Bopp (C/1995 O1)

Parameter	Model 1	Model 2	Model 3
	Defining		
Orbital eccentricity	0.9953	0.9953	0.9953
Semimajor axis	195 AU	195 AU	195 AU
Radius (R)	20 km	20 km	20 km
	Structural		
Bulk density (ρ)	0.8 g cm^{-3}	0.5 g cm^{-3}	0.5 g cm^{-3}
Porosity (p)	0.4	0.65	0.65
Pore size (d_0)	100 μm	100 μm	100 μm
Maximum particle size	1 cm	10 μm	10 μm
	Material		
Dust/ice ratio (by mass)	1	1	1
Fraction of trapped CO	0.05	0.04	0.12
Fraction of trapped CO_2	0	0.01	0.03
Albedo ($\mathcal{A}$)	0.03	0.04	0.04
Emissivity (ϵ)	0.5	0.5	0.5
Temperature	20 K	30 K	30 K

activity to H_2O-driven activity occurred at $r_{\rm H} \approx 3.4$ AU, after perihelion the transition occurred between $r_{\rm H} = 2 - 2.5$ AU. The diameter of the nucleus was estimated to be between 27 and 42 km.

We shall now illustrate the failures and successes of comet nucleus modeling, by means of a series of models aimed at explaining the apparently strange behaviour of Comet Hale-Bopp (C/1995 O1), based on different parameter combinations (Prialnik, 2002). The initial parameters were derived based on observations that were available at the time of calculation. As observations accumulated, the parameters changed and a better agreement between simulations and observations was achieved. The model parameters are listed in Table 10.1.

For all models, a radius of 20 km was adopted and the initial composition was assumed to be homogeneous and composed of water ice and dust in equal mass fractions. The key assumption was that the ice is amorphous, trapping a small fraction (5% by mass) of CO gas. A model of tortuous capillary tubes (Mekler et al., 1990) was adopted for describing the porous medium, with an average pore radius of 100 μm. The evolution calculation was started at aphelion.

For the first model (Prialnik, 1997), the porosity was taken to be 0.4, implying a bulk density of 800 kg m^{-3} for a very high dust particle density of 2650 kg m^{-3}. A power law (-3.5) size distribution was assumed for the dust particles (McDonnell et al., 1986) with a cut-off at a radius of 1 cm. Crystallization of the amorphous ice and release of the trapped CO started very gradually, propagating inward from the comet nucleus surface. However, near $r_{\rm H} = 7$ AU, the crystallization process accelerated. The emitted CO flux increased sharply, and the temperature in the outer layer of the nucleus rose abruptly, causing sublimation of water from the pore walls. At the same time the drag force exerted by the flowing gas became sufficient to entrain dust particles. Small dust particles were ejected with the gas while larger particles were left behind. Thus a very porous dust mantle gradually formed, growing in thickness to about 10 cm.

Quite remarkably, the date of discovery of the comet coincided with the onset of the runaway. The runaway subsided on a timescale of about 100 days. On a large scale, the average CO and dust emission rates reached a plateau, but exhibited a very high variability marked by several minor outbursts of CO and dust. It therefore appears that the various outbursts of Comet Hale-Bopp (C/1995 O1) that were detected for many months after discovery may be understood on the basis of the model, although they cannot be accurately simulated. Already before perihelion, when the crystallization front may have reached a depth of almost 10 m, its advance was considerably slowed and so was the rate of CO release. This was caused by the low temperature at this depth, which was controlled by the sublimation of CO gas that migrated inward. As a result, starting at $r_{\rm H} \approx 2$ AU pre-perihelion, the CO flux remained constant, at a relatively low value, unaffected by the surface temperature of the comet. The water gas production rate was found to exceed the CO gas release rate around 3 AU. The dust was now entrained by the H_2O molecules that flowed through the porous dust mantle. The pore size of the permeable, 10 cm thick mantle was of the order of 1 cm.

The assumptions of this first calculation regarding dust release led to the early formation of a dust mantle that quenched the rate of H_2O gas production around perihelion. Hence, although successful in reproducing the comet's behaviour at large heliocentric distances, this first model failed in explaining the comet's high perihelion activity.

For the second calculation (Prialnik, 1999), again the amorphous ice included 0.05% trapped gas, but this time 0.04% CO and 0.01% CO_2. The density was lower, at 500 kg m^{-3}, and the porosity, accordingly, higher (0.65). More important, the effective maximum dust particle size was taken to be 10μm, i.e. lower than the pore size, in order to prevent the formation of a mantle. As a result, the H_2O production rate at perihelion was higher than in the previous model by more than one order of magnitude, in good agreement with the rate derived from observations, as shown in the lower

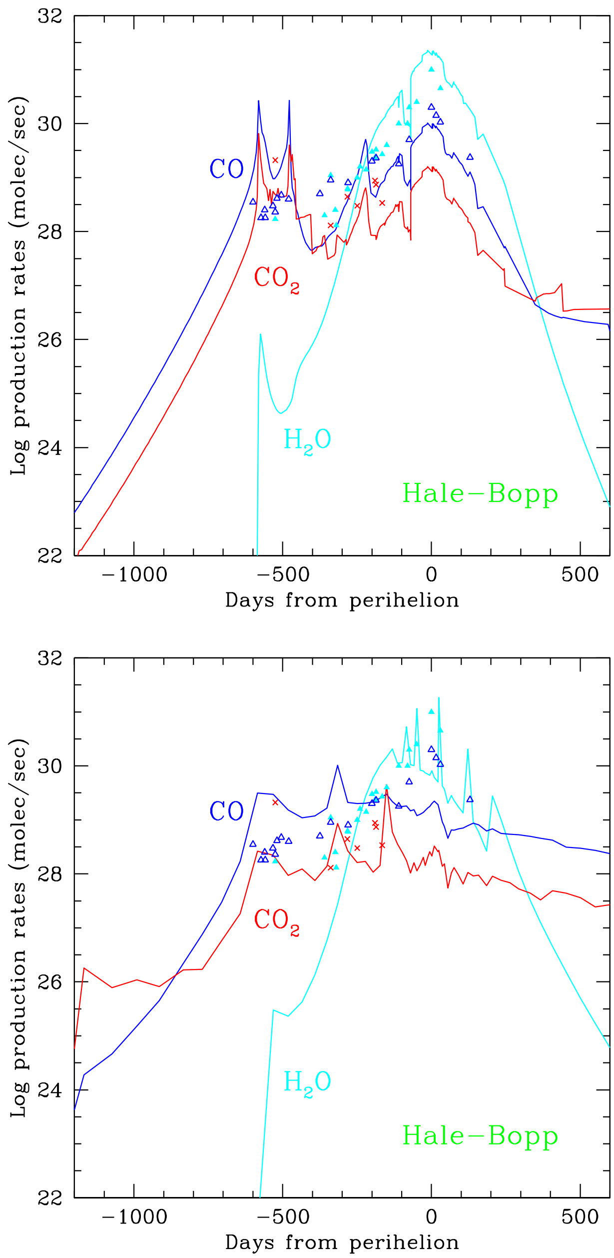

Figure 10.1: Models for the production rates of Comet Hale-Bopp (C/1995 O1) based on different assumptions: Model 1 from Table 10.1. Upper panel: slow release of CO gas from amorphous water ice. Lower panel: instantaneous release of CO gas.

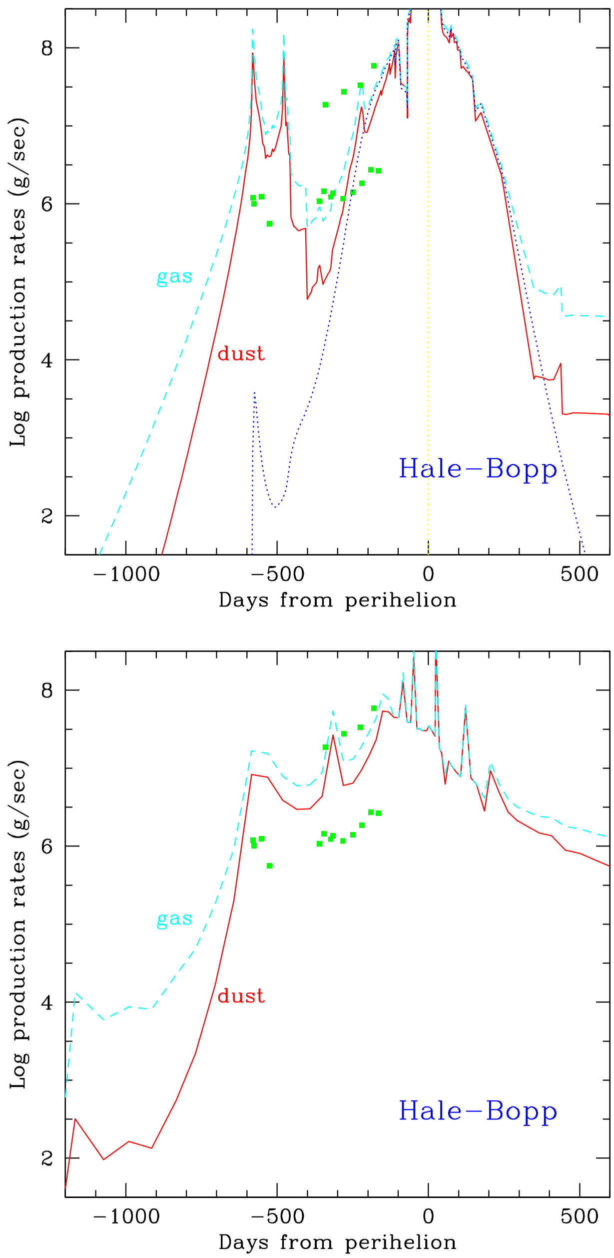

Figure 10.2: Models for gas and dust release rates of Comet Hale-Bopp (C/1995 O1) based on different assumptions. Model 2 from Table 10.1. Upper panel: slow release of CO gas from amorphous water ice. Lower panel: instantaneous release of CO gas.

panel of Fig. 10.1. A further improvement of this model was that the initial configuration was not homogeneous, but included a processed outer layer that was crystallized water ice depleted of volatiles. This should be expected of a comet that is likely to have passed through the inner Solar System in the past (Marsden, 1999). It is shown, however, that observations impose a strong constraint on the thickness of such a layer: if it exceeded 1 m, it would delay significantly the rise of production rates of CO and CO_2, and if it exceeded 10 m, the gas fluxes would not only be delayed, but would also be very low. Finally, the dust production rate was more than two orders of magnitude higher than in the first model, and quite close to the observed rates, as illustrated in the lower panel of Fig. 10.2. The remaining problem was the behaviour of the CO and CO_2 production rates close to and after perihelion: observations showed higher rates at perihelion and faster decline thereafter.

A solution to this problem was suggested by Rickman in a private communication, who drew attention to the results of laboratory experiments that show that gases are only partially released from amorphous ice during crystallization. A significant fraction remains trapped and escapes only when the crystalline ice sublimates. Including this effect in model calculations, while leaving the other parameters unchanged, yields the results shown in the upper panels of Fig. 10.1 and 10.2. There still remains the discrepancy between the high production rate of H_2O indicated by some observations at $r_{\rm H} > 3$ AU pre-perihelion and the results of model calculations. This could perhaps be explained by evaporation of ice-covered dust particles.

The main conclusion of this study is that the gas fluxes (CO and CO_2) in Comet Hale-Bopp (C/1995 O1) may not emanate from the respective ices, but from H_2O ice, either in the interior during crystallization of amorphous H_2O ice, or at the surface, with the sublimation of crystalline H_2O ice. In support of this conclusion, the high ejection velocities observed indicate that the gases have been released in a relatively warm medium. Characteristic temperatures at the crystallization front are found to be ~ 160 K, much higher than the sublimation temperature of, say, CO (~ 35 K) and even CO_2(~ 100 K). Nevertheless, CO and CO_2 ice may exist beneath the crystallization front. Gases released from the ice flow through the porous medium both outwards and inwards, since the temperature as well as the pressure peaks at the front (Prialnik and Bar-Nun, 1990). Gases that flow inward are bound to reach very cold regions, and hence refreeze. Calculations show that, while CO_2 freezes very close ahead of the crystallization front, CO freezes several metres deeper. This should lead to different production curves for different gas species that are now differentiated, but the behaviour would be history dependent.

In conclusion, we have shown how observations provide valuable constraints to comet nucleus models, which in turn help to interpret the (often puzzling) observed behaviour. In this particular case the inferences based on combining the results of modeling and observations (although not necessarily unique) are as follows:

- A model of porous grainy material made of gas-laden amorphous ice and dust *can* reproduce the general activity pattern of the comet.

- Particles should be mostly small, in order to prevent early formation of a dust mantle on the nucleus, which – even if very thin – would quench water production. Small, ice-laden particles would also make a more significant contribution to water production at large heliocentric distances, which is indicated by observations.

- The perihelion water production rate is not sensitive to structural parameter values, but is determined by the (active) surface area. For $R = 20$ km, the output exceeds 10^{31} molecules/s. The H_2O gas production rate becomes dominant at $r_H \approx 3$ AU.

- No simple correlation is found between production rates of different volatile gases and their relative abundances in the nucleus. Dust production is controlled mainly by CO and CO_2 at large heliocentric distances, and by water at heliocentric distances of less than $r_H \approx 3$ AU.

- A processed, volatile-free, surface layer cannot exceed a thickness of about 1 m, if activity is to set in around $r_H = 7$ AU, as observed. The gas emission rates are determined not only by the rate of crystallization, but also by sublimation of ices formed by the condensation of gases that were released at an earlier stage. While CO_2 freezes very close ahead of the crystallization front, CO freezes several metres deeper and its subsequent sublimation becomes weakly linked to the advance of the front. For different gaseous species, the two competing sources may lead to unusual activity patterns.

To strengthen these conclusions, we now turn to model calculations for the same comet carried out by different authors, using different algorithms (Capria et al. 2000a; 2002b). Additional aspects are considered in these studies and, as above, observations are used to guide the choice of parameters. The authors make several interesting points emerging from the observations of Comet Hale-Bopp (C/1995 O1) that a simulation should reproduce and explain: (a) water vapour production seems to have begun at $r_H \approx 4$ AU (Biver et al, 1997), where it could not be accounted for by sublimation from the surface (but see below); (b) the gas production rate of CO was high, even between 7 and 6 AU pre- (and post-) perihelion; (c) the production rate of CO gas and other minor volatile gases seems to have increased with the onset of water sublimation; (d) CO emission peaked with water emission at perihelion. There are three possible mechanisms that can contribute to the total measured CO production in a comet: (1) sublimation of the ice of CO from the nucleus; (2) release of CO gas trapped in amorphous water ice in the nucleus; (3) emission of CO from particles in the inner coma (distributed source). To match gas production rate observations with a numerical model, one needs to consider all of these emission mechanisms: success (or failure) in reproducing the observed behaviour may provide information about the relative importance of these mechanisms and the reservoir of observed CO.

Huebner and Benkhoff (1999) and Kührt (1999) disagree with point (a) above. They show that the water vapour production of Comet Hale-Bopp (C/1995 O1) can be reconciled with production from the surface in the entire range from 5 AU to perihelion. For the comparison with theoretical models, Huebner and Benkhoff (1999) compiled H_2O and OH observations from many observers. The data include radio observations, IR data, data from the visual range of the spectrum, and UV data. They report a less rapid increase in the gas production relative to the model predictions between 1 and 2 AU pre-perihelion. This reduced gas release rate is also observed for many other species. Thus, it appears as a global effect and may have several reasons: (1) the orientation of the spin axis may cause a seasonal effect (Kührt, 1999), or (2) dust may accumulate on the surface of the nucleus, reducing the efficiency of vapourisation at about 2 AU inbound, but then get entrained by the coma gas at about 1 AU inbound as a result of increased insolation and the accompanying increase in gas production. Alternatively, it has been suggested that icy particles contribute significantly to the gas release rates at large heliocentric distances (see, e.g. Bockelée-Morvan and Rickman, 1998).

In order to reproduce the dynamical evolution of the body (Bailey et al., 1996), computations were started at the aphelion of the pre-Jupiter encounter orbit (semimajor axis = 330 AU, eccentricity = 0.997223); then, after a few revolutions, the new orbit was invoked (semimajor axis = 195.4 AU, eccentricity = 0.99532) from an arbitrarily chosen point near 4.5 AU. This simulates that this comet was not dynamically new, and that the upper layers may have been differentiated to a depth depending on nucleus properties. When the computation was started, the comet was very far from the Sun and for a long time (thousands of years) nothing happened: all of the activity and the consequent mass loss are concentrated in a span of years – short with respect to the orbital period. This concentrated activity is coupled with a strong erosion that keeps sublimation and transition fronts close to the surface. We note that there is no need to suppose that the comet is dynamically new to explain why it does not seem to be very differentiated, because during each perihelion passage many metres of surface are lost and sublimation and transition fronts can always be found a few metres below the surface. When the comet arrives in the present orbit, the CO sublimation front is well under the surface. It should be noted that surface sublimation of CO ice is ruled out by its sublimation temperature.

If models are run with the usual nucleus composition, starting with a mixture of ices and dust, Capria et al. note that they can reproduce the water gas production rate at perihelion and the emission of CO far from the Sun, but the early water emission at 4 AU cannot be matched and the behaviour of CO production rate near perihelion cannot be reproduced. Activity starts very far from perihelion because CO is a very volatile ice: its sublimation front remains in a layer of almost constant temperature, even considering surface erosion, and can be reached by a thermal wave with a delay depending on its depth. A flat production curve is obtained, with a small peak after perihelion, when the heat wave reaches the sublimation front. Changing the initial amount of CO or bulk conductivity or the differentiation state of first layers cannot change the shape of the curve, but only move it up and down.

To explain water production between $R_{\mathrm{H}} = 3$ and 4 AU, water sublimation from icy particles in the inner coma should be introduced. To match the shape of the CO gas production curve, a mechanism able to confine CO near to the surface is required, otherwise the production peak at perihelion cannot be explained. Because of the very low sublimation temperature of CO ice, it is confined to deep layers in the nucleus. The mechanism of release of CO may be related to trapped gas during the transition from amorphous to the crystalline phase of water ice. This release may explain the abrupt increase in CO production when the phase transition should start, adding the CO released from amorphous ice to the CO directly sublimated from CO ice. This is not enough to completely explain the peak at perihelion, unless one assumes that the phase transition front is very close to the surface. This may be the case if the internal conductivity is very low. If the conductivity is not that low, there are still two possibilities: (1) A large fraction of CO may come from a distributed source in the inner coma, as was the case for Comet 1P/Halley. (2) As demonstrated in laboratory experiments, some of the trapped gas is released only with water sublimation. This would explain why the production rates of many minor volatiles seem to increase with the beginning of water ice sublimation. Presently, neither of these mechanisms can be ruled out, and perhaps they are working together. The CO gas production curve obtained with this last assumption is shown in Fig. 10.3.

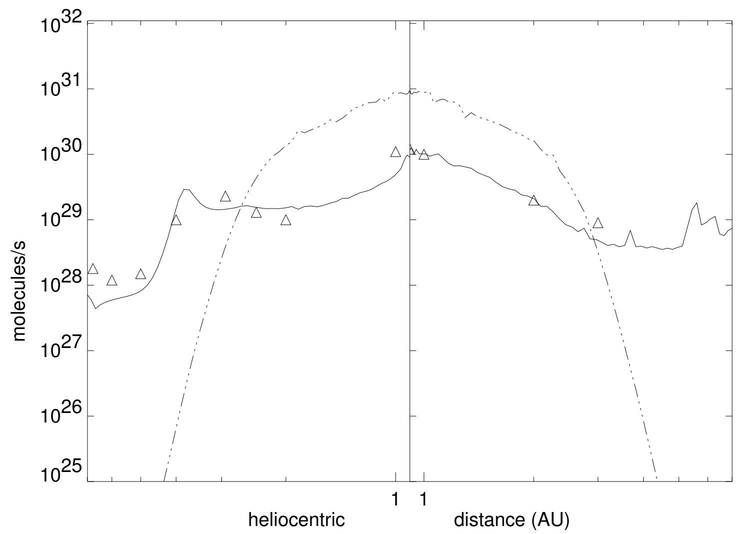

Figure 10.3: Gas production rates along one orbit of Comet Hale-Bopp (C/1995 O1): continuous and dashed-dotted lines represent, respectively, CO and water production rates obtained from the model, while triangles represent CO production from observation. The vertical line marks the perihelion.

10.1.2 Example 2: Comet 46P/Wirtanen

Comet 46P/Wirtanen is a Jupiter family comet with an orbital period of about 5 yr and a perihelion distance slightly greater than 1 AU, discovered in 1948 (Wirtanen, 1948). This comet has been extensively studied in the last years both from the ground and from space. From these detailed observations it has been deduced that 46P/Wirtanen has a small nucleus, one of the smallest ever observed to date. A detailed characterization of the nucleus was given by Lamy et al. (1998) using images taken with the Planetary Camera (WFPC2) of the Hubble Space Telescope. They obtained an effective radius of 0.59± 0.03 km from the V magnitude and 0.62± 0.02 km from the R magnitude. From the individual V and R apparent magnitudes of the nucleus, they constructed a light-curve and derived a spin period of 6± 0.3 hr. The comet is very active. Farnham and Schleicher (1998) derived an OH production rate of 7.8 $\times 10^{27}$ molecules/s at 1.07 AU from the Sun using narrow band photometry, while Bertaux (1997) reported a water gas production rate of about 7 $\times 10^{27}$ molecules/s. A'Hearn et al. (1995), on the basis of statistics of different comets and taking into account the localized activity, have estimated that the maximum emission rate of 46P/Wirtanen at perihelion should be about 10^{28} molecules/s. The observations performed by Colangeli et al. (1998) by means of ISOCAM inferred that the dust release rate, using a model developed by Fulle (1989), is less than that for most active comets. Theoretical models indicate that, for a comet of this size, the gas production values can be explained only if a large part of the comet surface is active. Thus, it seems that we are in the presence of a small object whose surface is almost completely active, but not in terms of dust release. This could happen if a very porous layer covers the comet, allowing gas emission but strongly inhibiting particle ejection.

Capria et al. (1996) gave first model results for dust and gas production rates and day and night surface temperatures. However, before the perihelion campaign of 1997, many important parameters were undetermined (e.g. radius and spin period). In a more recent model (De Sanctis et al., 1999) the results of the observational campaign were taken into account, including active and inactive regions. In this model, the nucleus is composed

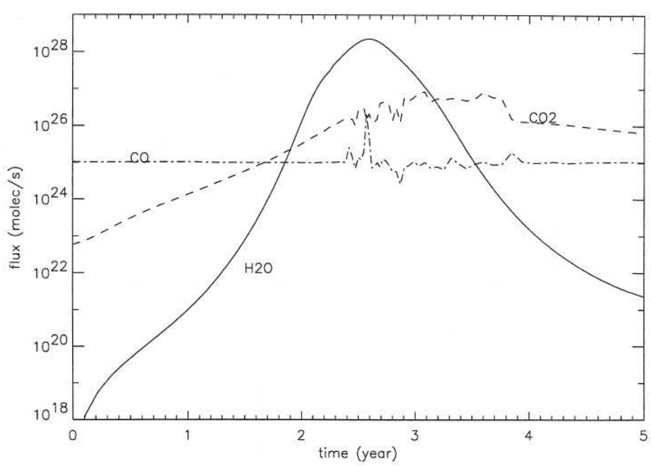

Figure 10.4: Flux rates of H_2O, CO_2, and CO along an orbit of Comet P/Wirtanen.

of ices (water, CO_2, and CO) and dust. These models, have been computed for many consecutive orbits, varying orbital parameters, simulating the so-called multistage capture process from the Kuiper belt to the final orbit of 46P/Wirtanen. A series of consecutive close encounters with the giant planets is thought to be the process allowing the transfer of a Kuiper belt object to a short-period orbit. When the model comet is inserted in the orbit of 46P/Wirtanen, its surface layers, initially undifferentiated and homogeneous, rapidly become depleted in CO_2 and CO ices and crystallization of amorphous H_2O ice is induced.

The selected 46P/Wirtanen models simulate the physical conditions leading to the formation of a non-volatile mantle. In the first group of models it is assumed that the mantle is formed by particles that cannot be entrained by the gas flux and remain on the surface. The main result for all these cases is that the formation of a stable mantle is impossible. A characteristic of all these models is the high activity with rapid erosion and strong depletion of volatile ices under the surface layers. At perihelion, the dominant flux is water, while the CO_2 flux is a maximum after perihelion. The CO flux, coming from deep layers, is continuous along the entire orbit (Fig. 10.4). The amount of dust accumulated on the nucleus surface changes along the orbit, but a stable mantle never forms. Only in polar regions can we see slow dust accumulation.

The difficulty in obtaining a stable mantle is not surprising. The critical dust particle radius is reduced by a large nucleus mass, by a low level of gas flux, by low gas velocity, and by a very long spin period. In the case of 46P/Wirtanen the estimated very short-period (6 hours) and the small radius (600 m) act against the formation of a mantle, even if we introduce very large particles into the dust distribution.

In a second group of models, it can be seen how the mantle affects the overall behaviour of the comet nucleus. The mantle can form on a nucleus assuming a process of particle trapping. In such a model dust mantle formation depends on the trapping of particles. When enough dust covers the surface the gas flow is quenched, increasing mantle stability. Only trapping of small dust particles in the pores of a mantle of larger particles stabilizes the mantle on the equatorial regions of 46P/Wirtanen. The higher thermal conductivity of the dust raises the temperature of the interior of the nucleus. The average surface temperature is about 100 K higher than that of the dust-free area. Strong temperature differences between the day and night hemispheres are confined to the subsurface layers. Deeper layers are not affected. Some metres below the surface the temperature remains constant over the time of one spin period. The regions covered by dust are less active than the exposed icy areas where free sublimation of water ice is allowed. The dust mantle on inactive areas can reach a thickness of the order of metres, depending on the heat conductivity. The temperature gradient in the insolating mantle can be high. The thicker the mantle, the more efficient is the quenching of the gas flux. The presence of very porous and insolating dust mantle determines the presence of high temperature spots on the surface. Capria et al. (2001) improved and completed the

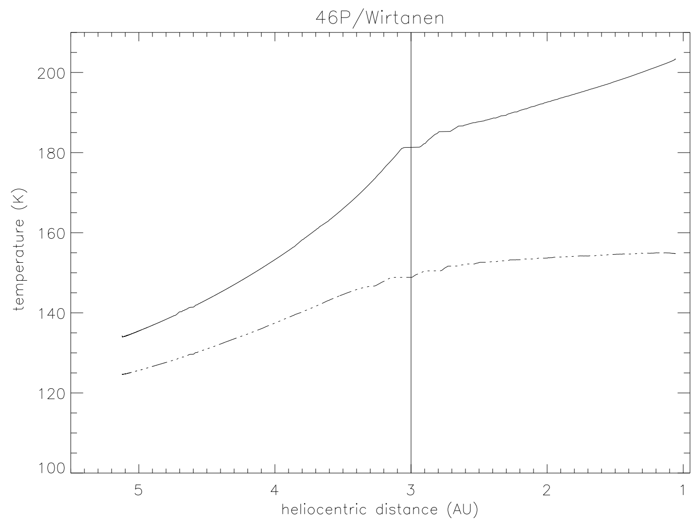

Figure 10.5: Maximum (solid line) and minimum (dashed-dotted line) daily temperatures from aphelion to perihelion at the surface of a bare (no dust mantle) comet nucleus in the orbit of Comet 46P/Wirtanen.

preceding simulations, taking into account the effects of the presence of organic materials in the refractory component and studying how it may modify the preceding results. The refractory component is described by two different physical properties, one with the characteristics of organic material.

Dust characteristics and their physical properties were chosen to simulate as much as possible findings from the Giotto mission to Comet 1P/Halley. The Particle Impact Analyzer instruments (PUMA and PIA) demonstrated that in 1P/Halley's refractory components two chemical phases existed. One phase was organic and of low atomic weight, called CHON, the other was a Mg-rich silicate (Jessberger and Kissel, 1991; McDonnell et al., 1991; Mumma, 1997). Measured particles were in the range of $10^{-16} - 10^{-11}$ g. Average densities were about 2500 kg m^{-3} for silicate particles, and about 1000 kg m^{-3} for CHON-dominated particles. There are indications that the density of larger particles is lower. These two materials have different physical properties for the density, thermal conductivity, tensile strength, cohesion, etc. As a consequence, the characteristics of a mantle composed of silicate particles alone would be different from a mantle composed of refractory organic materials. In this version of the model, one particle component is composed by silicates and the other component is a mixture of silicates and CHON. For the first component a thermal conductivity of 3 W $K^{-1}m^{-1}$, typical of silicates, was assumed, while for the CHON-dominated particles a value of 0.25 W $K^{-1}m^{-1}$, typical of organic substances thought to be analogues of cometary organic material (Kömle et al., 1996; Seiferlin et al., 1996), was assumed.

High values for the average density of 2500 kg m^{-3} for the first component and 1000 kg m^{-3} for the second were assumed. These densities suggest a rather compact structure, but there are indications that larger particles have lower densities, suggesting a more fluffy nature (McDonnel et al., 1991). Particles dominated by light elements should have a lower density and larger masses than particles that are dominated by rock-forming elements (Kissel, 1999). For these reasons a lower density than the average was assigned to larger particles.

The initial size distribution in the nucleus was defined following the reasoning explained in Section 4.5. A Gaussian size distribution was assumed (Coradini et al., (1977) based on the accretion of particles in the solar nebula. A slightly greater average radius was attributed to the particles of the organic distribution, to simulate the increased cohesive strength found experimentally (Kömle et al., 1996). This may result in larger particles. The mixture conductivity of a mantle is not well described by Russel's formula. Moreover, some laboratory data are available. The conductivity value, κ, depends on mantle material (see Section 4.9). In the KOSI experiments (Grün et al., 1993), the thermal conductivity of dust layers composed by silicate particles was found to be very low (about 10^{-2} – 10^{-3} W $K^{-1}m^{-1}$). Even a thin layer of dust causes a large temperature gradient. Following this result, a value of 0.01 W K^{-1} m^{-1} was assigned to the thermal conductivity of the mantle composed only of silicate particles.

As for the real nature of the organic material in comets, it is thought that it should behave like terrestrial tar or a mixture of hydrocarbons including low volatility components (Kömle et al., 1996). The volatility of these substances may be intermediate between that of minerals and ices. Most of the cometary organics may not sublimate, but metamorphose, at temperatures near to 400 K, into a quasi-fluid state, forming a high cohesive mantle (Kömle et al., 1996).

In the case of the organic component, lacking direct measurements, physical properties were adopted from the results of laboratory experiments conducted at the Space Research Institute of Graz by Kömle, Kargl, Thiel, and Seiferlin. They studied the thermal evolution of an analogue of cometary materials composed of a mixture of minerals, ices, and hydrocarbons. They obtained a cohesive mantle composed of minerals "glued" together by organics. This kind of mantle has a thermal conductivity higher than that of a purely siliceous mantle, and also has a greater cohesive strength. An admixture with organic material raises mantle conductivity by one order of magnitude or more with respect to a mantle composed of silicate particles alone (Kömle et al., 1996). Thus, the "organic" mantle was characterized by a higher thermal conductivity than a silicate particle mantle. A mantle composed mainly of organic materials was assigned a conductivity of 0.2 W $K^{-1}m^{-1}$.

With the input parameters described above, two models were constructed. In model A, the reference case, the refractory component consits only of silicates. In model B, the total dust/ice ratio is the same as in model A, but both dust components are present. The simulations are all performed at the equator. In both models a stable mantle was imposed, in the initial orbit. A trapping factor was introduced to compute surface temperatures.

Maximum and minimum temperatures obtained during a comet day along an orbit from aphelion to perihelion are shown in Fig. 10.5, for a model without the formation of a dust mantle. At perihelion a maximum daytime temperature of 203.5 K is reached, while the minimum nighttime temperature is 155 K. The difference between maximum and minimum temperatures is nearly 50 K at perihelion and about 10 K at aphelion.

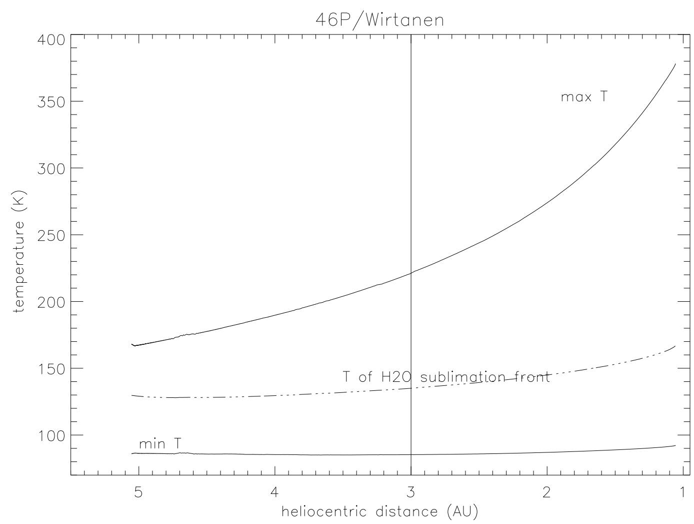

Figure 10.6: Model of comet 46P/Wirtanen: Maximum and minimum daily temperatures (solid lines) from aphelion to perihelion for a surface covered by a dust mantle (model A in text). The dashed-dotted line represents the temperature of the water sublimation front below the dust mantle.

Temperatures at the water sublimation front and typical maximum and minimum surface temperatures during a comet day from aphelion to perihelion are shown in Fig. 10.6, for the case when formation of a mantle with the trapping mechanism is imposed (model A). The maximum temperature rises with respect to that of an icy surface, to 379 K at perihelion, and the difference between daytime and nighttime temperatures is 289 K. The minimum temperature is very low and constant along the orbit. The sublimating water layer has a temperature of 167 K, which stays nearly constant during the comet day along the orbit. The mantle layer thickness is about 0.2 m. The thermal conductivity of 0.01 W K^{-1} m^{-1} makes the mantle a good insulator. However, a surface covered with such a mantle is not completely inactive because the mantle is assumed to be porous. The activity is about two orders of magnitude lower than for an exposed icy layer. It should be noted that the gas flux is also present during the comet night, but at a still lower level than during the day.

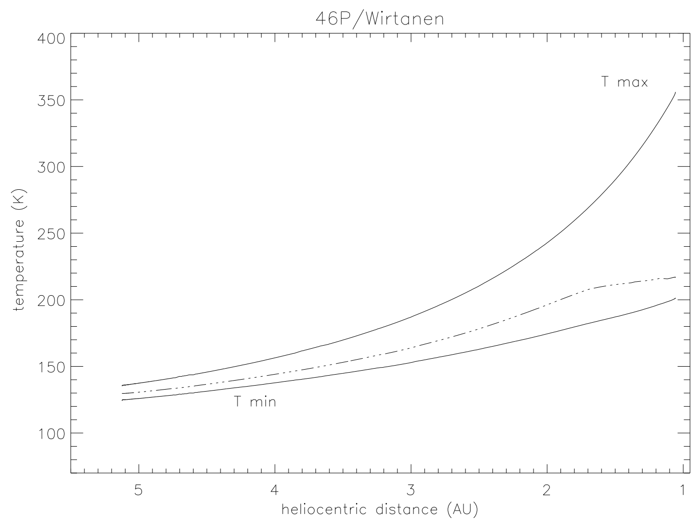

Figure 10.7: Maximum and minimum daily temperatures (solid lines) from aphelion to perihelion for a surface covered by a dust mantle (model B). The dashed-dotted line represents the temperature of the water sublimation front.

In model B, both dust components (30% silicates and 70% CHON particles) are present. Maximum and minimum temperatures on the surface are very similar to those of model A in the case of an active surface. When formation of a mantle is imposed, the temperatures, shown in Fig. 10.7, are very different from those of model A. Higher conductivity in the mantle results in a lower maximum daily temperature of 356 K and a higher night-time temperature of 200 K, both at perihelion. The water ice sublimation front, which in this case is at the same temperature during the night and during the day, has a higher temperature than in model A. This means that the water flux, quenched with respect to the active surface by slightly more than an order of magnitude, is low but continuous during the whole comet day. At perihelion it is 0.25×10^{27} molecules/s.

Our picture of 46P/Wirtanen, on the basis of the available data and models, is that of a very active comet on which formation of a stable mantle on the equatorial regions is unlikely. Although it is difficult to obtain a stable mantle on such a comet, locally and temporary patches of mantle may form. The temperatures reached on such areas greatly depend on their physical properties. It is unlikely that the composition and structure of a comet nucleus are as homogeneous as in the models. If some devolatilized areas have properties typical of organic materials, their temperatures may be lower than those usually assumed for a typical silicate mantle with very low conductivity. Moreover, a “mostly organic” mantle may not be as insulating as a silicate mantle. The existence of a range of variability in mantle physical properties may be verified by space missions.

Indeed, the Deep Impact mission to Comet 9P/Tempel 1 obtained temperature measurements on the surface of the nucleus as shown in Fig. 10.8. IR measurements were obtained when the comet was at about 1.5 AU heliocentric distance. The maximum temperature indicates a thermally well insulating dust mantle composed mostly of silicate particles.

10.2 Conclusions Based on Multiple Simulations

Comet 46P/Wirtanen has been investigated by several groups of comet modelers, using one-dimensional evolution algorithms and taking into account several volatile species, as well as dust. A comparison between the results would therefore be instructive, particularly since it should reveal the sensitivity of the model results to assumptions and approximations, which differ from group to group. The purpose of this comparison is also the opposite of that pursued in Chapter 7. There we were trying to establish how closely algorithms agree, when the only differences between them were of numerical nature. In the present case, we are interested to find how much they diverge, when the input physics and parameters differ.

The parameters used in the four different computations are listed in Table 10.2. Besides the different parameter values, there are differences in the thermal conductivities adopted and in the treatment of the dust. Capria et al. and Podolak and Prialnik include the flow of dust particles through the

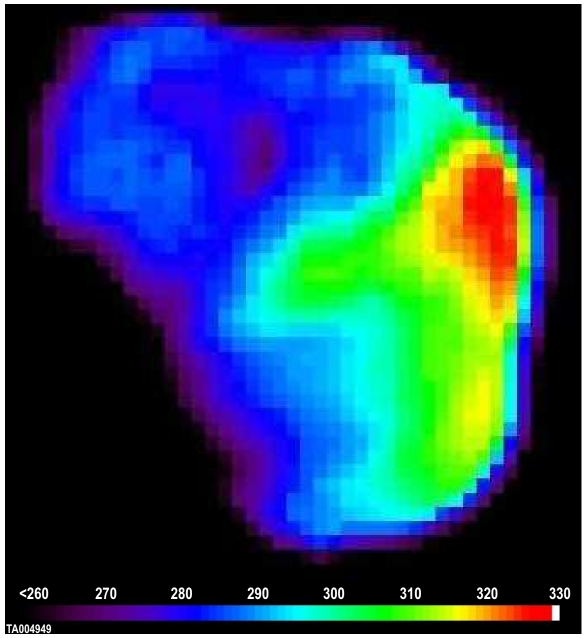

Figure 10.8: Map of the surface temperature of Comet 9P/Tempel 1 prior to impact. The scale is 160 m/pixel. Temperatures range from about 260 K to about 330 K on the sunlit portion of the nucleus. The temperature closely follows the topography, demonstrating the low thermal inertia of the body. (Courtesy Deep Impact Project. Analysis and map by O. Groussin).

pores. All except Benkhoff and Boice include the crystallization of amorphous ice. The other volatiles, essentially CO and CO_2, are taken either as ices [denoted (i) in Table 10.2] – depleted in the surface layer, or as trapped gases [denoted (t) in Table 10.2] that are released upon crystallization. Only Klinger et al. assume the gas release to entail absorption of latent heat. Klinger et al. and Capria et al. consider different values of insolation, corresponding to different latitudes. In all cases volatiles that flow through the porous nucleus are allowed to freeze on the pore walls, at sufficiently low temperatures.

Because of these differences between models, we cannot expect them to fully agree; nevertheless, in spite of the significant differences, some basic evolutionary patterns emerge from all models. Allowing for the limitations of a spherical comet nucleus model, and for the uncertainty in the values of initial parameters, these basic features should – with some confidence – be taken to describe comet nuclei in general, and the nucleus of Comet 46P/Wirtanen in particular:

Table 10.2: Initial parameters for Comet 46P/Wirtanen models

Parameter	B & B	C et al.	K et al.	P & P
Emissivity	0.96	0.96	0.9	0.50
Albedo	0.04	0.04	0.1	0.03
Radius [km]	1.8	0.7	5	2
$X_{\rm ice}/X_{\rm dust}$	1/3	1	1	1
CO/H_2O	0.06(i)	0.01(i)	0.05(t)	0.045(t)
CO_2/H_2O	0.12(i)	0.01(i)	–	0.005(t)
Porosity	0.5	0.8	0.8	0.4
Pore size [μm]	100	10	1	100
Temperature [K]	25	30	30	20
Ice phase	crystalline	amorphous	amorphous	amorphous

B & B – Benkhoff and Boice (1996); C et al. – Capria et al. (2001);
K et al. – Klinger et al. (1996); P & P – Podolak and Prialnik (1996).

1. The outer part of the nucleus is stratified, with layers of different compositions in the following sequence from the surface downwards: a very porous dust mantle 10 cm thick (or more), a denser layer of crystalline ice and dust, a layer composed of dust, amorphous or crystalline ice (see Table 10.2), and CO_2 ice, a thicker layer of dust, amorphous or crystalline ice, and CO ice, and only beneath it the unaltered composition. The thicknesses of these layers, the relative abundances of different components, the porosity, and the pore structure depend on the path of the comet in the inner Solar System (orbital parameters, whether constant or changing), as well as on the initial structure and composition. Accurate predictions are therefore difficult to make. We note, however, that qualitatively such a layered structure is predicted by all four studies, and it should be taken to characterize all evolved comet nuclei. However, one should keep in mind that the stratification may not be uniform, as 1-D models necessarily imply. Moreover, as the surface of a real nucleus is highly uneven, some areas may be bare, exposing ice and being much more active than the surroundings. Thus, different parameter combinations may describe not necessarily different comets, but different, separate areas of a single comet nucleus.

2. The production rate of H_2O gas varies strongly with heliocentric distance, that of CO_2 is less affected, while the production rate of CO gas is nearly constant throughout the orbit. This conclusion applies both to the case where the source of CO and CO_2 is crystallization of the amorphous ice releasing occluded, gases and to the case where the source is interior sublimation of CO and CO_2 ices. The reason for the resemblance is that

some of the gas released from the ice refreezes at some depth below the crystallization front, its origin being lost. The ice subsequently sublimates regardless of its history. In conclusion, relative abundances in cometary ejecta should *not* be taken to reflect the interior composition of the nucleus. For the most volatile species, the mass flux is almost constant throughout the orbit. Mixing ratios in the ejecta may vary by many orders of magnitude between perihelion and aphelion (see also Huebner and Benkhoff, 1999).

3. The surface temperature and the interior temperature profile are sensitive to model assumptions. For models including a dust mantle (Klinger et al., 1996 and Podolak and Prialnik, 1996), the surface temperature varies between about 200 K at perihelion and over 100 K at aphelion (although latitude variations may also be quite large). The internal temperature is affected down to a few metres for the Podolak and Prialnik (1996) model, a few tens of metres in the Benkhoff and Boice (1996) model and over 100 m in the Klinger et al. (1996) model. It is agreed, however, that the depth coincides with the presence of a CO (or other extremely volatile) ice layer, which acts as a thermostat, keeping the temperature near the sublimation point of that ice. The depth of such a layer is determined not only by initial parameters and assumptions, but also by the history of the comet (particularly, its orbital history in the inner Solar System).

Finally, a word of caution. Models of the active phase of comet nuclei consider only the evolution within the planetary system, either in a fixed orbit, or in an evolving orbit (e.g. Capria et al., 2001), assuming a homogeneous initial composition. One should keep in mind, however, that during earlier phases in the Oort cloud or the Kuiper belt, comets might not have been entirely inert and completely inactive. There still remains the potential source of energy provided by radioactive decay to be considered. According to Prialnik and Podolak (1995), porous comet nuclei composed initially of amorphous ice and dust retain the ice in the amorphous form if their radii do not exceed 20 km, and if the initial ^{26}Al content is negligible ($\leq 5 \times 10^{-9}$). If the radius is significantly larger than 20 km, the nucleus crystallizes even in the absence of ^{26}Al and only a thin outer layer preserves the pristine composition. The thickness of this layer (which may be considerable) depends on the thermal conductivity of the ice. The presence of ^{26}Al in the initial composition reduces the critical radius for crystallization.

10.3 Comet Outbursts

Comets are often found to be active at heliocentric distances far beyond the limit of about 5 AU, within which the activity may be explained by sublimation of water ice induced by insolation (Cochran et al., 1992; Jockers et al., 1992; Sekanina et al., 1992). Crystallization of amorphous ice has been recognized as a suitable mechanism for explaining such distant bursts of activity (Patashnick et al., 1974; Smoluchowski, 1981; Espinasse et al., 1991; Weissman, 1991; Prialnik and Bar-Nun, 1992).

Numerical models of the evolution of cometary nuclei containing amorphous ice agree that crystallization progresses in spurts, its onset, duration, and extent in depth being largely determined by the structure, composition, and thermal properties of the nucleus and by the comet's orbit (e.g. Herman and Podolak, 1985; Prialnik and Bar-Nun, 1987, 1990; Espinasse et al., 1991; Tancredi et al., 1994). Crystallization may be initiated by the heat wave propagating inwards from the insolated comet surface to the crystalline/amorphous ice boundary, provided that when reaching this boundary it still carries sufficient energy for raising the local temperature significantly. However, once this has occurred and the boundary has moved deeper into the nucleus, later heat waves originating at the surface will be too weak when reaching the boundary to rekindle crystallization. A quiescent period thus ensues, until the surface recedes (by sublimation) to a sufficiently shorter distance from the crystalline/amorphous ice boundary. At that point, a new spurt of crystallization will take place. Since in the meantime the interior temperature of the ice has risen to some extent, crystallization will advance deeper into the nucleus than at the previous spurt. This will, in turn, affect the time span to the next spurt of crystallization, since the rate of surface recession for a given comet nucleus is approximately constant (see Table 5.1).

In conclusion, crystallization would appear to be triggered sporadically, preferentially at large heliocentric distances, where comets spend most of their time. This could explain the distant activity – outbursts and, possibly, splitting – of comets.

The release of gas trapped in the amorphous ice provides the link between crystallization and the eruptive manifestations of comets, a few examples of which will be given below. We have already shown that numerical simulations are based on many simplifying assumptions, and often adopt parameters that are not well known. Hence, they should not be expected to accurately reproduce any particular observed outburst. Rather, such simulations should account for the basic characteristics of the observed outbursts.

On the other hand, other effects may also lead to activity and splitting at large heliocentric distances. For example, it may also be induced by the tumbling motion of comet nuclei. As the surface of a nucleus erodes from sublimation of ices, the moments of inertia of the nucleus change. In addition, sublimation of ices not only gives rise to non-gravitational forces affecting the orbit of the comet, it also changes the angular spin both in magnitude and in direction. These changes will be the larger the closer the erosion is to the extreme ends of an elongated nucleus. The misalignment between the principal axis of inertia and the spin axis of the nucleus gives rise to complex motions including tumbling, which cause internal stresses and strains that may lead to stretching and bending modes with different frequencies. It will take considerable time for these frequencies to approach an accidental resonance that may result in the tendency to realign different physical subsections of an agglomerated nucleus, thereby exposing fresh icy areas and even cause splitting of the nucleus. It may also be possible that a combination of various effects, such as the misalignment between principal axis of inertia and the spin axis and the amorphous/crystalline phase transition act together.

10.3.1 Distant Outbursts of Comet 1P/Halley

The behaviour of Comet 1P/Halley at large heliocentric distances, beyond $r_{\mathrm{H}} = 5$ AU, was characterized by outbursts of various magnitudes. During the most significant outburst, at $r_{\mathrm{H}} = 14$ AU (West et al., 1991), the total brightness increased by more than 5^{mag} and a large coma developed. The outburst subsided on a timescale of months. Klinger and his collaborators (see Espinasse et al., 1991; Weissman, 1991) and Prialnik and Bar-Nun (1992) showed that these features may be explained by ongoing crystallization of amorphous ice in the interior of the porous nucleus, at depths of a few tens of metres. According to this model, enhanced outgassing results from the release of trapped gases during crystallization of the ice. The orbital point where the gas flux reaches its peak was found to be strongly dependent on the porosity of the comet nucleus. Thus, in the case of a spherical nucleus of porosity 0.5 (Prialnik and Bar-Nun, 1990) crystallization was found to occur on the outbound leg of Comet 1P/Halley's orbit, at heliocentric distances between 5 and 17 AU (depending on the pore size assumed – typical pore sizes being 0.1 - 10 μm). Similar results were obtained by Schmitt et al. (1991). The duration of an outburst is the most difficult to predict. Depending on the pore size and on the mechanical properties of the ice, it may vary over three orders of magnitude. A time span of a few months lies within this range and is therefore attainable for a suitable choice of parameters.

10.3.2 Pre-Perihelion Activity of 2060 Chiron

2060 Chiron, first classified as an asteroid, was observed to develop a coma at random intervals before it reached perihelion in 1996 in its 50-year orbit.

Marcialis and Buratti (1993) summarized its brightness variations. The first episode of coma formation occurred in 1978, in the middle of the decline in brightness. The second episode, in 1989, when the coma reached vast dimensions, coincided with the maximal brightness. Even near aphelion, 2060 Chiron underwent a major outburst that lasted several years. Prialnik et al. (1995) were able to devise a model that agreed remarkably well with the observational data, by adopting a composition of 60% dust and 40% amorphous ice, occluding a fraction 0.001 of CO gas and assuming a low emissivity ($\epsilon = 0.25$). The optimal parameter combination was found after numerous trials of parameter combinations that proved far less successful. They found that spurts of crystallization started close to aphelion. As a rule, the CO production rate decreased slightly as the model comet approached the Sun from aphelion. This might explain the puzzling fading of 2060 Chiron between 1970 and 1985 (i.e. from $r_{\mathrm{H}} \approx 18$ AU to about 14 AU). The model produced the required CO emission rates, explained by release of trapped gases, and reproduced the estimated surface (colour) temperatures at different points of the orbit as derived by Campins et al. (1994). Capria et al. (2000b) also explained Chiron's activity by gas trapped in amorphous ice, although they also mentioned the possibility of CO ice close to the surface, which would imply that Chiron has been inserted in its present orbit only recently (e.g. see Fanale and Salvail, 1997).

10.3.3 Erratic Activity of 29P/Schwassmann-Wachmann 1

The orbit of Comet 29P/Schwassmann-Wachmann 1 is nearly circular and confined between the orbits of Jupiter and Saturn. Despite the fact that at such heliocentric distances the sublimation of H_2O ice is negligibly small, this comet exhibits irregular activity, i.e. unpredictable changes in its light-curve. Huebner and Weigert (1966) proposed that such activity might be explained by the appearance and disappearance of an ice-particle coma. Froeschlè et al. (1983) suggested that this might be associated with crystallization of amorphous water ice. This suggestion was further strengthened by the detection of CO released by the comet (Senay and Jewitt, 1994; Crovisier, et al. 1995), since Comet 29P/Schwassmann-Wachmann 1 is too distant for H_2O ice sublimation, its surface is too hot for the survival of CO ice. Subsequently, Klinger et al. (1996) showed by model calculations that the CO production pattern can be explained and simulated by gas trapped in the amorphous ice and released from the ice on crystallization. The chaotic behaviour results from the highly non-linear temperature dependence of the processes involved.

10.3.4 Distant Activity of Comet Hale-Bopp (C/1995 O1)

Comet Hale-Bopp (C/1995 O1) was characterized by an unusually bright coma at a distance of $r_{\rm H} \approx 7$ AU from the Sun. Jewitt et al. (1996) detected a very large flux of CO molecules, which increased dramatically. Such brightening is unlikely to have resulted from surface (or subsurface) sublimation of CO ice in response to insolation. CO ice should have been depleted much earlier in the comet's orbit, since at $r_{\rm H} \approx 7$ AU the surface temperature is already above $T = 100$ K, considerably higher than the sublimation temperature of CO. Jewitt et al. concluded that it would be highly improbable that the trend of CO emission increase be sustained until perihelion. Rather, it might indicate a transient brightening, similar to those exhibited by periodic Comet 29P/Schwassmann-Wachmann 1 or 2060 Chiron. Substantial emission of CO was also detected by Biver et al. (1996) on 20-21 September, but it was not detected on 16 and 23 August. This may be taken to indicate a sudden surge of activity. A jet-like feature of dust was detected on 25 August (Kidger et al., 1996), probably the result of an unusual outburst. In this case, too, the unusual activity could be explained on the basis of crystallization and release of occluded CO accompanied by ejection of dust entrained by the gas (Prialnik 1999, 2002; Capria et al., 2002).

10.4 Coma Versus Nucleus Abundances

10.4.1 Multi-Volatile Model of Comet 67P/Churyumov-Gerasimenko

After the delayed launch of *Rosetta* at the beginning of 2003, a new target comet had to be selected for the mission because the initial target, Comet 46P/Wirtanen, could no longer be reached within a reasonable time. Thus, Comet 67P/Churyumov-Gerasimenko, discovered in October 1969, was selected as the new target. The comet has a particularly unusual history. Its perihelion distance decreased from $q \approx 4$ AU after an encounter with Jupiter and the orbit shifted inwards to a perihelion distance of $q \approx 3$ AU. From there it slowly decreased further to 2.77AU, from which a further Jupiter encounter in 1959 moved it into the recent orbit with a perihelion distance of $q = 1.28$ AU. The period is about 6.57 years. After the comet was discovered in 1969, it returned to perihelion six times. The nucleus of 67P/Churyumov-Gerasimenko is estimated to be about 4 km in diameter.

Assuming a spherical model comet in the orbit of 67P/Churyumov-Gerasimenko with its orbital period of about 6.57 years, gas fluxes of different molecules were calculated for a wide range of nucleus parameters (see

Benkhoff, 2002 for details). The spin axis was assumed to be perpendicular to the orbital plane and a spin period of 12 hr was adopted. The results are calculated for nine different latitudes, starting with a homogeneous mixture of nine ices (H_2O, CO_2, CO, CH_3OH, CH_4, HCN, H_2S, C_2H_2, C_2H_6) and dust at a constant starting temperature of $T = 10$ K and a constant mass density distribution. The relative mass abundances of the ices are as follows: $X(H_2O)$:$X(CO_2)$:$X(CO)$:$X(CH_3OH)$:$X(CH_4)$:$X(HCN)$:$X(H_2S)$:$X(C_2H_2)$:$X(C_2H_6)$= 0.885 :0.02 :0.03 :0.025 :0.015 :0.01 :0.005 :0.005 :0.005 .

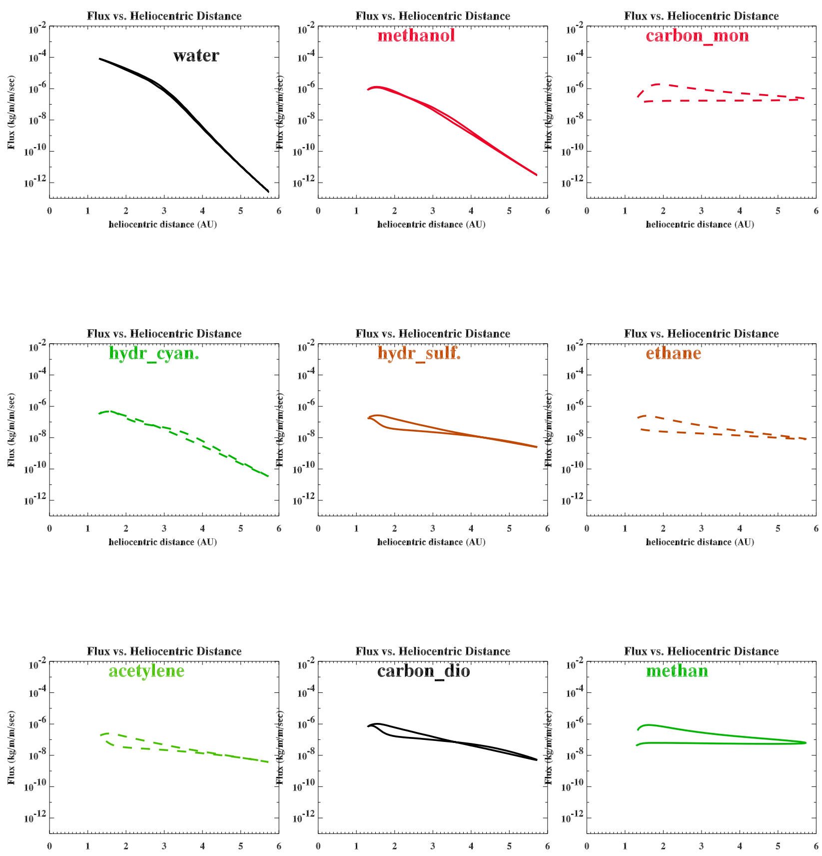

Figure 10.9: Mass fluxes of H_2O, CO, CO_2, CH_3OH, HCN, H_2S, C_2H_2, C_2H_6 and CH_4 from the surface as a function of heliocentric distance for models assuming a heat conductivity of 0.01 times the conductivity of pure water ice.

Due to heating of the body and sublimation of the volatile components, the initially homogeneous body differentiates into a multi-layer body, where the deepest layer has the original composition. The layers above are successively depleted of volatiles, with the outermost layer containing only dust.

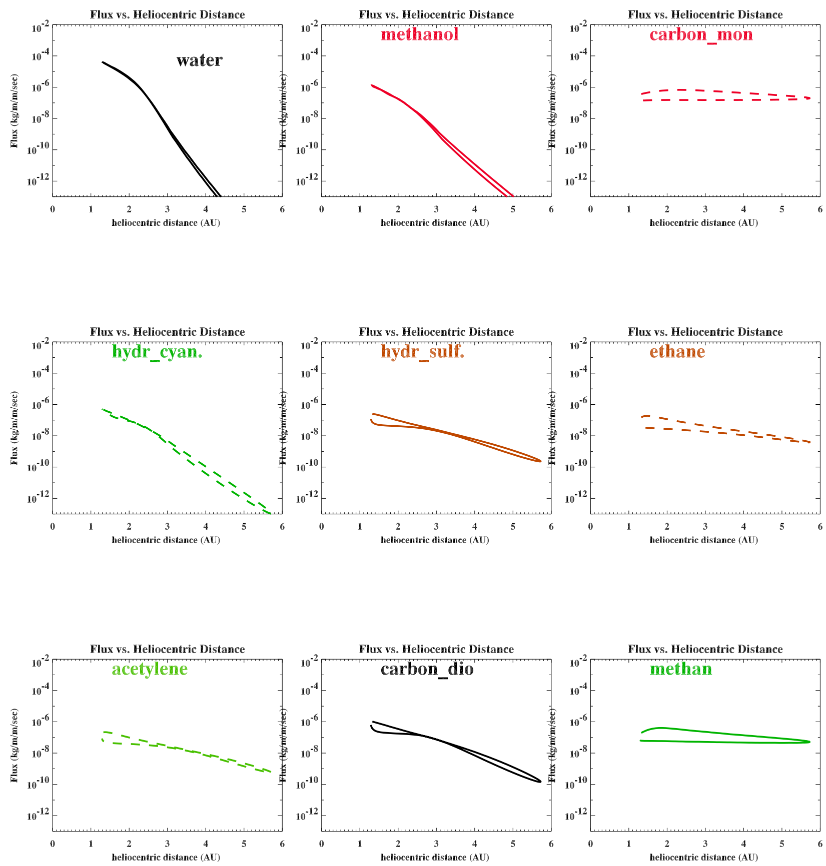

Figure 10.10: Mass fluxes of H_2O, CO, CO_2, CH_3OH, HCN, H_2S, C_2H_2, C_2H_6 and CH_4 from the surface as a function of heliocentric distance for models assuming a heat conductivity of 0.01 times the conductivity of pure water. Fluxes originate from a belt of $\pm 10°$ around latitude 60°.

An understanding of the energy balance of the nucleus of a comet is essential to explain its chemical composition and its physical behaviour. The number of molecules leaving the surface of the nucleus is strongly related to the amount of energy that is available for sublimation. The energy input depends mainly on heliocentric distance, rotational state, spin period, scattering properties, reflectivity of the surface, and heat conductivity of the matrix material.

Most of these parameters are poorly known. Thus, assumptions and parameter variation studies are necessary in order to obtain clues regarding the chemical and physical behaviour of the nucleus. In the present calculations, as in the models described in Chapter 7, the conductivity of the solid was reduced by a Hertz factor of 0.01 to take porosity and the reduced contact area into account.

In Fig. 10.9 the calculated gas fluxes of H_2O, CO, CO_2, CH_3OH, HCN, H_2S, C_2H_2, C_2H_6 and CH_4 molecules from the surface into the coma are given. Calculations are carried out for nine different latitudes and the total flux is obtained by integration over the whole nucleus. The flux is given in kg m^{-2} s^{-1}. The H_2O mass flux varies by several orders of magnitude during one orbit. The mass flux depends strongly on the amount of energy transported to the sublimation front of water ice. The total maximum flux at perihelion is about 1×10^4 kg m^{-2} s^{-1} or 2×10^{29} molecules s^{-1} (assuming a radius of 2000 m and a 100% active surface. If one assumes that only 5 % of the surface of Comet 67/Churyumoy-Gerasimenko is active, then the total flux is only about 10^{28} molecules s^{-1}, which is in good agreement with observations. Average mass fluxes of CH_3OH and HCN vary by about 5 orders of magnitude during one orbit.

The fluxes obtained at perihelion are in the order of 2×10^6 kg m^{-2} s^{-1} for methanol and 8×10^7 kg m^{-2} s^{-1} for HCN. The CO_2, H_2S, and C_2H_6 fluxes show smaller orbital variations of about 2 to 3 orders of magnitude, while CO, C_2H_2, and CH_4 fluxes vary only by small factors. Due to the inward motion of the sublimation fronts and the thermal inertia of the matrix material, the maximum flux is shifted slightly to distances past perihelion.

At perihelion one obtains a CO mass flux of about 2×10^6 kg m^{-2} s^{-1} or 4×10^{27} molecules s^{-1} assuming a radius of 2000 m and a 100% active surface. No CO flux has been measured for this comet. This is not in conflict with the model results, because the calculated values are below the detection limit of the instruments. Generally, it was found by comparing calculated results with measured data that a low heat conductivity leads to a better fit to observations.

Instead of averaging gas fluxes over the whole sphere and comparing these average fluxes with measurements, results obtained at different latitudes are considered in order to show how the flux will change if it originates from different parts of the surface. In Fig. 10.10 we show the calculated gas fluxes of H_2O, CO, CO_2, CH_3OH, HCN, H_2S, C_2H_2, C_2H_6 and CH_4, originating from a belt of $\pm 10°$ around latitude $60°$.

We note that these fluxes decrease rapidly with heliocentric distance. The absolute values are also significantly smaller than the values given in Fig. 10.9. If these results fit measured data better, this could be a hint that the measured fluxes may originate from active areas at higher latitudes. Several processes must be taken into account to understand the results as a function of heliocentric distance. Energy is needed to sublimate surface water ice. Dust is entrained by the evaporating gas. The dust emission is linked to the gas, but because of the lack of a measured dust size distribution, results are very vague. It is possible to put a limit on the size of particles entrained by the gas, but this also depends on the shape and state of the dust particles.

Distributed sources from the dust in the coma, which contribute to coma gas, are not included in the nucleus models, but could play an important role (e.g. in understanding the source of CO). Gases evaporating from the nucleus interior are more volatile ices than water ice and diffuse outwards into the coma depending on porosity. The results will only provide some hints about the gas flux and the energy balance at the surface, the conductivity that is consistent with the measurements, the influence of the rotational state, and the possible molecular densities in the coma.

10.4.2 Volatile Production Rates Compared with Nucleus Composition

A comet nucleus is expected to include many different volatile species as observed in the coma. If water ice is crystalline, these volatiles will be frozen out as separate phases; if water ice is amorphous, the volatiles may be trapped in the amorphous ice. In the first case, as the heat absorbed at the surface penetrates inwards, ices other than water ice will sublimate and the gas will flow in part to the surface and into the coma and in part to the colder interior, where it will refreeze. Since sublimation rates are strongly temperature dependent and vary widely between gas species, several distinct sublimation fronts are expected to form, and also several separate layers of refrozen gases. These ice layers will sublimate, in turn, when erosion of the nucleus brings them closer to the surface. Hence, the layered structure may move towards the centre, but at the same time remain constant in depth relative to the surface.

Characteristics of several different species are summarized in Table 10.3. Constants A and B correspond to the coefficients of the Clausius-Clapeyron equation for the saturation vapour pressure

$$P_v(T) = A\mathrm{e}^{-B/T} \tag{10.1}$$

Table 10.3: Volatile properties

Ice	A	B	T_s	ΔH	$\dot{r}$
	10^{10} N m^{-2}	K	K	10^6 J kg^{-1}	cm/d
H_2O	356.	6141.67	133	2.830	0.8
HCN	3.8665	4024.66	97	1.240	37
NH_3	61.412	3603.60	81	1.760	26
CO_2	107.9	3148.00	70	0.594	78
CH_4	0.597	1190.20	30	0.617	75
CO	0.1263	764.16	20	0.227	200

which also serves to calculate the typical sublimation temperature

$$T_s = B/\ln(A/\mathrm{const}) \tag{10.2}$$

The rate of advance of the sublimation front $\dot{r}$ into the nucleus is then estimated for each species by assuming that the conduction flux inward from the surface (typically of order 100 W m^{-2}) is used entirely for the sublimation of that species, $\dot{r} = F_{\mathrm{in}}/(\rho X_{\mathrm{ice}}\Delta H)$.

If gas is trapped in amorphous ice, it will start to escape when the ice crystallizes. This means that all species will escape together and they will escape, generally, at higher temperatures than those typical for sublimation. Once they are released from the ice, these gases will behave similarly to gases that sublimated from the pore walls, flowing in part towards the surface and in part towards the interior. In this case a layered structure of refrozen volatiles will develop and will eventually sublimate at a later stage.

Table 10.4: Parameters for Comet 67P/Churyumov-Gerasimenko models

Property	Value
Semi-major axis	3.507 AU
Eccentricity	0.6316
spin period	12.69 hr
Radius	1.98 km
Bulk density	500 kg m^{-3}

This complex behaviour is expected to result in gas production rates particular for each species. Thus, abundance ratios in the coma may be vastly different from those in the nucleus, even before molecules are further processed by solar radiation. In order to test this inference and asses the extent of the discrepancy between ejecta and nucleus compositions, several models were calculated (Prialnik, 2006), adopting the characteristic parameters of Comet 67P/Churyumov-Gerasimenko, listed in Table 10.4.

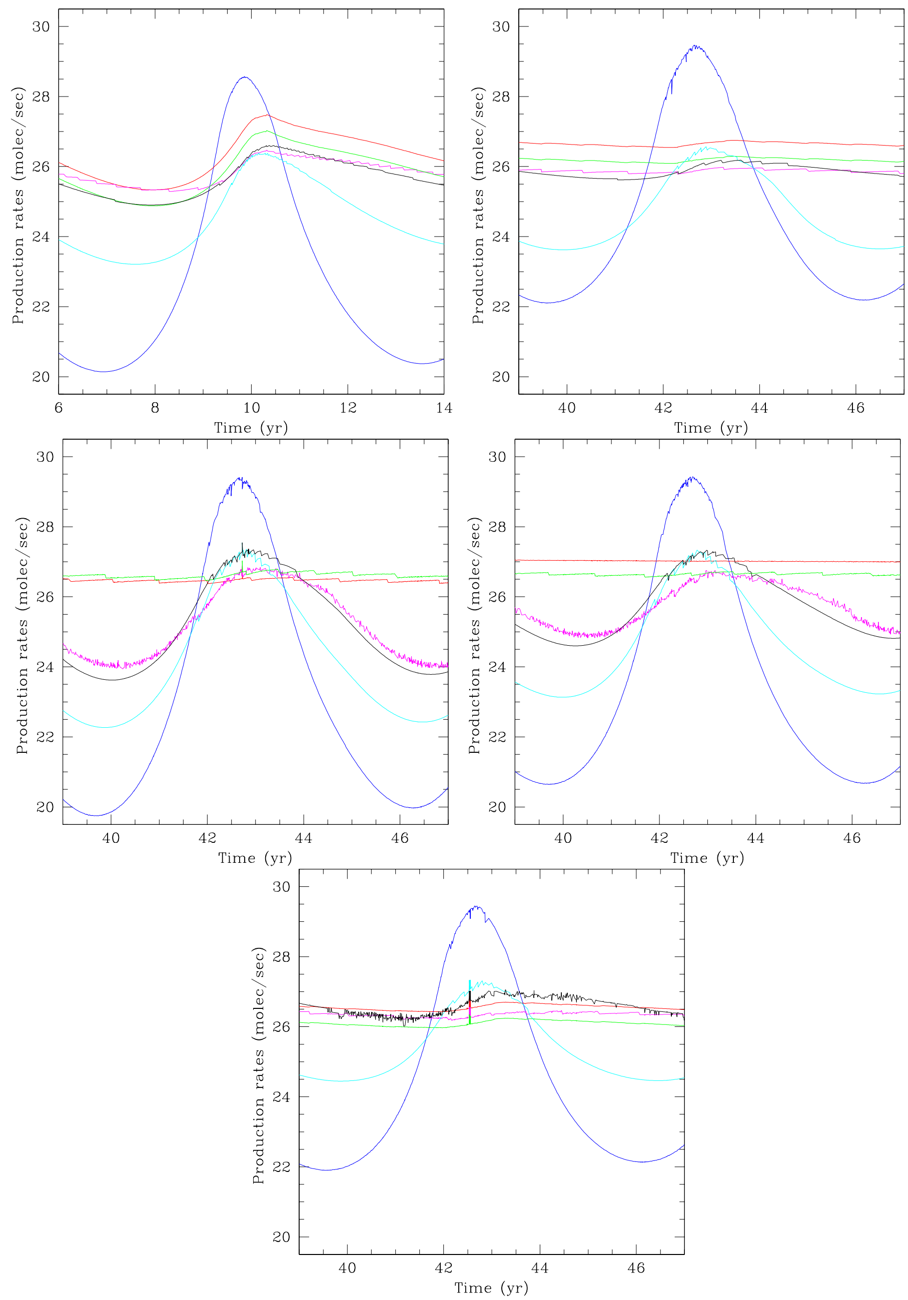

Figure 10.11: Production rates for one orbital revolution: red – CO; magenta – CO_2; green – CH_4; cyan – HCN; black – NH_3. Models, as listed in Table 10.5, are: top left - 1; top right - 2; middle left - 3; middle right - 4; and bottom - 5. The upper models include only trapped volatiles, the middle ones include only ices, while the bottom one includes both.

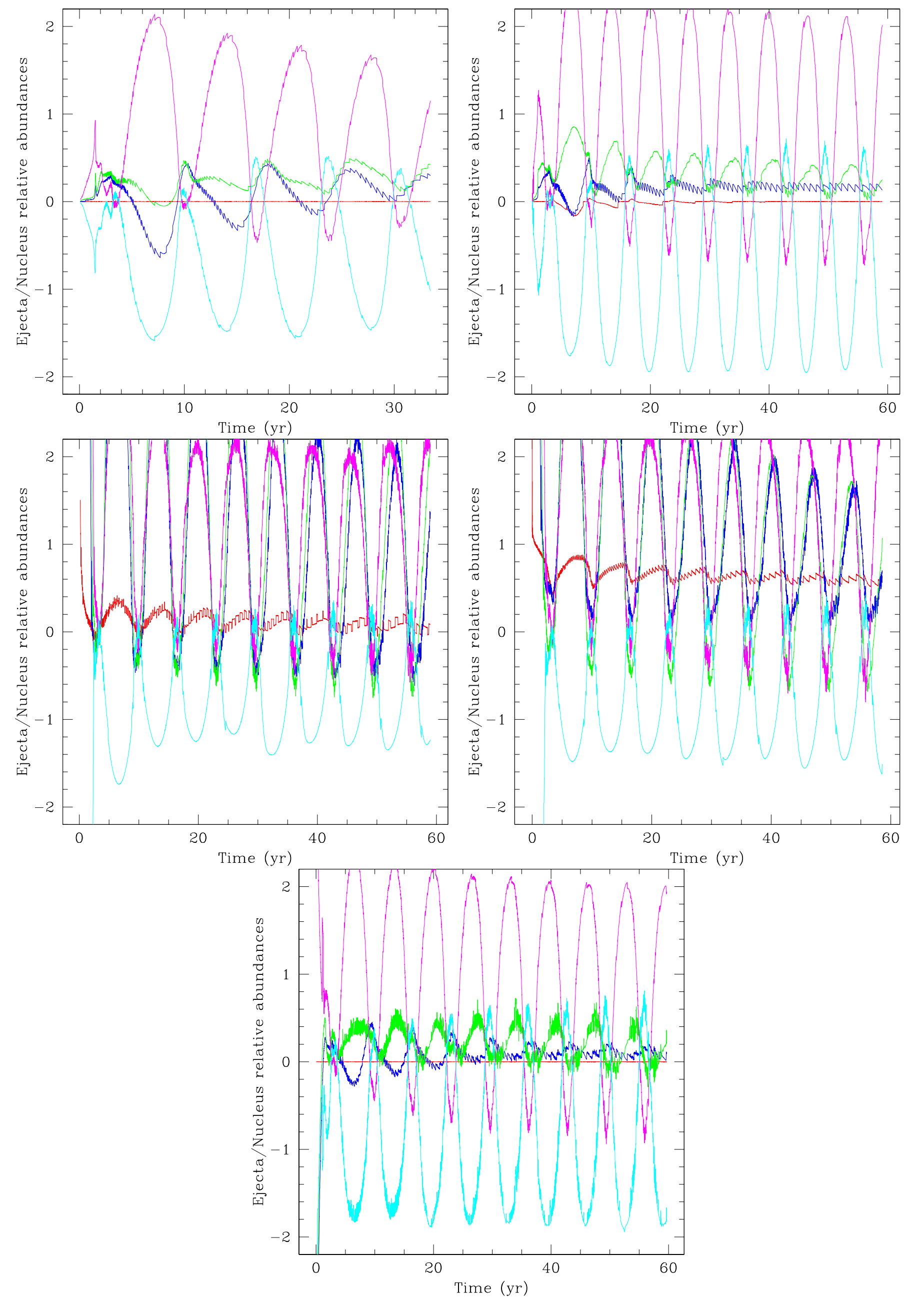

Figure 10.12: Final abundance ratios relative to initial abundance ratios (log scale): blue $CO\,/\,CO_2$; green $CH_4\,/\,NH_3$; cyan $HCN\,/\,NH_3$; magenta $CO_2\,/\,HCN$; red $CO\,/\,CH_4$. Models from Table 10.5: top left - 1; top right - 2; middle left - 3; middle right - 4; and bottom - 5. Models 1, 2 include only trapped volatiles, 3 and 4 include only ices, while 5 includes both.

The compositions adopted for the different models (labeled 1 to 5) are listed in Table 10.5. It includes three types of volatile mixtures: amorphous water ice and trapped gases, crystalline water ice mixed with ices of other volatiles and also, a combination of amorphous water ice and trapped gases mixed with ices of the same species of gas.

Table 10.5: Initial volatile abundances: first row – frozen (mass fractions); second row – percentage trapped in amorphous ice

Model	T_0	X_d	X_{ice}	CO	CO_2	CH_4	HCN	NH_3
1.	50 K	0.50	0.50	—	—	—	—	—
			am	5%	2%	1%	1%	1%
2.	50 K	0.20	0.80	—	—	—	—	—
			am	5%	2%	1%	1%	1%
3.	20 K	0.25	0.60	0.03	0.03	0.03	0.03	0.03
			cr	—	—	—	—	—
4.	40 K	0.25	0.60	0.03	0.03	0.03	0.03	0.03
			cr	—	—	—	—	—
5.	50 K	0.20	0.71	—	0.03	—	0.03	0.03
			am	5%	2%	1%	1%	1%

The results of these model calculations are summarised in Figs. 10.11 and 10.12, which show production rates of volatiles along one full orbital revolution, and abundance ratios in the ejecta relative to those of the nucleus, respectively. It is clearly illustrated that abundances in the material ejected from the nucleus may differ from the initial abundances of the nucleus composition by up to factors of 100. This effect is related to the stratified structure of the nucleus (see Section 11.2 below) to which refreezing of volatiles makes a significant contribution. Exceptions are supervolatile species, which preserve their relative abundances. We note that the production rates of these species remain nearly constant along the orbit, while those of the least volatile species change considerably (see also Fig. 10.3). This is correlated with the depth at which gases are produced: the higher the volatility, the colder and hence deeper the zone of origin. Deep layers are less affected by orbital variations in insolation.

— 11 —

Internal Properties of Comet Nuclei

"...I propose to investigate the possibility that the molecules responsible for most of the light of comets near perihelion arise primarily from gases long frozen in the nuclei of comets. Furthermore, I propose that these primitive gases constitute an important, if not a predominant, fraction of the mass of a "new" or undisintegrated comet. On the basis of these assumptions, a model comet nucleus then consists of a matrix of meteoric material with little structural strength, mixed together with the frozen gases—a true conglomerate."

Fred L. Whipple, *Astrophysical Journal, 111*, 1950.

11.1 Temperature Profiles

The heat transported into a nucleus in part increases its internal energy and in part sublimates ices. Heating of the subsurface layers of a nucleus that contains amorphous ice is illustrated for one spin period in Fig. 11.1. The affected region is only a few metres deep. At larger heliocentric distances, r_{H}, the layer of temperature inversion is only about 1 cm thick. The change in slope of the profile occurs at the boundary between the outer crystalline layer, which is a better heat conductor, leading to a mild temperature variation with depth and the inner amorphous ice region, where conductivity is poorer and the temperature profile is steep. The typical steep rise in temperature at 1.68 AU pre-perihelion is caused by heat released in crystallization of amorphous ice, which proceeds at a fast rate at that point. We note the shift of the surface caused by erosion.

The evolution of the temperature profile for models of two different compositions, Models 1 and 5 of Table 10.5, is shown in Fig. 11.2. We note that heat is dissipated to larger depths in the case of crystalline ice, which is a better heat conductor. For the same reason, cooling is more efficient, as shown by the narrower temperature peaks as function of time around perihelion. In both cases, an almost steady pattern of temperature variation with both time and depth is achieved after only a few revolutions. The orbital skin depth, of about 10 m, is clearly apparent.

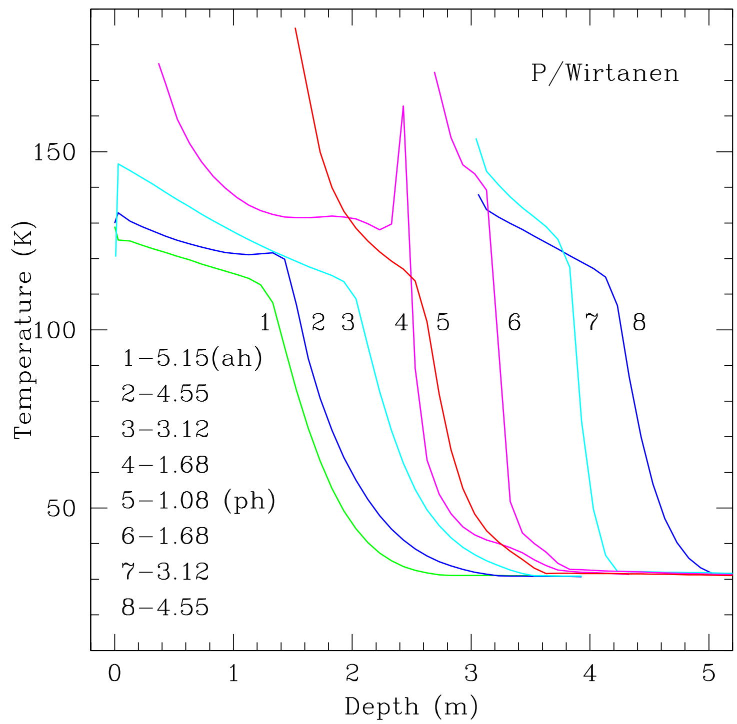

Figure 11.1: Modeled temperature profiles in the upper layer of a nucleus in the orbit of 46P/Wirtanen at several points along the orbit, pre-perihelion (curves 1 - 4) and post-perihelion (curves 6 - 8). Aphelion (ah) at $r_{\mathrm{H}} =$ 5.15 AU, perihelion (ph) at $r_{\mathrm{H}} = 1.08$ AU.

11.2 Stratification of Composition

Heat that is conducted into the interior of a porous nucleus may reach ices more volatile than water ice. In a comet nucleus, many different volatile species are expected to be present (e.g. Table 10.3). If the ice is crystalline, then volatile ices are frozen out as separate phases. As heat diffuses inward, each volatile constituent forms its own sublimation front depending on its change in enthalpy of sublimation. If amorphous ice is present, it will change to crystalline ice, forming an exothermic front for the phase transition. At this front, gases trapped by the amorphous ice will be released. As an ice species sublimates, or is released from the amorphous ice, the gas pressure at the sublimation or crystallization front increases towards its maximum (equilibrium) value at that temperature. The pressure forms a gradient that is negative in the outward direction and positive in the inward direction from the front. This pressure gradient drives the gas flow.

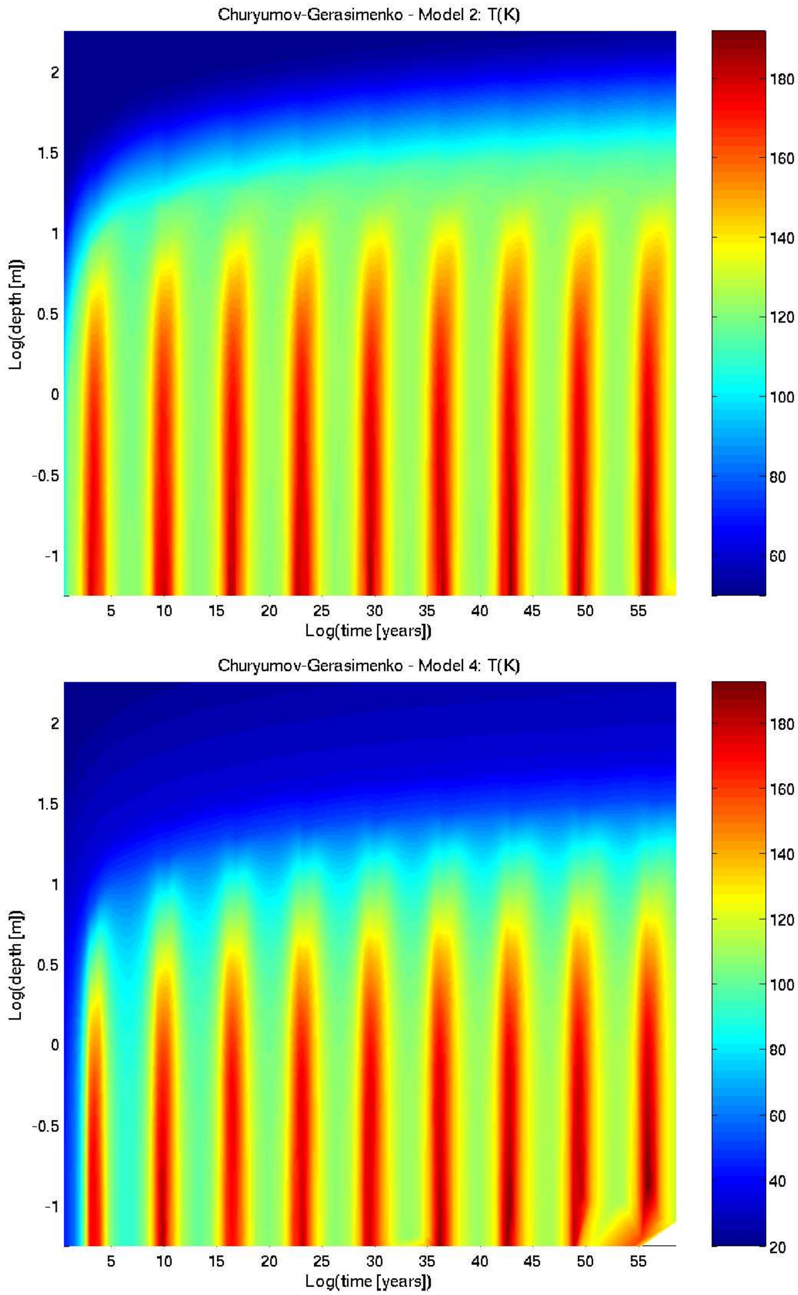

Figure 11.2: Temperature evolution within a comet nucleus model in the orbit of 67P/Churyumov-Gerasimenko through repeated revolutions about the Sun for different initial compositions: *upper panel* - amorphous water ice, occluded gases, and dust; *lower panel* - crystalline water ice mixed with other ices, and dust.

The gas flowing outwards will diffuse through the comet nucleus and escape through its surface into the coma. The gas flowing inwards will recondense a short distance below the sublimation or crystallization front and release its latent heat. This is an additional heat transport mechanism into the interior, which surpasses advection by flowing gas (Prialnik, 1992; Steiner and Kömle, 1993). It was observed by Benkhoff and Spohn (1991a) during the KOSI experiments on cometary ice analogues. Recondensation occurs within a thermal skin depth. The effect is illustrated in Fig. 11.3, where we note the advance of crystallization, accompanied by freezing of the CO gas flowing inwards into the colder regions below the crystallization front. The decrease of X_c (crystalline ice mass fraction) near the surface is caused by sublimation.

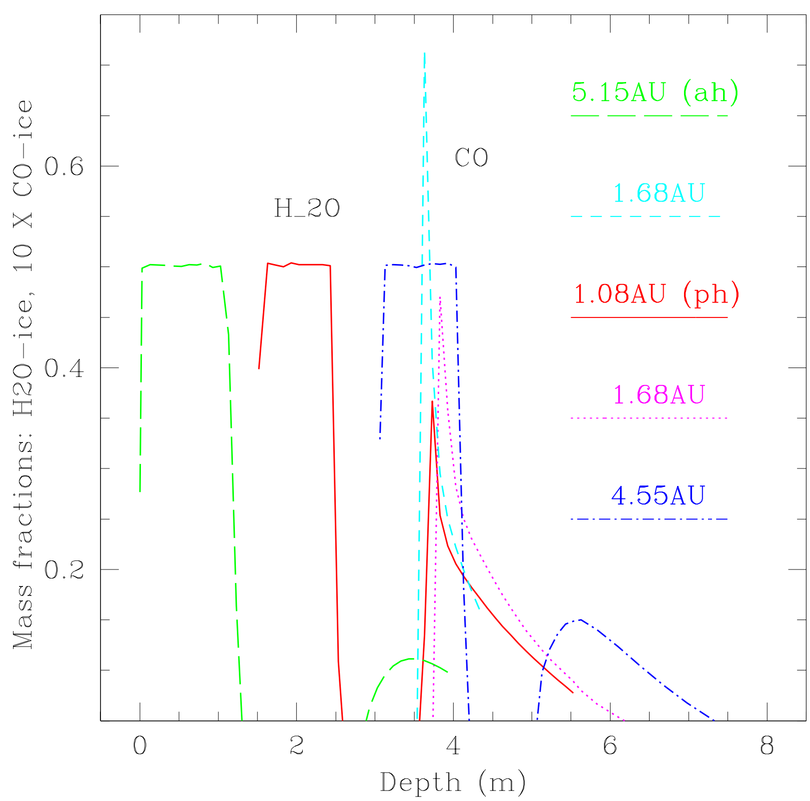

Figure 11.3: Mass fraction profiles in the outer layers of a model nucleus near the subsolar point: X_c - H_2O ice that has crystallized, X_{CO-ice} (multiplied by 10) - frozen CO originating from CO gas released from amorphous water ice. The initial composition is $X_a = 0.5$ (amorphous water ice), $f_{CO} = 0.05$, and $X_d = 0.5$ (dust). The model is the same as that of Fig. 11.1.

Because of heat and gas diffusion, the nucleus will be chemically differentiated in layers. The least volatile material (dust) will be at the top of the nucleus. It will be followed by a layer of dust and water ice. In the deepest layers we would find dust and all ices including the most volatile species (such as CO and CH_4). An example of the stratified structure of the nucleus is shown in Fig. 11.4, where the mass fraction of volatiles other than H_2O is mapped as a function of depth and time. The different peaks as a function of depth at any given time correspond to different volatiles, the deepest arising from the most volatile, and subsequent ones in order of volatility (see Table 10.3).

In the lower panel, representing an initial composition of mixed ices, the enriched volatile fractions arise from refreezing of gases that migrated inwards into colder regions after sublimating from their ices. The low initial temperature assumed for the model ($T = 20$ K) allowed for refreezing even of CO. Although a composition of amorphous ice with trapped gases follows a similar pattern, only three enriched layers are observed in the upper panel of Fig. 11.4, since both CO and CH_4 cannot refreeze because of the higher initial temperature of the model ($T = 50$ K). The dips in the enriched layers arise at perihelion as a result of erosion of the nucleus surface, which reduces the depth of those layers periodically.

11.3 Dust Mantle Thickness

When working with our reference models, dust (if present) was not considered to be entrained by the escaping coma gas. This gave rise to a rapidly growing mantle, whose effect on surface temperature and gas fluxes can be seen in Figs. 7.5, 7.6 and 7.7, in Chapter 7. Surface temperature in models 4a and 4b is much higher after a mantle is formed, and gas fluxes are smaller by orders of magnitude, but still present because the mantle is assumed to be porous. The thickness of the mantle is steadily growing, because all the freed dust particles remain on the surface. Being porous, the mantle is a good insulator. A steep temperature gradient forms between the ice and the dust mantle. Generally speaking, dust mantle properties and evolution are strongly dependent on the modeling assumptions and on the way the mantle is formed.

When the formation of a mantle on a model nucleus is not forced, i.e. dust entrainment by gas is permitted, the mantle development depends on the dust particle size distribution, on the solar input, on the spin period, and on dust and surface properties, such as sticking coefficients between particles that can inhibit ablation of a dust layer once it is formed. Following the criterion of critical dust particle radius (see Section 3.5), a mantle forms

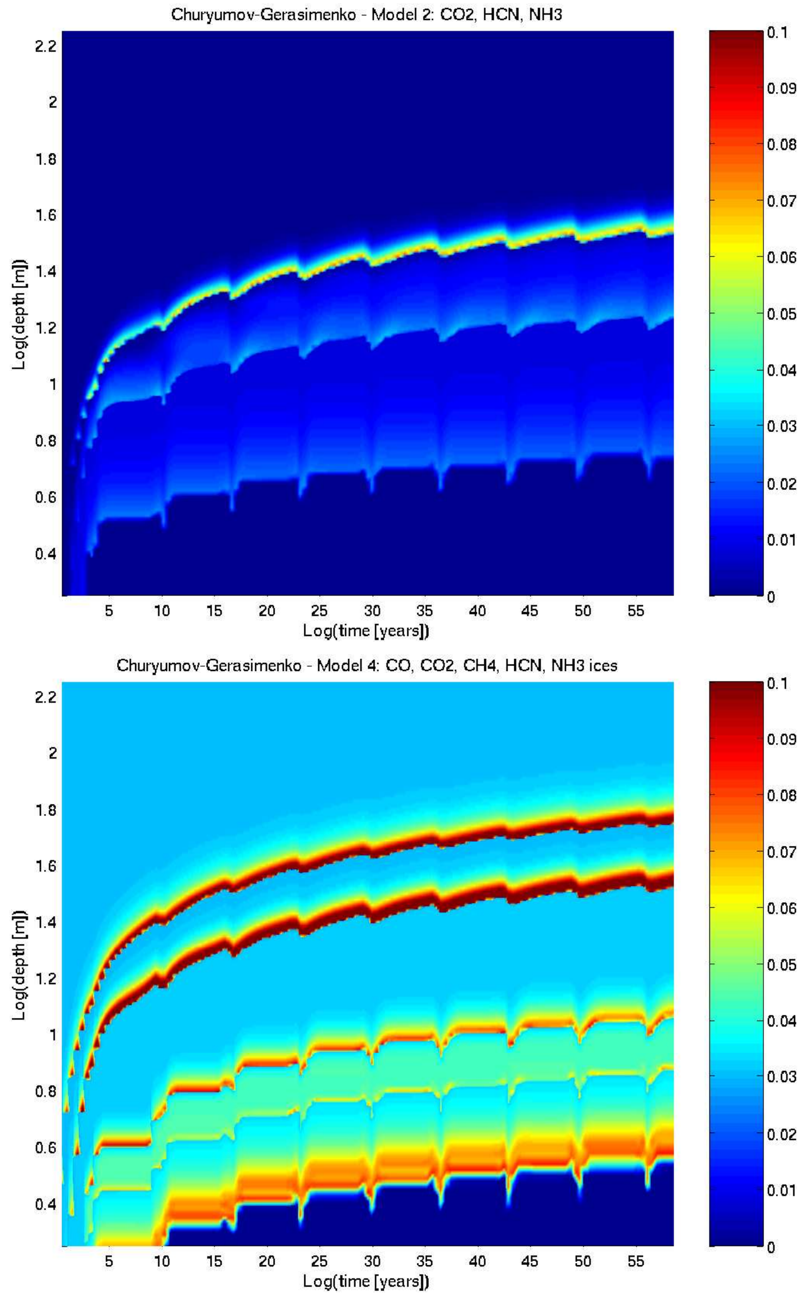

Figure 11.4: Evolution of volatile mass fractions within a comet nucleus model in the orbit of 67P/Churyumov-Gerasimenko through repeated revolutions around the Sun for different initial compositions: *upper panel* - amorphous water ice, occluded gases, and dust; *lower panel* - crystalline water ice mixed with other ices, and dust.

when ice is sublimating but the gas flux is not strong enough to entrain all the dust particles that are freed. Among the conditions favouring the formation process, we can list particle size (large particles are more difficult to remove), spin period (a slowly spinning nucleus enhances dust mantle formation), surface roughness, and solar input.

Once the dust mantle has formed, its thickness and stability depend on the orbit, on the cometocentric latitude, and on the spin period, that is on the temperature reached by the surface layer and on how long a high temperature lasts. It should be noted that mantle formation is usually favoured at high cometocentric latitudes (if the spin axis is approximately normal to the orbit plane), and is more difficult close to the equator. In some cases, a thick mantle may form, becoming thicker with every orbit because the gas flux is not able to destroy the mantle and entrain the particles on the surface. On the other hand, if the gas flux (e.g. at perihelion) is strong enough to entrain all the dust particles, the mantle may be destroyed shortly after its formation: in this case we can have a cyclic mantle, accreting on the way to and from aphelion and disappearing near perihelion. It is generally assumed that the mantle layer is porous, so the flow of gases through it is allowed, but this flux is quenched even for a thin layer of dust.

The dust mantle can reach temperatures much higher than an ice layer: at 1 AU heliocentric distance, temperatures between 350 K and 380 K, depending on the physical characteristics attributed to the dust particles, can be attained. This is in agreement with the high temperatures measured on the surface of Comet 1P/Halley during the Vega-1 flyby (Emerich et al., 1987). Once a dust layer is formed, it acts as a powerful insulator: even a thin layer has typically a very low thermal conductivity (Grün et al., 1993). In Figs. 10.6 and 10.7 the surface temperature profiles of a nucleus with and without a dust mantle are shown; note the strong temperature difference between the surface and the non-devolatilized layers close to the surface.

— 12 —

Conclusions

> "...Moreover, it seems reasonable that by this rarefaction the vapour - continually dilated – is finally diffused and scattered throughout the whole heavens, and then is by degrees attracted toward the planets by its gravity and mixed with their atmospheres. For just as the seas are absolutely necessary for the constitution of this Earth, so that vapours may be abundantly enough aroused from them by the heat of the Sun, which vapours either – being gathered into clouds – fall in rains and irrigate and nourish the whole earth for the propagation of vegetables, or – being condensed in the cold peaks of mountains (as some philosophize with good reason) – run down into springs and rivers; so for the conservation of the seas and fluids on the planets, comets seem to be required, so that from the condensation of their exhalations and vapours, there can be a continual supply and renewal of whatever liquid is consumed by vegetation and putrefaction and converted into dry earth. ... Further, I suspect that the spirit which is the smallest but most subtle and most excellent part of our air, and which is required for the life of all things, comes chiefly from comets."
>
> Isaac Newton, *Principia*, Book 3, Proposition 41, 1687 [1]

The general conclusion that emerges from simulations of the evolution of comet nuclei is that a nucleus model of porous, grainy material, possibly made of gas-laden amorphous ice and dust, is capable of reproducing activity patterns of comets. This is quite remarkable, keeping in mind the complexity of the processes that may take place within them, the uncertainties involved, and the fact that we still have very little direct information regarding the nature of cometary materials.

[1]Translation from I.B. Cohen and A. Whitman, *Isaac Newton - The Principia*, University of California Press, Berkeley, 1999.

12.1 Numerical Algorithms

One of our most important conclusions concerns the numerical procedures that must be followed when modeling heat and gas diffusion in porous, icy materials exposed to and warmed by solar radiation. This is particularly true when the temperature gradient into the surface of a spinning body is very steep because of volatile ices below the surface. The amount of heat flowing into the interior is critical for the amount and speed of sublimation of the volatile ices. When the temperature gradient is calculated from temperature differences on a fine spatial grid, it is important that the temperature values at the grid points have numerically converged. (Numerical convergence should not be confused with a physical steady state.) This depends on the grid spacing, the time step (since the object is spinning), and the coupling algorithm between the time step and the spatial grid (see Section 6.1).

Thus, one of the most important conclusions of our study of heat and gas diffusion in comet nuclei is:

- Steep temperature gradients normal to the surface into a spinning nucleus require careful selection of time steps, spatial grid, and special procedures for coupling these independent variables to guarantee convergence of dependent variables, such as the temperature (see Chapter 7).

- The flux of extremely volatile ices, such as CO, needs further investigation (e.g. see Chapter 7). Problems with the CO flux may be related to the steep temperature gradient at the surface of the nucleus. The large difference between the sublimation temperatures of H_2O and CO can cause steep temperature gradients.

12.2 Goals of Comet Nucleus Modeling

The purpose of modeling comet nuclei is not to predict their behaviour based on an initial set of parameters. Given the large number of parameters and their wide range of possible values, predictions may be misleading, as we have shown in Chapter 10. The purpose of modeling is to reproduce the observed behaviour, and thereby derive internal properties and processes characteristic of comet nuclei that are inaccessible to observations. In this respect, the fact that comet nuclei – unlike the models used to explain them – are nonspherical (e.g. 1P/Halley, 19P/Borrelly) should not change the basic conclusions; thus, stratification patterns, both in structure and in composition, will not be described by simple concentric spherical surfaces, but rather by far more irregular surfaces, defined by isotherms (since the internal processes are essentially thermal), which in turn will be determined by the real shape of the nucleus and its spin properties.

12.2.1 Derivation of Internal Properties

The manner in which internal properties are derived is basically by a "trial and error" procedure, which involves a great deal of art and assiduity. For a particular comet, given orbital parameters and size, a full set of structural and compositional parameters is assumed and evolution calculations are carried out. These yield results that can be compared with observations of that comet, such as production rates for various volatile gases, dust release rates, surface temperatures, etc. More often than not, the agreement on the first trial will be poor. Usually, discrepancies can be attributed to one or more of the initial set of parameters. Changing the values of these parameters usually improves the agreement between computation results and observations. However, a series of such adjustments is usually necessary in order to achieve acceptable agreement and sometimes tens of different parameter combinations are required. An example of this procedure may be found in modeling 2060 Chiron (Prialnik et al., 1995). Even then, the combination of parameters that reproduces the observed characteristics may not be unique. However, given the high sensitivity of models to these parameters, the plausibility that they represent reality is high.

As an illustrative example, from the models of Comet Hale-Bopp (C/1995 O1) (see Chapter 10) we have learned that the nucleus is probably bare, that is not covered by a dust mantle, and therefore the dust particles must be small (or the dust particle size distribution be steep). The processed outer layer cannot be thick. Fluxes of CO and CO_2 may not emanate only from the respective ices, but from H_2O ice, either in the interior or just below the surface during crystallization of amorphous H_2O ice (if amorphous water ice exists in comets). However, CO and CO_2 ice may occur beneath the crystallization front. Gases released from the ice flow through the porous matrix both outward and inward, since the temperature as well as the gas density peak at the front. Gases that flow inward are bound to reach very cold regions, and hence refreeze; while CO_2 freezes very close below the crystallization front, CO freezes somewhat deeper. This leads to different production curves for different gas species, which are now differentiated. Although we should keep in mind that the behaviour should be history dependent, we can state with confidence that the abundance ratio of ejected volatiles does not represent the nucleus abundances (Huebner and Benkhoff, 1999).

The closer a simulation is to observed reality, the more reliable are our inferences on the elusive nature of comet nuclei and on the clues they hold to the understanding of the Solar System's beginnings.

12.2.2 Identification of Internal Processes

The behaviour of comet nuclei, with its wealth of manifestations, sometimes erratic and unexpected, can be explained in many different ways. For comet outbursts, for example, a number of very different mechanisms have been proposed, including collisions, association with solar flares, chemical reactions, crystallization of amorphous ice, internal strains and stresses. However, even if a mechanism is successful in one case (for a particular outburst of a particular comet), it may fail in other cases. In principle, it is possible that each outburst has its own mechanism, but this is highly improbable. Thus, another goal of comet nucleus modeling is to identify processes that can account for a large variety of behaviour patterns. In the case of outbursts, for example, such a mechanism can be suggested (for more details, see Chapter 10).

Crystallization of amorphous ice has been recognized as a possible mechanism for explaining distant bursts of activity that comets often display (see Section 10.3).

Numerical models of the evolution of cometary nuclei (e.g. Prialnik and Bar-Nun, 1987, 1990, 1992; Espinasse et al., 1991; Tancredi et al., 1994), found that crystallization progresses in spurts, their onset, duration and extent in depth being largely determined by the structure, composition, and thermal properties of the nucleus, and by the comet's orbit. The release of gas trapped in the amorphous ice provided the link between crystallization and the eruptive manifestations of comets. The mechanism proved successful for explaining different types of outbursts. One should keep in mind, however, that as numerical simulations are based on many simplifying assumptions, and often adopt parameters that are not well known, they should not be expected to accurately reproduce any particular observed outburst. Rather, such simulations should account for the basic characteristics of the observed outbursts and in this respect they have been quite successful. It must also be kept in mind that amorphous ice has not been identified in the interstellar medium, nor do we have direct evidence of its existence in comet nuclei.

12.3 General Characteristics of Comet Nuclei

General characteristics that may be expected of comets on the basis of evolution models are summarized as follows:

- *Loss of ices of extremely volatile species:* Calculations of the long-term evolution of comets far from the Sun, under the influence of radioactive heating, show that the internal temperatures attained may be quite high, at least several tens of Kelvin. As a result, comets may have lost some volatiles that sublimate below about 40-50 K. Detection of such volatiles in comets suggests that they were trapped in amorphous H_2O ice undergoing crystallization, or that radioactive heating was ineffective or did not occur.

- *Amorphous water ice:* There is no direct evidence that amorphous water ice exists in comet nuclei, nor has it been observed in the interstellar medium or in molecular clouds. On the other hand, there are many observations of the ices of H_2O, CO (e.g. Thi et al., 2002; Pontoppidan et al., 2003a, 2005; Spoon et al., 2003), CO_2, CH_3OH (e.g. Taban et al., 2003; Pontoppidan et al., 2003b, 2005), NH_3, and CH_4 in star-forming regions. Boogert and Ehrenfreund (2004) compiled and updated a list of detected interstellar ice absorption features as a function of wavelength, λ, which can be found at: www.astro.caltech.edu/ acab/icefeatures.html.

- *Stratified composition and inhomogeneous structure:* While the inner part may have been altered by early evolution, the outer layers are altered by exposure to cosmic radiation in the Oort cloud and in the Kuiper belt and by recent activity in the inner Solar System. Thus, the internal composition of comet nuclei is stratified, with increasingly volatile species at increasingly greater depths. Similarly, the internal structure of comets is very likely not uniform: density, porosity, H_2O ice phases, and strength vary with depth. Increased porosity arises from volatile depletion, decreased porosity from recondensation. Weak regions may form where sharp density changes occur.

- *Lack of correlation between abundances in the coma and in the nucleus:* As a result of the inhomogeneous structure that develops with thermal evolution, gas production rates at any given time should not be taken to reflect the composition (abundances of ices) of the nucleus (Huebner and Benkhoff, 1999).

12.4 General Behaviour Patterns

Three types of comet activity, all associated with the flow of volatiles through and out of a porous nucleus, can be identified. They have observable outward manifestations on the one hand, and lasting effects on the structure of the nucleus on the other.

- Sublimation of volatiles from the pore walls and the subsequent flow of vapour is the source of gas for the coma and tails, but may also lead to the formation of an icy crust of enhanced strength below the surface of the nucleus. Gases flowing to the interior may refreeze when reaching sufficiently cold regions, at depths correlated with the volatility of the gas. The resulting effects are a compositionally stratified nucleus.
- Crystallization of amorphous ice, accompanied by the release of heat as well as trapped gases, may account for comet outbursts and may also result in fracture of the porous material.
- Entrainment of dust particles by escaping gas leads to the observable dust coma and tail. The largest particles may accumulate on the surface of the nucleus and lead to the formation of a gas-quenching dust mantle that might turn a comet into an asteroid-like object.

In conclusion, the thermal evolution and activity patterns of porous comet nuclei differ from the old view of solid icy bodies that are controlled by sublimation from the surface in response to solar heating. The structure that emerges is shown schematically in Fig. 12.1.

The thermal evolution of comet nuclei may be divided into two phases: a long phase – of the order of the Solar System's age – spent at large distances from the Sun (in the Oort cloud or the Kuiper belt) , and a second, much shorter phase, spent in orbits around the Sun within the planetary system. There is also an intermediate, transient phase during which a comet nucleus is gradually perturbed into its final orbit. Much of the fascination and interest comets arouse is due to the clues they hold as to the formation of the Solar System and the possible origins of life.

12.5 Input Data Required from Observations and Experiments

The success of the thermal evolution theory described in this text in explaining the structure and activity of comet nuclei is hindered by the lack of information regarding critical parameters. As a result, explanations about observed behaviour may be ambiguous; that is, different parameter combinations – within the same model – may lead to similar results, or some observed behaviours may remain inexplicable with parameters deemed to be reasonable. Consequently, additional input is required both from laboratory studies and from observations. The input required from laboratory studies includes:

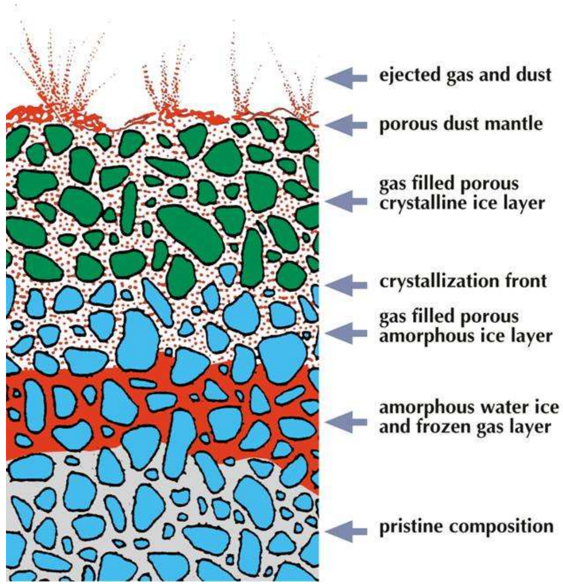

Figure 12.1: Schematic layered structure of a cometary nucleus.

- Vapour pressure measurements of ices at low temperatures.
- Measurements of changes in enthalpy of sublimation and phase change.
- Thermal conductivity of mixtures and in particular of amorphous ice (Huebner and Altwegg, 2005).
- Sublimation studies of mixtures.
- Measurements of the strengh of porous ice or ice and dust mixtures.

From observations, we need more information on dynamical properties: spin axis orientations, spin periods, and shapes of nuclei. It would be interesting to determine and understand whether an ellipsoid (as is suspected), rather than spherical shape, is typical of small bodies of negligible self-gravity. Upcoming in-situ measurements should provide information about the porous structure – porosity and pore size – as well as material strength.

In order to constrain the parameters used in comet nucleus models, it becomes necessary to carry out well defined laboratory experiments. A physical process that is thought to play a key role in the thermal evolution of comet nuclei is the trapping of volatiles in a matrix of amorphous water ice. This problem has already been considered by several working groups (Allamandola et al., Blake et al., Bar-Nun et al., Kouchi et al., Schmitt et al.). Up to now no general agreement exists on the conductive properties, the amount of trapped gas, on the outgassing process during the warming up of the sample, or on the possibility of clathrate hydrates forming when the amorphous ice reorganizes. In particular, no systematic study in the context of applications to comet models has yet been completed. It would be particularly important to study trapping of molecules that have been identified in comets, such as CH_3OH, CH_4, CO, CO_2, HCN, C_2H_2, C_2H_6, and C_3H_4. The type of experiment that should be carried out in a systematic manner could be as follows:

- Of very high priority is a new and independent measurement of the thermal conductivity of amorphous ice (see, e.g. Huebner and Altwegg, 2005).
- Rapidly co-deposit water vapour with one or more of the above mentioned gases at temperatures where water vapour condenses as an amorphous solid, i.e. between 10 K (a typical temperature of cold molecular clouds) and say 100 K (a temperature that may have occurred in certain regions of the presolar nebula).
- Check the structure of the deposit by an appropriate method (spectral signatures in the infrared, X-ray, or electron diffraction).
- Measure the enthalpy change during the warm-up, monitor the content of guest molecules in the *solid* phase by an appropriate method, for example by infrared spectroscopy, and verify the structure of the matrix.

Such experiments should be carried out for different concentrations of molecular gases. In this way it is possible to determine the change in enthalpy associated with the crystallization of the amorphous matrix. This change in enthalpy is a very important parameter in thermal models of comet nuclei. Furthermore, it is very important to gather more information about the loss of guest molecules as a function of temperature. In this context, it is also very important to determine the conditions under which gas molecules can be stored in clathrate hydrates. The formation of such compounds has been reported for low pressure conditions. Equally important is the detection and identification of amorphous ice in the interstellar medium, for example in interstellar clouds.

We have mentioned a rather long list of assumptions that are common to most theoretical studies to date. Some of these assumptions should be relaxed in future, more sophisticated models.

12.5.1 Recommended Advances for Numerical Modeling

- Use of adaptive grid methods for dealing with receding surfaces during perihelion passages.
- Development of full-scale 3-D models that allow for lateral flow of heat and gas.
- Inclusion of boundary conditions accounting for nucleus–coma exchange interactions.
- Implementation of modern methods for the simultaneous solution of a multiple component nucleus.
- Study of surface roughness and topography effects.

12.5.2 Physical Processes

- Coupling between gas phases and rigorous treatment of mixtures.
- Construction of models for stress - strain relationships and for fracture and crack propagation.
- Treatment of surface properties, such as roughness, topography, shadowing, heterogeneous physico-chemical and thermal properties, and radiative transfer in the outermost porous layer (e.g. Huebner and Markiewicz, 1993, 2000; Davidsson and Skorov, 2002a, b; Huebner, 2006).
- Modeling of the creation and evolution of the dust mantle on the nucleus surface.

12.5.3 Modeling the Evolution of Comet Nuclei

- Modeling comet formation including asteroid – comet transition objects by accretion.
- Long-term evolution over the age of the Solar System, considering potential gravitational interactions and orbital evolution.
- Improve modeling comet to asteroid transitions through evolution (e.g. Coradini et al., 1997a).
- Modeling nucleus shape evolution as a result of erosion and ablation.

Appendix A: Orbital Parameters and Sizes of Comet Nuclei

In the following tables we list orbital parameters [2] for short-period comets whose sizes have been determined from observations. The first, short table lists 5 comets for which the shape of the nucleus is well determined, and thus the axes lengths are known (L_a, L_b and L_c, given in km). About 100 comets are listed in the next table: estimates for the radius of the nucleus (in km) are based mainly on a recent data set provided by Tancredi et al. (2006), labelled R_{a}; additional radius estimate are listed, obtained by Meech et al. (2004), labelled R_{b}. Rotation periods are summarized and discussed in an extensive review by Samarasinha et al. (2004).

Comet	q (AU)	e	$L_a \times L_b \times L_c$	$\mathcal{A}$	P_{spin}
1P/Halley	0.58597811	0.96714291	15.5 ×8.5 ×8	0.04	68.2
9P/Tempel 1	1.50612525	0.51756748	5.04×6.14×4.8	0.05	41.0
10P/Tempel 2	1.42664936	0.53549253	16 × 8× 8	0.04	9.0
19P/Borrelly	1.35820317	0.62390848	8× 4× 4	0.03	25.0
81P/Wild 2	1.58489778	0.53975820	5.5× 4.0× 3.3	0.04	$\sim$ 12

[2] supplied by http://ssd.jpl.nasa.gov/dat/ELEMENTS.COMET

Comet	q (AU)	e	$R_{(a)}$ (km)	$R_{(b)}$ (km)	P_{spin} (hr)
2P/Encke	0.33541700	0.84859557	2.10		11.
4P/Faye	1.65749925	0.56814362	1.83		
6P/d'Arrest	1.65749925	0.56814362	1.66	1.52-1.70	6.67
7P/Pons-Winnecke	1.25726995	0.63412259	1.83		
14P/Wolf	2.40614959	0.40838829	1.91		
15P/Finlay	1.03408498	0.71055148	1.21		
16P/Brooks 2	1.83516105	0.49207985	1.59		
17P/Holmes	2.16512855	0.41272851	1.59		
21P/Giacobini-Zinner	1.03789477	0.70565515	1.00		9.5
22P/Kopff	1.58326283	0.54332250	1.83		12.3
24P/Schaumasse	1.20501004	0.70480036	0.91		
26P/Grigg-Skjellerup	0.99681861	0.66379625	1.21		
28P/Neujmin 1	1.55215690	0.77541331	9.58	10.83	12.67
29P/Schwassmann-Wachmann 1	5.72233300	0.04410215		15.4	14.0-32.3
30P/Reinmuth 1	1.87739414	0.50187000	1.00		
31P/Schwassmann-Wachmann 2	3.40889591	0.19386657	3.03		5.58
32P/Comas-Solá	1.83354932	0.56983541	2.52		
33P/Daniel	2.15738391	0.46333049	0.91		
36P/Whipple	3.08827962	0.25880575	2.10		
37P/Forbes	1.57240363	0.54139288	1.00		
40P/Väisälä 1	1.79597439	0.63291236	1.66		
41P/Tuttle-Giacobini-Kresák	1.04780498	0.66041820	0.69		
42P/Neujmin 3	2.01471456	0.58515624	0.69		
43P/Wolf-Harrington	1.58173143	0.54409635	2.10		
44P/Reinmuth 2	1.90345012	0.46603475	1.52		

Comet	q (AU)	e	$R_{(a)}$ (km)	$R_{(b)}$ (km)	P_{spin} (hr)
45P/Honda-Mrkos-Pajdusakova	0.52839781	0.82507079	0.33		
46P/Wirtanen	1.06170446	0.65725604	0.58		6.0
47P/Ashbrook-Jackson	2.30712043	0.39702587	2.64		> 44
48P/Johnson	2.30958336	0.36665416	2.19		29.0
49P/Arend-Rigaux	1.36859401	0.61164042	3.54	5.1	13.47
50P/Arend	1.91685288	0.53007409	0.96		
51P/Harrington	1.56831730	0.56220236	0.23		
52P/Harrington-Abell	1.75706533	0.54299945	1.10		
53P/Van Biesbroeck	2.41486785	0.55229060	3.32	3.33-3.37	
56P/Slaughter-Burnham	2.53496984	0.50367142	1.45	1.55	
58P/Jackson-Neujmin	1.38117347	0.66150673	0.60		
59P/Kearns-Kwee	2.33930581	0.47645561	1.00		
60P/Tsuchinshan 2	1.76637969	0.50713897	0.69		
61P/Shajn-Schaldach	2.33009391	0.39027755	0.83		> 18
63P/Wild 1	1.96086133	0.64982138	1.45		
64P/Swift-Gehrels	1.33901500	0.69443283	1.83		
65P/Gunn	2.44384420	0.31935915	4.59		
67P/Churyumov-Gerasimenko	1.28931109	0.63193560	2.10		12.3
68P/Kremola	1.75418716	0.64109193	2.52		
69P/Taylor	1.94782838	0.46598352	2.10		
70P/Kojima	2.00355008	0.45455070	1.26		> 22
71P/Clark	1.55538354	0.50130728	0.83	1.31	
74P/Smirnova-Chernykh	3.55298598	0.14854619	3.17		> 20
75P/Kohoutek	1.78465694	0.49630740	1.83		

Comet	q (AU)	e	$R_{(a)}$ (km)	$R_{(b)}$ (km)	P_{spin} (hr)
77P/Longmore	2.30955544	0.35818984	2.30		
78P/Gehrels 2	2.00867457	0.46226392	1.74		
79P/du Toit-Hartley	1.22997814	0.59410787	1.21		
82P/Gehrels 3	3.62616828	0.12387435	0.80		> 50
84P/Giclas	1.84573781	0.49329493	1.05		
86P/Wild 3	2.31028192	0.36447645	0.53	0.65-0.73	> 11
87P/Bus	2.18087829	0.37480091	0.53		> 25
88P/Howell	1.36725589	0.56124367	0.96		
89P/Russell 2	2.28984773	0.39779498	1.15		
90P/Gehrels 1	2.96591125	0.50913673	2.64		
91P/Russell 3	2.60192197	0.33066477	1.26		
92P/Sanguin	1.80804078	0.66308226	1.21	1.19	
94P/Russell 4	2.23119189	0.36445056	2.00		
97P/Metcalf-Brewington	2.61089722	0.45620917	1.45		
98P/Takamizawa	1.58522671	0.57524677	2.89		
99P/Kowal 1	4.71876340	0.22633678	4.80		
101P/Chernukh	2.35049100	0.59383868	2.19		
103P/Hartley 2	1.03718776	0.69956650	1.21		
104P/Kowal 2	1.39660195	0.58532519	1.45		
105P/Singer-Brewster	2.04130488	0.41097421	0.83		
106P/Schuster	1.54968456	0.58777572	0.83		
107P/Wilson-Harrington	0.99289408	0.62369170		1.92-1.96	6.10
108P/Ciffréo	1.71336017	0.54236246	0.83		
109P/Swift-Tuttle	0.95951616	0.96322576		13.73	67.2
110P/Hartley 3	2.47847172	0.31398179	2.00		10

Comet	q (AU)	e	$R_{(a)}$ (km)	$R_{(b)}$ (km)	P_{spin} (hr)
111P/Helin-Roman-Crokett	3.47757904	0.14048021	1.15		
112P/Urata-Niijima	1.45781503	0.58776040	0.76		
113P/Spitaler	2.12725266	0.42354904	1.15		
114P/Wiseman-Skiff	1.56946350	0.55644468	0.87		
115P/Maury	2.04137496	0.52079387		1.11	
116P/Wild 4	2.17054010	0.37567697	3.32		
117P/Helin-Roman-Alu 1	3.71399575	0.17332990	3.64		
118P/Shoemaker-Levy 4	2.00955266	0.42279028	1.91		
119P/Parker-Hartley	3.04443318	0.29049872	1.83		
120P/Mueller 1	2.74680763	0.33667688	0.83		
121P/Shoemaker-Holt 2	2.64844424	0.33878869	2.00		
123P/West-Hartley	2.12837050	0.44826919	2.00		
124P/Mrkos	1.46706280	0.54270322	1.74		
125P/Spacewatch	1.52845126	0.51159372	0.83		
129P/Shoemaker-Levy 3	2.80721831	0.24962164	1.66		
130P/McNaught-Hughes	2.10424203	0.40591321	1.59		
131P/Mueller 2	2.42406482	0.34222181	0.80		
134P/Kowal-Vávrová	2.57526168	0.58684094	1.45		
135P/Shoemaker-Levy 8	2.72110392	0.28956774	1.38		
137P/Shoemaker-Levy 2	1.86737635	0.57951640	2.76		
143P/Kowal-Mrkos	2.53947146	0.41037417	4.59		17.2
144P/Kushida	1.43112836	0.62882352	1.15		
152P/Helin-Lawrence 1	3.10561963	0.30717058	2.10		
154P/Brewington	1.59036887	0.67164174	1.66		

Appendix B: Thermodynamic Properties

B.1 Vapour Pressures and Changes in Enthalpy of Sublimation

It is important that the vapour pressure of sublimation and the corresponding change in enthalpy of sublimation are internally consistent. Fits for vapour pressures given below are of the standard form

$$\log P(T) = A + \frac{B}{T} + C \log T + DT \tag{B-1}$$

Consistency between vapour pressure and change in molar enthalpy for sublimation under *equilibrium* conditions is achieved through the use of the Clausius-Clapeyron equation

$$\Delta H_{\mathrm{s,e}}(T) = \frac{\mathcal{R}_{\mathrm{g}} T^2}{P(T)} \cdot \frac{dP(T)}{dT} \tag{B-2}$$

Here, $\mathcal{R}_{\mathrm{g}}$ is the universal gas constant. Using Eq. (B-1) in Eq. (B-2) gives

$$\Delta H_{\mathrm{s,e}}(T) = \left[-B \ln(10) + CT + D \ln(10) T^2\right] \mathcal{R}_{\mathrm{g}} \tag{B-3}$$

If $\mathcal{R}_{\mathrm{g}} = 8.314510$ J g-mol^{-1} K^{-1}, then the change in enthalpy for sublimation under equilibrium conditions is in J/g-mol. To convert the enthalpy to units of J kg^{-1}, it is necessary to divide by the $10^{-3}M$, where M is the gram-molecular weight.

The equilibrium enthalpy of sublimation includes the work $P\Delta V$ of the gas sublimating from the ice on its own vapour pressure. Ices from a comet sublimate into near vacuum. Thus, to obtain the change of enthalpy for sublimation into vacuum, it is necessary to subtract this energy. For an ideal gas this energy is $\mathcal{R}_{\mathrm{g}}T$. Thus the equation of sublimation into vacuum in units of J/kg is

$$\Delta H_{\mathrm{s}}(T) = \left[E + FT + GT^2\right] \frac{R_{\mathrm{o}}}{10^{-3}M} \tag{B-4}$$

where $E = -B \ln(10)$, $F = C - 1$, and $G = D \ln(10)$. Table 1 gives the constants A through G and the gram-molecular weights, M, for several ices for which reliable data are available to be fitted by Eq. (B-1) and that are of potential interest for comets. Except for water ice, the data for the fits come from the CRC Handbook of Chemistry and Physics (Lide, 2001). The constant A is adjusted to give the pressure in units of Pa. The temperature range of validity of the fits is also indicated.

Table B1. Constants for Vapour Pressures and Changes of Enthalpy for Sublimation into Vacuum

Molec	A	B	C	D	E	F	G	M	$T_{\min} - T_{\max}$
H_2O_{cr}	4.07023	-2484.986	3.56654	-0.00320981	5721.892	2.56654	-0.00739086	18.015	100-273.16
CO	53.2167	-795.104	-22.3452	0.0529476	1830.79	-23.3452	0.121916	28.0105	50-70
CO_2	49.2101	-2008.01	-16.4542	0.0194151	4623.61	-17.4542	0.0447049	44.0099	110-220
CH_4	26.6055	-708.756	-8.02377	0.0107439	1631.97	-9.02377	0.0247387	16.043	50-95
C_2H_2	-41.7289	-206.410	23.1873	-0.0262842	475.277	22.1873	-0.0605216	26.038	120-200
C_5H_{12}	14.9933	-1742.54	-1.40729	-0.00101225	4012.35	-2.40729	-0.00233079	72.152	166-256.6
HCN	240.713	-7395.48	-94.0317	0.0733612	17028.7	-95.0317	0.168920	27.026	190-260
NH_3	24.3037	-1766.28	-5.64472	0.00740241	4067.01	-6.64472	0.0170447	17.031	130-200
N_2	17.5901	-435.37	-3.88851	0.0063423	1002.5	-4.88851	0.014604	28.0134	37-63
C_2N_2	39.0771	-2313.54	-11.4553	0.0106139	5327.12	-12.4553	0.0244394	52.0356	146-218
NO	23.1144	-1134.73	-3.5911	-0.00997388	2612.81	-4.5911	-0.0229657	30.0061	70-110
N_2O	53.985	-2010.5	-18.18	0.0163	4629.3	-19.18	0.0375	44.0128	106.16-160.26
H_2S	6.96156	-903.815	0.258812	0.00873804	2081.11	-0.741188	0.0201201	34.08	120-190
Ne	-23.3389	15.0153	21.8046	-0.103136	-34.5740	20.8046	-0.237479	20.179	12.16-21.16
Ar	-9.4588	-259.379	10.581	-0.0353158	597.242	9.581	-0.0813176	39.948	45-85
Kr	122.595	-1858.73	-55.6008	0.112819	4279.88	-56.6008	0.259775	83.8	60-120
Xe	166.211	-3185.37	-71.4244	0.099896	7334.59	-72.4244	0.230256	131.3	100-160

Since water ice is an important constituent of comets, we give the data for the vapour pressure and change of enthalpy for sublimation into vacuum specifically. For crystalline water ice and $100 \leq T \leq 273$K

$$\log P_{\mathrm{c-H_2O}} = 4.07023 - \frac{2484.986}{T} + 3.56654 \log T - 0.00320981 \cdot T \quad \text{(B-5)}$$

where $P_{\mathrm{c-H_2O}}$ is in Pa. This vapour pressure in Eq. (B-5) is of highest quality over the widest temperature range (Gibbins, 1990) and is based on the work of Goff (1942) and Goff and Gratch (1946).

The corresponding change in molar enthalpy for sublimation in the range $100 \leq T \leq 273$K is

$$\Delta H_{\mathrm{c-H_2O}}(T) = (5721.892 + 3.56654 \cdot T - 0.00739086 \cdot T^2)\mathcal{R}_{\mathrm{g}} \quad \text{(B-6)}$$

where $\mathcal{R}_{\mathrm{g}} = 8.314510$ J g-mol^{-1} K^{-1} is the universal gas constant. The change in enthalpy for sublimation into vacuum in the temperature range $100 \leq T \leq 273$K is

$$\Delta H_{\mathrm{c-H_2O}}(T) = (5721.892 + 2.56654 \cdot T - 0.00739086 \cdot T^2)\mathcal{R}_{\mathrm{g}} \quad \text{(B-7)}$$

For amorphous water ice, fit parameters are not available in the standard form [Eqs. (B-1) and (B-3)]. The vapour pressure for amorphous water ice, with $P_{\mathrm{a-H_2O}}$ in Pa, is

$$\log P_{\mathrm{a-H_2O}} = 3.286 - \frac{2391}{T} + 4 \log T - 0.0005065 \cdot T^{1.4} \quad \text{(B-8)}$$

B.2 Specific Heat

Hexagonal Water Ice:

$$c_{\mathrm{c-H_2O}} = 7.5 \cdot T + 90 \qquad [\mathrm{Jkg^{-1}K^{-1}}] \quad \text{(B-9)}$$

Klinger (1980).

B.3 Thermal Conductivity

Crystalline Water Ice:

$$\kappa_{\mathrm{c-H_2O}} = 567/T \qquad [\mathrm{Wm^{-1}K^{-1}}] \quad \text{(B-10)}$$

as determined by Klinger (1980).

B.4 Phase Transitions

Amorphous to Crystalline Water Ice:
The phase transition from amorphous to crystalline water ice is highly exothermic, with a heat release during the transformation of 1620 J g-mol^{-1} (Ghormley, 1968). An activation law, determined experimentally by Schmitt et al. (1989), gives the crystallization time t_{cr} as a function of temperature

$$t_{\mathrm{cr}} = 9.54 \times 10^{-14} \cdot e^{5370/T} \qquad [\mathrm{s}] \tag{B-11}$$

The energy released by the phase transition from amorphous to crystalline ice, can be written as

$$Q_{\mathrm{tr}} = \frac{1620\ cdot N_{\mathrm{a-H_2O}}}{t_{\mathrm{cr}}} \qquad [\mathrm{Jm^{-3}s^{-1}}] \tag{B-12}$$

where $N_{\mathrm{a-H_2O}}$ is the number of g-moles of amorphous ice in the unit volume.

Glossary

Scientific terms used in research discussed and described in this book are defined as follows:

Adzumi equation: see Slip Flow.

Albedo: Ratio of outgoing solar radiation reflected by an object to the incoming solar radiation incident upon it.

Asteroid: Rocky, metallic, 100 m – 1000 km-sized objects, orbiting the Sun, mostly in the Asteroid Main Belt between the orbits of Mars and Jupiter; consist of pristine solar material; most likely bodies that never coalesced into planets.

Bulk Composition: Chemical composition of an object averaged over its whole volume.

Chemical Fractionation: see differentiation.

CHON Particle: Polycondensate of carbon, hydrogen, oxygen, nitrogen, and sulphur compounds.

Coma: Continually renewing and escaping atmosphere of gas and dust of a comet when it is close to the Sun.

Differentiation: Physico-chemical separation of materials in a body during sublimation (vapourisation), allowing chemically distinct zones (layers), e.g. a dust mantle.

Dust Mantle: Accumulation of dust and regolith on the surface of a comet nucleus.

Dust Particle: Aggregate of dust particles.

Dust Tail: Collection of micrometre and submicrometre-sized dust particles that are moved into a tail-like formation by solar radiation pressure.

Enstatite: $MgSiO_3$; rocky material belonging to the pyroxene group.

Ion Tail: See Plasma Tail.

Jet-like Feature: Collimated beam of gas or gas and dust in the coma.

Magnetite: Fe_3O_4; member of the spinel group.

Meteor: A meteoroid as it enters the atmosphere at speeds of 15 – 70 km/s.

Meteorite: Solid object striking a planet's surface, categorized as stony, iron, and stony-iron; mainly of asteroidal origin; a few from Mars or Moon.

Meteoroid: Interplanetary debris, from asteroids and comets.

Nucleus: Solar System body composed of ice and dust, the source of all cometary activity; formed in the outer Solar System beyond the asteroid belt.

Obliquity: Tilt of the spin axis from the perpendicular from the orbit plane.

Olivine: $(Mg, Fe)_2SiO_4$; rocky silicate mineral.
Phase Transition: Transition of matter from one state with specific physical and chemical properties to another, e.g. transition of a solid from an amorphous to a crystalline structure.
Planetesimal: 1 m to 100 km-sized body that is a building block of planets.
Plasma Tail: Collection of ions that are moved into a tail-like formation by interaction with the solar wind.
Porosity: Fraction of a material volume that consists of open spaces.
Pyroxene: $(Fe, Mg, Ca)SiO_3$; group of ferromagnesian silicates with a single chain of silicon-oxygen tetrahedral.
Refractory Material: Any chemical material that vapourises at higher temperatures; see Volatile Material.
Regolith: Layer of loose, pulverized debris (unconsolidated dust) created on the surface of an airless or nearly airless body by evaporation of ices or by meteoritic impacts.
Resonances: Gravitational relationship with a planet that forces the orbit of an asteroid or comet nucleus to change, usually toward larger eccentricity. Simple resonances have integer ratios, such 2:1 and 3:2, between the orbit of the asteroid or comet nucleus and the planet's orbit.
Reynolds Number: A measure of turbulence.
Slip Flow: Flow regime intermediate to Knudsen and Poiseuille flow.
Sodium Tail: Collection of neutral sodium atoms that are moved into a tail-like formation by solar radiation pressure.
Tail: See dust tail, plasma tail, sodium tail.
Tidal Stress: Differential gravitational force per unit area acting on a body by the Sun, a planet, or a moon.
Trail: Large cometary dust particles in comet orbit.
Volatile Material: Any chemical material that vapourises at relatively low temperatures (e.g. H_2O, CO_2, CO, CH_4, NH_3).

Bibliography

This list collects papers referenced in the text and papers on comet nucleus modeling published in the last fifty years. When a paper is cited in the text, the chapter and the section in which it is cited appear in brackets.

Bibliography

A'Hearn, M. F., Millis, R. L., Schleicher, D. G., Osip, D. J., Birch, P. V., The Ensemble Properties of Comets: Results from narrowband photometry of 85 comets, 1976-1992, *Icarus* **118**, 223, 1995. [1, 3.5, 8.2, 10.1]

Allamandola, L. J., Bernstein, M. P., Sandford, S. A., Walker, R. L., Evolution of interstellar ices, *Space Sci. Rev.*, **90**, 219, 1999. [8.2]

Anders, E., Ebihara, M., Solar system abundances of the elements, *Geochim. Cosmochim. Acta* **46**, 2363, 1982. [2.1]

Andersson, O., Suga, H., Thermal conductivity of the Ih and XI phases of ice, *Phys. Rev. B* **50**, 6583, 1994. [3.2, 4.5]

Arakawa, M., Higa, M., Leliwa-Kopystyński, J., Maeno, N., Impact cratering of granular mixture targets made of H_2O ice - CO_2 ice-pyrophylite, *Planet. Space Sci.* **48**, 1437, 2000.

Bailey, M. E., Chambers, J. E., Hahn, G., Origin of Sun-grazers: A frequent cometary end-state, *Astron. Astrophys.* **257**, 315, 1992. [8.5]

Bailey, M. E., Emel'Yanenko, V. V., Hahn, G., Harris, N. W., Hughes, K. A., Muinonen, K., Scotti, J. V. Orbital evolution of Comet 1995 O1 Hale-Bopp, *Mon. Not. Roy. Astron. Soc.* **281**, 916, 1996. [10.1]

Baratta, G. A., Castorina, A. C., Leto, G., Palumbo, M. E., Spinella, F., Strazzulla, G., Ion irradiation experiments relevant to the physics of comets, *Planet. Space Sci.* **42**, 759, 1994. [3.5]

Bar-Nun, A., Owen, T., Trapping of gases in water ice and consequences to comets and the atmospheres of the inner planets, in *Solar System Ices*, (eds. B. Schmitt, C. de Bergh, and M. Festou), Dordrecht, Kluwer Academic Publishers, 353, 1998. [2.4, 3.2, 4.5]

Bar-Nun, A., Herman, G., Laufer, D., Rappaport, M. L., Trapping and release of gases by water ice and implications for icy bodies, *Icarus* **63**, 317, 1985. [2.4, 3.2]

Bar-Nun, A., Prialnik, D., Laufer, D., Kochavi, E., Trapping of gases by amorphous water ice and implications for icy bodies, *BAAS* **18**, 813, 1986. [2.4]

Bar-Nun, A., Dror, J., Kochavi, E., Laufer, D., Amorphous water ice and its ability to trap gases, *Phys. Rev. B* **35**, 2427, 1987. [3.2]

Belton, M. J. S., Characterization of the rotation of cometary nuclei, in *Comets in the Post-Halley Era*, (eds. R. L. Newburn, Jr., M. Neugebauer, and J. Rahe), Kluwer Academic Publishers, p. 691, 1991. [9.5]

Benkhoff, J., Energy balance and the gas flux from the surface of comet 46P/Wirtanen, *Planet. Space Sci.* **47**, 735, 1999. [6.3]

Benkhoff, J., The emission of gas and dust from comets, *Adv. Space Res.* **29**, 1177, 2002. [10.4]

Benkhoff, J., Spohn, T., Thermal histories of the KOSI samples, *Geophys. Res. Lett.* **18**, 261, 1991a. [2.4, 10.4, 11.2]

Benkhoff, J., Spohn, T., Results of a coupled heat and mass transfer model applied to KOSI sublimation experiments, in *Theoretical Modeling of Comet Simulation Experiments*, (eds. N. I. Kömle, S. J. Bauer, and T. Spohn), Verlag der Österreichischen Akademie der Wissenschaften, p. 31, 1991b. [2.4]

Benkhoff, J., Huebner, W. F., Influence of the vapor flux on temperature, density, and abundance distributions in a multi-component, porous, icy body, *Icarus* **114**, 348, 1995. [2.4]

Benkhoff, J., Boice, D. C., Modeling the thermal properties and the gas flux from a porous, ice body in the orbit of P/Wirtanen, *Planet. Space Sci.* **44**, 665, 1996. [6.3, 10.2]

Benkhoff, J., Huebner, W. F., Modeling the gas flux from a Jupiter-family comet, *Planet. Space Sci.* **44**, 1005, 1996.

Benkhoff, J., Seidensticker, K. J., Seiferlin, K., Spohn, T., Energy analysis of porous water ice under space-simulated conditions: Results from the KOSI-8 experiment, *Planet. Space Sci.* **43**, 353, 1995. [2.4]

Bertaux, J.-L., Comet 46P/Wirtanen, *IAU Circ.* 6565, 2, 1997. [10.1]

Biermann, L., Huebner, W. F., Lüst, Rh., Aphelion clustering of 'new' comets: Star tracks through Oort's cloud, *Proc. Natl. Acad. Sci. USA* **80**, 5151, 1983. [8.2]

Binzel, R. P., Xu, S., Bus, S. J., Bowell, E., Small main-belt asteroid lightcurve survey, *Icarus* **99**, 225, 1992. [2.3]

Bird, M. K., Janardhan, P., Wilson, T. L., Huchtmeier, W. K., Gensheimer, P., Lemme, C., K-band radio observations of Comet Hale-Bopp: Detections of ammonia and (possibly) water, *Earth, Moon, Planets* **78**, 21, 1998.

Biver, N., Rauer, H., Despois, D., Moreno, R., Paubert, G., Bockelée-Morvan, D., Colom, P., Crovisier, J., Gérard, E., Jorda, L., Substantial outgassing of CO from Comet Hale-Bopp at large heliocentric distance, *Nature* **380**, 137, 1996. [10.3]

Biver, N., Bockelée-Morvan, D., Colom, P., Crovisier, J., Davies, J. K., Dent, W. R. F., Despois, D., Gérard, E., Lellouch, E., Rauer, H., Moreno, R., Paubert, G., Evolution of the outgassing of Comet Hale-Bopp (C/1995 O1) from radio observations, *Science* **275**, 1915, 1997. [2.1, 10.1]

Blake, D., Allamadola, L. J., Sandford, S., Hudgins, D., Freund, F., Clathrate hydrate formation in amorphous cometary ice analogs in vacuo, *Science* **245**, 58, 1991.

Bockelée-Morvan, D., Crovisier, J., Formaldehyde in comets. II - Excitation of the rotational lines, *Astron. Astrophys.* **264**, 282, 1992. [2.3]

Bockelée-Morvan, D., Rickman, H., C/1995 O1 (Hale-Bopp): Gas production curves and their interpretation, *Earth Moon Planets* **79**, 55, 1998. [4.5, 10.1]

Boehnhardt, H., Comet splitting - Observations and model scenarios, *Earth, Moon, Planets* **89**, 91, 2002. [3.6]

Boogert, A. C. A, Ehrenfreund, P., Interstellar ices. In *Astrophysics of Dust.* (eds. A. N. Witt, G. C. Clayton, and B. T. Draine), ASP Conference Series 309, p. 547, 2004. [12.3]

Bouziani, N., Fanale, F. P., Physical chemistry of a heterogeneous medium: Transport processes in comet nuclei, *Astrophys. J.* **499**, 463, 1998.

Brailsford, A., Major, K. G., The thermal conductivity of aggregates of several phases, including porous materials, *Brit. J. Appl. Phys.* **15**, 313, 1964.

Brin, G. D., Mendis, D. A., Dust release and mantle development in comets, *Astrophys. J.* **229**, 402, 1979. [3.5, 4.5]

Britt, D. T., The surface processes of Comet 19/P Borrelly, *Am. Astron. Soc.* **34**, 2703, 2002.

Brucato, J. R., Castorina, A. C., Palumbo, M. E., Strazzulla, G., Satorre, M. A., Ion irradiation and extended CO emission in cometary comae, *Planet. Space Sci.* **45**, 835, 1997.

Burns, J., Safronov, V., Asteroid nutation angles, *Mon. Not. Roy. Astron. Soc.* **165**, 403, 1973. [9.5]

Cameron, A. G. W., Schneck, P. B., Density of matter assembled from randomly incident particles, *Icarus* **4**, 396, 1965. [3.5]

Campins, H., Telesco, C. M., Osip, D. J., Rieke, G. H., Rieke, M. J., Schulz, B., The color temperature of (2060) Chiron: A warm and small nucleus, *Astron. J.* **108**, 2318, 1994. [10.3]

Capria, M. T., Capaccioni, F., Coradini, A., De Sanctis, M. C., Espinasse, S., Federico, C., Orosei, R., A P/Wirtanen evolution model, *Planet. Space Sci.* **44**, 987, 1996. [4.7, 10.1, 11.3]

Capria, M. T., Coradini, A., De Sanctis, M. C., Orosei, R., CO emission mechanisms in C/1995 O1 (Hale-Bopp), *Astron. Astrophys.* **357**, 359, 2000a. [10.1]

Capria, M. T., Coradini, A., De Sanctis, M. C., Orosei, R., Chiron activity and thermal evolution, *Astron. J.* **119**, 3112, 2000b. [10.3]

Capria, M. T., Coradini, A., De Sanctis, M. C., Blecka, M. I., P/Wirtanen thermal evolution: Effects due to the presence of an organic component in the refractory material, *Planet. Space Sci.* **49**, 907, 2001. [4.7, 10.1, 10.2, 11.3]

Capria, M. T., Coradini, A., De Sanctis, M. C., A model of the activity of Comet Wild 2, *Adv. Space Res.* **29**, 709, 2002. [10.3]

Capria, M. T., Coradini, A., De Sanctis, M. C., C1995 O1 Hale-Bopp: Short and long distance activity from a theoretical model, *Earth, Moon, Planet* **90**, 1, 2003. [10.1]

Carman, P. C., *Flow of Gases Through Porous Media*, Butterwoths Scientific Publications, London, 1956.

Carslaw, H. S., Jaeger, J. C. *Conduction of Heat in Solids*, Oxford University Press, 1986. [6.2]

Carusi, A., Kresak, L., Valsecchi, G. B. Perturbations by Jupiter of a chain of objects moving in the orbit of Comet Oterma, *Astron. Astrophys.* **99**, 262, 1981. [8.3]

Carusi, A., Kresák, L., Perozzi, E., Valsecchi, G. B., *Long Term Evolution of Short Period Comets*, Adam Hilger, Bristol, 1985. [8.2]

Carusi, A., Valsecchi, G., Dynamical evolution of short-period comets, in *Interplanetary Matter*, (eds. Z. Ceplecha and P. Pecina), 21, 1987. [1, 8.3]

Carusi, A., Valsecchi, G. B., Dynamics of comets, in *Chaos, Resonance, and Collective Dynamical Phenomena in the Solar System*, Proceedings of the 152nd Symposium of the IAU, (eds. S. Ferraz-Mello), Kluwer Academic Publishers, 255, 1992. [8.3]

Chen, J., Jewitt, D. C., On the rate at which comets split, *Icarus* **108**, 265, 1994. [9.5]

Cheng, P., Hsu, C.-T., The effective stagnant thermal conductivity of porous media with periodic structures, *J. Porous Media* **2**, 19, 1999. [4.9]

Chochol, D., Rušin, V., Kulčár, L., Vanýsek, V., Emission features in the solar corona after the perihelion passage of Comet 1979 XI, *Astrophys. Space Sci.* **91**, 71, 1983. [8.5]

Choi, Y.-J., Cohen, M., Merk, R., Prialnik, D., Long-term evolution of objects in the Kuiper belt zone - effects of insolation and radiogenic heating, *Icarus* **160**, 300, 2002. [6.4]

Chu, B., *Molecular Forces – Based on the Baker Lectures of Peter J. W. Debye*, Interscience Publishers, 1967. [3.5]

Clifton, R. J., Simonson, E. R., Jones, A. H., Green, S. J., Determination of the critical-stress-intensity factor K_{Ic} from internally pressurized thick-walled vessels, *Exper. Mech.* **16**, 233, 1976.

Cochran, A. L., Barker, E. S.,Ramseyer, T. F., Storrs, A. D., The McDonald

Observatory Faint Comet Survey - Gas production in 17 comets, *Icarus* **98**, 151, 1992. [10.3]

Cochran, A. L., Barker, E. S., McDonald Observatory spectral observations of Comet 19P/Borrelly, *Icarus* **141**, 307, 1999. [11.2]

Cohen, M., Prialnik, D., Podolak, M., A quasi-3D model for the evolution of shape and temperature distribution of comet nuclei - application to Comet 46P/Wirtanen, *New Astron.* **8**, 179, 2003. [6.3, 8.1, 9.3, 9.4]

Colangeli, L., Bussoletti, E., Cecchi-Pestellini, C., Fulle, M., Mennella, V., Palumbo, P., Rotundi, A., ISOCAM imaging of Comets 65P/Gunn and 46P/Wirtanen, *Icarus* **134**, 35, 1998. [10.1]

Colbeck, S. C., Theory of metamorphism of dry snow, *J. Geophys. Res.* **88**, 475, 1983. [2.4]

Colwell, J. E., Jakosky, B. M., Sandor, B. J., Stern, S. A., Evolution Of topography on comets. II – Icy craters and trenches, *Icarus* **85**, 205, 1990. [3.4]

Cook, R. F., Effective-medium theory for the fracture of fractal porous media, *Phys. Rev. B* **39**, 2811, 1989.

Coradini, A., Federico, C., Magni, G., Grain accretion processes in a protoplanetary nebula: Accretion times and mass limits, *Astrophys. Space Sci.* **48**, 79, 1977. [10.1]

Coradini, A., Federico, C. and Lanciano, P., Earth and Mars: Early Thermal Profiles, *Physics of the Earth and Planetary Interiors* **31**, 145, 1983. [8.2]

Coradini, A., Capaccioni, F., Capria, M. T., De Sanctis, M. C., Espinasse, S., Orosei, R., Salomone, M., Federico, C., Transition elements between comets and asteroids. I. Thermal evolution models, *Icarus* **129**, 317, 1997a. [4.7, 8.3, 9.5, 12.5]

Coradini, A., Capaccioni, F., Capria, M. T., De Sanctis, M. C., Espinasse, S., Orosei, R., Salomone, M., Federico, C., Transition elements between comets and asteroids. II. From the Kuiper belt to NEO orbits, *Icarus* **129**, 337, 1997b. [8.3, 9.5]

Cowan, J. J., A'Hearn, M. F., Vaporization of comet nuclei – Light curves and life times, *Moon Planets* **21**, 155, 1979. [5.1]

Crifo, J. F., Rodionov, A. V., The dependence of the circumnuclear coma structure on the properties of the nucleus. I. Comparison between homogeneous and inhomogeneous spherical nucleus with application to P/Wirtanen, *Icarus* **127**, 319, 1997.

Crovisier, J., Solids and volatiles in comets, in *Formation and Evolution of Solids in Space*, (eds. J. M. Greenberg and A. Li), Kluwer Academic Publishers, 389, 1999. [4.5]

Crovisier, J., Biver, N., Bockelée-Morvan, D., Colom, P., Jorda, L., Lelouch, E., Paubert, G., Despois, D., Carbon monoxide outgassing from Comet

Schwassmann-Wachmann 1, *Icarus* **115**, 213, 1995. [8.4, 10.3]

Davidsson, B. J. R., Tidal splitting and rotational breakup of solid spheres, *Icarus* **142**, 525, 1999.

Davidsson, B. J. R., Tidal splitting and rotational breakup of solid biaxial ellipsoids, *Icarus* **149**, 375, 2001.

Davidsson, B. J. R., Skorov, Y. V., On the light-absorbing surface layer of cometary nuclei: I. Radiative transfer, *Icarus* **156**, 223, 2002a. [12.5]

Davidsson, B. J. R., Skorov, Y. V., On the light-absorbing surface layer of cometary nuclei: II. Thermal modeling, *Icarus* **159**, 239, 2002b. [12.5]

Davis, D. R., Farinella, P., Collisional evolution of Edgeworth-Kuiper belt, *Icarus* **125**, 50, 1997. [8.2]

De Almeida, A. A., Huebner, W. F., Benkhoff, J., Boice, D. C., Singh, P. D., The three sources of gas in the comae of comets, *Rev. Mex. Astron. Astrof.* **4**, 110, 1996. [1]

Delsemme, A. H., Miller, D. C., Physico-chemical phenomena in comets - III. The continuum of comet Burnham (1960 II): The differentiation of a short period comet, *Planet. Space Sci.* **19**, 1229, 1971. [3.1, 3.4, 5.1]

De Sanctis, M. C., Capaccioni, F., Capria, M. T., Espinasse, S., Coradini, A., Orosei, R., Salomone M., Federico, C., Model of P/Wirtanen nucleus: Active zones versus non-active zones, *Planet. Space Sci.* **47**, 855, 1999. [4.7, 10.1]

De Sanctis, M. C., Capria, M. T., Coradini, A., Orosei, R., Thermal evolution of the Centaur object 5145 Pholus, *Astron. J.* **120**, 1571, 2000.

De Sanctis, M. C., Capria, M. T., Coradini, A., Thermal evolution and differentiation of Kuiper belt objects, *Astron. J.* **121**, 2792, 2001. [3, 4.2, 6.4, 8.2]

De Sanctis, M. C., Capria, M. T., Coradini, A., Models of P/Borrelly: Activity and dust mantle formation, *Adv. Space Res.* **31**, 2519, 2003.

Dickens, J. E, Irvine, W. M., Nummelin, A., Mllendal, H., Saito, S., Thorwirth, S., Hjalmarson, A., Ohishi, M., Searches for new interstellar molecules, including a tentative detection of aziridine and possible detection of propenal. Spectrochim, *Acta A, Mol. Biomol. Spectr.* **57**, 643, 2001. [2.1]

Domingue, D. L., Lockwood, G. W., Thompson, D. T., Surface textural properties of icy satellites: A comparison between Europa and Rhea, *Icarus* **115**, 228, 1995. [3.5]

Donn, B., The origin of icy cometary nuclei. *Icarus* **2**, 396, 1963.

Dullien, F. A. L., *Porous Media - Fluid Transport and Pore Structure*, Academic Press, New York, 1979.

Duncan, M. J., Levison, H. F., A scattered comet disk and the origin of Jupiter family comets, *Science* **276**, 1670, 1997. [8.2]

Eberhardt, P., Krankowsky, D., Schulte, W., Dolder, U., Lämmerzahl, P., Berthelier, J. J., Woweries, J., Stubbemann, U., Hodges, R. R., Hoffman, J. H., Illiano, J. M., The CO and N_2 Abundance in Comet P/Halley, *Astron. Astrophys.* **187**, 481, 1987.

Edgeworth, K. E., The evolution of our planetary system, *J. Brit. Astron. Assoc.* **53**, 181, 1943. [8.2]

Edgeworth, K. E., The origin and evolution of the solar system, *Mon. Not. Roy. Astron. Soc.* **109**, 600, 1949. [8.2]

Ehrenfreund, P., Boogert, A. C. A., Gerakines, P. A., Schutte, W. A., Thi, W. F., Tielens, A. G. G. M., Vanden Bussche, B., van Dishoeck, E. F., Whittet, D. C. B., Ices in star-forming regions: Highlights from ISO, laboratory and theory, in *First ISO Workshop on Analytical Spectroscopy*, (eds. A. M. Heras, K. Lech, N. R. Trams, and M. Perry), ESA SP-**419**, 3, 1997a. [2.1]

Ehrenfreund, P., d'Hendecourt, L., Dartois, E., Jourdain de Muizon, M., Breitfellner, M., Puget, J. L., Habing, J. H., *Icarus* **130**, 1, 1997b. [2.1]

Eluszkiewicz, J., Leliwa-Kopystyński, J., Kossacki, K. J., Metamorphism of solar system ices, in *Solar System Ices*, (eds. B. Schmitt, C. de Bergh, and M. Festou), Kluwer Academic Press, 119, 1998.

Emerich C., Lamarre, J. M., Moroz, V. I., Combes, M., Sanko, N. F., Nikolsky, Y. V., Rocard, F., Gispert, R., Coron, N., Bibring, J. P., Encrenaz, T., Crovisier, J., Temperature and size of the nucleus of Comet P/Halley deduced from IKS infrared VEGA-1 measurements, *Astron. Astrophys.* **187**, 839, 1987. [11.3]

Enzian, A., Cabot, H., Klinger, J., A 2 1/2 D thermodynamic model of cometary nuclei, *Astron. Astrophys.* **319**, 995, 1997. [6.3]

Enzian, A., Klinger, J., Schwehm, G., Weissman, P. R., Temperature and gas production distribution on the surface of a spherical model nucleus in the orbit of 46P/Wirtanen, *Icarus* **138**, 74, 1999. [6.3]

Espinasse, S., Klinger, J., Ritz, C., Schmitt, B., Modeling of the thermal behaviour and of the chemical differentiation of cometary nuclei, *Icarus* **92**, 350, 1991. [10.3, 12.2]

Espinasse, S., Coradini, A., Capria, M. T., Capaccioni, F., Orosei, R., Salomone, M., Federico, C., Thermal evolution and differentiation of a short-period comet, *Planet. Space Sci.* **41**, 409, 1992.

Everhart, E., Close encounters of comets and planets, *Astron. J.* **74**, 735, 1969. [8.3]

Fanale, F. P., Salvail, J. R., An idealized short-period comet model: Surface insolation, H_2O flux, dust flux and mantle evolution, *Icarus* **60**, 476, 1984. [4.4, 5.1, 7.3]

Fanale, F. P., Salvail, J. R., The loss and depth of CO_2 ice in comet nuclei, *Icarus* **72**, 535, 1987. [B.2]

Fanale, F. P., Salvail, J. R., The influence of CO ice on the activity and near-surface differentiation of comet nuclei, *Icarus* **84**, 403, 1990.

Fanale, F. P., Salvail, J. R., The cometary activity of Chiron: A stratigraphic model, *Icarus* **125**, 397, 1997. [10.3]

Farinella, P., Davis, D. R., Short-period comets: Primordial bodies or collisional fragments?, *Science* **273**, 938, 1996. [8.2]

Farinella, P., Froeschlé, C., Froeschlé, C., Gonczi, R., Hahn, G., Morbidelli, A., Valsecchi, G. B., Asteroids falling into the Sun, *Nature* **371**, 314, 1994a. [8.5]

Farinella, P., Froeschlé, C., Gonczi, R., Meteorite delivery and transport, in *Asteroids, Comets, Meteors* 93, (eds. A. Milani, M. Di Martino, and A. Cellino), Kluwer Academic Press, 205, 1994b. [8.5]

Farnham, T. L., Schleicher, D. G., Narrowband photometric results for Comet 46P/Wirtanen, *Astron. Astrophys.* **335**, L50, 1998. [10.1]

Fegley Jr., B., Chemical and physical processing of presolar materials in the solar nebula and the implications for preservation of presolar materials in comets, *Space Sci. Rev.* **90**, 239, 1999. [8.2]

Fernandez, J. A., On the existence of a comet belt beyond Neptune, *Mon. Not. Roy. Astron. Soc.* **192**, 481, 1980. [8.2]

Froeschlé, C., Klinger, J., Rickman, H., Thermal models for the nucleus of comet P/Schwassmann-Wachmann 1, in *Asteroids, Comets, Meteors* **83**, 215, 1983. [10.3]

Fulle, M., Evaluation of cometary dust parameters from numerical simulations - Comparison with an analytical approach and the role of anisotropic emissions, *Astron. Astrophys.* **217**, 283, 1989. [10.1]

Geiss, J., Composition in Halley's comet: Clues to origin and history of cometary matter, *Rev. Mod. Astron.* **1**, 1, 1988. [2.1]

Ghormley, J. A., Enthalpy change and heat-capacity changes in the transformations from high-surface-area amorphous ice to stable hexagonal ice, *J. Chem. Phys.* **48**, 503, 1968. [2.4, 3.2, 4.2, 5.4, B.2]

Gibbins, C. J., A survey and comparison of relationships for the determination of the saturation vapour pressure over plane surfaces of pure water and of pure ice, *Ann. Geophys.* **8**, 859, 1990. [3.1, 5.1, B.2]

Goff, J. A., Saturation pressure of ice from 32 to -280 F, *Trans. Am. Soc. Heat. Vent. Eng.* **48**, 299, 1942. [B.2]

Goff, J. A, Gratch, S., Low-pressure properties of water from -160 to 212 F, *Trans. Am. Soc. Heat. Vent. Eng.* **52**, 95, 1946. [B.2]

Gol'dyanskii, V. I., *Soviet. Phys. Dokl.* **22**, 417, 1977. [2.4]

Gombosi, T. I., *Gaskinetic Theory*, Cambridge Univ. Press, 1994. [3.3]

Greenberg, J. M., What are comets made of? A model based on interstellar dust, in *Comets*, (ed. L. L. Wilkening), University of Arizona Press, 131, 1982.

Greenberg, J. M., The chemical composition of comets and possible contribution to planet composition and evolution, in *The Galaxy and the Solar System*, (eds. R. Smoluchowski, J. N. Bahcall, and M. S. Matthews), University of Arizona Press, 103, 1986.

Greenberg, J. M., Making a comet nucleus, *Astron. Astrophys.* **330**, 375, 1998. [2.1, 2.2]

Greenberg, J. M., Mizutani, H., Yamamoto, T., A new derivation of the tensile strength of cometary nuclei: The fit to Comet Shoemaker-Levy 9, *Astron. Astrophys.* **295**, L35, 1995. [2.2]

Grün, E., Jessberger, E. K., Dust, in *Physics and Chemistry of Comets*, (ed. W. F. Huebner), Springer-Verlag, 113, 1990. [2.1]

Grün, E., Kochan, H., Roessler, K., Stöffler, D., Simulation of cometary nuclei, ESA SP- **278**, 501, 1987.

Grün E., Bar-Nun, A., Benkhoff, J., Bischoff, A., Düren, H., Hellmann, H., Hesselbarth, P., Hsiung, P., Keller, H. U., Klinger, J., Knölker, J., Kochan, H., Kohl, H., Kölzer, G., Krankowsky, D., Lämmerzahl, P., Mauersberger, K., Neukum, G., Oehler, A., Ratke, L., Roessler, K., Schwehm, G., Spohn, T., Stöffler, D., Thiel, K., Laboratory simulation of cometary processes: Results from first KOSI experiments, in *Comets in the Post-Halley Era* **1**, (eds. R. L. Newburn, Jr., M. Neugebauer, and J. Rahe), Kluwer Academic Publishers, 277, 1991a. [2.4]

Grün E., Benkhoff, J., Heidrich, R., Hesselbarth, P., Kohl, H., Kührt, E., Energy balance of the KOSI 4 experiment, *Geophys. Res. Lett.* **18**, 257, 1991b. [2.4]

Grün, E., Kochan, H., Seidensticker, K. J., Laboratory simulation, a tool for comet research, *Geophys. Res. Lett.* **18**, 245, 991c.

Grün, E., Gebhard, J., Bar-Nun, A., Benkhoff, J., Düren, H., Eich, G., Hische, R., Huebner, W. F., Keller, H. U., Klees, G., Kochan, H., Kölzer, G., Kroker, H., Kührt, E., Lämmerzahl, P., Lorenz E., Markiewicz, W. J., Möhlmann, D., Oehler, A., Scholz, J., Seidensticker, K. J., Rössler, K., Schwehm, G., Steiner G., Thiel, K., Thomas, H., Development of a dust mantle on the surface of an insolated ice-dust mixture: Results from the KOSI-9 experiment, *J. Geophys. Res.* **98**, 15091, 1993. [1, 2.4, 3.5, 10.1, 11.3]

Gutiérrez, P. J., Ortiz, J. L., Rodrigo, R., Lopez-Moreno, J. J., A Study of water production and temperature of rotating irregularly shaped cometary nuclei, *Astron. Astrophys.* **355**, 809, 2000. [3.4, 6.3]

Hahn, G., Bailey, M. E., Long-term evolution of 1991 DA: A dynamically evolved extinct Halley type, in *Asteroids, Comets, Meteors* 91, (eds. A.

Harris and E. Bowell), Lunar and Planetary Institute, 227, 1992. [8.5]

Handbook of Chemistry and Physics, CRC Press, 2004. [2.2]

Hapke, B., van Horn, H., Photometric studies of complex surfaces with applications to the Moon, *J. Geophys. Res.* **68**, 4545, 1963. [3.5]

Harmon, J. K., Campbell, D. B., Ostro, S. J., Nolan, M. C., Radar observations of comets, *Planet. Space Sci.* **47**, 1409, 1999. [4.5]

Harris, N. W., Bailey, M. E., Dynamical evolution of cometary asteroids, *Month. Not. Roy. Astron. Soc.* **297**, 1227, 1998. [2.3]

Haruyama, J., Yamamoto, T., Mizutani, H., Greenberg, J. M., Thermal history of comets during residence in the Oort cloud: Effect of radiogenic heating in combination with the very low thermal conductivity of amorphous ice, *J. Geophys. Res.* **98**, 15079, 1993. [2.2, 4.9, 8.2]

Herman, G., Podolak, M., Numerical simulation of comet nuclei. I. Water-ice comets, *Icarus* **61**, 252, 1985. [5.1, 10.3]

Herman, G., Weissman, P. R., Numerical simulation of cometary nuclei. III. Internal temperatures of cometary nuclei, *Icarus* **69**, 314, 1987. [5.1]

Horai, K., Susaki, J., The effect of pressure on the thermal conductivity of silicate rocks up to 12 kbar, *Phys. Earth Planet. Inter.* **55**, 292, 1989. [2.2]

Horai, K., Thermal Conductivity of Hawaiian basalt: A new interpretation of Robertson and Peck's data, *J. Geophys. Res.* **96**, 4125, 1991. [4.9]

Horanyi, M., Gombosi, T. I., Cravens, T. E., Korosmezey, A., Kecskemety, K., Nagy, A. F., Szego, K., The friable sponge model of a cometary nucleus, *Astrophys. J.* **278**, 449, 1984. [4.7]

Houpis, H. L. F., Ip, W.-H., Mendis, D. A., The chemical differentiation of the cometary nucleus: The process and its consequences, *Astrophys. J.* **295**, 654, 1985.

Hudson, R. L., Donn, B., An experimental study of the sublimation of water ice and the release of trapped gases, *Icarus* **94**, 326, 1991. [2.4, 3.2]

Huebner, W. F., Über die Gasproduktion der Kometen, *Z. Astrophys.* **63**, 22, 1965. [3.1, 5.1]

Huebner, W. F., Dust from cometary nuclei, *Astron. Astrophys.* **5**, 286, 1970. [4.7]

Huebner, W. F. First polymer in space identified in Comet Halley, *Science* **237**, 628, 1987. [2.4]

Huebner, W. F., Composition of comets: Observations and models, *Earth, Moon, Planets* **89**, 179. 2002. [2.1]

Huebner, W. F., A quantitative model for comet nucleus topography, *Adv. Space Sci. Res.* **31**, 2555, 2006. [3.4, 4.7, 12.5]

Huebner, W. F., Weigert, A., Eiskörner in der Koma von Kometen, *Z. Astrophys.*, **64**, 185, 1966. [5.1, 10.3]

Huebner, W. F., Boice, D. C., Polymers in comet comae. In *Solar System Plasma Physics: Geophysical Monograph* **54**, (eds.) J. H. Waite, Jr., J. L. Burch, and R. L. Moore. American Geophysical Union, Washington, DC, p.453, 1989. [2.4]

Huebner, W. F., Boice, D. C., On the 3-D time-dependent modeling of comet nucleus surface-layers, *Ann. Geophysicae - Atmospheres Hydrospheres and Space Sciences* **10**, 169, 1992. [6.3]

Huebner, W. F., Markiewicz, W. J., Sublimation in das Vacuum, in *8. Kometenwerkstatt*, (eds. K. Roessler and K. Thiel), Forschungszentrum Jülich GmbH report, 46, 1993. [3.4, 5.1, 12.5]

Huebner, W. F., Benkhoff, J., From coma abundances to nucleus composition, in *Proceedings of the ISSI Workshop: The Origin and Composition of Cometary Material*, (eds. K. Altwegg, P. Ehrenfreund, J. Geiss, and W. F. Huebner), *Space Sci. Rev.* **90**, 117, 1999. [1, 4.5, 10.1, 10.2, 12.2, 12.5]

Huebner, W. F., Markiewicz, W. J., The temperature and bulk flow speed of a gas effusing or evaporating from a surface into a void after reestablishment of collisional equilibrium. *Icarus*, **148**, 594, 2000. [3.4, 5.1, 12.5]

Huebner, W. F., Altwegg, K., Comets and their interstellar connections, ISSI Anniversary volume, in press, 2005. [12.5]

Huebner, W. F., Benkhoff, J., Capria, M. T., Coradini, A., De Sanctis, M. C., Enzian, A., Orosei, R., Prialnik, D., Results from the comet nucleus model team at the International Space Science Institute, Bern, Switzerland, *Adv. Space Res.* **23**, 1283, 1999. [7.1]

Huebner, W. F., Boice, D. C., Schwadron, N. A., Sungrazing comets as solar probes, *Adv. Space Sci. Res.*, submitted 2006. [8.5]

Ibadinov, K. I., Rahmonov, A. A., Bjasso, A. S., Laboratory simulation Of cometary structures, in *Comets in the Post-Halley Era*, **1**, (eds. R. L. Newburn, Jr., M. Neugebauer, and J. Rahe), Kluwer Academic Publishers, 299, 1991. [2.4]

Ip, W.-H., Fernandez, J. A., On dynamical scattering of Kuiper belt objects in 2:3 resonance with Neptune into short-period comets, *Astron. Astrophys.* **324**, 778, 1997. [8.2]

Irvine, W. M., Leschine, S. B., Schlörb, F. P. , Thermal history, chemical composition and relationship of comets to the origin of life, *Nature* **283**, 748, 1980.

Irvine, W. M., Kaifu, N., Ohishi, M., Chemical abundances in cold, dark interstellar clouds, *Icarus* **91**, 2, 1991.

Irvine, W. M., Dickens, J. E., Lovell, A. J., Schloerb, F. P., Senay, M., Bergin, E. A., Jewitt, D., Matthews, H. E., Chemistry in cometary comae, in *Chemistry and Physics of Molecules and Grains in Space, Faraday Discussions*, **109**, Faraday Div. Roy. Soc. Chem., 475, 1998. [2.1]

Irvine, W. M., Dickens, J. E., Lovell, A. J., Schloerb, F.P., Senay, M., Bergin, E. A., Jewitt, D., Matthews, H. E., The HNC/HCN ratio in comets, *Earth, Moon, Planets* **78**, 295, 1999 [2.1]

Jenniskens, P., Blake, D. F., Structural transitions in amorphous water ice and astrophysical implications, *Science* **265**, 753, 1994. [3.2]

Jenniskens, P., Blake, D. F., Kouchi, A., in *Solar System Ices*, (eds. B. Schmitt, C. de Bergh, and M. Festou), Kluwer Academic Publishers, Dordrecht, 1998. [3.2]

Jessberger, E. K., Kissel, J., Chemical properties of cometary dust and a note on carbon isotopes, in *Comets in the Post-Halley Era.*, (eds. R. L. Newburn, Jr., M. Neugebauer, and J. Rahe), Kluwer Academic Publishers, Vol. 2, p. 1075, 1991. [10.1]

Jewitt, D., Cometary rotation: An overview, *Earth, Moon, Planets* **79**, 35, 1997. [9.5]

Jewitt, D., Luu, J., Discovery of the candidate Kuiper belt object 1992 QB1, *Nature* **362**, 730, 1993. [8.2]

Jewitt, D., Senay, M., Matthews, H., Observations of carbon monoxide in Comet Hale-Bopp, *Science* **271**, 1110, 1996. [10.3]

Jockers, K., Bonev, T., Ivanova, V., Rauer, H., First images of a possible CO^+-tail of Comet P/Schwassmann-Wachmann 1 observed against the dust coma background, *Astron. Astrophys.* **260**, 455, 1992. [10.3]

Johnson, R. E., *Energetic Charged Particle Interactions with Atmospheres and Surfaces*, Springer-Verlag, 1990.

Johnson, R. E., Sputtering and desorption from icy surfaces, in *Solar System Ices*, (eds. B. Schmitt, C. de Bergh, and M. Festou), Kluwer, Netherlands, 30, 1998. [2.4]

Johnson, R. E., Carlson, R. W., Cooper, J. F., Paranicas, C., Moore, M. H., Wong, M., Radiation effects on the surfaces of the Galilean satellites, in *Jupiter: Planet, Satellites, and Magnetosphere*, (ed. F. Bagenal), Cambridge University Press, 2003. [2.4]

Jorda, L., Rickman, H., Comet P/Wirtanen, summary of observational data, *Planet. Space Sci.* **43**, 575, 1995. [8.4]

Julian, W. H., Samarasinha, N. H., Belton, M. J. S., Thermal structure of cometary active regions: Comet 1P/Halley, *Icarus* **144**, 160, 2000. [6.3]

Kajmakov, E. A., Sharkov, V. I., Laboratory simulation of icy cometary nuclei, in *The Motion, Evolution of Orbits, and Origin of Comets*, (eds. G. A. Chebotarev, E. I. Kazimirchak-Poanskaya, and B. G. Marsden), Reidel Publ. Comp., 304, 1972. [2.4]

Kaponen, A., Kataja, M., Timonen, J., Permeability and effective porosity of porous media, *Phys. Rev. E* **56**, 3319, 1997.

Keller, H. U., The nucleus, in *Physics and Chemistry of Comets*, (ed. W. F. Huebner), Springer-Verlag, p. 13, 1990. [1, 2.1]

Keller, H. U., Arpigny, C., Barbieri, C., Bonnet, R. M., Cazes, S., Coradini, M., Cosmovici, C. B., Delamere, W. A., Huebner, W. F., Hughes, D. W., Jamar, C., Malaise, D., Reitsema, H. J., Schmidt, H. U., Schmidt, W. K. H., Seige, P., Whipple, F. L., Wilhelm, K., First Halley multicolour camera imaging results from Giotto, *Nature* **321**, 320, 1986. [2.1, 2.3]

Keller, H. U., Delamere, W. A., Huebner, W. F., Reitsema, H. J., Schmidt, H. U., Whipple, F. L., Wilhelm, K., Curdt, W., Kramm, J., Rainer, T. N., Arpigny, C., Barbieri, C., Bonnet, R. M., Cazes, S., Coradini, M., Cosmovici, C. B., Hughes, D. W., Jamar, C., Malaise, D., Schmidt, K., Schmidt, W. K. H., Seige, P., Comet P/Halley's nucleus and its activity, *Astron. Astrophys.* **187**, 807, 1987. [2.1]

Kidger, M. R., Serra-Ricart, M., Bellot R., Luis R., Casas, R., Evolution of a spiral jet in the inner coma of Comet Hale-Bopp (1995 O1), *Astrophys. J. Lett.* **461**, L119, 1996. [10.3]

Kissel, J., 1999. [10.1]

Kittel, C., Kroemer, H., *Thermal Physics*, W. H. Freeman & Co., San Francisco, London, 1980. [3.4, 4.3].

Klinger, J., Low-temperature heat conduction in pure, monocrystalline ice, *J. Glaciol.* **14**, 517, 1975. [2.2]

Klinger, J., Influence of a phase transition of the heat on ice and mass balance of a comet, *Science* **209**, 271, 1980. [3.2, 4.5, 4.9, B.2]

Klinger, J., Some consequences of a phase transition of water ice on the heat balance of comet nuclei, *Icarus* **47**, 320, 1981. [4.9]

Klinger, J., Espinasse, S., Schmidt, B., Some considerations on cohesive forces in Sun-grazing comets, ESA SP- **12**, 197, 1989.

Klinger, J., Levasseur-Regourd, A. C., Bouziani, N., Enzian, A., Towards a model of cometary nuclei for engineering studies for future spacecraft missions to comets, *Planet. Space Sci.* **44**, 637, 1996. [10.2, 10.3]

Kochan, H. et al., Comet simulation experiments in the DFVLR space simulators, *Adv. Space Res.* **9**, 113, 1987.

Kochan, H., Rössler, K., Ratke, L., Heyl, M., Hellman, H., Schwehm, G., Crustal strength of different model comet materials, ESA SP- **302**, 115, 1989.

Kömle, N. I., Kargl, G., Thiel, K., Seiferlin, K., Thermal properties of cometary ices and sublimation residua including organics, *Planet. Space Sci.* **44**, 675, 1996. [2.4, 10.1]

Konno, I., Huebner, W. F., Modeling the dust size distribution in comets with dust fragmentation, in *Workshop on Observations of Recent Comets*, (eds. W. F. Huebner, P. A. Wehinger, J. Rahe, and I. Konno), 150, 1990. [4.7]

Konno, I., Huebner, W. F., Modeling dust fragmentation in comets, in *Origin and Evolution of Interplanetary Dust*, (eds. A. C. Levasseur-Regourd and H. Hasegawa), Kluwer Academic Publishers, 221, 1991. [4.7]

Konno, I., Huebner, W. F., Boice, D. C., A model of dust fragmentation in near-nucleus jet-like features on Comet Halley, *Icarus* **101**, 84, 1993. [4.7]

Kossacki, K. J., Szutowicz, S., Leliwa-Kopystyński, J., Comet 46P/Wirtanen: Evolution of the subsurface layer, *Icarus* **142**, 202, 1999.

Kossacki, K. J., Kömle, N. I., Kargl, G., Steiner, G., The influence of grain sintering on the thermoconductivity of porous ice, *Planet. Space Sci.* **42**, 383, 1994. [4.9]

Kouchi, A., Greenberg, J. M., Yamamoto, T., Mukai, T., Extremely low thermal conductivity of amorphous ice – relevance to comet evolution, *Astrophys. J.* **388**, L73, 1992. [3.2, 4.5]

Kouchi, A., Yamamoto, T., Kozasa, T., Kuroda, T., Greenberg, J. M., Conditions for condensation and preservation of amorphous ice and crystallinity of astrophysical ices, *Astron. Astrophys.* **290**, 1009, 1994. [2.2, 3.2, 8.2]

Krankowsky, D., Eberhardt, P., Evidence for the composition of ices in the nucleus of Comet Halley, in *Comet Halley 1986: World-Wide Investigations, Results, and Interpretations*, (eds. J. Mason and P. Moore), Ellis Horwood Ltd., p. 273, 1990. [2.1]

Kreutz, H., Untersuchungen über das System der Cometen 1843 I, 1880 I und 1882 II, *Publ. Sternwarte Kiel*, Nr. 6, p. 67, 1891. [8.5]

Kronk, G. W., *Cometography: A Catalogue of Comets*, **1**, Cambridge University Press, 1999. [1]

Kührt, E., Temperature profiles and thermal stresses in cometary nuclei, *Icarus* **60**, 512, 1984. [5.1]

Kührt, E., H_2O activity of Comet Hale-Bopp, in *Proceedings of the ISSI Workshop: The Origin and Composition of Cometary Material*, (eds. K. Altwegg, P. Ehrenfreund, J. Geiss, and W. F. Huebner), *Space Sci. Rev.* **90**, 75, 1999. [10.1]

Kührt, E., Keller, H. U., The formation of cometary surface crusts, *Icarus* **109**, 121, 1994. [3.5]

Kuiper, G. P., On the origin of the Solar System, in *Proceedings of a Topical Symposium, Commemorating the 50th Anniversary of the Yerkes Observatory and Half a Century of Progress in Astrophysics*, (ed. J. A. Hynek), McGraw-Hill, 357, 1951. [8.2]

Lamy, P. L., Toth, I., Fernández, Y. R., Weaver, H. A., The sizes, shapes, albedos, and colors of cometary nuclei, in *Comets II* (eds. M. C. Festou, H.

U. Keller, H. A. Weaver), University of Arizona Press, 223, 2004. [Ap.A]

Lamy, P. L., Toth, I., Jorda, L., Weaver, H. A., A'Hearn, M., The nucleus and inner coma of Comet 46P/Wirtanen, *Astron. Astrophys.* **335**, L25, 1998. [11.3]

Lamy, P. L., Toth, I., Weaver, H. A., Hubble Space Telescope observations of the nucleus and inner coma of Comet 19P/1904 Y2 (Borrelly), *Astron. Astrophys.* **337**, 945, 1998. [11.2]

Lanciano, P., Federico, C., Coradini, A., Primordial Thermal History of Growing Planetary Objects, *Lunar and Planetary Sci.* **XII**, 586, 1981. [8.2]

Lee, T., Papanastassiou, D., Wasserburg, G. J., Demonstration of ^{26}Mg excess in Allende and evidence for ^{26}Al, *Geophys. Res. Lett.* **3**, 109, 1976.

Levin, B. J. Gas evolution from the nucleus of a comet as related to the variations in its absolute brightness, *Comp. Rend. Acad. Sci. URSS* **38**, 72 (1943a); Ber. Akad. Wiss. USSR **38**, 82 (1943a) (Russian). [5.1]

Levin, B. J. Variation der Helligkeit der Kometen in Abhngigkeit von ihrer Sonnendistanz, (Russian) *Astron. Z.* **25**, 246 (1943b), (German) *Abh. Sowj. Astron.* **1**, 105 (1951). [5.1]

Levison, H. F., Duncan, M. J., The long-term dynamical behaviour of short-period comets, *Icarus* **108**, 18, 1987. [1]

Levison, H. F., Duncan, M. J., The long-term dynamical behaviour of short-period comets, *Icarus* **108**, 18, 1994. [8.5]

Lide, D. R., ed., *CRC Handbook of Chemistry and Physics*, Sect. 6, 82nd edition, CRC Press Inc., 2001. [B.2]

Loeb, L., *Kinetic Theory of Gases*, 2nd edition, Dover, 1980. [3.4]

Lovell, A. J., Schlörb, F. P., Bergin, E. A., Dickens, J. E., Devries, C. H., Senay, M. C., Irvine, W. M., HCO^+ in the coma of Comet Hale-Bopp, *Earth, Moon, Planets* **77**, 253, 1999. [2.1]

Lugmair, G. W., Shukolyukov, A., Early solar system events and timescales, *Meteor. Planet. Sci.* **36**, 1017, 2001.

Luré, A. I., McVean, D. B., Radok, J. R. M., *The Three-Dimensional Problems of the Theory of Elasticity*, Interscience, New York, 1964. [3.6]

Luu, J. L., Jewitt, D. C., High resolution surface brightness profiles of near-Earth asteroids, *Icarus* **97**, 276, 1992. [2.3]

Luu, J., Marsden, B. G., Jewitt, D., Trujillo, C. A., Hergenrother, C. W., Chen, J., Offutt, W. B., A new dynamical class in the trans-Neptunian solar system, *Nature* **387**, 573, 1997. [8.2]

MacPherson, G. J., Davis, A. M., Zinner, E. K., The distribution of aluminum-26 in the early solar system – a reappraisal, *Meteoritics* **30**, 365, 1995.

Mahoney, W. A., Ling, J. C., Wheaton, W. A., Jacobson, A. S., Heao, Discovery of ^{26}Al in the interstellar medium, *Astrophys. J.* **286**, 578, 1984.

Marcialis, R. L., Buratti, B. J., CCD photometry of 2060 Chiron in 1985 and 1991, *Icarus* **104**, 234, 1993. [10.3]

Marsden, B. G., Orbit Determination and Evolution of Comet C/1995 O1 (Hale-Bopp), *Earth, Moon, Planets* **79**, 3, 1999. [10.1]

Maxwell, J. C., *A Treatise on Electricity and Magnetism*, Clarendon Press, Oxford, 1873. [4.9]

McDonnell, J. A. M., Alexander, W. M., Burton, W. M., Bussoletti, E., Evans, G. C., Evans, S. T., Firth, J. G., Grard, R. J. L., Green, S. F., Grün, E., Hanner, M. S., Hughes, D. W., Igenbergs, E., Kissel, J., Kuczera, H., Lindblad, B. A., Langevin, Y., Mandeville, J.-C., Nappo, S., Pankiewicz, G. S. A., Perry, C. H., Schwehm, G. H., Sekanina, Z., Stevenson, T. J., Turner, R. F., Weishaupt, U., Wallis, M. K., Zarnecki, J. C., The dust distribution within the inner coma of Comet P/Halley 1982i: Encounter by Giotto's impact detectors, *Astron. Astrophys.* **187**, 719, 1987. [2.2]

McDonnell, J. A. M., Alexander, W. M., Burton, W. M., Bussoletti, E., Clark, D. H., Grard, R. J. L., Grün, E., Hanner, M. S., Sekanina, Z., Hughes, D. W., Igenbergs, E., Kuczera, H., Lindblad, B. A., Mandeville, J.-C., Minafra, A., Schwehm, G. H., Sekanina, Z., Wallis, M. K., Zarnecki, J. C., Chakaveh, S. C., Evans, G. C., Evans, S. T., Firth, J. G., Littler, A. N., Massonne, L., Olearczyk, R. E., Pankiewicz, G. S., Stevenson, T. J., Turner, R. F., Dust density and mass distribution near Comet Halley from Giotto observations, *Nature* **321**, 338, 1986. [10.1]

McDonnell, J. A. M., Lamy, P. L., Pankiewicz, G. S., Physical properties of cometary dust, in: *Comets in the post-Halley Era.* (eds. R. L. Newburn, Jr., M. Neugebauer, and J. Rahe), Kluwer Academic Publishers, Vol. 2, p. 1043, 1991. [10.1]

McFadden, L. A., Cochran, A. L., Barker, E. S., Cruikshank, D. P., Hartmann, W. K., The enigmatic object 2201 Oljato – is it an asteroid or an evolved comet? *J. Geophys. Res.* **98**, E2, 3031, 1993. [2.3]

McKay, C. P., Squyres, S. W., Reynolds, R. T., Methods for computing comet core temperatures, *Icarus* **66**, 625, 1985. [5.1]

Meech, K. J., Belton, M. J. S., Mueller, B. E. A., Dicksion, M. W., Li, H. R., Nucleus properties of P/Schwassmann-Wachmann 1, *Astron. J.* **106**, 1222, 1993. [9.5]

Meech, K. J., Hainaut, O. R., Marsden, B. G., Comet nucleus size distribution from HST and Keck telescopes, *Icarus* **170**, 463, 2004. [Ap.A]

Meier, R., Eberhardt, P., Krankowsky, D., Hodges, R. R., The extended formaldehyde source in comet P/Halley, *Astron. Astrophys.* **277**, 677,

1993. [2.4]

Mekler Y., Podolak, M., Formation of amorphous ice in the protoplanetary nebula, *Planet. Space Sci.* **42**, 865, 1994.

Mekler, Y., Prialnik, D., Podolak, M., Evaporation from a porous cometary nucleus, *Astrophys. J.* **356**, 682, 1990. [3.3, 4.3, 4.4, 4.6, 4.8, 10.7]

Mendis, D. A., Wickramasinghe, N. C., Composition of cometary dust: The case against silicates, *Astrophys. Space Sci.* **37**, L13, 1975. [4.2]

Mendis, D. A., Brin, G. D., Monochromatic brightness variations of comets. II – Core-mantle model, *Moon* **17**, 359, 1977.

Merk, R., Thermodynamics and accretion of asteroids, comets and Kuiper belt objects – a computer simulation study in planetary physics, Ph.D. Thesis, University of Muenster, 2003.

Merk, R., Breuer, D., Spohn, T., Numerical modeling of ^{26}Al- induced melting of asteroids considering accretion, *Icarus* **159**, 183, 2002.

Miller, H., *Landolt-Börnstein Tables, New Series* **5**, Springer-Verlag, 1982. [3.5, 3.6]

Millis, R. L., Schleicher, D. G., Rotational period of Comet Halley, *Nature* **324**, 646, 1986. [9.5]

Moore, M. H., Hudson, R. L., Gerakines, P. A., Mid and far infrared spectroscopic studies of the influence of temperature, ultraviolet photolysis and ion irradiation on cosmic type ices, *Spectrochim. Acta* **A57**, 841, 2001. [2.4]

Morbidelli, A., Chaotic diffusion and the origin of comets from the 2/3 resonance in the Kuiper Belt, *Icarus* bf 127, 1, 1997. [8.2]

Morbidelli, A., Origin of multi-kilometre near Earth asteroids: A new scenario, *Meteorite* **5**, 34, 1999. [8.2]

Moroz, L. V., Arnold, G., Korochantsev, A. V., Wäsch, R., Natural solid bitumens as possible analogs for cometary and asteroid organics: 1. Reflectance spectroscopy of pure bitumens, *Icarus* **134**, 253, 1998. [2.4]

Moroz, L. V., Schade, U., Wäsch, R., Reflectance spectra of olivine orthopyroxene bearing assemblages at decreased temperatures: Implications for remote sensing of asteroids, *Icarus* **147**, 79, 2000.

Moroz, L. V., Baratta, G., Distefano, E., Strazzulla, G., Starukhina, L. V., Dotto, E., Barucci, M. A., Ion Irradiation of asphaltite: optical effects and implications for trans-Neptunian objects and Centaurs, *Earth, Moon, Planets* **92**, 279, 2003. [2.4]

Moroz, L. V., Baratta, G., Strazzulla, G., Starukhina, L. V., Dotto, E., Barucci, M. A., Arnold, G., Distefano, E., Optical alteration of complex organics induced by ion irradiation: I. Laboratory experiments suggested unusual space weathering trend, *Icarus* **170**, 214, 2004. [2.4]

Moroz, L. V., Starukhina, L. V., Strazzulla, G., Baratta, G., Dotto, E., Barucci, M. A., Arnold, G., Optical alteration of complex organics induced by ion irradiation: II. Implications for primitive small bodies of solar system., *Icarus*, submitted, 2005. [2.4]

Morris, C. S., The lightcurve of periodic Comet Wirtanen, *Int. Comet Q.* **92**, 178, 1994.

Mueller, B. E. A., Ferrin, I., Change in the rotational period of Comet P/Tempel 2 between the 1988 and 1994 apparitions, *Icarus* **123**, 463, 1996. [9.5]

Mumma, M. J., Organic volatiles in comets: Their relation to interstellar ices and solar nebula material, in *From Stardust to Planetesimals*, Symposium 108th Annual meeting of the ASP held at Santa Clara, California, 1996, ASP Conference Series **122**, (ed. Y. J. Pendleton, A. G. G. M., p. 369, 1997 [10.1]

Nikolaeva, O., Tobelko, K., Korochantsev, A., Kreslavsky, M., Reference materials for organic matter of Meteorites and asteroids, *Ann. Geophys. Suppl.* **9**, 083, 1991. [2.4]

Notesco, G., Bar-Nun, A., Enrichment of CO over N_2 by their trapping in amorphous ice and implications to Comet P/Halley, *Icarus* **122**, 118, 1996. [2.4]

Oort, J. H., The structure of the cloud of comets surrounding the Solar System and a hypothesis concerning its origin, *Bull. Astron. Inst. Neth.* **11**, 91, 1950. [1, 8.2]

Öpik, E. J., *Meteor Flight in the Atmosphere*, Interscience, New York, 1958. [4.7]

Öpik, E. J., Photometry, dimensions, and ablation rates of comets, *Irish Astron. J.* **6**, 93, 1963. [2.3]

Orosei, R., Capaccioni, F., Capria, M. T., Coradini, A., Espinasse, S., Federico, C., Salomone, M., Schwehm, G. H., Gas and dust emission from a dusty porous comet, *Astron. Astrophys.* **301**, 613, 1995.

Orosei, R., Capaccioni, F., Capria, M. T., Coradini, A., De Sanctis, M. C., Federico, C., Salomone, M., Huot, J. P., Numerically improved thermochemical evolution models of comet nuclei, *Planet. Space Sci.* **47**, 839, 1999. [6.2, 6.5]

Parrott, J. E., Stukes, A. D., *Thermal Conductivity of Solids*, Pion Limited, 1975.

Patashnick, H., Rupprecht, G., Schuerman, D. W., Energy source for comet outbursts, *Nature* **250**, 313, 1974. [10.3]

Pironello, V., Brown, W. L., Lanzerotti, L. J., Marcantonio, K. J., Simmons, E. H., Formaldehyde formation in a H_2O/CO_2 ice mixture under irradiation by fast ions, *Astrophys. J.* **262**, 636, 1982. [2.4]

Podolak, M., Herman, G., Numerical simulations of comet nuclei. II. The

effect of the dust mantle, *Icarus* **61**, 267, 1985.
Podolak, M., Prialnik, D., Models of the structure and evolution of Comet P/Wirtanen, *Planet. Space Sci.* **44**, 655, 1996. [3.5, 4.7, 10.2]
Podolak, M., Prialnik, D., ^{26}Al and liquid water environments in comets, in *Comets and the Origin of Life*, (eds. P. Thomas, C. Chyba, and C. McKay), Springer-Verlag, 259, 1997.
Podolak, M., Prialnik, D., Conditions for the production of liquid water in comet nuclei, in *Bioastronomy '99: A New Era in Bioastronomy*, (eds. G. A. Lemarchand and K. J. Meech), Sheridan Books, 231, 2000.
Pontoppidan, K. M., Fraser, H. J., Dartois, E., Thi, W.-F., van Dishoeck, E. F., Boogert, A. C. A., d'Hendecourt, L., Tielens, A. G. G. M., Bisschop, S. E. A 3-5 m VLT spectroscopic survey of embedded young low mass stars. I. Structure of the CO ice, *Astron. Astrophys.* **408**, 981-1007, 2003a. [12.3]
Pontoppidan, K. M., Dartois, E., van Dishoeck, E. F., Thi, W.-F., d'Hendecourt, L. Detection of abundant solid methanol toward young low mass stars, *Astron. Astrophys.* **404**, L17, 2003b. [12.3]
Pontoppidan, K. M., Dartois,, E., Thi, W.-F., van Dishoeck, E. F. Processed and unprocessed ices in disks of low-mass YSOs, in *Formation of Cometary Materials, Highlights of Astronomy, Joint Discussion 14*, in press, 2005. [12.3]
Prialnik, D., Crystallization, sublimation, and gas release in the interior of a porous comet nucleus, *Astrophys. J.* **388**, 196, 1992. [4.2, 4.4, 4.6, 10.4]
Prialnik, D., A Model for the Distant Activity of Comet Hale-Bopp, *Astrophys. J. Lett.* **478**, L107, 1997. [10.1]
Prialnik, D., Modelling gas and dust release from Comet Hale-Bopp, *Earth, Moon, Planets* **77**, 223, 1999. [10.1, 10.3, 12.4]
Prialnik, D., Modeling the comet nucleus interior; application to Comet C/1995 O1 Hale-Bopp, *Earth, Moon, Planets* **89**, 27, 2002. [10.1, 10.3]
Prialnik, D., What makes comets active?, in *Proceedings IAU Symposium No. 229, 2005*, (eds. D. Lazzaro, S. Ferraz Mello, J. Fernandez), Cambridge University Press, 2006. [10.4]
Prialnik, D., Bar-Nun, A., On the evolution and activity of cometary nuclei, *Astrophys. J.* **313**, 893, 1987. [5.1, 10.3, 12.2]
Prialnik, D., Bar-Nun, A., The formation of a permanent dust mantle and its effect on cometary activity, *Icarus* **74**, 272, 1988. [3.5]
Prialnik, D., Bar-Nun, A., Gas release in comet nuclei, *Astrophys. J.* **363**, 274, 1990. [3.6, 10.1, 10.3, 12.2]
Prialnik, D., Mekler, Y., The formation of an ice crust below the dust mantle of a cometary nucleus, *Astrophys. J.* **366**, 318, 1991. [3.5]
Prialnik, D., Bar-Nun, A., Crystallization of amorphous ice as the cause of comet P/Halley's outburst at 14 AU, *Astron. Astrophys.* **258**, L9, 1992.

[10.3, 12.2]

Prialnik, D., Podolak, M., Radioactive heating of porous comet nuclei, *Icarus* **117**, 420, 1995. [3, 4.2, 5.3, 8.2, 10.2]

Prialnik, D., Bar-Nun, A., Podolak, M. Radiogenic heating of comets by ^{26}Al and implications for their time of formation, *Astrophys. J.* **319**, 993, 1987. [8.2]

Prialnik, D., Egozi, U., Bar-Nun, A., Podolak, M., Greenzweig, Y., On pore size and fracture in gas-laden comet nuclei, *Icarus* **106**, 499, 1993. [3.6, 4.8, 5.1, 5.3]

Prialnik, D., Brosch, N., Ianovici, D., Modelling the activity of 2060 Chiron, *Mon. Not. Roy. Astron. Soc.* **276**, 1148, 1995. [10.3, 12.2]

Prialnik, D., Benkhoff, J., Podolak, M., Modeling the structure and activity of comet nuclei, in *Comets II* (eds. M. C. Festou, H. U. Keller, and H. A. Weaver), University of Arizona Press, 359, 2004. [10.4]

Quinn, T., Tremaine, S., Duncan, M., Planetary perturbations and the origins of short-period comets, *Astrophys. J.* **355**, 667, 1990. [8.2, 8.3]

Rayleigh, Lord, On the influence of obstacles arranged in rectangular order upon the properties of a medium, *Philos. Magaz.*, **LVI**, 481, 1892. [4.9]

Reach, W. T., Sykes, M. V., Lien, D. J., Davies, J. K., The formation of Encke Meteoroids and dust trail, *Icarus* **148**, 80, 2000.

Remson, I., Hornberger, G. M., Molz, F. J., *Numerical Methods in Subsurface Hydrology*, Wiley-Interscience, 1971.

Rickman, H., The nucleus of Comet Halley: Surface structure, mean density, gas and dust production, *Adv. Space Res.* **9**, 59, 1989. [1]

Rickman, H., Cometary Nuclei, *Asteroids, Comets, Meteors: Proceedings of the 160th International Astronomical Union Symposium.* (eds. A. Milani, M. Di Martino, A. Cellino, Kluwer Academic Publishers, Dordrecht, p. 297, 1993. [3]

Rickman, H., Fernández, J. A., Gustafson, B., Formation of stable dust mantles on short-period comet nuclei, *Astron. Astrophys.* **237**, 524, 1990. [3.5, 4.7]

Rodgers, S. D., Charnley, S. B., HNC and HCN in comets, *Astrophys. J. Lett.* **501**, 227, 1998. [2.1]

Rodriguez, E., Ortiz, J., Lopez-Gonzalez, M., Rolland, A., Hobart, M., Sanchez-Blanco, E., Gutierrez, P., Short-term variability in Comet C/1995 O1 Hale-Bopp, *Astron. Ap.* **324**, L61, 1997. [9.5]

Ross, R. G., Kargel, J. S., Thermal conductivity of solar system ices with special reference to Martian polar caps, in *Solar System Ices*, (eds. B. Schmitt, C. de Bergh, and M. Festou), Kluwer Academic Press, 33, 1998.

Russel, H. W., Principles of heat flow in porous insulators, *J. Am. Ceram. Soc.* **18**, 1, 1935. [4.9, 7.2]

Sagdeev, R. Z., Elyasberg, P. E., Moroz, V. I., Is the nucleus of Comet Halley a low density body? *Nature* **331**, 240, 1988. [1]

Sandford, S. A., Allamandola, L. J., The condensation and vaporization behaviour of H2O:CO ices and implications for interstellar grains and cometary activity, *Icarus* **76**, 201, 1988. [2.4]

Samarasinha, N., Mueller, B., Spin axis direction of Comet 19P/Borrelly based on observations from 2000 and 2001, *Earth, Moon, Planets*, **90**, 473, 2002. [9.5]

Samarasinha, N., Mueller, B., Belton, M., Jorda, L., Rotation of Cometary Nuclei, in *Comets II* (eds. M. C. Festou, H. U. Keller, and H. A. Weaver), University of Arizona Press, 281, 2004. [Ap.A]

Saunders, R. S., Fanale, F. P., Timothy, J. P., Stephens, J. B., Sutton, S, Properties of filamentary sublimate residues from dispersions of clay in ice, *Icarus* **66**, 94, 1986. [2.4]

Scheidegger, A. E., *The Physics of Flow Through Porous Media*, University of Toronto Press, 1963. [4.6]

Schmitt, B., Espinasse, S., Grim, R. J. A., Greenberg, J. M., Klinger, J., Laboratory studies of cometary ice analogues, ESA SP- **302**, 65, 1989. [3.2, 4.2, 8.2, B.2]

Schmitt, B., Espinasse, S., Klinger, J., A possible mechanism for outbursts of comet P/Halley at large heliocentric distances, *Meteoritics* **26**, 392, 1991. [10.3]

Sears, D. W. G., Kochan, H., Huebner, W. F., Simulation experiments and surface processes on comet nuclei, *Meteor. Planet Sci.* **34**, 497, 1999. [1]

Seidensticker, K. J., Kochan, H., Gas dynamics of sublimating ice/dust samples, *BAAS* **24**, 1019, 1992. [2.4]

Seiferlin, K., Spohn, T., Benkhoff, J., Cometary ice texture and the thermal evolution of comets, *Adv. Space Res.* **15**, 35, 1995a.

Seiferlin, K., Spohn, T., Kömle, N., Kargl, G., Measurements of the thermal conductivity of porous H_2O ice, CO_2 ice and mineral powders under space conditions, *Ann. Geophys.* **13**, Suppl. III, Part III, C 791, 1995b. [2.4]

Seiferlin, K., Kömle, N. I., Kargl, G., Spohn, T., Line heat-source measurements of the thermal conductivity of porous H_2O ice, CO_2 ice and mineral powders under space conditions, *Planet. Space Sci.* **44**, 691, 1996. [2.4, 10.1]

Sekanina, Z., Fan-Shaped Coma, Orientation of rotation axis, and surface structure of a cometary nucleus. I – Test of a model on four comets, *Icarus* **37**, 420, 1979a. [9.4]

Sekanina, Z., Relative motions of fragments of the split comets. III. A test of splitting and comets with suspected multiple nuclei, *Icarus* **38**, 300, 1979b. [4.4]

Sekanina, Z., Rotation and precession of cometary nuclei, *Ann. Rev. Earth Planet. Sci.* **9**, 113, 1981. [9.5]

Sekanina, Z., The problem of split comets in review, in *Comets* University of Arizona Press, 251, 1982. [8.5]

Sekanina, Z., Disappearance and disintegration of comets, *Icarus* **58**, 81, 1984. [8.5]

Sekanina, Z., The problem of split comets revisited, *Astron. Astrophys.* **318**, L5, 1997. [3.6]

Sekanina, Z., Larson, S. M., Hainaut, O., Smette, A., West, R. M., Major outburst of periodic Comet Halley at a heliocentric distance of 14 AU, *Astron.Astrophys.* **263**, 367, 1992. [10.3]

Sekanina, Z., Jehin, E., Boehnhardt, H., Bonfils, X., Schuetz, O., Recurring outbursts and nuclear fragmentation of Comet C/2001 A2 (LINEAR), *Astrophys. J.* **572**, 679, 2002. [3.6]

Senay, M. C., Jewitt, D., Coma formation driven by carbon monoxide release from Comet P/Schwassmann-Wachmann 1, *Nature* **371**, 229, 1994. [10.3]

Shoshani, Y., Heifetz, E., Prialnik, D., Podolak, M., A model for the changing pore structure and dust grain size distribution in a porous comet nucleus, *Icarus* **126**, 342, 1997. [4.7]

Shoshany, Y., Podolak, M., Prialnik, D., A Monte-Carlo model for the flow of dust in a porous comet nucleus, *Icarus* **137**, 348, 1999.

Shoshany, Y., Prialnik, D., Podolak, M., Monte-Carlo modeling of the thermal conductivity of cometary ice, *Icarus* **157**, 219, 2002. [4.9]

Shul'man, L. M., The evolution of cometary nuclei, in *The Motion, Evolution of Orbits and Origin of Comets*, (eds. G. A. Chebotarev, E. I. Kazimirchak-Polonskaya, and B. G. Marsden), Reidel, 271, 1972. [3.5, 4.7]

Shul'man, L. M., The contribution of dust grains of condensation origin to the integral brightness of comets, *Astrometr. Astrofiz.* **46**, 68, (Russian) 1982. [9.4]

Shul'man, L. M., The contemporary model of cometary nucleus and the prospects of its improvement by space research., *Adv. Space Res.* **1**, 91, 1991. [10.1]

Simpson, J. A., Rabinowitz, D., Tuzzolino, A. J., Ksanformality, L. V., Sagdeev, R. Z., The dust coma of Comet P/Halley: Measurements on the Vega-1 and Vega-2 spacecraft, *Astron. Astrophys.* **187**, 742, 1987. [2.2]

Sirono, S., Greenberg, J. M., Do cometesimal collisions lead to bound rubble piles or to aggregates held together by gravity? *Icarus* **145**, 230, 2000. [2.2]

Sirono, S., Yamamoto, T., Thermal conductivity of granular materials relevant to the thermal evolution of cometary nuclei, *Planet. Space Sci.* **45**, 827, 1997. [2.2]

Skorov, Y. V., Kömle, N. I., Keller, H. U., Kargl, G., Markiewicz, W. J., A model of heat and mass transfer in a porous cometary nucleus based on a kinetic treatment of mass flow, *Icarus* **153**, 180, 2001.

Skorov, Y. V., Rickman, H., A kinetic model of gas flow in a porous cometary mantle, *Planet. Space Sci.* **43**, 1587, 1995.

Skorov, Y. V., Rickman, H., Simulation of gas flow in a cometary Knudsen layer, *Planet. Space Sci.* **46**, 975, 1998.

Skorov, Y. V., Rickman, H., Gas flow and dust acceleration in a cometary Knudsen layer, *Planet. Space Sci.* **47**, 935, 1999. [3.4]

Smoluchowski, R., Amorphous ice and the behaviour of cometary nuclei, *Astrophys. J.* **244**, L31, 1981. [4.9, 10.3]

Smoluchowkski, R., Heat transport in porous cometary nuclei, *J. Geophys. Res.* **87**, A422, 1982. [2.4]

Soderblom, L. A., Becker, T. L., Bennett, G., Boice, D. C., Britt, D. T., Brown, R. H., Buratti, B. J., Isbell, C., Giese, B., Hare. T., Hicks, M. D., Howington-Kraus, E., Kirk, R. L., Lee, M., Nelson, R. M., Oberst, J., Owen, T. C., Rayman, M. D., Sandel, B. R., Stern, S. A., Thomas, N., Yelle, R. V., Observations of Comet 19P/Borrelly by the Miniature Integrated Camera and Spectrometer aboard Deep Space 1, *Science* **296**, 1087, 2002. [11.2]

Spohn, T., Benkhoff, J., Thermal history models for KOSI sublimation experiments, *Icarus* **87**, 358, 1990. [2.4]

Spohn, T., Benkhoff, J., Seiferlin, K., Thermal conductivities and diffusivities of porous ice samples at low pressures and temperatures and possible modes of heat transfer in near surface layers of comets, in *Proceedings of an International Workshop on Physics and Mechanics of Cometary Material*, ESA SP-302, 77, 1989. [2.4, 3.5]

Spoon, H. W. W., Moorwood, A. F. M., Pontoppidan, K. M., Cami, J., Kregel, M., Lutz, D., Tielens, A. G. G. M. Detection of strongly processed ice in the central starburst of NGC 4945, *Astron. Astrophys.* **402**, 499, 2003. [12.3]

Squires, R. E., Beard, D. B., Physical and orbital behaviour of comets, *Astrophys. J.* **133**, 657, 1961. [5.1]

Squyres, S. W., McKay, C. P., Reynolds, R. T., Temperatures within comet nuclei, *J. Geophys. Res.* **90**, 12381, 1985. [4.9, 5.1]

Srinivasan, G., Goswami, J. N., Bhandari, N., ^{26}Al in Eucrite Piplia Kalan: Plausible heat source and formation chronology, *Science* **284**, 1348, 1999.

St. Cyr, O., Burkepile, J., Stanger, A., Pitone, D., Twambly, B., Marsden, B. G., IAU Circ. 4884, 1989. [8.5]

Stagg, C. R., Bailey, M. E., Stochastic capture of short-period comets, *Mon.*

Not. Roy. Astron. Soc. **241**, 507, 1989. [8.2]

Starukhina, L. V., Shkuratov, Yu. G., A model for ion bombardment. Induced organic synthesis on carbon bearing surfaces in cosmic space, *Icarus* **113**, 442, 1995. [2.4]

Steiner, G., Kömle, N., A model of the thermal conductivity of porous water ice at low gas pressures, *Planet. Space Sci.* **39**, 507, 1991a. [2.4, 6.5]

Steiner, G., Kömle, N. I., Thermal budget of multicomponent porous ices, *J. Geophys. Res.* **96**, 18897, 1991b. [4.9, 6.5]

Steiner, G., Kömle, N. I., Evolution of a porous H_2O-CO_2-ice sample in response to irradiation, *J. Geophys. Res.* **98**, 9065, 1993. [10.2, 10.4]

Steiner, G., Kömle, N., Kührt, E., Thermal modelling of comet simulation experiments, in *Proceedings of an International Workshop on Physics and Mechanics of Cometary Materials*, ESA SP- **302**, 1990. [3.3, 4.8, 7.2]

Steiner, G. Kömle, N. I., Kührt, E., Thermal modeling of comet simulation experiments, in *Theoretical Modeling of Comet Simulation Experiments*, (eds. N. I. Koemle et al., Verlag der Österreichischen Akademie der Wissenschaften, 11, 1991. [6.5]

Stevenson, D. J., Lunine, J. I., Rapid formation of Jupiter by diffuse redistribution of water vapor in the solar nebula, *Icarus* **75**, 146, 1988. [8.2]

Stöffler, D., Düren, H., Knölker, J., Hische, R., Bischoff, A., Cometary analogue material: Preparation, composition and thin section petrography, *Geophys. Res. Lett.* **18**, 285, 1991. [2.4]

Strazzulla, G., Ion bombardment of comets, in *From Stardust to Planetesimals*, (eds. Y. J. Pendleton and A. G. G. M. Tielens), ASP Conf. Series Book, 423, 1997. [2.4]

Strazzulla, G., Chemistry of ice induced by energetic charged particles, in *Solar System Ices*, (eds. B. Schmitt, C. de Bergh, and M. Festou), Kluwer, 281, 1998. [2.4]

Strazzulla, G., Ion irradiation and the origin of cometary materials, *Space Sci. Rev.* **90**, 269, 1999. [8.2]

Strazzulla G., Baratta, G. A., Johnson, R. E., Donn, B., The primordial comet mantle: Irradiation production of a stable, organic crust, *Icarus* **91**, 101, 1991. [2.4, 3.5]

Strazzulla, G., Baratta, G. A., Palumbo, M. E., Vibrational spectroscopy of ion-irradiated ices, *Spectrochim. Acta*, **A57**, 825, 2001. [2.4]

Strazzulla, G., Johnson, R. E., Irradiation effects on comets and cometary debris, in *Comets in the Post-Halley Era*, (eds. R. L. Newburn, Jr., M. Neugebauer, and J. Rahe), Kluwer, 243, 1991. [2.4]

Sykes, M. V., Lebofsky, L. A., Hunten, D. M., Low, F., The discovery of dust trails in the orbits of periodic comets, *Science* **232**, 1115, 1986. [4.5]

Sykes, M. V., Lien, D. J., Walker, R. J., The Tempel 2 dust trail, *Icarus*

86, 236, 1990. [4.5]

Taban, I. M., Schutte, W. A., Pontoppidan, K. M., van Dishoeck, E. F., Stringent upper limits to the solid NH3 abundance towards W 33A from near-IR spectroscopy with the Very Large Telescope, *Astron. Astrophys.* **399**, 169, 2003. [12.3]

Tancredi, G., Fernández, J. A., Rickman, H., Licandro, J., Nuclear magnitudes and the size distribution of Jupiter family comets, *Icarus*, in press, 2006. [Ap.A]

Tancredi, G., Rickman, H., Greenberg, J. M., Thermochemistry of cometary nuclei. 1. The Jupiter family case, *Astron. Astrophys.* **286**, 659, 1994. [3.2, 4.4, 10.3, 12.2]

Taylor, S. R., *Solar System Evolution: A New Perspective*, Cambridge University Press, 1992. [2.4]

Thi, W.-F., Pontoppidan, K. M., van Dishoeck, E. F., Dartois, E., d'Hendecourt, L., Detection of abundant solid CO in the disk around CRBR 2422.8-3423, *Astron. Astrophys.* **394**, L27, 2002. [12.3]

Uzzo, M., Raymond, J. C., Biesecker, D., Marsden, B., Wood, C., Ko, Y.-K., Wu, R., Results from UVCS and LASCO observations of the sungrazing Comet C/2000 C6, *Astrophys. J.* **558**, 403, 2001. [8.5]

Vaisberg, O. L., Smirnov, V., Omelchenko, A., Gorn, L., Iovlev, M., Spatial and mass distribution of low-mass dust particles ($m < 10^{-10}$ g) in Comet P/Halley's coma, *Astron. Astrophys.* **187**, 753, 1987. [2.2]

Valsecchi, A., Manara, G. B., Dynamics of comets in the outer planetary region. II. Enhanced planetary masses and orbital evolutionary paths, *Astron. Astrophys.* **323**, 986, 1997. [8.2]

Vanýsek, V., Wickramasinghe, N. C., Formaldehyde polymers in comets, *Astrophys. Space Sci.* **33**, L19, 1975. [2.4]

Wallis, M. K., Radiogenic heating of primordial comet interiors, *Nature* **284**, 431, 1980. [8.2]

Wallis, M. K. , Rotation of cometary nuclei, *Phil. Trans. Roy. Soc. A* **313**, 165, 1984. [9.5]

Washburn, E. W., The vapor pressure of ice and water up to 100° C. Internat. Crit. Table **3**, McGraw-Hill, p. 210, 1928. [5.1]

Weidenschilling, S. J., The origin of comets in the solar nebula: A unified model, *Icarus* **127**, 290, 1997.

Weissman, P., Why did Halley hiccup? *Nature* **353**, 793, 1991. [10.3]

Weissman, P. R., Cometary reservoirs. in *The New Solar System*, (eds. J. K. Beatty, C. C. Peterson, and A. Chaikin), Cambridge University Press, 1999, p. 59. [8.2]

Weissman, P. R., A'Hearn, M. F., Rickman, H., McFadden, L. A., Evolution of comets into asteroids, in *Asteroids II* Tucson, AZ, University of

Arizona Press, 1989, p. 880. [3.5]

Weissman, P., Kieffer, H. H., Thermal modeling of cometary nuclei, *Icarus* **47**, 302, 1981.

Weissman, P., Kieffer, H. H., An improved thermal model for cometary nuclei, *J. Geophys. Res.* **89**, Suppl. C358, 1984. [5.1]

Weissman, P. R., Levison, H. F., Origin and evolution of the unusual object 1996 PW: Asteroids from the Oort Cloud? *Astrophys. J. Lett.* **488**, L133, 1997. [8.2]

Weissman, P. R., Lowry, S. C., The size distribution of Jupiter-family cometary nuclei, *34th Annual Lunar and Planetary Science Conf.*, abs. 2003, 2003. [Ap.A]

West, R. M., Hainaut, O., Smette, A., Post-perihelion observations of P/Halley. III – An outburst at $R = 14.3$ AU, *Astron. Astrophys.* **246**, L77, 1991. [10.3]

Wetherill, G. W., Where do the Apollo objects come from? *Icarus* **76**, 1, 1988. [2.3]

Whipple, F. L., A comet model. I. Acceleration of comet Encke, *Astrophys. J.* **111**, 375, 1950. [5.1]

Whipple, F. L., A comet model. II. Physical relations for comets and Meteors, *Astrophys. J.* **113**, 464, 1951. [5.1]

Whipple, F. L., Comets: Problems of the cometary nucleus, *Astron. J.* **66**, 375, 1961. [9.5]

Whipple, F. L., On the structure of the cometary nucleus, in *The Moon, Meteorites and Comets*, (eds. G. P. Kuiper and B. Middlehurst), University of Chicago Press, p. 639, 1963. [5.1]

Whipple, F. L., The rotation of cometary nuclei, in *Comets*, (ed. L. L. Wilkening), University of Arizona Press, p. 227, 1982. [9.5]

Whipple, F. L., Stefanik, R., On the physics and splitting of cometary nuclei, *Mem. Soc. Roy. Sci. Liege* **12**, 33, 1966. [8.2, 9.5]

Wirtanen, C. A., Comet 1948b, Iau Circ. 881, 1948. [10.1, 11.3]

Wickramasinghe, N. C., Formaldehyde polymers in interstellar space, *Nature* **252**, 462, 1974. [2.4]

Wood, J. A., Origin of the solar system, in *The New Solar System*, (eds. J. K. Beatty, C. C. Peterson, and A. Chaikin), Cambridge University Press, 1999, p. 13. [8.2]

Wright, R. B., Varma, R., Grün, D. M., Raman scattering and SEM studies of graphite and silicon carbide surfaces bombarded with energetic protons, deuterons and helium, *J. Nucl. Mater.* **63**, 415, 1976. [2.4]

Yabushita, S., Thermal evolution of cometary nuclei by radioactive heating and possible formation of organic chemicals, *Mon. Not. R. Astron. Soc.* **260**, 819, 1993. [8.2]

Subject Index